

# **Combined Palaeomagnetic and Anisotropy of Magnetic Susceptibility (AMS) Study of High Grade Rocks from Kondapalle Area, Eastern Ghats Belt, India**

**Thesis submitted to Jadavpur University  
For the degree of Doctor of Philosophy (Science)**

**By**

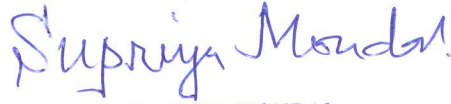
**DEBESH GAIN**

**INDEX No.: 167/15/Geol. Sc./24**

**Geophysical Laboratory  
Department of Geological Sciences  
Jadavpur University  
Kolkata-700032, India  
2022**

## CERTIFICATE FROM THE SUPERVISORS

This is to certify that the thesis entitled “**Combined Palaeomagnetic and Anisotropy of Magnetic Susceptibility (AMS) Study of High Grade Rocks from Kondapalle Area, Eastern Ghats Belt, India**” submitted by **SRI DEBESH GAIN** who got his name registered on **08.10.2015** for the award of **Ph. D. (Science)** degree of Jadavpur University, is absolutely based upon his own work under the supervision of **Prof. Supriya Mondal** and **Prof. Nathani Basavaiah** and that neither this thesis nor any part of it has been submitted for either any degree / diploma or any other academic award anywhere before.



**DR. SUPRIYA MONDAL**  
Professor  
Department of Geological Sciences  
JADAVPUR UNIVERSITY  
Kolkata-700032, W.B.(India)

**Date: 21.09.2022**

---

**Professor Supriya Mondal**



**Prof. NATHANI BASAVAI AH**  
**INDIAN INSTITUTE OF GEOMAGNETISM**  
Kalamboli, New Panvel, Navi Mumbai-40210  
Tel : 022-27484142  
Email : basg@igs.ii gm.rrw.in

**Date: 19.09.2022**

---

**Professor Nathani Basavaiah**

***Dedicated to my Parents  
and Mentors***

## ACKNOWLEDGEMENTS

The first place in this acknowledgement goes to my supervisors, Prof. Supriya Mondal, Department of Geological Sciences, Jadavpur University, Kolkata and Prof. Nathani Basavaiah, Professor-G, Indian Institute of Geomagnetism, Navi Mumbai, India for their constant guidance, support and meticulous supervision throughout the work. It would be impossible to complete the work without their guidance and advice.

I would like to thank UGC (Non-NET fellowship scheme) and CSIR (JRF and SRF), Govt. of India for the financial support during this research work and the Environmental Magnetism Laboratory, Indian Institute of Geomagnetism, Navi Mumbai, India and Department of Earth, Ocean, and Ecological Sciences, University of Liverpool, UK for the necessary laboratory facilities. Besides, I am pleased with the staffs of Ph.D. (Science) Section, Jadavpur University for their cooperation. I would like to thank Head of the Department of Geological Sciences, all the faculty members, the research scholars and non-teaching staffs for their help and support during the course of my work.

I would like to specially thank my friend Dr. Saurodeep Chatterjee for his selfless support throughout this work. Besides, Dr. Alip Roy, Dr. Rimjhim Maity, Dr. Dipanjan Majumder, Punyotoya Paul and Solanky Das of the Department of Geological Sciences, Jadavpur University are acknowledged for their constant support towards this research work. I would always remain grateful to my parents, my brother and other family members and friends for their support, love and encouragement throughout the work.

Date: 27.09.2022

Place: KOLKATA

Debesh Gain

DEBESH GAIN

# CONTENTS

	<b>Page No.</b>
Abstract	<b>i-ii</b>
List of Abbreviations	<b>iii-iv</b>
<b>1. Introduction</b>	<b>1-5</b>
<b>2. Geological Set-up and Sampling</b>	<b>6-20</b>
2.1. Background Geology	6-10
2.2. Lithology and Geological Structures	10-15
2.3. Geochronology and Tectonic Evolution	15-19
2.4. Sampling Process and Sample Preparation	19-20
<b>3. Petrography</b>	<b>21-40</b>
3.1. Introduction	21
3.2. Mineral Assemblages	21-39
3.3. Mutual Textural Relations of Minerals	39-40
<b>4. Generation of Fe-Ti Oxides</b>	<b>41-63</b>
4.1. Introduction	41-44
4.1.1. Classification of the Fe-Ti Oxides	41-43
4.1.2. Solid Solution Series of the Fe-Ti Oxides	43-44
4.2. Oxidation of Fe-Ti Oxides	44-59
4.3. Generations of Fe-Ti oxide and its tectonic implications	59-63
<b>5. Anisotropy of Magnetic Susceptibility study</b>	<b>64-77</b>
5.1. Introduction	64-65
5.2. AMS and magnetic fabrics in Rocks of KPLC	65-75
5.2.1. Introduction	65-67
5.2.2. Low field magnetic susceptibility and anisotropy	67-69
5.2.3. Magnetic Fabrics	69-73
5.2.4. Magnetic fabric versus mesoscopic fabric	73-75
5.3. Summary: Tectonic implications	75-77

<b>6. Rock Magnetic Studies</b>	<b>78-105</b>
6.1. Introduction	78-79
6.2. Rock Magnetic Measurements	80-84
6.2.1. Thermo-magnetic Study	80-81
6.2.2. Magnetic Hysteresis Study	81-83
6.2.3. Isothermal Remanent Magnetization (IRM) Study	83-84
6.3. Mineral Magnetic Studies	84-99
6.3.1. Magnetic Susceptibility Measurement	84-86
6.3.2. Anhyseretic Remanent Magnetization (ARM) Measurement	87-88
6.3.3. Saturation Isothermal Remanent Magnetization (SIRM) Measurement	88-89
6.3.4. Frequency-dependent Susceptibility ( $\chi_{fd}$ %) Measurement	90-93
6.3.5. SIRM/ $\chi$ , ARM/ $\chi$ and ARM/SIRM	93-95
6.3.6. Partial IRMs: Hard IRM, Soft IRM and S-ratio	95-98
6.3.7. SIRM versus Magnetic Susceptibility ( $\chi$ ) Plot	98-99
6.4. Summary of Rock Magnetic Studies	99-105
<b>7. Palaeomagnetic Studies</b>	<b>106-120</b>
7.1. Introduction	106
7.2. Natural Remanent Magnetization (NRM)	106-108
7.3. Koenigsberger (Q) Ratio	109-110
7.4. AF Demagnetization	110-116
7.5. ChRM and Pole Positions	116-118
7.6. Pole Positions and its Geological Implications	118-120
<b>8. Conclusions</b>	<b>121-122</b>
<b>9. Appendix</b>	<b>123-132</b>
<b>10. References</b>	<b>133-149</b>

## ABSTRACT

The present study is an integrated approach towards the petrography, rock magnetic, Anisotropy of Magnetic Susceptibility (AMS) and palaeomagnetic studies of the high-grade metamorphic rocks in and around Kondapalle Pangidi Layered Complex (KPLC), Eastern Ghats Belt (EGB), India. This study aims at determining the petrography, generations of Fe-Ti oxides, rock magnetic properties, magnetic remanence carriers, magnetic fabrics and the stable magnetic vectors (ChRM) present in the studied rocks and its corresponding pole positions.

The rock magnetic properties and the magnetic fabrics from AMS studies are used to determine their tectonic implications. Magneto-mineralogical study reveals that the chief remanence carrier mineral is titanomagnetite. There are three generations of Fe-Ti oxides are observed. They are primary homogeneous titanomagnetite, primary inhomogeneous titanomagnetite (high temperature and low temperature phases) and secondary ultra-fine grained Fe-Ti oxides. Rock magnetic studies including Isothermal Remanent Magnetization (IRM), back-field IRM, hysteresis loop studies, and thermomagnetic studies reveal the same. The magnetic hysteresis parameters (remanence and coercivity) are used to determine the magnetic domains from a modified Day plot. The magnetic domains lie within Stable Single Domain (SSD) and Pseudo Single Domain (PSD) ranges, thereby explaining their potential to record an ancient magnetic field. Also, mineral magnetic measurements and related inter-parametric ratios (e.g.,  $\chi$ , ARM, SIRM, ARM/ $\chi$ , SIRM/ $\chi$ ,  $\chi_{fd}$  %, S-ratio) exhibit the same. Besides the ferrimagnetic remanence carriers, paramagnetic silicates are also dominant which controlled the development of magnetic fabric, which is revealed from the AMS study. The magnetic fabric bears analogy with the regional structures and bear tectonic implications related to the post-rifting closure of the ocean followed by subduction of the ocean basin, accretionary orogeny and felsic magmatism in the Indo-Antarctic continental blocks.

Three mean ChRM components have been determined from alternate field (AF) demagnetization analysis of the rocks with predominant remanent component over induced component. These components do not include a significant record of the present earth's magnetic field. These are D<sub>1</sub> (D/I=20.8°/35.1°), D<sub>2</sub> (D/I=312.5°/53.7°)

and  $D_3$  ( $D/I=42.6^\circ/-10.3^\circ$ ). These vectors are carried by primary high temperature and low temperature phases of titanomagnetites and probably acquired over a long period of geologic time during post-metamorphic uplift-related cooling. Each mean ChRM direction defines palaeomagnetic pole positions, which are  $K_1$  ( $70.04^\circ\text{N}/159.61^\circ\text{E}$ ),  $K_2$  ( $44.12^\circ\text{N}/22.43^\circ\text{E}$ ), and  $K_3$  ( $42.56^\circ\text{S}/14.28^\circ\text{E}$ ) respectively. The poles were dated (correlating with the existing accepted pole positions available in the literature) to be of the age group  $\sim 1700$ - $1900$  Ma,  $\sim 1500$ - $1700$  Ma and  $\sim 1100$ - $1200$  Ma respectively. The acquisition of first two ChRM components correspond to UHT metamorphism and emplacement of KPLC respectively while the third acquired during post-metamorphic uplift related tectonism.

Results from all the parameters and attributes together contribute towards the genesis of the various magnetic properties of the Kondapalle Pangidi Layered Complex of the Eastern Ghats Belt, India.



## LIST OF ABBREVIATIONS

**AF:** Alternating Field

**AMS:** Anisotropy of Magnetic Susceptibility

**APW:** Apparent Polar Wander

**APWP:** Apparent Polar Wandering Path

**ARM:** Anhysteretic Remanent Magnetization

**ChRM:** Characteristic Remanent Magnetization

**CRM:** Chemical Remanent Magnetization

**CMZ:** Central Charnockite-Migmatite Zone

**D:** Declination

**DRM:** Detrital Remanent Magnetization

**EGB:** Eastern Ghats Belt

**EMF:** Earth's Magnetic Field

**EKZ:** Eastern Khondalite Zone

**FD:** Frequency Dependent

**HF:** High Frequency

**HIRM:** Hard Isothermal Remanent Magnetization

**I:** Inclination

**IBC:** Isobaric Cooling

**IP:** Irreversibility Parameter

**IPx:** New Irreversibility Parameter

**IRM:** Isothermal Remanent Magnetization

**ITD:** Isothermal Decompression

**KPLC:** Kondapalle Pangidi Layered Complex

**LF:** Low Frequency

**MD:** Multi Domain

**NRM:** Natural Remanent Magnetization

**pDRM:** Post Depositional Remanent Magnetization

**PGE:** Platinum Group of Element

**PPL:** Plane Polarised Light

**PSD:** Pseudo Single Domain

**SD:** Single Domain

**SI:** Standard International

**SIRM:** Saturating Isothermal Remanent Magnetization

**Soft IRM:** Soft Isothermal Remanent Magnetization

**SP:** Super Paramagnetic

**SSD:** Stable Single Domain

**TRM:** Thermal Remanent Magnetization

**UHT:** Ultra High Temperature

**VRM:** Viscous Remanent Magnetization

**WCZ:** Western Charnockite Zone

**WKZ:** Western Khondalite Zone

**XPL:** Cross Polarised Light

**Chapter 1**  
**Introduction**

## **INTRODUCTION**

Plate tectonics has taught us to view the Earth's lithosphere as a dynamic system of spreading oceanic ridges, transform faults, and subduction zones. Continental drift is now accepted as a corollary of plate tectonics, and the complexity of orogenic belts is leading to an appreciation of the mobility of continental crust. The margins of continents are often tectonically active especially above subduction zones. Portions of continental crust can rift from a continent and move, as Baja California is doing today. Continental fore-arc regions may also be displaced during intervals of oblique subduction. Palaeomagnetism has played a central role in this developing view of continental geology.

Lithospheric plates carrying continents have experienced intervals of rapid motion, and oceanic plateaus, seamounts, and island arcs have been accreted (become attached) to continental margins. Although details are debatable, many geologists now view much of the western Cordillera of North America as a collage of tectono-stratigraphic terranes (Coney et al., 1980) these terranes are generally fault-bounded regions (dimensions up to hundreds of kilometers) with geologic histories that are distinct from those of neighboring regions. Some terranes are composed of rocks that originated in oceanic basins far from their present locations; others have experienced little or no motion with respect to the continental interior. Palaeomagnetism is one of the primary methods of deciphering tectonic histories of terranes.

The Eastern Ghats belt (EGB) along the east coast of India preserves vestiges of ultra-high temperature metamorphism with a characteristic retrograde near-isobaric cooling P-T path. Reassembly of east Gondwana has juxtaposed the EGB against the parts of east Antarctica. The identification of metamorphic events and magneto-stratigraphy in the EGB and their comparison with the evolutionary history of the east Antarctic granulites are crucial, not only to understanding the spatial and temporal variation of Precambrian orogenic processes, but also to provide important and independent constraints on the configuration of east Gondwana before ~ 500 Ma. In the EGB, a wide range of variation in rock types is exposed here. These rock units exhibit

a wide range of geological age. The palaeomagnetic investigations can only correlate the tectonic history of the rocks.

Palaeomagnetic and anisotropy of magnetic susceptibility (AMS) analysis of deep crustal rocks of Kondapalle Pangidi Layered Complex (KPLC), EGB have two important contributions to make to the geophysical study of the deep continental crust:

(i) Firstly, the Precambrian deep crustal rocks invariably possess a strong and stable record of the ancient magnetic field acquired at stages of the early tectonic history of these terrains. The magnetism is typically resident in one or more phases of magnetite growth and has recorded the palaeomagnetism over protracted periods of geologic time. This palaeomagnetic record will provide the only evidence for the ancient tectonic history of the EGB, India and is the essential information required for correlating the deep crustal rocks of EGB, India with that elsewhere.

(ii) Secondly, magnetic fabrics of the rocks is an important character, which can be measured from anisotropy of magnetic susceptibility (AMS) study in high-grade metamorphic rocks because they are related to the metamorphic and tectonic events. The AMS ellipsoids are useful indicators of the geometry of the magnetic fabrics in metamorphic terrains. The geometry of the magnetic fabrics can resolve complex tectonic problems and large-scale deformations can also be traced from AMS signatures. Magnetic mineralogy and rock magnetic properties also useful to determine magnetic nature of the rocks and the magnetic remanence carriers. Thus, this terrain is ideal for studying rock magnetic properties and magnetic fabrics in relation to tectonics.

The permanent magnetism present in a rock before any treatment is termed as Natural Remanent Magnetization (NRM). Often the magnetization remaining after various natural demagnetization treatments, is also referred as NRM. Majority of crustal rocks possess NRM which is acquired by different physical processes depending on the mode of formation of the rocks. They are as follows: Thermoremanent Magnetization (TRM), Detrital Remanent Magnetization (DRM), Chemical Remanent Magnetization (CRM), Viscous Remanent Magnetization (VRM), Isothermal Remanent Magnetization (IRM), and Post Depositional Remanent Magnetization (pDRM).

Metamorphic rocks overlain by the sedimentary / igneous rocks, form the bulk of the continental crust are exposed in the Precambrian shields and mobile belts. These

rocks acquire primary magnetization (TRM) in the geomagnetic field. Later they subjected to metamorphic and tectonic processes, which introduce secondary remanence components within the rocks. These secondary magnetization components (CRM, VRM, IRM), which can overprint primary thermo-remanent magnetization (TRM). Superimposed primary and secondary remanences are carried by two coexisting magnetic minerals or by coexisting multi-domain (MD), single-domain (SD) and stable single domain (SSD) states of the same mineral (McClelland-Brown, 1982). The rocks from KPLC, EGB are mainly igneous and metamorphic rocks, so TRM and CRM are taken into account.

The NRM is usually the vector sum of the primary magnetization acquired during the formation of a rock and the secondary magnetization (which may include several components) acquired during subsequent period of geological time. The major part of all palaeomagnetic investigations involves the recognition and separation of these magnetic components and identification of Characteristic Remanent Magnetism (ChRM) from all the magnetic components. Magnetic components are commonly isolated by partial demagnetization processes of the natural remanence (thermal demagnetization or alternate field demagnetization) because the stability to demagnetization procedures is different of the magnetic components. After removal of the secondary magnetization components, the magnetizations of partially demagnetized specimens are called Characteristic Remanent Magnetism (ChRM). ChRM of a rock is a vector quantity which has both direction (declination and inclination) and magnitude (intensity). Using these directions of remanent magnetization, the palaeolatitude of the sampling site can be obtain from the relationship:

$$2 \tan \lambda = \tan I \quad (\text{Keary et al., 2009})$$

where  $\lambda$  is the palaeolatitude and  $I$  is the inclination of that magnetic vector. The palaeopole position (latitude and longitude) can also be obtained by applying various mathematical equations (Butler, 1992). This information of past direction and the intensity of the geomagnetic field through geological time is essential for quantifying the past movements of the tectonic plates (e.g., Butler, 1992).

There is very little palaeomagnetic data on the Precambrian rocks of India. No reliable palaeomagnetic pole positions have so far been obtained from the KPLC of

EGB. It is expected that the magnetic data (rock magnetic, AMS and palaeomagnetic) of the Precambrian layered complexes may be very useful in defining Apparent Polar Wander (APW) segment of the Proterozoic times but also in recording deformation stages in rock history which cannot be obtained otherwise. The palaeomagnetic and anisotropy of magnetic susceptibility data can be combined to place rock fabrics within a plate tectonic framework.

A detailed geological and geophysical studies of the KPLC are carried out in this present study. This study mainly deals with the determination the rock magnetic characters, AMS analysis and palaeomagnetic investigations of the different litho-units of the Proterozoic high-grade metamorphic rocks of KPLC. For that, first oriented block samples have been collected from various litho-units. Apart from the collection of oriented block samples, field work also involves collection of structural data and preparation of geological map. For measurements of mineral magnetic parameters, powdered samples are required. From the collected samples, polished thin sections were prepared for microscopic studies both in transmitted and reflected lights to identify the petrological characteristics, magnetic minerals and their textures (generations of Fe-Ti oxides) and their textural relationship with associated silicate minerals. Rock magnetic studies help to identify the nature of magnetic minerals and their domain state (SSD, PSD or MD). The rock magnetic studies include measurements of thermomagnetic behaviors, magnetic hysteresis and isothermal remanent magnetization. In mineral magnetic parameters, magnetic susceptibility ( $\chi$ ), anhysteretic remanent magnetization (ARM) and isothermal remanent magnetization (IRM) are measured using powdered rock samples and inter-parametric ratios were calculated to identify the concentration, composition and effective grain size of the magnetic minerals within the rocks. The AMS study carried out by measuring the oriented core samples drilled out from the oriented block samples. The AMS study determines the magnetic fabrics, correlated with the crystal and grain shape alignment i.e., the microstructures. The AMS fabric can help to evaluating the deformational history of high-grade metamorphic rocks because the textures formed at high temperatures are typically obliterated by post-tectonic recrystallization; the orientation of foliation and / or lineation is then difficult to determine by field and microscopic studies. In palaeomagnetic study the magnetic remanence (NRM) of the rocks is measured, and the different components of the

remanent magnetization are determined by the progressive demagnetization by alternate field (AF) demagnetization process. The magnetization history of the rocks obtained from these processes are then tried to correlate them with the age of the recorded field. The  $\chi$  determined the induced magnetization and NRM determined the total remanence, so the relative importance of the remanent and the induced components was evaluated. When a rock passing through a geothermal gradient (30°C/km), the remanence acquisition occurs at a depth corresponding the upper limit of the blocking temperature range (~ 560°C for magnetite or ~ 670°C for hematite). Therefore, magnetic remanences (NRM and TRM) record the palaeo-field (magnetic) of the ancient Earth, which provides information about the time of magmatic and metamorphic events and the relative position of the magmatic geologic unit.

Thus, the principle aims of this study is to explore the potential of the Mesoproterozoic high-grade rocks to recording ancient EMF, to unfold the orientation anisotropy of the minerals, the nature of the magnetic fabrics and the factors responsible for the magnetic fabrics and through AMS studies, and The Characteristic Remanent Magnetism (ChRM) directions and the palaeo-pole position of the pole to identify the Proterozoic magnetization events recorded in the area.

The main objectives of the present study are:

- i) Identification the magnetic remanence carrier and their nature residing within the studied rocks.
- ii) Determination of magnetic fabric of the rocks through AMS and correlate them with the mesoscopic fabrics and microstructures to implicate their tectonic significances.
- iii) Unraveling the magnetization history of the rocks and its tectonic implications.
- iv) Determination of the palaeo-pole positions of the studied rocks.

Since these approaches are based on the magnetic analysis of rock cores, it is logical to combine them to determine both the magnetization of the deep crustal rocks of Eastern Ghats Belt, India and its earliest recoverable tectonic history.



## **Chapter 2**

# **Geological Set-Up and Sampling**

## **GEOLOGICAL SET-UP AND SAMPLING**

### **2.1. Background Geology**

The Eastern ghats Belt (EGB) is a NE-SW trending curved Proterozoic fold belt consisting of high-grade metamorphic rocks. It extends towards SW for about 900 km along the east coast of Indian subcontinent from Brahmani River (north of Cuttack) in Orissa to Ongole in Andhra Pradesh. The belt has a maximum width of 300km in the NE part (Mahalik, 1996) and it tapers to merely few tens of km in width in the SW part where it is overlain by the Phanerozoic sediment cover. The average width of the belt is about 100 km. The fold belt is surrounded by three cratonic blocks, namely Singhbhum craton in the north, the Bastar craton in the west, and the Dharwar craton in the south and south west (Fig. 2.1). To the south-east EGB is truncated by the Bay of Bengal and accreted by the Phanerozoic Continental marginal sediments in the east coast of India. The Mahanadi graben in the north and the Godavari graben in the south, break the continuity by hosting Gondwana sediments. The EGB consists largely of igneous and high-grade metamorphic rocks whose principal structural trends are parallel to the NNE-SSW elongation of EGB. (Kaila and Bhatia, 1981). The boundary between these three cratons and the EGB is termed the transition zone, having characteristics common to both (Bhattacharya and Kar, 2002). A thrust along the western margin of the EGB has been confirmed by deep seismic sounding. The contact of western belt of the EGB against Bastar craton is gradational. The contact between EGB and Singhbhum craton is also marked by shear zones, predominantly Sukinda thrust. The craton-mobile belt boundary is characterized by the occurrence of alkaline rocks in the Bastar and Singhbhum cratons, like those of Prakasan alkaline province in the Transition zone of Dharwar craton to the south of Godavari graben (Leelanandam, 1990). Alkaline rocks, mainly nepheline syenites are also reported at the contact zone of EGB-Singhbhum craton in the north as well as in the western part of the EGB, where they are grouped as Khariar Alkaline Complex. These alkaline rocks are deformed and their lenses are seen nearly parallel to the gneissic foliation. The alkaline complex in general has U–Pb and Pb–Pb emplacement ages of 1400–1500 Ma (Upadhyaya et al., 2006a). Bhattacharya (1996) gave an overview of the EGB. Charnockitic and

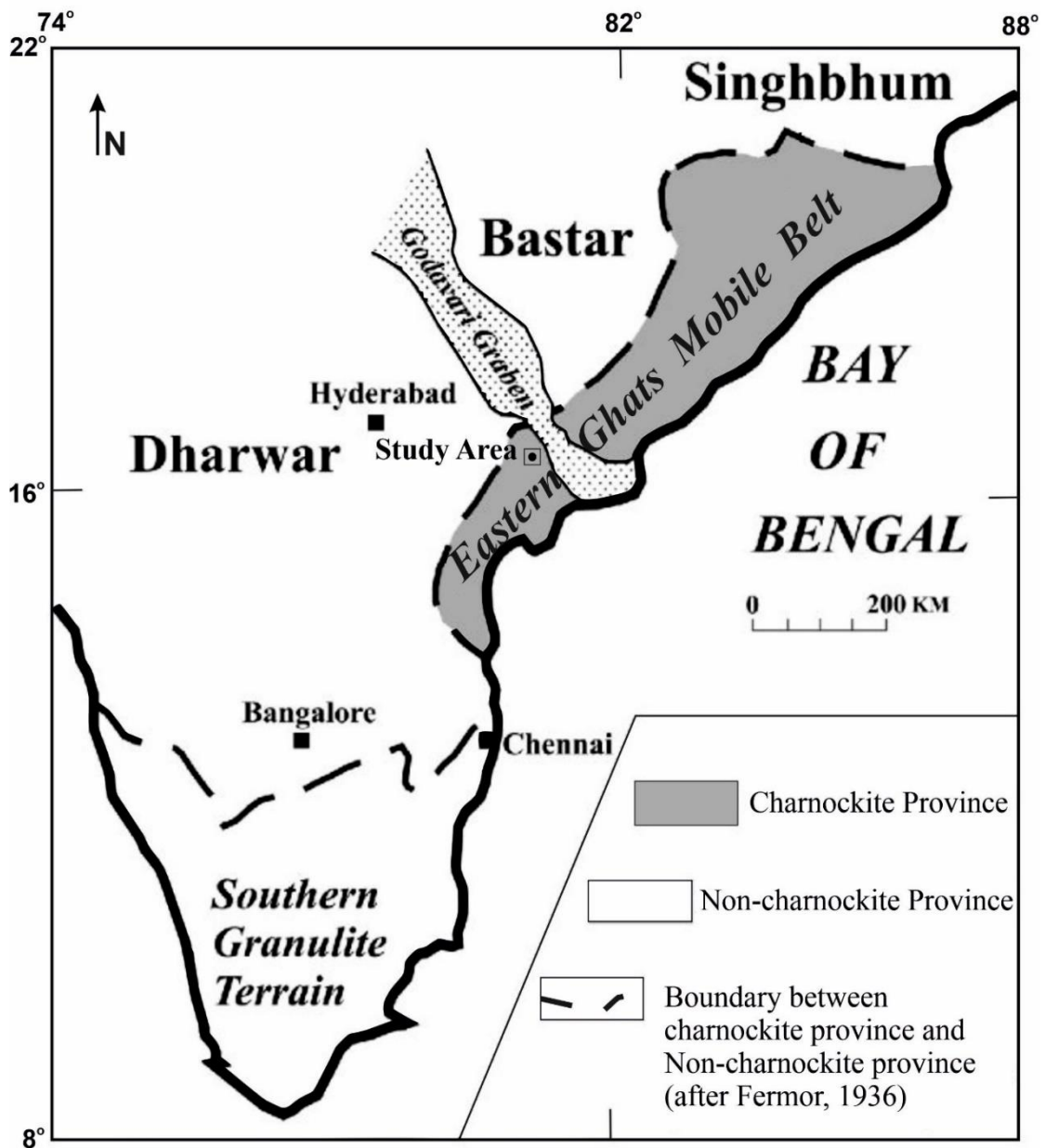


Fig. 2.1: Geological Map of Peninsular India, showing the location of the EGB with respect the Dharwar, Bastar and Singhbhum Cratons. (From Gupta et al., 2020).

khondalitic group of rocks are the main constituents of the EGB. The charnockitic group consists of mafic to acidic charnockites, hypersthene-bearing granulites, gneisses and leptynites. The khondalitic group consists garnet-sillimanite gneisses, quartzites and calc-silicates. The belt is broadly divided into four longitudinal zones based on the dominant lithological assemblages (Ramakrishnan et al., 1998). These divisions from West to East are: (a) Western Charnockite Zone (WCZ), dominantly charnockite and enderbite with lenses of mafic-ultramafic rocks and minor metapelites. (b) Western Khondalite Zone (WKZ), dominated by metapelite (khondalite) with intercalated

quartzite, calc-silicate rocks, marble and high Mg–Al granulites. Intrusion of later charnockite/enderbite in metapelitic granulites are common. (c) Central Charnockite-Migmatite Zone (CMZ), dominated by migmatitic gneisses with some high Mg–Al granulites and calc-silicate rocks, all of which are intruded by later charnockite/enderbite, porphyritic granitoids and massive-type anorthosite (Chilka Lake region), and (d) Eastern Khondalite Zone (EKZ), having lithological similarity with WKZ, but without anorthosite (Fig. 2.2a). Rickers et al. (2001) demarcated five isotopic domains in EGB, which are IA, IB, II, III and IV. The domain IA, IB and IV correspond to the WCZ and the domains II and III correspond to the WKZ, CMZ and EKZ of Ramakrishnan et al. (1998) (Fig. 2.2b). Domain II is separated from domain III by Nagavalli-Vamsadhara shear zone. Dobmeier and Raith (2003) divided the EGB into four provinces and several domains based on their distinct geological histories. They are (a) Krishna Province, (b) Jeypore Province, (c) Rengali Province and (d) Eastern Ghats Province. The first three provinces correspond to WCZ, whereas the Eastern Ghats Province corresponds WKZ, CMZ and EKZ of Ramakrishnan et al. (1998) (Fig. 2.2c). The main difference between subdivisions by Rickers et al. (2001) and Dobmeier

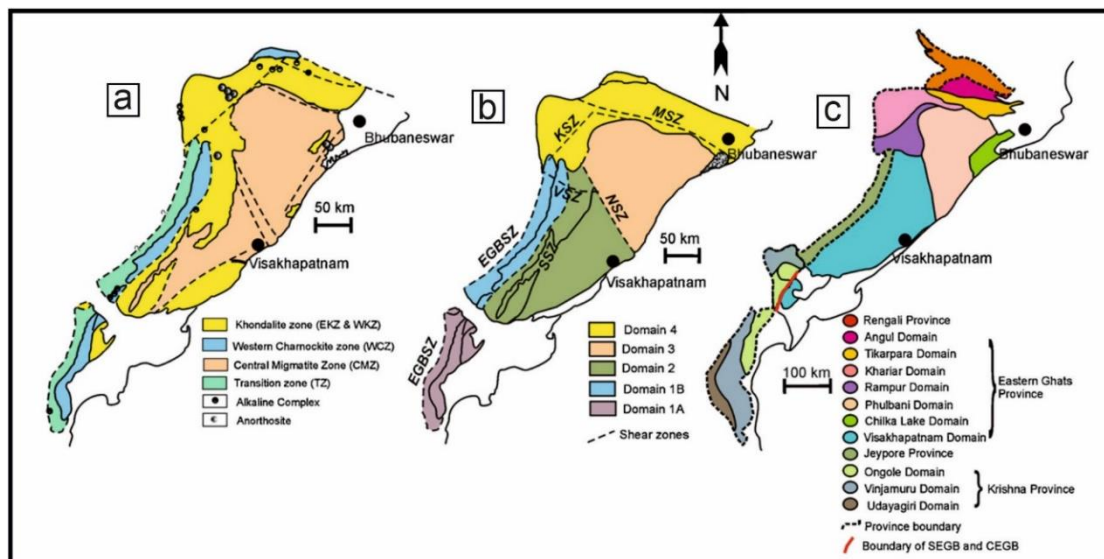


Fig. 2.2: Divisions and classifications of EGB based on (a) lithological characters (Ramakrishnan et al., 1998), (b) isotopic (Nd-model age) characters (Rickers et al., 2001) and (c) combination of lithological, metamorphic and isotopic characters (Dobmeier and Raith, 2003). (From Dasgupta et. al., 2013).

and Raith (2003) is subdivision by Dobmeier and Raith (2003) does not include Nagavalli-Vamsadhara shear zone as a province boundary. Dasgupta and Sengupta (1998) proposed the division of EGB into southern and northern mobile belt separated by Godavari rift.

The Kondapalle and Pangidi hill ranges (in Krishna District of Andhra Pradesh) and adjoining areas belongs to the granulite-facies Ongole domain (equivalent to the southern part of the WCZ' of Ramakrishnan et al., 1998) of Krishna Province of Dobmeier and Raith (2003) along with other two domains (Vinjamuru and Udayagiri) together known as low to medium-grade Nellore-Khammam Schist Belt. The Krishna province is situated at the South of the Godavari Graben. The Krishna province is dominantly composed of feldspathic and calc-granulites), mafic and felsic granulites, alkaline rocks, S-type granites, and massif-type anorthosites as well as layered igneous complexes in the southern sector. The granulite facies rocks of the Ongole Domain extend from Ongole in the south to the south-western margin of the Godavari Rift and re-appear on the other side of the rift.

The Kondapalle and Pangidi hill ranges cover an area about 200 sq km surrounded by Kondapalle to the South and Pangidi to the North (Lat. 16° 35' N to 16° 46' N and Long. 80° 26' E to 80° 33' E). A general Geological Map of the Kondapalle and Pangidi area is provided in the Fig. 2.3. Kondapalle and Pangidi area comprising anorthosite-gabbro-pyroxenite-chromitite, referred as a layered igneous complex (Nanda and Natarajan, 1980; Leelanandam, 1967, 1997, 1998; Dharma Rao et al., 2004). Both complexes are co-spatial (Nanda and Natarajan, 1980). They are studied separately by many workers of the Kondapalle (e.g., Sengupta et al., 1999; Bhui et al., 2007) and the Pangidi layered complexes (Dharma Rao, 1998; Dharma Rao and Satish Kumar, 2001; Dharma Rao et al., 2004). The Kondapalle and Pangidi complexes together designated as the Kondapalle Pangidi layered complex (KPLC) as they show same petrological, structural and geochemical features (Dharma Rao and Santosh, 2011) which pointing towards a regionally extensive arc related magmatic event (Dharma Rao and Santosh, 2011).

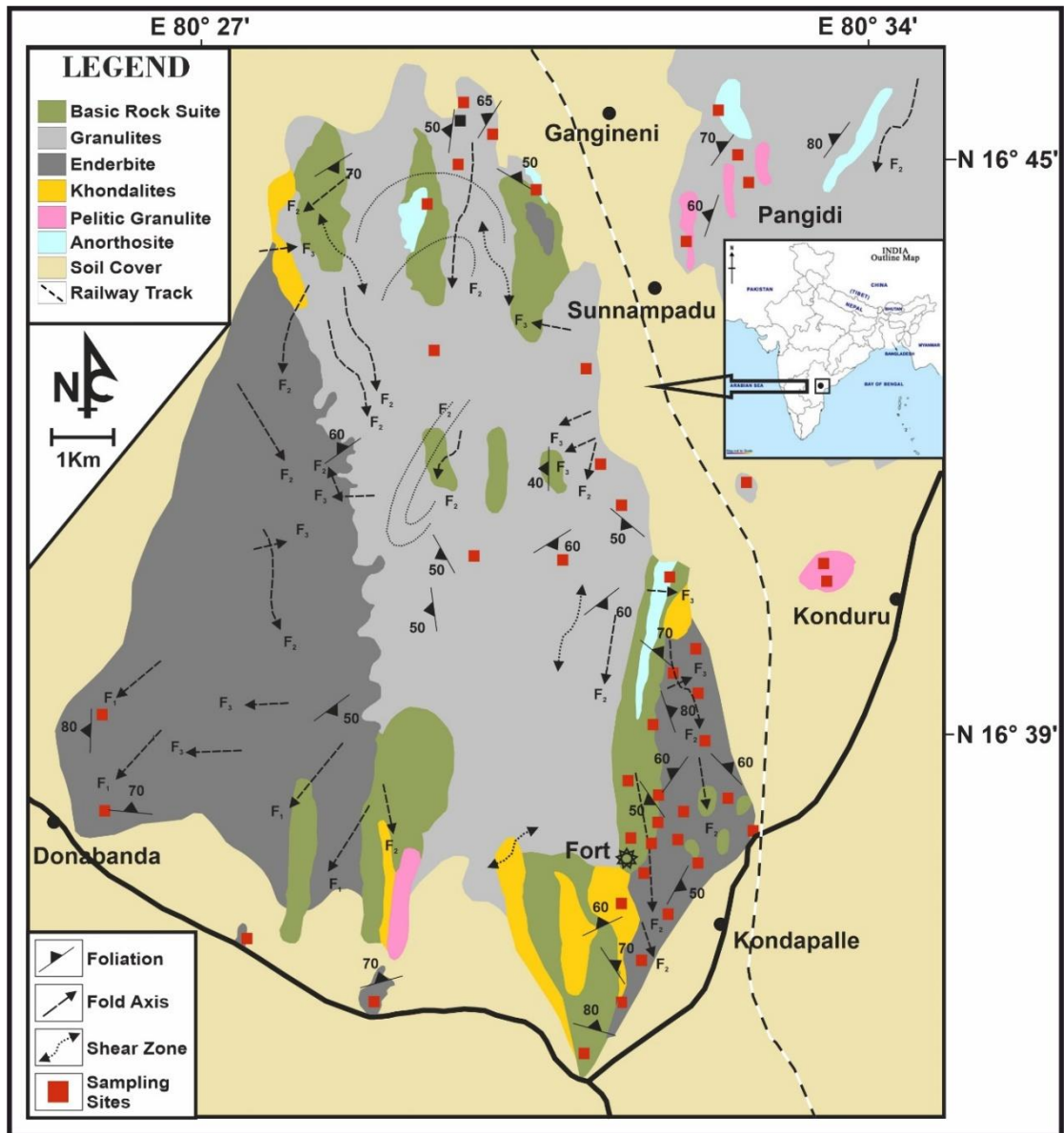


Fig. 2.3: Geological Map of the Kondapalle area (after Dharma Rao et al., 2012; Sengupta et al., 1999).

## 2.2. Lithology and Geological Structures

The EGB consists of igneous and high-grade metamorphosed rock. The principal rock types are mafic schist, metapelitic gneisses or khondalite (garnet-sillimanite-perthite-quartz gneiss), charnokite, orthopyroxene bearing quartzofeldspathic gneisses (mainly enderbite), leptynite (garnet-plagioclase-quartz-perthite gneiss without sillimanite and orthopyroxene), two pyroxenes mafic granulite,

sapphirine-spinel granulite along with intrusive anorthosite/layered complexes and alkaline rocks (Bhowmik, 1997; Dasgupta and Sengupta, 1995). Mafic schists include biotite, muscovite, and amphibole bearing schists. Khondalite and related rocks, including calc-silicates are metasediments. Charnokites are silica-rich, quartzo-feldspathic assemblages containing hypersthene. Mafic granulite commonly occurs as conformable layers in the charnockite and khondalite and consists of plagioclase, orthopyroxene, clinopyroxene, and minor amount of amphibole. Massif type anorthosites / layered complexes consist of a sequence of anorthosite, gabbro, norites and minor more differentiated rocks. Dunites and serpentinites are commonly associated with chromite and form a small and generally conformable bodies. Alkaline rocks occur as a number of post-tectonic bodies throughout the EGB.

The KPLC is dominated by several magmatic rocks including the gabbro-norite – pyroxene – anorthosite layered complex and later enderbite to charno-enderbite intrusives. The mafic-ultramafic layered complex consists predominantly of gabbro-norite, which, at places, grades into leuco-gabbro-norite to anorthosite. The later two rocks show magmatic layering defined by alternate pyroxene and plagioclase rich bands. Clinopyroxenite (locally with orthopyroxene and plagioclase) and chromite bearing enstatite are the dominant ultramafic rocks in the KPLC, the former occurring as thin to thick layers or pods of various dimensions in all these mafic members, whereas large pods of the latter rock (often several meters in length) are found only in the leuco-gabbro-norite and anorthosite. Layering (few centimeters to few meters) of chromite and enstatite is a common feature in this rock. There is local development of basic types with which chromite is associated in KPLC. The rocks are garnet bearing at places and show banding with garnet. The basic and ultrabasic types are of restricted distribution and occur as inter-banded. The chief ultrabasic rock is a pyroxenite composed largely or entirely of enstatite-hypersthene, without olivine. The occurrence of mafic pegmatites associated with the KPLC chromitites containing sulphides suggests the possibility of the presence of the platinum group elements (PGE) (Mathez, 1989; Naldrett et al., 1990; Roberts et al., 1990). The following sequence of rocks is proposed for Kondapalle and surrounding areas by Sinha and Mall (1974):

---

Dolerite

Acid charnockites, enderbites and granite gneisses and their variants.

Hybrid rocks formed by reaction of charnockite magma with pyroxene granulites of basement (Intermediate charnockite)

Chromiferous ultrabasics, dunites and anorthosites

Two pyroxene granulites. Hornblende granulites (Basic charnockites) and pyroxenites, amphibolites and their variants (Ultra basic charnockites)

Khondalite suite of rocks

---

The KPLC are variably deformed. The different components occur as isolated sheets, bands or lenses of various dimensions. The contacts of these components with the enclosing granulites are generally concealed, but are assumed to be tectonic in nature and modified by some shearing and also probably by hybridization (Leelanandam, 1997). Chilled margins and contact metamorphic effects of the complexes are not preserved. Most rocks of the KPLC exhibit remnant of layering, except the anorthositic and gabbroic group of rocks that occasionally display well developed layering and banding on different scales and styles (Fig. 2.4a, Fig. 2.4b) (Leelanandam, 1997). Small-scale slump and folded structures (Fig. 2.4c, Fig. 2.4d), imperfect low angle local unconformities, mineral lamination, flow folds (due to syn-consolidation deformation), and modally graded layers are rare (Leelanandam, 1997).

EGB broadly trends NE-SW, is a product of close parallelism of banding, compositional layering and lithological contacts. This trend is almost parallel to the axial planar foliation with steep easterly dips on the long limbs of major isoclinal / reclined folds. Narayanswami (1975) regarded NE-SW trend related to the earlier phase of folding (EGB trend) followed by cross folds along the NW-SE trends (Dharwar trend). Dome and basin structures or folded ovals resulting from fold interference are abundantly seen in the CMZ with the fold cores occupied by diapiric granitoids (Hopgood, 1968; Natarajan and Nanda, 1981). Detailed map pattern of the principal lithologies is very complex Generally, charnokites occupy the western, marginal part



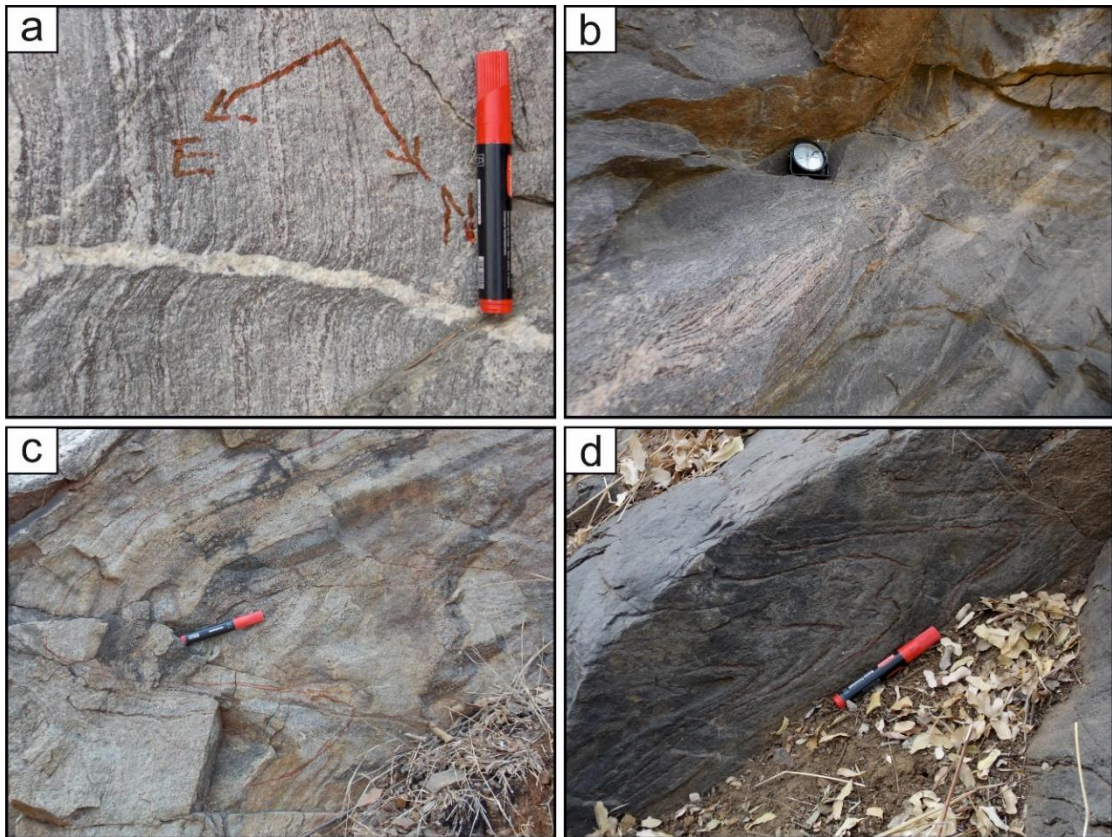


**Fig. 2.4: Field photographs showing (a), (b) Layering of dark and light colored mineral within the rocks and local scale shearing (c), (d) Small scale folds, with thick hinge and thinner limb. The limbs of the folds are refolded.**

of the belt, and khondalites and other pyroxene-free rocks occur predominantly to the east (Viswanathan, 1969). Sarkar et al. (1981) suggested that, the rocks have been affected by three phases of deformation. (a) D<sub>1</sub> deformation producing ENE-WSW to NE-SW trending isoclinal folds, (b) Cross – folding on north-south and N-S and NNW-SSE axes during D<sub>2</sub> deformation, and (c) D<sub>3</sub> deformation producing E-W trending gentle antiformal and synformal wraps. The D<sub>1</sub> and D<sub>2</sub> deformations produced penetrative planar structures, axial planar to the folds. Sarkar et al. (1981) suggested that the two earlier deformations were associated with high grade metamorphism and the D<sub>3</sub> deformation is correlatable with syntectonic emplacement of anorthosite, alkaline rocks and carbonatites. On contrary Bhattacharya et al., (1994) postulated that the first- and second-generation folds are reclined and coaxial while the third set is commonly open and upright fold.

The KPLC comprises of two oval bodies, which shows a NE- SW trend at the surface level. Two apparently separate outcrops of the same mafic intrusion are detached with a thin bridge of migmatitic terrain within a graben structure. The KPLC and the

associated rocks of the EGB display a NE-SW trending foliation dipping towards SE to NW (Fig. 2.3). The rocks of the study area were suffered polyphase deformation. Three subsequent episodes of deformation are being reported in the area. According to Dharma Rao et al. (2012), the initial folding ( $F_1$ ) developed tight to overturned reclined folds with NE-SW axial planes which forms the regional scale foliation. This is the most prevalent planar structure, a shallow dipping foliation ( $S_1$ ) axial planar to  $F_1$ . The emplacement of the enderbite–charnoenderbite also occurred along this planar structure (Sengupta et al., 1999). This is succeeded by the second phase of folding,  $F_2$ , which leads to the development of an N-S to NNW-SSE trending linear fabric. The anorthosites are emplaced along the antiformal structures of  $F_2$  folds and are thus genetically related to this phase of deformation. Small scale faults and shear zones are

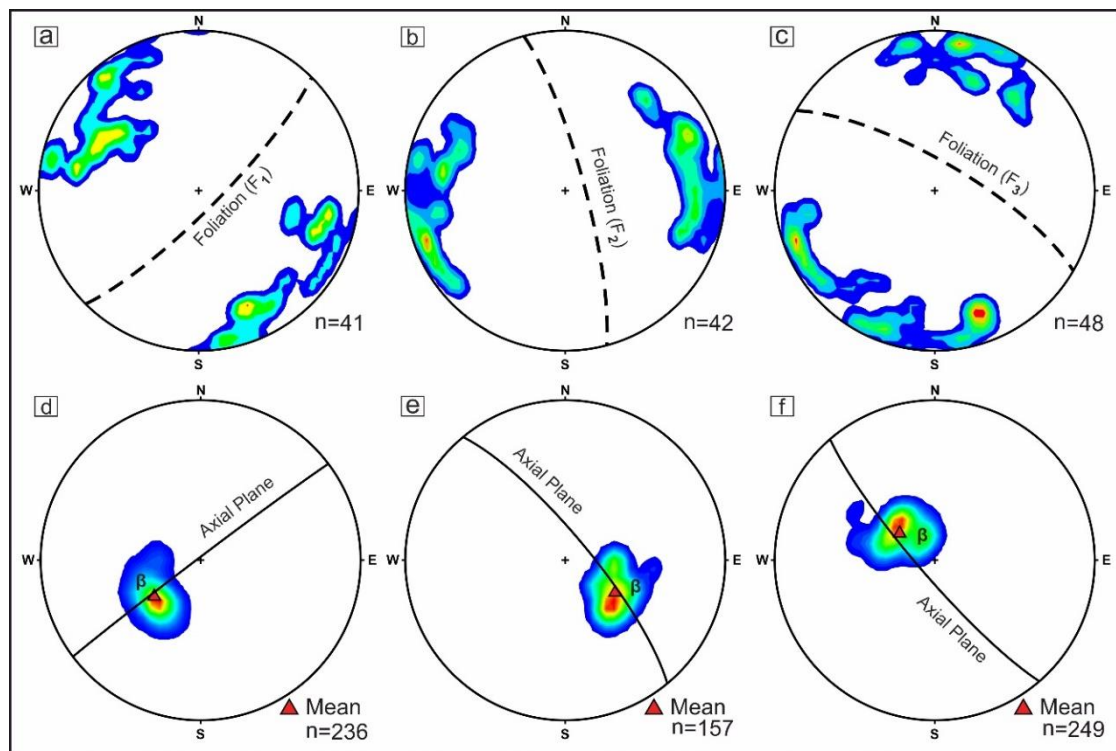


**Fig. 2.5: Mesoscopic fabrics (field data) in the KPLC. Fold axes and corresponding axial planes are averaged using the  $\beta$  pole.**

common along the hinges of the  $F_2$ . Post  $F_2$ , the  $F_3$  event is marked by open folding of the  $F_2$  limbs with WNW-ESE to E-W trending axial planes. Interference of these folds has resulted in a complex outcrop pattern in the layered rocks. The anorthosite (and gabbro) bodies trend variably from NE-SW to NNW-SSE. Color banding is quite common in the gabbro-anorthosite suite of rocks in the KPLC. However, the color

banding varies in scale with the location. The major structural elements that are reported in the KPLC from the present study are represented in lower hemisphere equal area diagrams in (Fig. 2.5). Finally, a set of roughly N–S trending subparallel shear zones (dip  $>70^\circ\text{E}$  to almost subvertical) have cut across all the rock types. The host rocks in the shear zones show extensive recrystallization and development of amphibole (Sengupta et al., 1999). These structural complexities introduce an element of ambiguity in establishing the magmatic stratigraphy of the KPLC (C. Leelanandam, 1997). The generalized succession of the Kondapalle area (Sengupta et al., 1999) as follows:

---

**YOUNG** Development of N–S ductile shear zones, fluid fluxing and formation of retrograde hydrous and carbonatic phases in all litho-units. Ar–Ar cooling age of hornblende  $\sim 1100$  Ma.

Emplacement of allanite-bearing granitic pegmatite. U–Pb cooling ages of allanite ( $\sim 1600$  Ma) and monazite (1672 Ma).

Emplacement of dolerite dyke.

F<sub>2</sub>–F<sub>4</sub> folding, emplacement of noritic dyke along F<sub>3</sub>.

Emplacement of pegmatoidal enderbite.

F<sub>1</sub> recumbent folding, emplacement of enderbite–charnoenderbite along the axial plane (S<sub>2</sub>).

Emplacement of basic magma, fractionation (ultramafic–basic-anorthosite) at 35–40 km depth, UHT metamorphism of the pelitic rocks, partial melting and segregation of leucosomes and melanosomes (S<sub>1</sub>).

**OLD** Deposition of supracrustal rocks (mainly pelites).

---

### 2.3. Geochronology and Tectonic Evolution

Geochronological study on the EGB was initiated in mid-sixties. Since then although considerable amount of information regarding age of rock has been gathered, but most of the generated data lack proper correlation with tectono-thermal, thermal, and tectonic perturbations in the history of the belt. The geochronological data from the EGB rocks show a wide spread (3100–500 Ma) in the Rb–Sr whole rock, Sm–Nd

isochron, and K-Ar biotite ages. Lal et al. (1987) pointed out that several episodes of metamorphism and magmatism can be identified from the age dating. Taking cognizance of acquired data, these can be recognized as:

(1) A metamorphism event at 3090 Ma from the Rb-Sr whole-rock age of a khondalite (Perraju et al., 1979).

(2) An event of felsic and basic magmatism at ~ 3000-2900 Ma from model Nd (TDM) age (Paul et al., 1990).

(3) A metamorphic event at 2600+100 Ma from Rb-Sr whole-rock age of a Khondalite (Vinogradov et al., 1964).

(4) A metamorphic and magmatic event in late Proterozoic [Rb-Sr age of 1400 Ma from anorthosite (Sarkar et al., 1981); Rb-Sr age of garnetiferous gneisses between 1370 and 1100 Ma (Perraju et al., 1979); Pb-Pb whole-rock isochron age for carbonatite and alkaline rocks (Clark and Subbarao, 1971); Rb-Sr whole-rock age of 1211 Ma for leptynite (Perraju et al., 1979); Pb-Pb ages between 1700 and 1000 Ma (Grew and Manton, 1986)].

(5) A metamorphic event between 600 and 450 Ma as indicated by the K-Ar biotite age (Aswathanarayan, U., 1964).

These above-mentioned episodes show that the EGB granulites witnessed four metamorphic events at ~3100 Ma, 2600+100 Ma, 1400-1000Ma and 600-450 Ma. And magmatic events occurred at ~3000-2900 Ma and ~1400-1200 Ma. Sarkar et al. (1981) correlated the D<sub>1</sub>, D<sub>2</sub> and D<sub>3</sub> deformations with the three earlier metamorphic events. The youngest metamorphic event has been correlated with the Indian Ocean orogenic cycle (Lal et al., 1987).

Recently Dasgupta (1995) postulated that EGB was metamorphosed under extreme P-T conditions (~950-1000°C and 8-9kb) with an anticlockwise P-T trajectory comprising a prograde path, followed by near isobaric cooling (IBC) and near isothermal decompression (ITD), with late hydration at lower temperature. Fe-Al granulites from Kondapalle suffered a UHT metamorphism (>1000°C) and deep crustal heating cooling trajectory (Sengupta et al., 1999). The emplacement of mafic-ultramafic suite of Kondapalle causes the UHT metamorphism. According to Bhui et al. (2007) the emplacement of charnoenderbites at ~1.7 Ga is younger than the high-

grade metamorphism. Also, Bose et al. (2011) interpreted U-Pb zircon ages of from Kondapalle to reflect an older UHT metamorphism (1.76 Ga). Recently, Dharma Rao et al. (2012) dated the age of emplacement of the KPLC at ~1.69-1.63 Ga and was inferred to be emplaced in a continental arc environment (Dharma Rao and Santosh, 2011; Vijaya Kumar et al., 2011).

The EGB appears to be a product of continent-continent collision, like Limpopo mobile belt of South Africa. After the evolution of Mesoproterozoic sedimentary basins, the rifting of the continental margin at ~1500 Ma saw the deposition of shelf sediments and the intrusion of alkaline rocks and some anorthosite massif at 1300 ~ 1400 Ma. Regional compression from the East, combined with strike slip movement caused the development of crustal – scale shear zones parallel to the regional NE trend. Intense deformation, granulite facies metamorphism and attendant migmatization at 1000 Ma marked the climax of the orogeny. Post-orogenic magmatism was marked by emplacement of granites and alkaline rocks at ~800 Ma. The geological setting and tectonic evolution of the belt appear to be matched with events in east Gondwana to provide the best fit with Antarctica and Srilanka.

The EGB was compared to a geosyncline or mobile belt, having miogeosyncline of Khondalite Group and eugeosyncline of charnockites and basic granulites, forming the oldest orogeny in peninsular India (Narayanaswamy 1966, Murthy et al., 1971). The belt was compared with “ensialic graben to proto-oceanic rift system” following Windley (1973) by Ray and Bose (1975), and as an ensialic rift – aulacogen association by Katz (1978). Subrahmanyam (1978) interpreted the belt as a Proterozoic cryptic suture like Grenville. Chetty and Murthy (1994) visualised EGB as a collisional belt, Sarkar (1994) views it in terms of a Wilson Cycle. The oldest activity was deposition of silty and shaley sediments (now khondalites), carbonates (now calc-silicates) and intercalated basalts (now mafic granulites). There was deposition of mafic volcano sedimentary sequence now occur as schist belts (Nellore, Khammam) along western edge. Granulite terrains across the world are, indeed, the windows on the deep crust. The composition and evolution of the deep crust and its interaction with mantle and upper crust provide us with fundamental knowledge about the formation and stabilization of continents. Although our understanding about the mechanism of granulite formation, physical conditions of metamorphism, role and source of fluids has

been improved quite a lot during the last two decades (Harley, 1989; Vielzeuf and Vidal, 1990; Newton, 1987; Santosh et al., 1990, 1991).

The KPLC represents typical 'layered-type' anorthosite complex (Nanda and Natarajan, 1980; Dharma Rao et al., 2004). A whole-rock Sm–Nd isochron age of  $1739 \pm 220$  Ma has been reported from the Pangidi anorthosite (Dharma Rao et al., 2004). On the other hand, mean  $^{207}\text{Pb}/^{206}\text{Pb}$  ages of  $1634 \pm 18$  Ma has been reported for the anorthosite from Pangidi (Dharma Rao, 2011). The mean  $^{207}\text{Pb}/^{206}\text{Pb}$  ages of anorthosite from Kondapalle are  $1628 \pm 36$  Ma and  $1639 \pm 110$  Ma (Dharma Rao et al., 2004). The age and emplacement histories of magmatic complexes in the EGB suggested that the Krishna province is a dominantly Mesoproterozoic terrane and preserves evidence for a major crustal growth event during this time. Sarkar et al. (2015) obtained U–Pb ages of Zircon 1750 Ma widespread magmatic activity in Ongole domain. In KPLC allanite and monazite from the pegmatite have yielded U–Pb cooling ages of  $1672 \pm 4$  Ma (monazite) and  $\sim 1600$  Ma (allanite), and the  $^{40}\text{Ar}$ – $^{39}\text{Ar}$  age of a retrograde hornblende from the shear zone is  $\sim 1100$  Ma (Mezger et al., 1996; Mezger and Cosca, 1999). The field features and these mineral age data, thus, collectively indicate the high-grade metamorphism of khondalites is older than 1640 Ma (Sengupta et al., 1999). This is the first unequivocal documentation of pre-Grenvillian granulite facies metamorphism in the EGB. The  $\sim 1100$  Ma  $^{40}\text{Ar}$ – $^{39}\text{Ar}$  amphibole age documents a localized Grenvillian thermal overprint (up to amphibolite facies). The U–Pb cooling ages of allanite and monazite further suggest that the Grenvillian granulite facies metamorphism, which is pervasive in the northern sector (Grew and Manton, 1986; Aftalion et al., 1988; Paul et al., 1990; Mezger et al., 1996), is absent in the study area (Sengupta et al., 1999).

Krishna province is a dominantly Mesoproterozoic terrane and preserves evidence for a major crustal growth event during that time. A prominent tectono-magmatic event, reflecting mantle- and crustal-derived magma addition in Krishna Province, is placed around 1.75 Ga (Kovach et al., 2001). The KPLC reflects the 1.85–1.7 Ga subduction related magmatism as represented in the EGB, which is correlated with the accretion of the napier complex to proto-India, attending the formation of Columbia (Dobmeier and Raith, 2003). There are many geodynamic models related to the formation of Ongole domain of southern EGB. According to Dharma Rao et al.

(2011) generation of the subduction related arc magmas of KPLC at ~1.6 Ga (Dharma Rao et al., 2012) due to a Paleo-Mesoproterozoic (1.85-1.33 Ga) long-lived active continental margin along the southeastern margin of India, which terminate in continental collision with the Napier Complex of East Antarctica in the Neoproterozoic (~1.0 Ga) related to the amalgamation of the supercontinent Rodinia.

## 2.4. Sampling Process and Sample Preparation

Rock magnetic, palaeomagnetic and anisotropy of magnetic susceptibility studies require oriented core samples (2.54 cm x 2.20 cm). Such oriented core samples were prepared (by core drilling machines) from oriented block samples. The Comprehensive oriented blocks were collected from different rock types from the Kondapalle and Pangidi area for rock magnetic, palaeomagnetic and anisotropy of magnetic susceptibility studies. The oriented block samples were collected from the different sites from studied area as shown in the Fig. 2.3. Oriented block samples were collected from the different rock types under study on ease of accessibility.

Relatively fresh samples were oriented with the help of Brunton compass and were also marked before removing from the in-situ outcrops. The samples were oriented in in-situ condition by marking parallel horizontal lines on two adjacent side walls of the rock by Brunton compass and demarcating the geographical north direction on the top surface (Fig. 2.6). Another process of block samples orientation is used when there is no adjacent vertical wall. Then, the attitude of the top surface of

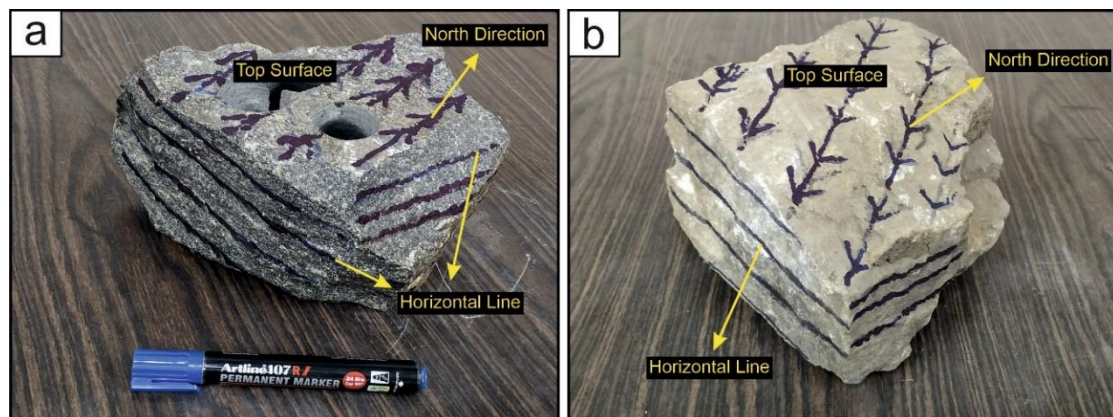
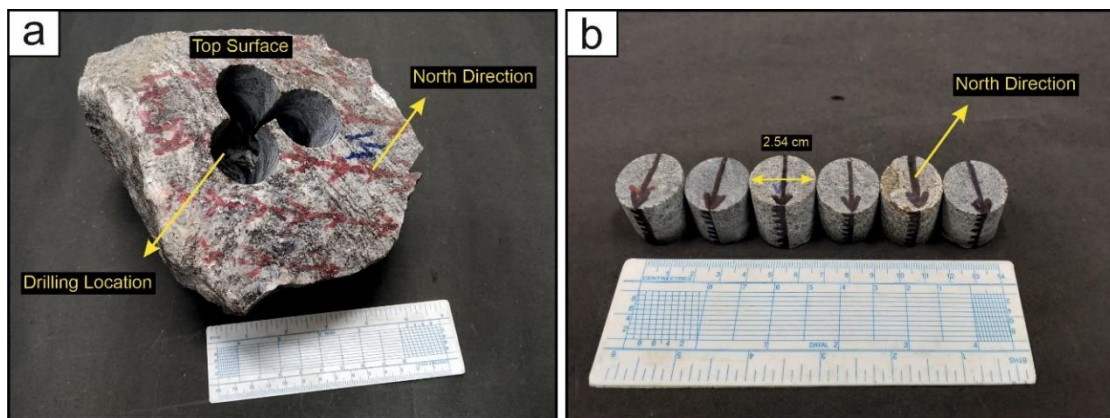


Fig. 2.6: Orientation processes to collect the oriented block samples.

the in-situ sample was measured and noted. Both the processes were followed in the present study for the collection of the oriented block samples.

During field work, samples were collected from all variety of rock types observed within the field. For petrographic studies and studies related to the generation of the Fe-Ti oxides, polished thin sections were prepared from small chips extracted from the oriented block samples. Besides, powdered rock samples were prepared for the measurement of rock magnetic parameters. These samples were prepared at the Sample preparation laboratory of the Department of Geological Sciences, Jadavpur University, Kolkata.

For palaeomagnetic, rock magnetic and anisotropy of magnetic susceptibility studies, the oriented samples were drilled to 6-8 numbers of cores from each block (with a dimension of 2.54 cm in diameter and 2.2 cm in height) by vertical core drilling on the top surface of the samples such that the north marking on the top is preserved for marking the North direction on the top of each core samples (Fig. 2.7). Then the core samples were marked and oriented with heat proof marker. This marking further helps in setting the core to different orientation in various geophysical instruments. The samples were drilled at the Department of Geological Sciences, Jadavpur University, India with non-magnetic diamond drilling bit.



**Fig. 2.7:** (a) Oriented sample being vertically drilled at suitable locations to extract cylindrical cores leaving out hollow spaces. (b) Oriented core samples of precise dimension.



**Chapter 3**  
**Petrography**

## **PETROGRAPHY**

### **3.1. Introduction**

Debates and uncertainty prevail regarding the metamorphism of the rocks of the EGB. According to Sen et al. (1995), the rocks have several stages of decompression and cooling starting from a temperature of about 1100°C and >10 Kbar pressure, however, reviews of Dasgupta and Sengupta (2003) finds such an explanation was not a viable one from that particular study and also from later works. The study area is mainly dominated by several magmatic rocks including the gabbro-norite, pyroxenite, anorthosite layered complex and later enderbite to charno-enderbite intrusives. The mafic-ultramafic layered complex consists predominantly of gabbro-norite, which, at places, grades into leuco-gabbro-norite to anorthosite (Nanda and Natarajan, 1980; Dharma Rao et al., 2004). These rocks show banding, with accessory garnet at places. The basic and ultrabasic rocks are restricted to inter banded occurrences.

Most of the study area consists of orthopyroxene granulite, with lesser occurrences of mafic granulite, khondalite, leptynite, enderbite and anorthosite. Mafic granulites occur not only as distinct litho-unit, but also as pockets or lenses of varying dimension within orthopyroxene granulite and khondalite. Khondalite co-existing with leptynite occurs as lensoid body within orthopyroxene granulite.

Microscopic studies of the rocks from the area under study have revealed that the occurrences of orthopyroxene granulite, mafic granulite, khondalite, leptynite, enderbite and anorthosite. This study involved careful identification of both mineral assemblages and textural associations of silicate minerals and opaque oxides. Thin-polished sections of the rock samples from KPLC have been prepared and studied under microscope with transmitted light set up.

### **3.2. Mineral Assemblages**

The major litho-units of studied area are orthopyroxene granulite, mafic granulite, Khondalite, leptynite, enderbite and anorthosite. Mineral assemblages and

textural association of different litho-units in and around KPLC are described as follows:

### Orthopyroxene Granulite:

The orthopyroxene granulite of the studied area is coarse grained mesocratic rock. Microscopically it contains orthopyroxene, plagioclase, k-feldspar, quartz, garnet and opaque minerals. It shows crude to well-foliated gneissic band where gneissosity is defined by alternate banding of quartzo-feldspathic and ferromagnesian phases (Fig. 3.1a, Fig. 3.1b).

The orthopyroxenes are mainly occurred as porphyroblasts. It contains inclusions of biotite, plagioclase and quartz (Fig. 3.1c, Fig. 3.1d). It shows sharp

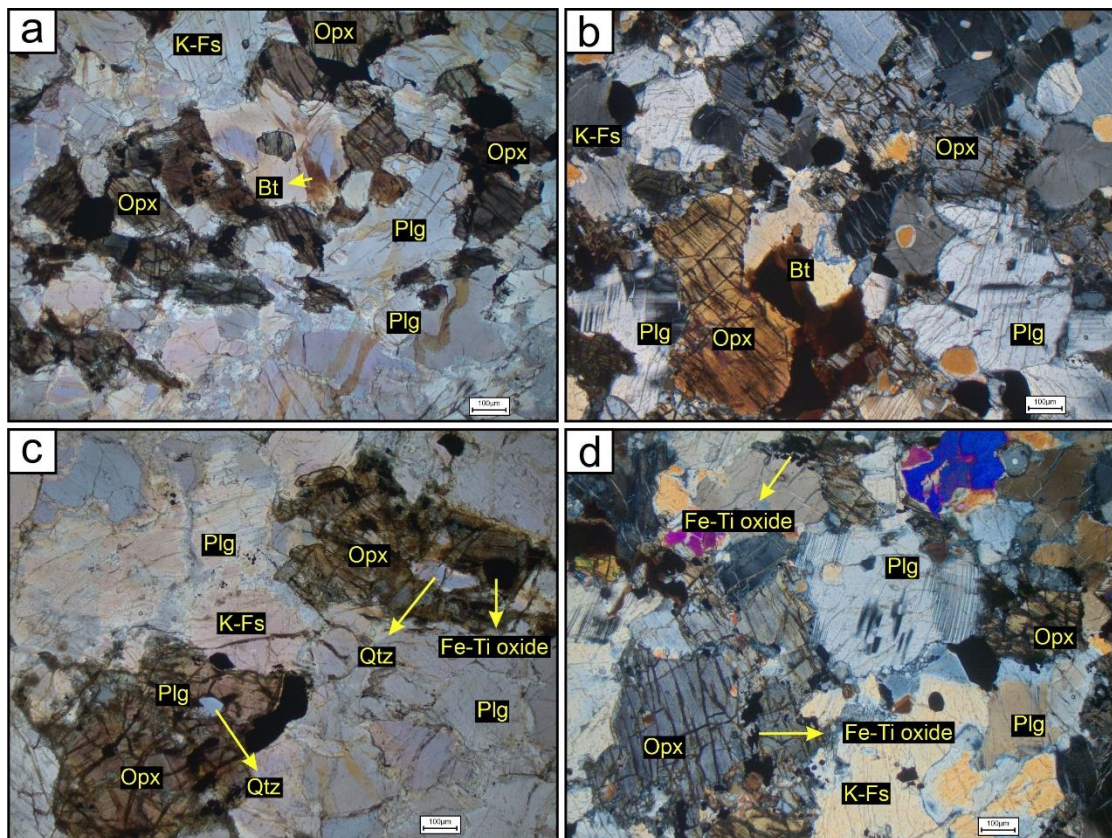


**Fig. 3.1:** (a) and (b) Orthopyroxene granulite displaying granoblastic texture defined by orthopyroxene, plagioclase, k-feldspar with minor biotite and opaque (PPL, XPL). (c) and (d) Inclusion of quartz, biotite and opaque within orthopyroxene grains (PPL, XPL).

boundary with k-feldspar. Orthopyroxenes are separated from the plagioclase porphyroblasts and opaque by the development of coronal garnet (Fig. 3.2a, Fig. 3.2b). At places opaque (magnetite) minerals are present along the cleavages of orthopyroxene

(Fig. 3.1b). In high strain zone, grains of orthopyroxene show varying degrees of deformation and recrystallisation into small strain free grains.

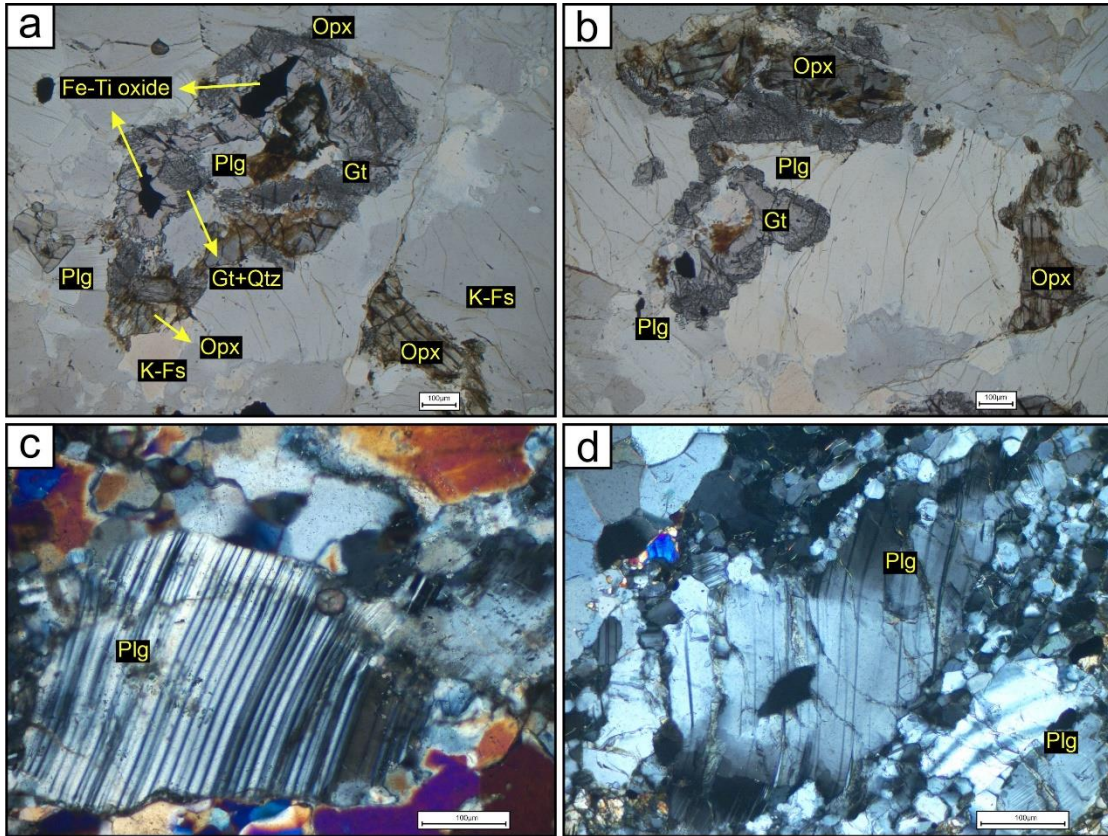


**Fig. 3.2:** (a) and (b) Coronal garnet developed between Plagioclase-opaque, plagioclase orthopyroxene, orthopyroxene-opaque grain boundary. The coronal garnets are mainly garnet -quartz symplectite (PPL). (c) and (d) Bent twin lamellae within the plagioclase porphyroblasts. It is also noted that strain free recrystallized grains are present along the grain boundary (XPL).

The plagioclase shows lamellar twinning and occurs in three modes. One is subhedral to anhedral porphyroblastic plagioclase. Porphyroblastic plagioclase is separated from the orthopyroxene and magnetite by the coronal garnet or garnet-quartz symplectite (Fig. 3.2a, Fig. 3.2b). In the zone of intense deformation, porphyroblasts shows bent twin lamellae (Fig. 3.2c, Fig. 3.2d) and wedge-shaped twin lamellae (Fig. 3.3a, Fig. 3.3b). These grains are often surrounded by recrystallized small strain free grains (Fig. 3.2d). In myrmekite, worm like inter growth of plagioclase and quartz is found to replace porphyroblastic k-feldspar along the periphery (Fig. 3.3c, Fig. 3.3d). Besides these textural varieties, plagioclase also found as lamellae within large K-feldspar grains to form perthite (Fig. 3.4a).

The k-feldspars are subhedral to anhedral in shape. K-feldspar is of orthoclase

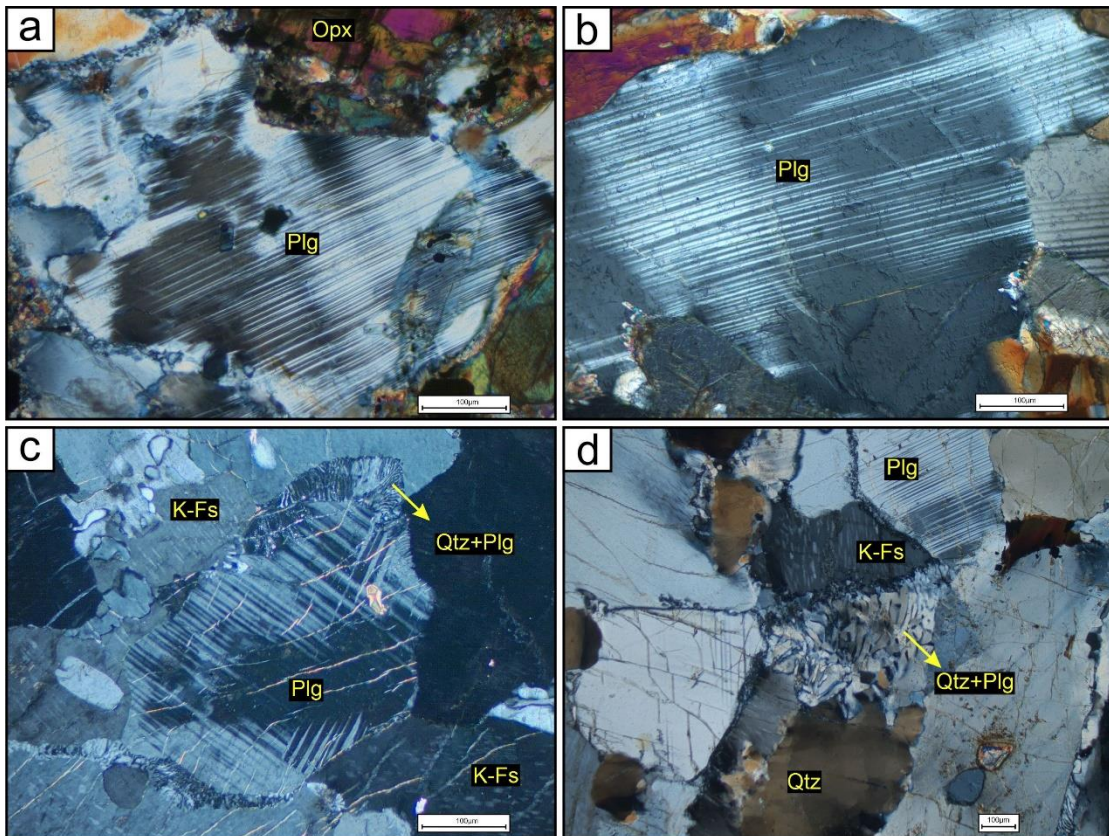


**Fig. 3.3:** (a) Plagioclase porphyroblasts show wedge-shaped bent twin lamellae (XPL). (b) Plagioclase porphyroblasts show wedge-shaped twin lamellae (XPL). (c) and (d) Myrmekite replacing the periphery of k-feldspar (XPL).

and microcline variety. Microcline exhibits a combination of both albite and pericline twinning (Fig. 3.4b). Most of the k-feldspars show perthitic texture (Fig. 3.4a). K-feldspar also occur as anti-perthite, crystallographically intergrown in the plagioclase host (Fig. 3.5a). Perthite probably resulted from un-mixing of k-feldspar with small

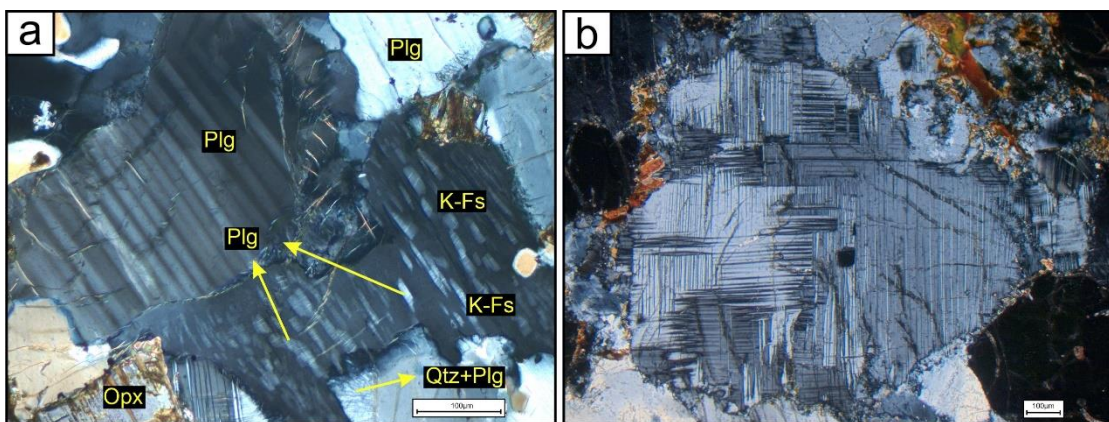


**Fig. 3.4:** (a) K-feldspar shows perthitic texture as an intergrowth of plagioclase within it. It is also noted that myrmekite replaces the k-feldspar at the periphery (XPL). (b) Microcline shows pericline twinning (XPL).

portion of plagioclase feldspar at low temperature. On the other hand, presence of anti-perthite indicates high temperature of magma consolidation (Tilley, 1936).

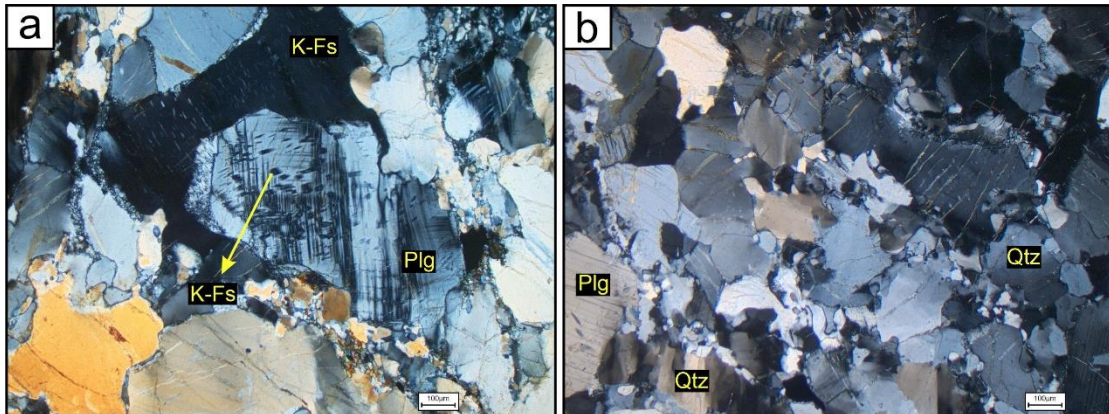


**Fig. 3.5:** (a) Plagioclase shows anti-perthitic texture as an intergrowth of k-feldspar within it. It is also noted that the twin lamellae of the grain are bent (XPL). (b) Elongated quartz grains show preferred orientation and shows undulose extinction (XPL).

Quartz shows a wide range of grain size. Some quartz grains are elongated and show preferred orientation in the high strain zones (Figur 3.5b). There are inclusions of quartz within garnet (Fig. 3.6a). Symplectic growth of quartz with garnet, plagioclase (myrmekite) and biotite are also observed. In biotite-quartz intergrowth, the grain size of quartz varies widely (Fig. 3.7b).

Garnet occurs in two modes in the studied rocks. (a) Porphyroblastic garnet and (b) Coronal garnet. Porphyroblastic garnet is polygonal and enclose inclusions of quartz, plagioclase, biotite and magnetite (Fig. 3.6a, Fig. 3.7a). These garnets show

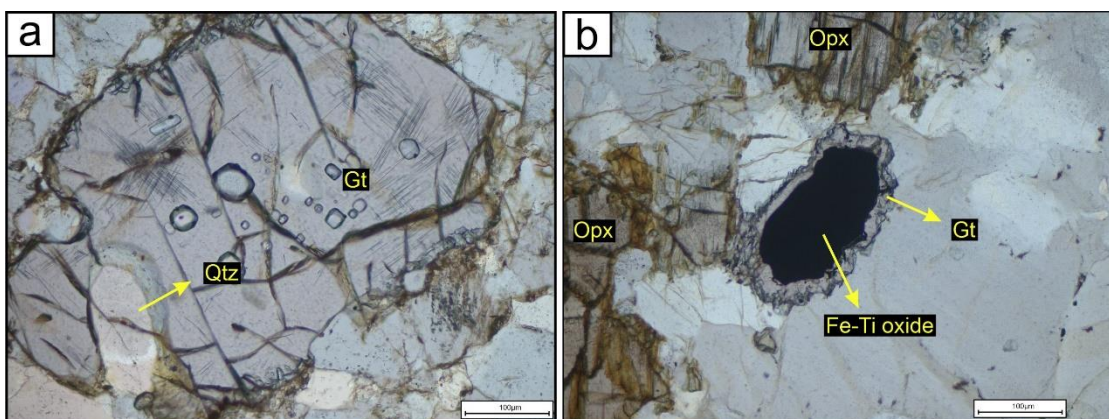


**Fig. 3.6:** (a) Inclusion of quartz within porphyroblastic garnet (PPL). (b) Coronal garnet rimming around opaque minerals (PPL).

mutual boundary with porphyroblastic orthopyroxene and k-feldspar. Coronal garnet is frequent and found to occur along the periphery of orthopyroxene, plagioclase and porphyroblastic magnetite and ilmenite (Fig. 3.2a, Fig. 3.2b, Fig. 3.6b). In many cases, coronal garnet is symplectic, containing thread like intergrowth of quartz and second-generation ilmenite (Fig. 3.2a, Fig. 3.2b).

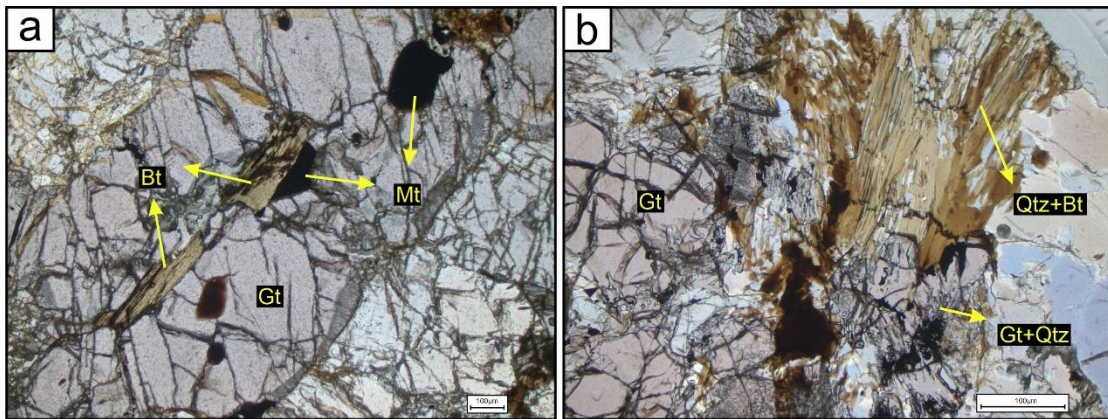


**Fig. 3.7:** (a) Inclusion of magnetite and biotite within porphyroblastic garnet (PPL). (b) Quartz-biotite-garnet symplectite (PPL).

Biotite occurs in two modes. One as inclusion within orthopyroxene, garnet and k-feldspar probably it of prograde type (Fig. 3.1b, Fig. 3.7a). Another is associated with k-feldspar magnetite, garnet and orthopyroxene. Biotite-quartz symplectite, probably it of retrograde type (Fig. 3.7b).

### **Mafic Granulite:**

The mafic granulites of the studied area are mesocratic, medium to fine grained rock. Microscopically it contains orthopyroxene, clinopyroxene, plagioclase, k-feldspar, quartz, garnet, opaque and biotite (Fig. 3.8a). The occurrence of garnet is sporadic in the rock.

The orthopyroxene is subhedral and occur as porphyroblast. The grains of orthopyroxene are hosted into quartzo-feldspathic matrix with no preferred orientation. In majority, there is a sharp contact with magnetite (Fig. 3.8b). Porphyroblastic orthopyroxene contain inclusions of magnetite and quartz (Fig. 3.8c). The clinopyroxene occurs in two modes, porphyroblastic clinopyroxene and symplectic clinopyroxene. Subhedral porphyroblastic clinopyroxene often contain inclusion of opaque and quartz (Fig. 3.8d). Symplectic clinopyroxene is associated with coronal

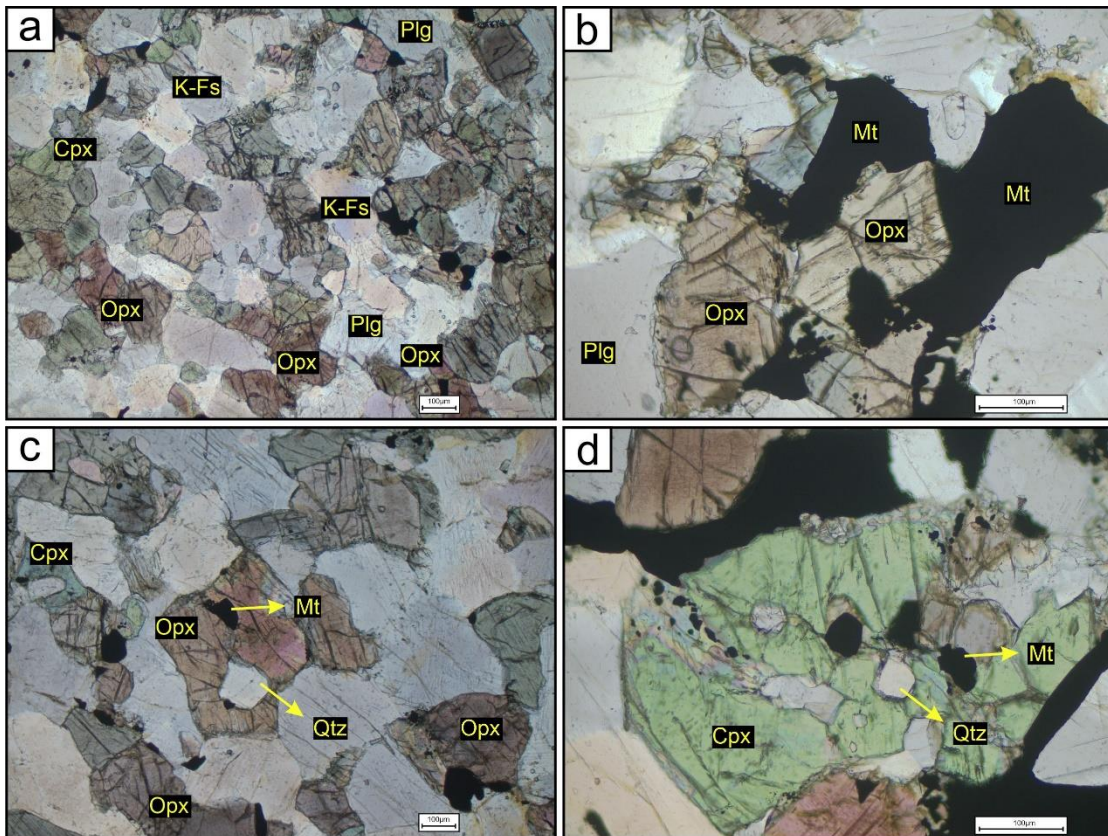


**Fig. 3.8:** (a) Mafic granulite consisting of orthopyroxene, clinopyroxene, feldspar, quartz and opaque (PPL). (b) Sharp contact between orthopyroxene and opaque (PPL). (c) Inclusion of opaque and quartz within orthopyroxene porphyroblasts (PPL). (d) Clinopyroxene porphyroblasts contain inclusions of opaque and quartz. (PPL).

garnet, quartz and opaque and rimming the porphyroblasts of orthopyroxene, plagioclase and clinopyroxene (Fig. 3.9a).

The plagioclase occurs in three modes. First one is subhedral to anhedral porphyroblastic plagioclase, which is separated from the orthopyroxene and magnetite

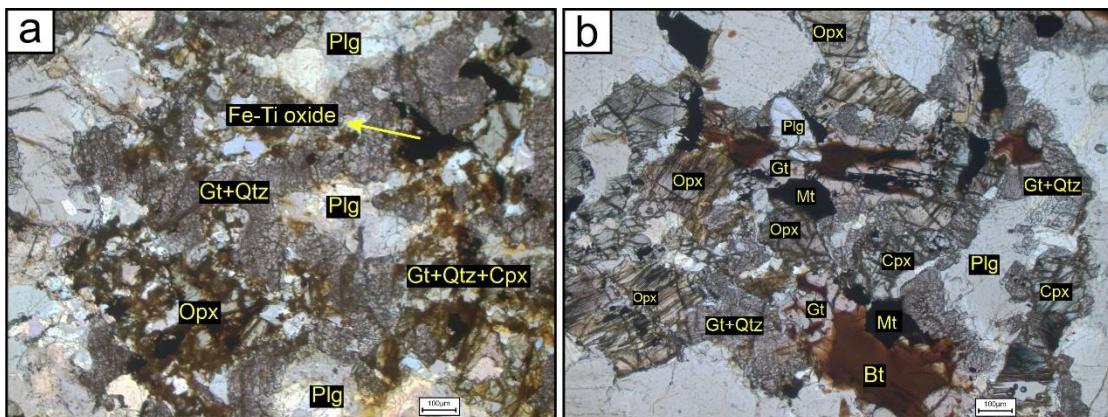


**Fig. 3.9:** (a) Symplectitic overgrowth of quartz-garnet-clinopyroxene-opaque rimming orthopyroxene, plagioclase and opaque (PPL). (b) Coronal garnet developed between Plagioclase-opaque, plagioclase orthopyroxene, orthopyroxene-opaque grain boundary. The coronal garnets are mainly garnet-quartz symplectite (PPL).



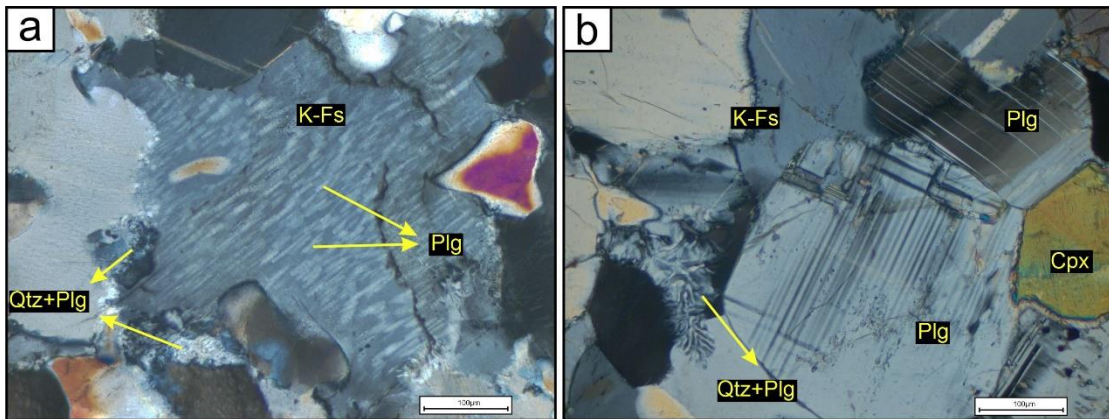


**Fig. 3.10:** (a) K-feldspar shows perthitic texture as an intergrowth of plagioclase within it (XPL). (b) Myrmekite replacing the periphery of k-feldspar (XPL).

by coronal garnet (Fig. 3.9b). Second one as intergrowth within k-feldspar in the form of perthite (Fig. 3.10a). And the last one is worm like inter growth of plagioclase and quartz in the form of myrmekite (Fig. 3.10b). Intergrowth of k-feldspar enclosed in plagioclase host in the form of aniperthite is also seen (Fig. 3.11a).

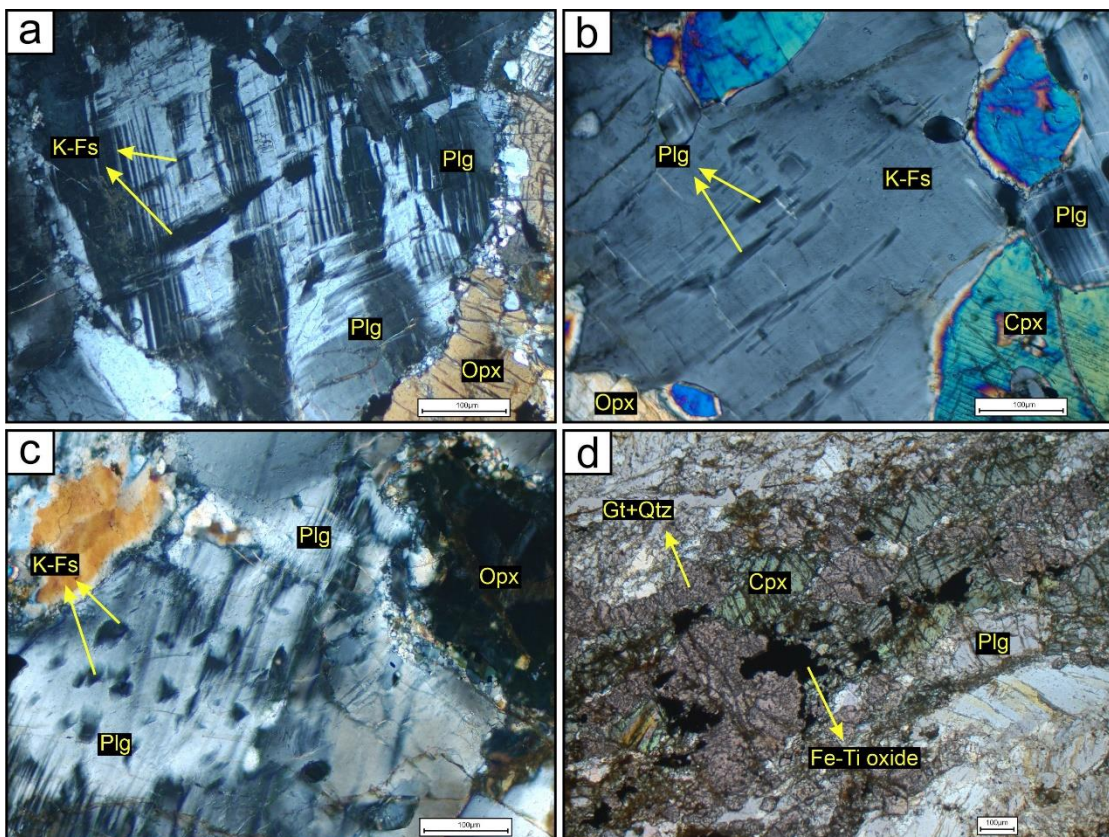


**Fig. 3.11:** (a) Plagioclase shows anti-perthitic texture as an intergrowth of k-feldspar within it (XPL). (b) K-feldspar shows perthitic texture as an intergrowth of plagioclase within it (XPL). (c) Plagioclase shows anti-perthitic texture as an intergrowth of k-feldspar within it. It is also noted that the twin lamellae of the grain are bent (XPL). (d) Coronal garnet (garnet-quartz symplectite) rimming around clinopyroxene, opaque and plagioclase (PPL).

The subhedral to anhedral k-feldspars shows perthitic texture with plagioclase intergrowth (Fig. 3.10a, Fig 3.11b). Another mode of occurrence of k-feldspar is as antiperthite (Fig. 3.11c). Abundance of antiperthite within these rocks indicates high temperature of magma consolidation (Tilley, 1936).

Quartz grains are fine to medium sized subhedral to anhedral in shape. Quartz also occurs as inclusion within garnet and orthopyroxene (Fig. 3.8c). Symplectic growth of quartz with garnet is also observed (Fig. 3.11d). Quartz shows polygonization in certain domain (Fig. 3.12a). Quartz also occurs in myrmekite (Fig. 3.12b).

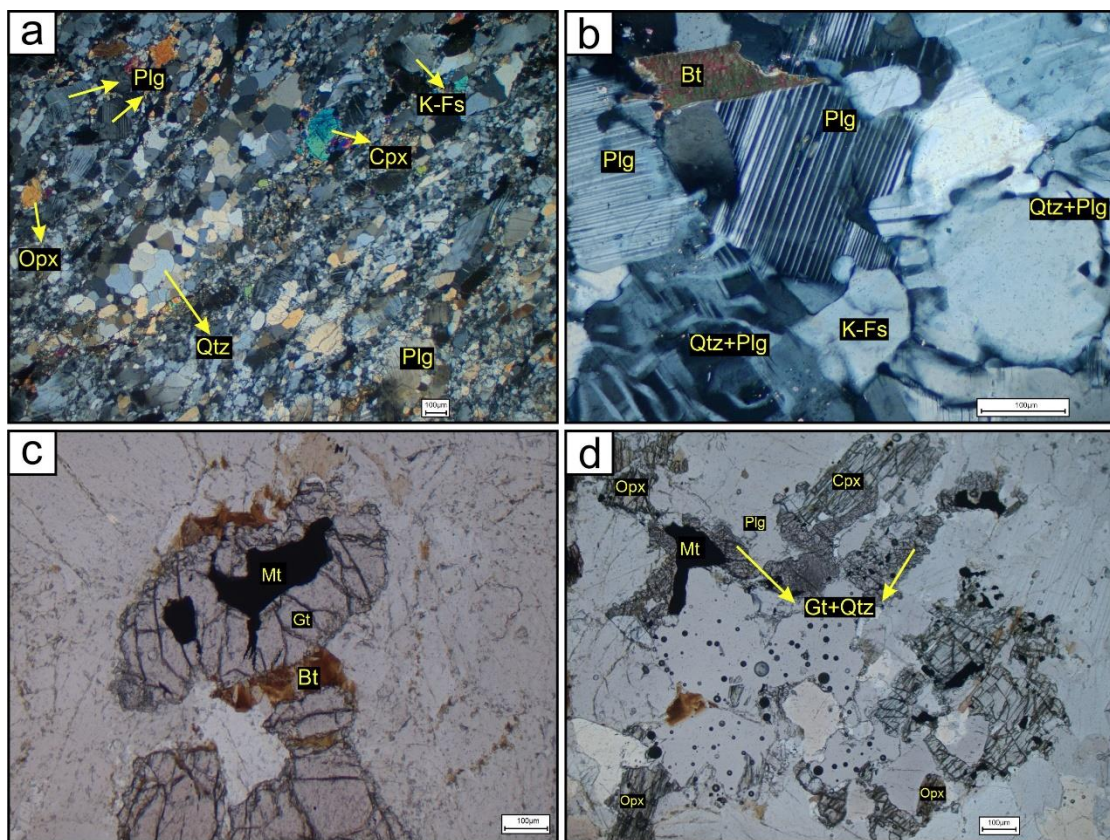


**Fig. 3.12:** (a) Polygonization of quartz grains (XPL). (b) Myrmekite replacing the periphery of k-feldspar (XPL). (c) Garnet rimming around large opaque grain (PPL). (d) Coronal garnet (quartz-garnet symplectite) rimming around orthopyroxene, clinopyroxene, plagioclase and opaque (PPL).

The garnet mainly occurs as corona in the mafic granulite. Coronal garnet rimming both the orthopyroxene and opaque oxide (Fig. 3.1ca, Fig. 3.12d). Coronal garnet also found to occur along the periphery of clinopyroxene and quartz (Fig. 3.13a, Fig. 3.13b). The garnet coronas contain fine grained inclusion of clinopyroxene, biotite and opaque (Fig. 3.13a). Such coronal garnet is symplectite in many cases.

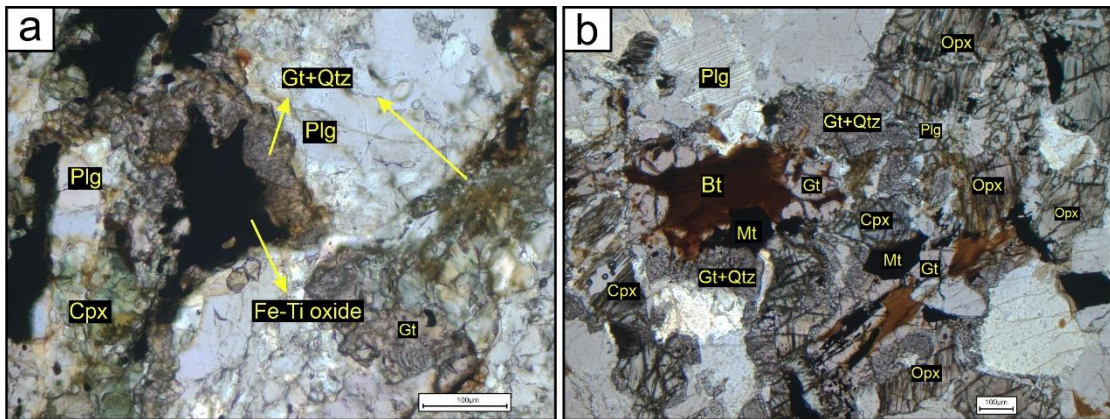


**Fig. 3.13:** (a) Garnet (quartz-garnet-clinopyroxene-biotite-opaque symplectite) rimming around opaque grain (PPL). (b) Coronal garnet developed between Plagioclase-opaque, plagioclase orthopyroxene, orthopyroxene-opaque grain boundary. The coronal garnets are mainly garnet-quartz symplectite (PPL).

### Khondalite:

Khondalite is leucocratic, medium to coarse grained rock. Microscopically it contains quartz, feldspar, garnet and aluminosilicates (Fig. 3.14a). A strong gneissosity in khondalite is observed which is defined by Garnet and sillimanite rich bands alternate with quartz-feldspar rich bands (Fig. 3.14b).

Garnet is anhedral to subhedral porphyroblastic with inclusion of quartz, sillimanite and biotite (Fig. 3.15a). Colourless sillimanite occurs as stumpy lath shaped grains having textural equilibration with garnet (Fig. 3.14b, Fig. 3.15b).

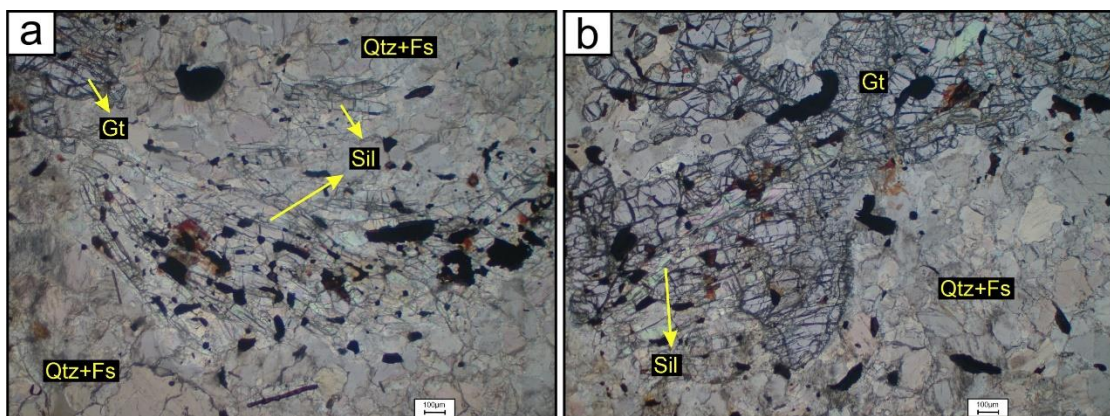


**Fig. 3.14:** (a) Khondalite consisting quartz, plagioclase, garnet, sillimanite, biotite and opaque (PPL). (b) Gneissosity defined by garnet-sillimanite rich band alternate with quartz-feldspathic band (PPL).

K-feldspar is subhedral medium to coarse grained. Medium grained variety of quartz occurs in the groundmass whereas the fine-grained variety occurs as inclusion

within garnet (Fig. 3.16a). Medium grained quartz shows the imprints of deformation in the form of undulose extinction (Fig. 3.16b).

Biotites are mostly of secondary origin and occur as patches around the margin and along the fractures of garnet grain (Fig. 3.14b). However, some prograde biotites are also present as inclusion within garnet (Fig. 3.16a).

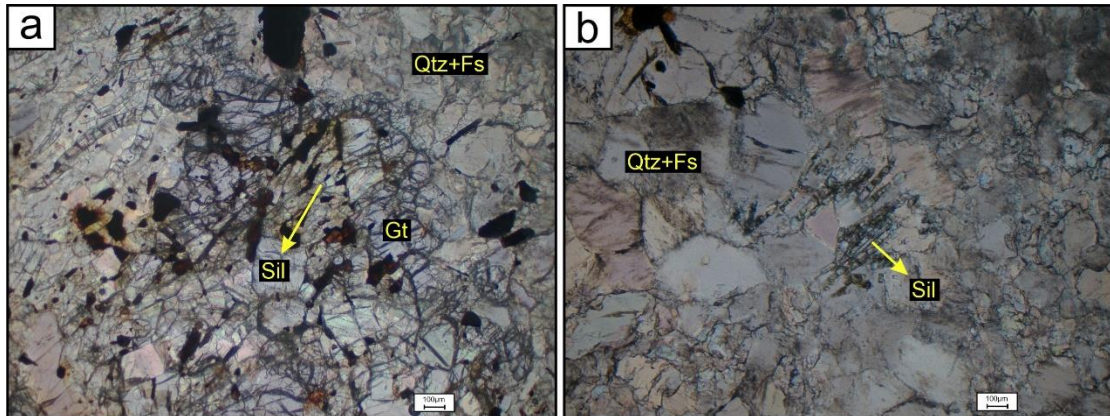


Fig. 3.15: (c) Garnet porphyroblast contain inclusion of quartz sillimanite and biotite. Biotite also occurs along fracture of the garnet grain (PPL). (d) stumpy lath shaped sillimanite grains (PPL).

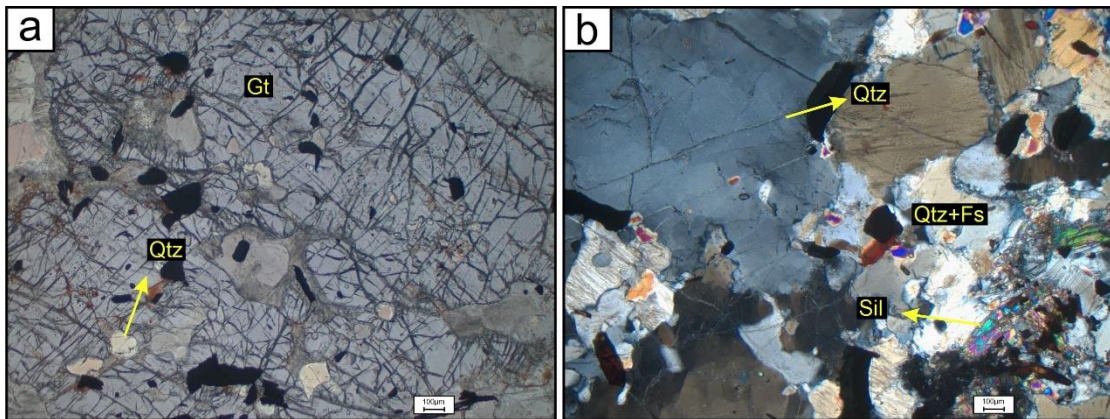
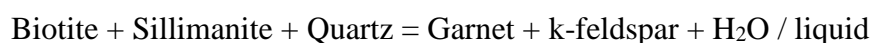


Fig. 3.16: (a) Inclusion of quartz, magnetite and biotite within porphyroblastic garnet (PPL). (b) Quartz shows undulose extinction (XPL).

Textural relation such as inclusion of biotite, sillimanite and quartz in the porphyroblastic garnet together with equilibrium relation between k-feldspar and garnet suggest following dehydration / melting reaction:



**Leptynite:**

Leptynite of the studied area is leucocratic, fine to medium grained rock. Microscopically it contains quartzo-feldspathic material (dominantly k-feldspar, quartz and plagioclase) along with garnet and biotite (Fig. 3.17a). In thin section, the gneissic fabric is evident from the parallel to subparallel alternate bands of quartzo-feldspathic bands and garnet-biotite bands (Fig. 3.17b).

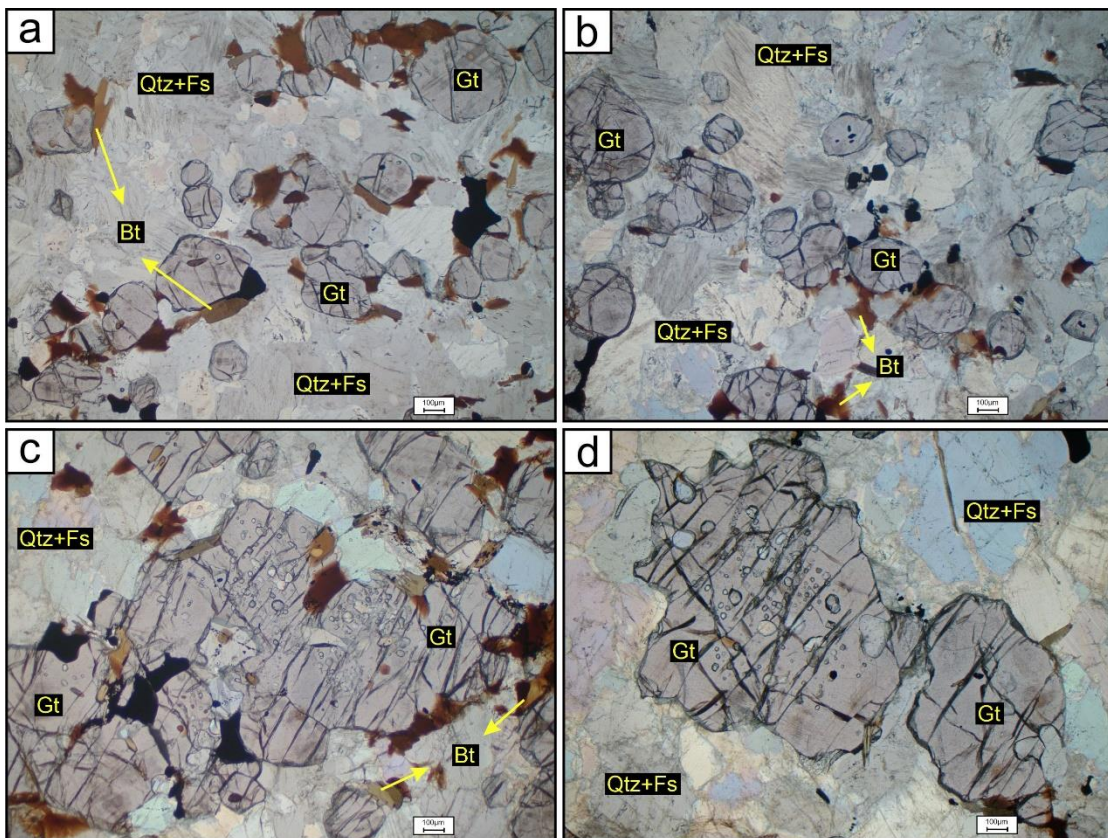


**Fig. 3.17:** (a) Leptynite consists of feldspar, quartz, garnet, biotite and opaque (PPL) (b) Gneissosity defined by garnet-biotite rich band alternate with quartzo-feldspathic band (PPL). (c) and (d) Inclusion of quartz, biotite and opaque within garnet porphyroblasts (PPL).

Large garnet grains typically show inclusion of quartz, biotite and opaque (Fig. 3.17c, Fig 3.17d). Secondary coronal garnet is found to rim around Fe-Ti oxide (Fig. 3.18a). Most of the cases these coronal garnets are symplectic with quartz (Fig. 3.18a, Fig. 3.18b).

The plagioclase grains exhibit myrmekitic texture (Fig. 3.18c). Most of the plagioclase grains shows anti-perthitic texture with exsolved k-feldspar (Fig. 3.18d). Bend twin lamellae, wedge-shaped lamellae within plagioclase grains are common

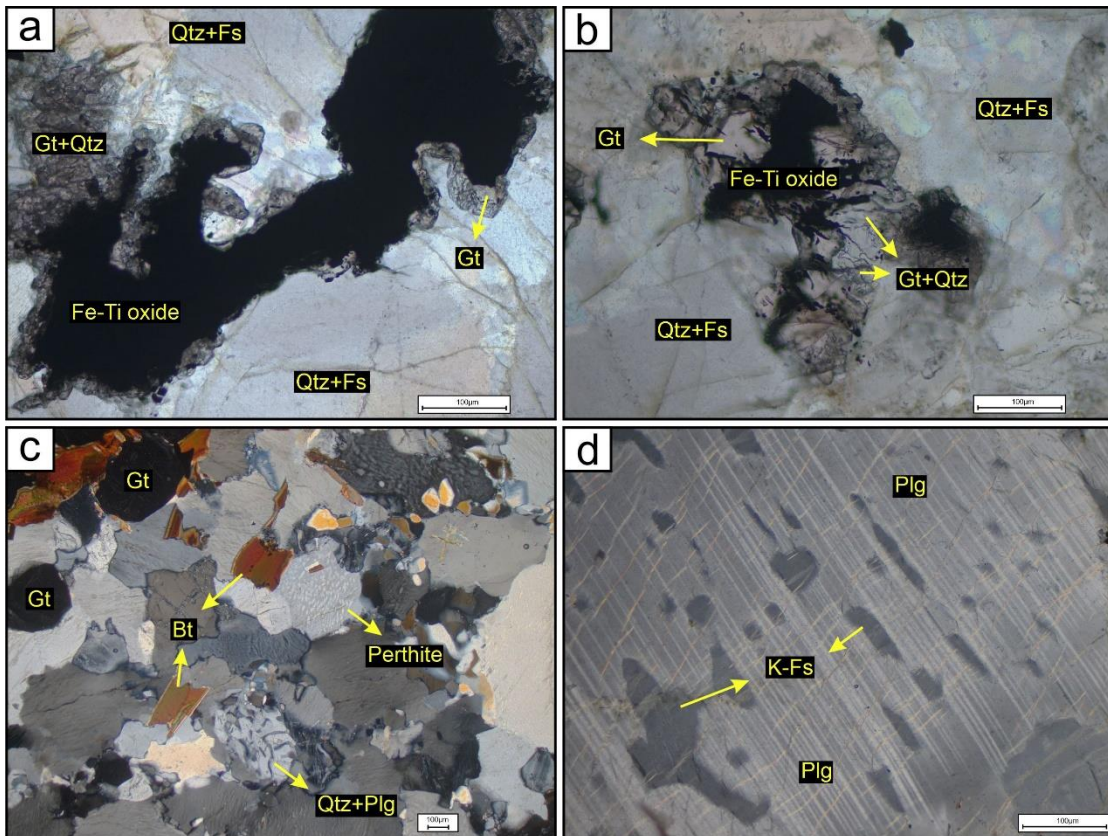


**Fig. 3.18:** (a) and (b) Coronal garnet (garnet-quartz symplectite) rimmed around Fe-Ti oxide (PPL). (c) Myrmekite replacing the periphery of k-feldspar (XPL). (d) Plagioclase shows anti-perthitic texture as an intergrowth of k-feldspar within it (XPL).

(Fig. 3.19, Fig. 3.20). K-feldspars show perthitic texture with exsolved lamellae of plagioclase (Fig. 3.21a).

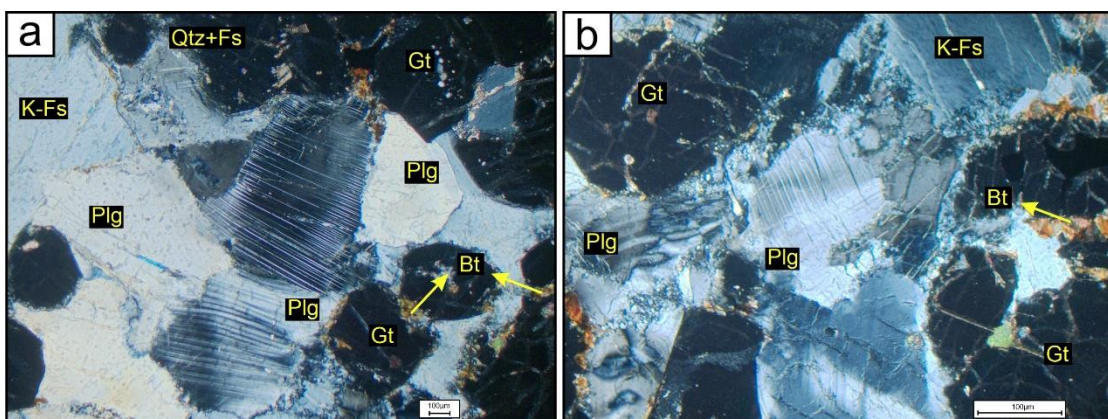


**Fig. 3.19:** (a) Plagioclase porphyroblasts show bent twin lamellae (XPL). (b) Plagioclase porphyroblasts show deformed twin lamellae. It is also noted that the plagioclase porphyroblast recrystallizes along the periphery (XPL).

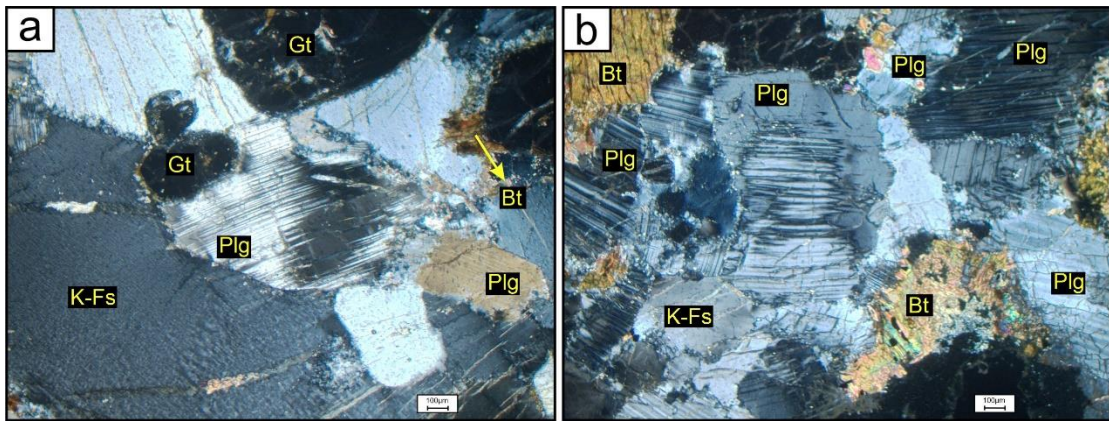


Fig. 3.20: (a) and (b) Plagioclase porphyroblasts shows wedge-shaped twin lamellae (XPL).

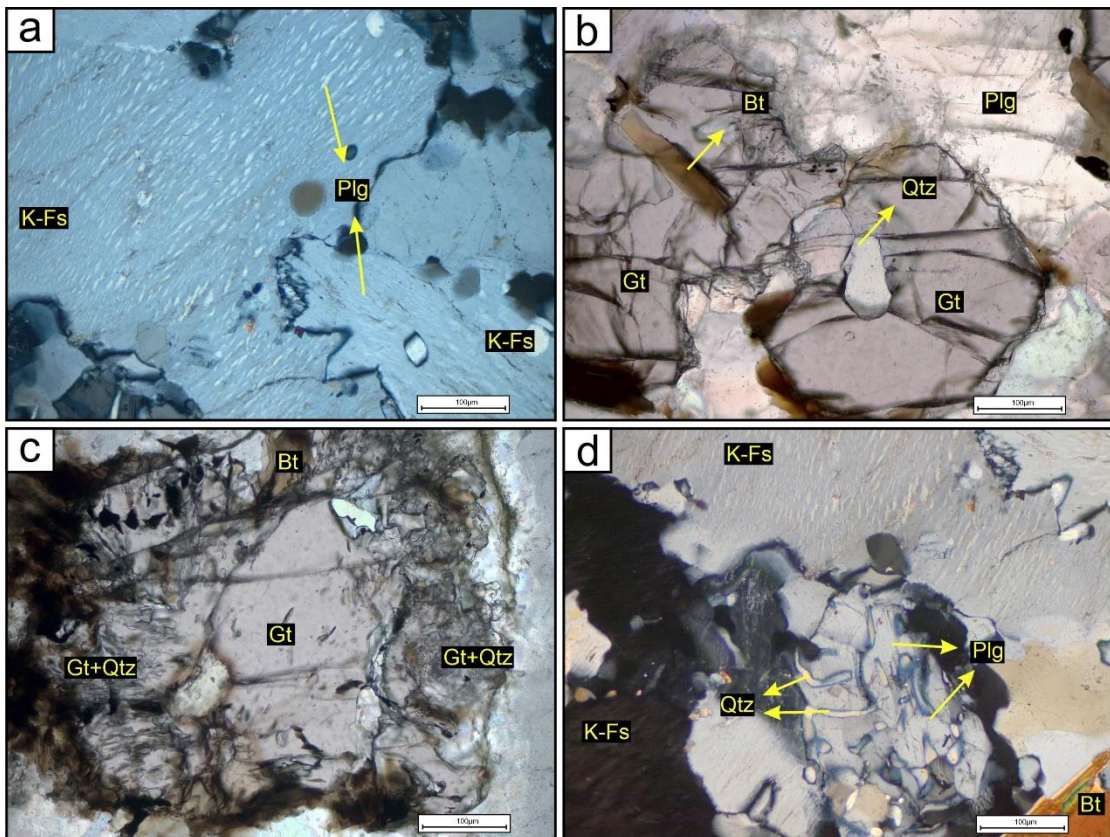
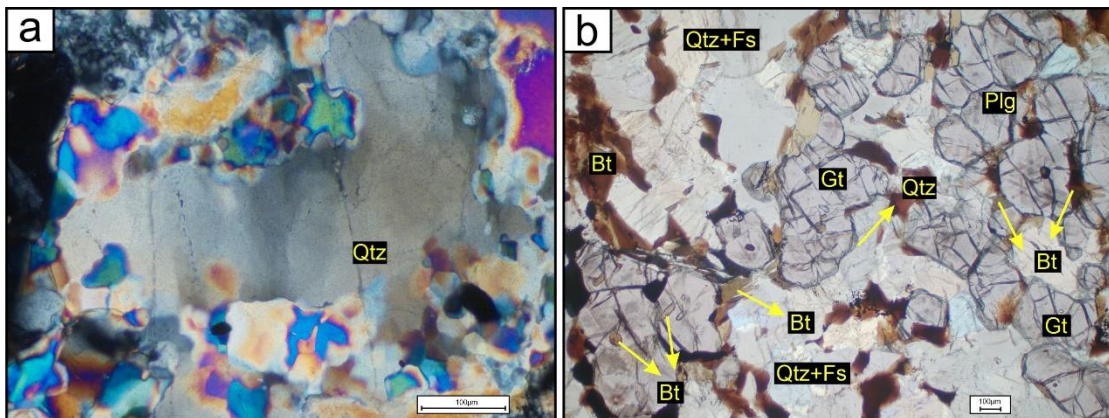


Fig. 3.21: (a) K-feldspar shows perthitic texture as an intergrowth of plagioclase within it (XPL). (b) Inclusion of quartz and biotite within garnet porphyroblasts (PPL). (c) Symplectitic intergrowth of quartz and garnet (PPL). (d) Myrmekite replacing the periphery of k-feldspar (XPL).

Fine to medium grained quartz is subhedral to anhedral in shape. Quartz occurs as inclusion within garnet (Fig. 3.21b). Symplectitic intergrowth of quartz and garnet is also observed (Fig. 3.21c). It also occurs as intergrowth with plagioclase (Fig. 3.21d). Undulose extinction within quartz shows imprints of deformation (Fig. 3.22a).



**Fig. 3.22:** (a) Quartz shows undulose extinction (XPL). (b) Biotite occurs as inclusion within garnet as well as along the grain boundary and fracture plane of the garnet (PPL).

Biotites occur as inclusion within garnet (Fig. 3.22b). It also occurs as patches around the margin and along the fractures of garnet grain (Fig. 3.22b).

#### **Enderbite:**

Enderbite of the studied area coarse grained granular rock. Microscopically it contains plagioclase, k-feldspar, clinopyroxene, orthopyroxene and opaque with or without garnet and biotite (Fig. 3.23).

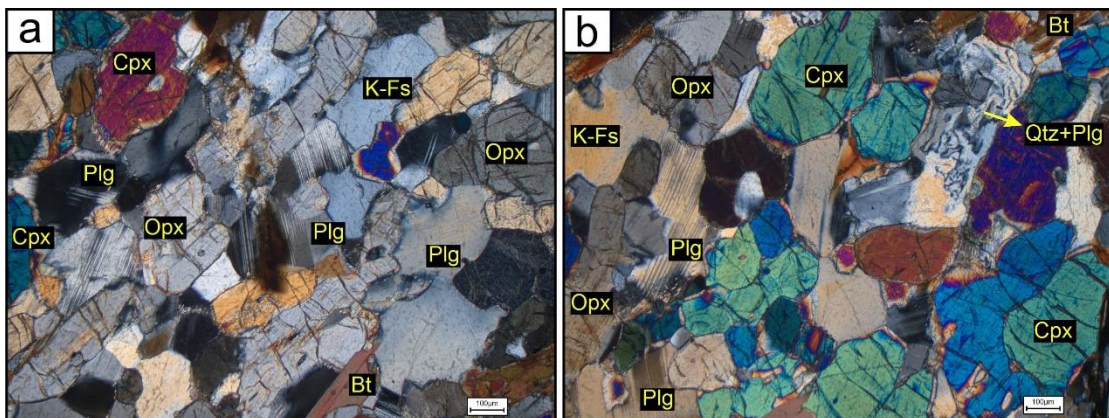


**Fig. 3.23:** (a) and (b) Enderbite consisting of plagioclase, k-feldspar, orthopyroxene, clinopyroxene and biotite (XPL).

Plagioclase and pyroxene grains show bimodal grain size distribution. The finer grains are present within the spaces between the coarse grains (Fig. 3.24a). Plagioclase shows deformed/wedge shaped twins (Fig. 3.24b). Most of the plagioclase feldspars in these rocks are strongly anti-perthitic while some of these grains are devoid of antiperthitic texture with the development of simple twinning (Fig. 3.25a, Fig. 3.25b, Fig. 3.25c). Abundance of anti-perthite within these rocks indicates high temperature



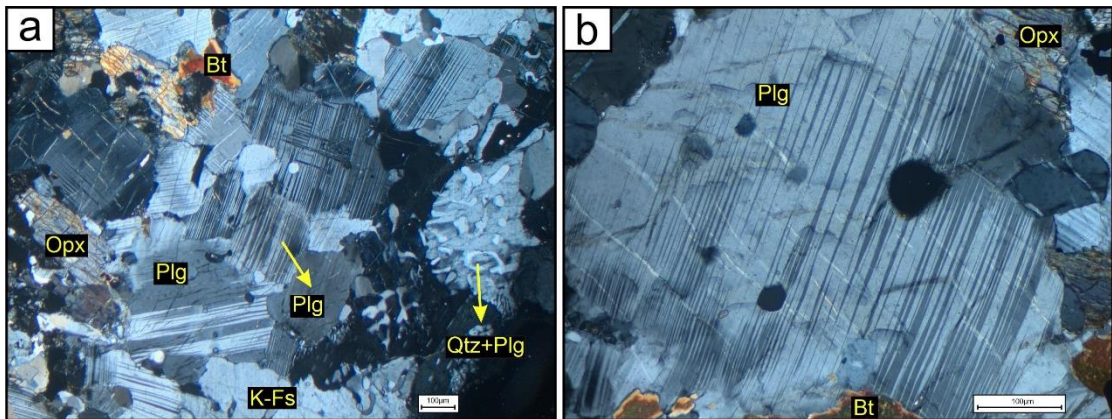


**Fig. 3.24:** (a) Bimodal distribution of plagioclase grain (XPL) (b) Plagioclase porphyroblasts shows wedge-shaped twin lamellae (XPL).

of magma consolidation (Tilley, 1936). The k-feldspars are perthitic in nature (Fig. 3.25d), which suggests that they form under high temperature (above 600° C) condition (Bowen and Tuttle's diagram, 1950). At places K-feldspars are replaced by myrmekite (Fig.3.26a, Fig. 3.26b).

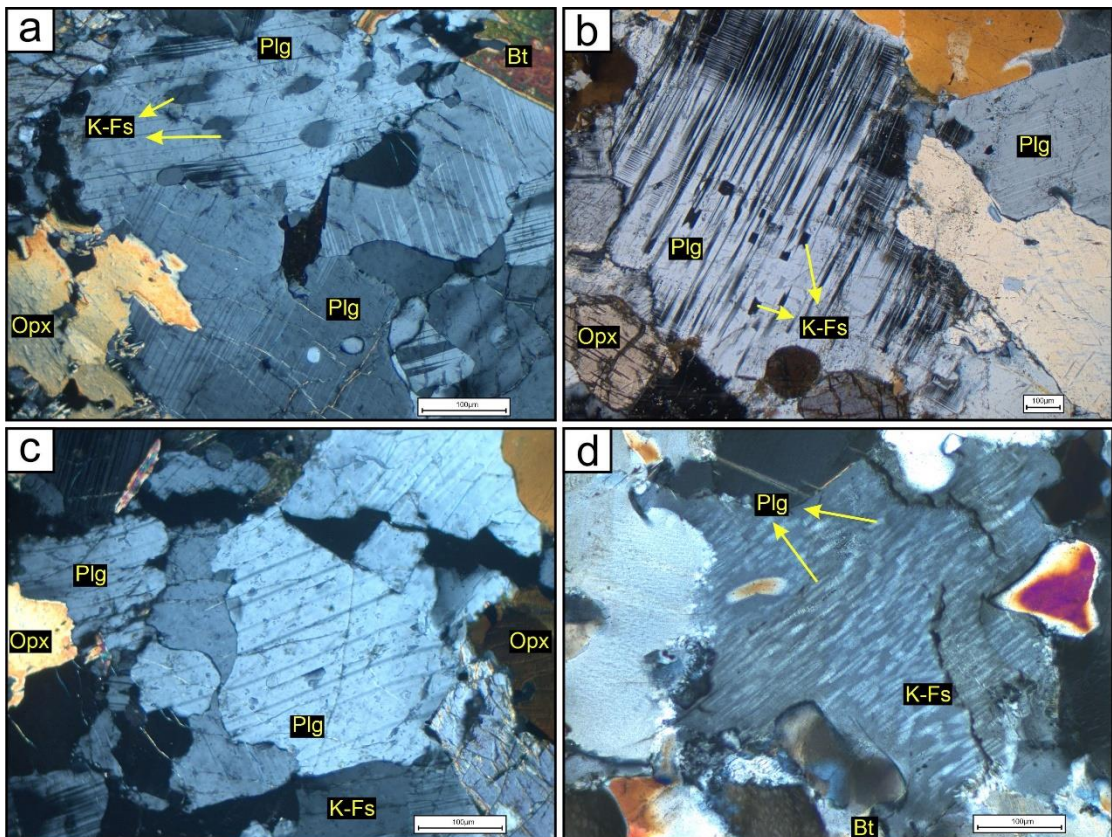


**Fig. 3.25:** (a) and (b) Plagioclase shows anti-perthitic texture as an intergrowth of k-feldspar within it (XPL). (c) Plagioclase shows bimodal distribution and devoid of anti-perthite with bent and wedge-shaped twin lamellae (XPL). (d) K-feldspar shows perthitic texture as an intergrowth of plagioclase within it (XPL).

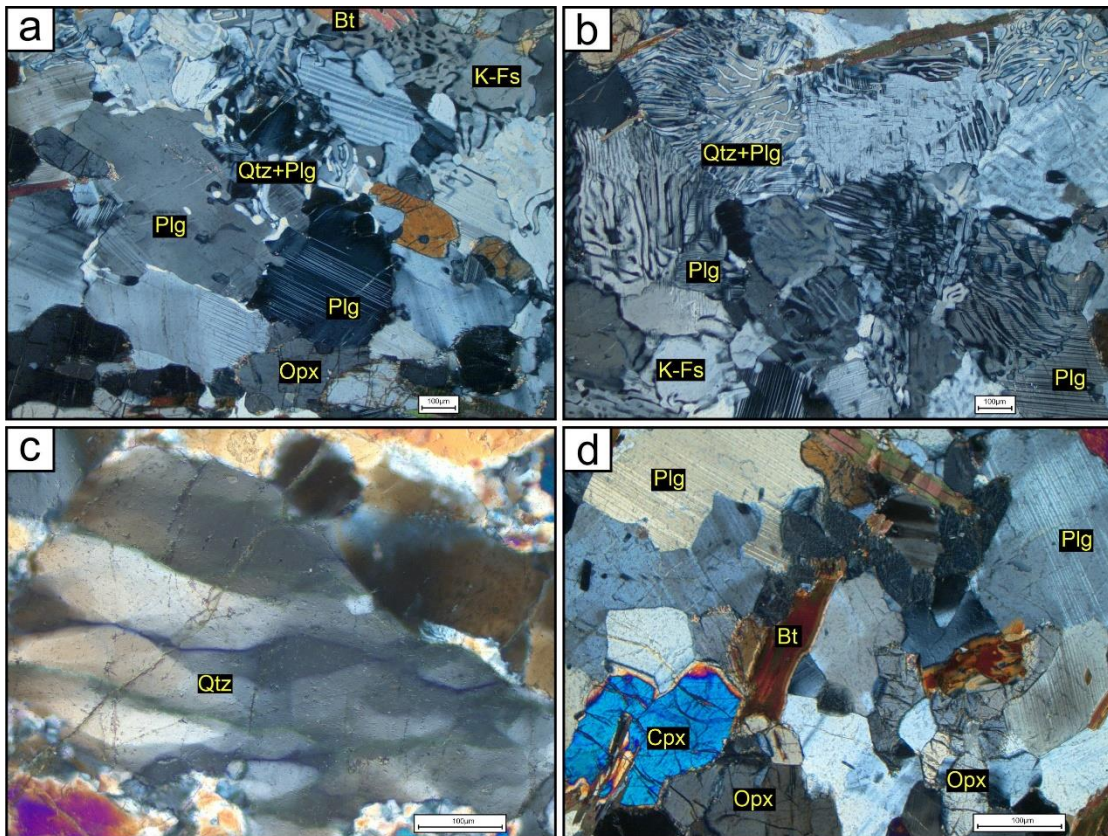


**Fig. 3.26:** (a) and (b) Myrmekite replacing the periphery of k-feldspar (XPL). (c) Quartz shows undulose extinction (XPL).

The orthopyroxene and clinopyroxene occur as randomly oriented idioblasts in quartz-feldspar matrix (Fig. 3.23). Quartz occurs as subhedral fine to medium sized grains with undulatory extinction (Fig. 3.26c). It also occurs as myrmekite (Fig. 3.26b) replacing k-feldspar along periphery. Biotite occurs within the inter-granular spaces and is devoid of its typical lath shape (Fig. 3.26d).

### **Anorthosite:**

The anorthosite of the studied area is leucocratic rock, shows granoblastic texture. Microscopically it composed of plagioclase cumulus with interstitial orthopyroxene, clinopyroxene, amphibole and magnetite (Fig. 3.27).

The plagioclase in the anorthosite occur in two modes: (a) Porphyroblasts and (b) recrystallized grains. Porphyroblastic plagioclase grains show bent twin lamellae, wedge-shaped and tapered lamellae (Fig. 3.28, Fig. 3.29a) as imprints of deformation and occurs as polygonal-granoblastic cumulates and exhibit planar boundaries and

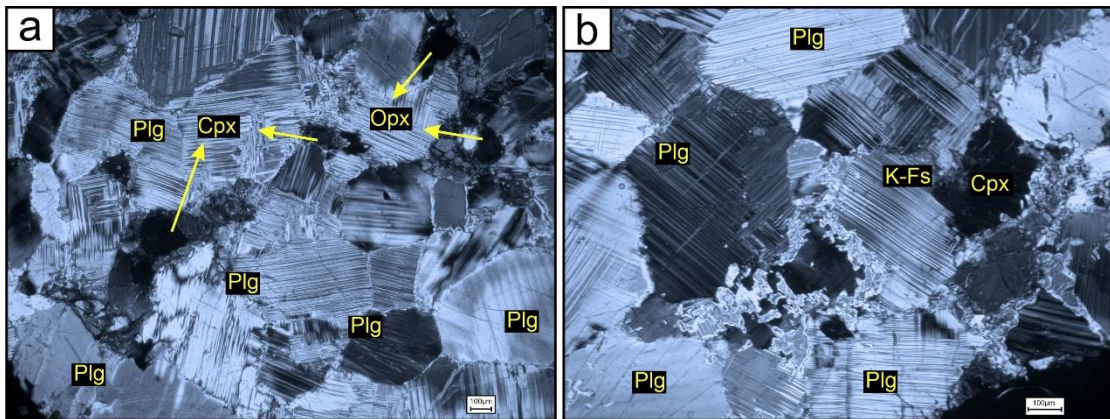


**Fig. 3.27: (a) Bent and tapered lamellae occur within plagioclase porphyroblast (XPL). (b) Plagioclase porphyroblasts enclosing inclusions of amphibole and biotite (XPL).**

triple junctions (Fig. 3.27). In some cases, plagioclase porphyroblasts contain inclusions of amphibole and biotite (Fig. 3.29b). Secondary recrystallized plagioclase

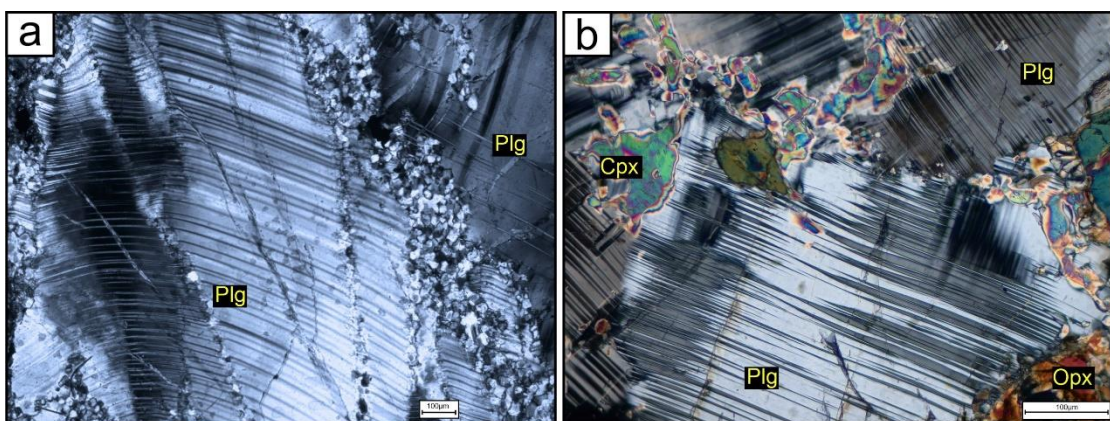


**Fig. 3.28: (a) Bent lamellae occur within plagioclase porphyroblast (XPL). (b) Wedge-shaped and tapered lamellae occur within plagioclase grains (XPL).**

grains occur along with small amphibole and pyroxene grains aligned across the porphyroblasts (Fig. 3.30a). They are smaller in size and show no twinning.

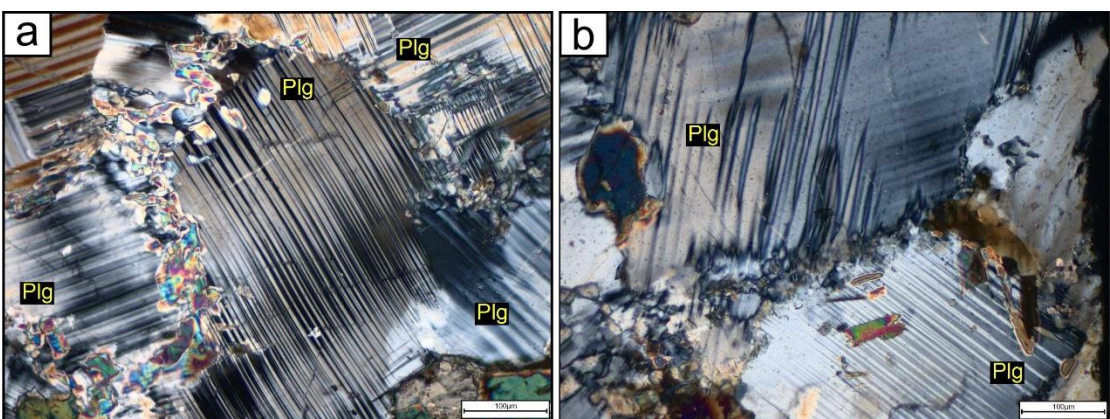


**Fig. 3.29: (a) Bent and tapered lamellae occur within plagioclase porphyroblast (XPL). (b) Plagioclase porphyroblasts enclosing inclusions of amphibole and biotite (XPL).**

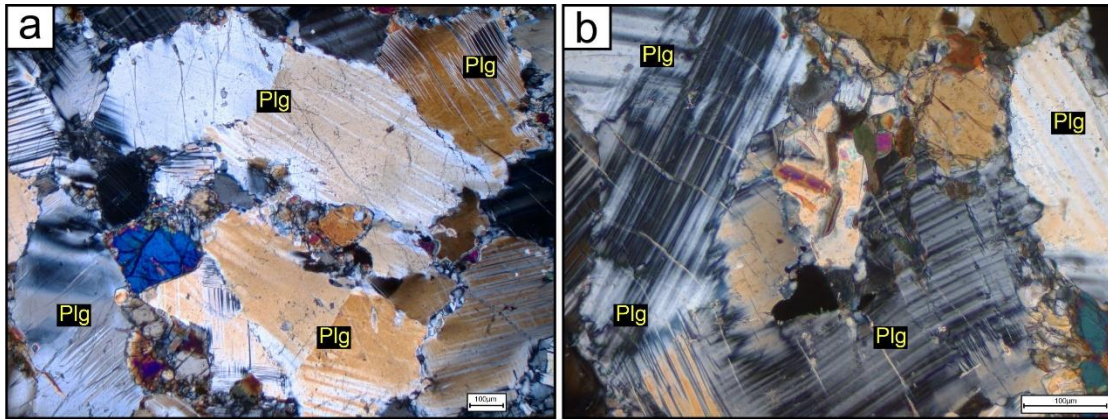
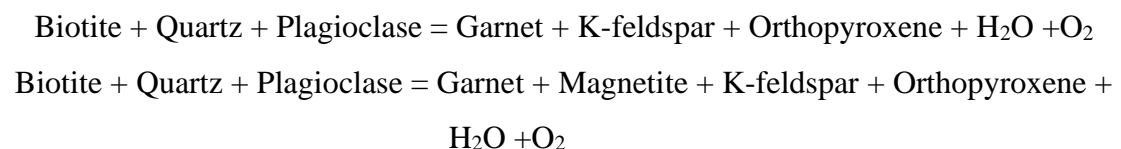


**Fig. 3.30:** (a) The secondary recrystallized plagioclases occur along with small amphibole and pyroxene grains aligned across the plagioclase porphyroblast (XPL). (b) biotites and recrystallized plagioclase vein occurs within plagioclase porphyroblasts (XPL).

The clinopyroxenes typically occur in the spaces between plagioclase cumulates. Small biotites and recrystallized plagioclase also occur as micro veins within the large plagioclase crystals (Fig. 3.30b).

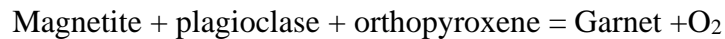
### 3.3. Mutual Textural Relations of Minerals

According to the textural relationship of orthopyroxene granulites, it may infer that the rock suffered three stages of metamorphism. During prograde metamorphism garnet, opaque oxide and orthopyroxene were formed when temperature and pressure were increasing. The textural associations observed within the rocks are described earlier which are mainly: (a) Inclusion of plagioclase, biotite, quartz, k-feldspar and opaque within orthopyroxene (Fig. 3.1c, Fig. 3.1d). (b) Inclusion of biotite, quartz and opaque within garnet porphyroblast (Fig. 3.6a, Fig. 3.7a). (c) Sharp mutual boundary between orthopyroxene and garnet (Fig. 3.2a), k-feldspar with both orthopyroxene and plagioclase (Fig. 3.1). These textural association could be result from the following reactions:

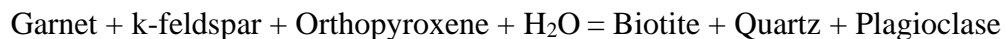
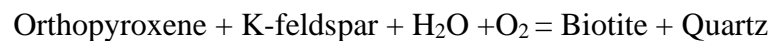
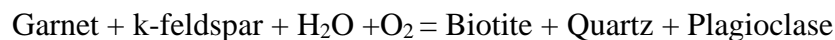


At peak condition of metamorphism coronal garnet was formed, when pressure decreased but temperature remained constant at peak condition of metamorphism. The textural associations observed within the rocks are described earlier which are mainly:

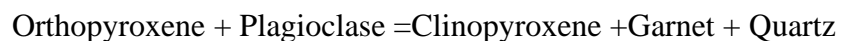
(a) Coronal garnet rimming around plagioclase and orthopyroxene (Fig. 3.2a, Fig. 3.2b) as results they are separated by the garnet. (b) Opaques are separated from plagioclase and orthopyroxene by garnet (Fig. 3.6b). (c) Symplectic overgrowth between garnet and quartz (Fig. 3.2a) and inclusion of opaque within coronal garnet (Fig. 3.2c). These textural association may result from the following reactions:



During retrograde metamorphism when temperatures were decreasing. The textural associations observed within the rocks are described earlier which are mainly: (a) Occurrence of patchy biotite grains along the boundary and fractures of orthopyroxene and garnet which is in contact with opaque (Fig. 3.1d, Fig. 3.7). (b) Symplectite of quartz and biotite (Fig. 3.7b). (c) Presence of myrmekite replacing k-feldspar along periphery (Fig. 3.3c, Fig. 3.3d). These textural association could be result from the following reactions:



The textural relationships observed within the mafic granulites of the studied area are mainly: (a) Coronal garnet rimming the orthopyroxene grains and also separated from plagioclase (Fig. 3.9b), (b) Garnet-quartz symplectite separates orthopyroxene from plagioclase (Fig. 3.9a, 3.12d), (c) No sharp contact between clinopyroxene and orthopyroxene (Fig. 3.8a, 3.8c). This type of textural association may suggest the following reaction:



**Chapter 4**  
**Generation of Fe-Ti Oxides**

## GENERATION OF Fe-Ti OXIDES

### 4.1. Introduction

A rock is a heterogeneous assemblage of minerals (ferrimagnetic, paramagnetic and diamagnetic), each grain of which makes its own contribution to the total (bulk) susceptibility. The most important factors influencing rock magnetism and palaeomagnetism are the type of magnetic minerals (remanence carriers), its grain size, and the manner in which it acquires a remanent magnetization. The most important magnetic minerals are Iron-Titanium oxides. Iron–Titanium (Fe-Ti) oxide minerals constitute the major opaque oxides in many metamorphic rocks, partially in granulitic rocks. The magnetic properties of high-grade rocks are functions of their Fe-Ti oxide minerals and their subsequent changes during metamorphism. So, the primary Fe-Ti oxide mineralogy plays an important role in the field of rock-magnetism.

This chapter deals with the generation of the Fe-Ti Oxides present within the rocks from KPLC. Before getting into the detailed results, some basic concepts of magnetic mineralogy are discussed. This will include the basic knowledge of classification and solid solution series of the Fe-Ti oxides and their oxidation states.

#### 4.1.1. Classification of the Fe-Ti Oxides

For the classification of the Fe-Ti Oxides based on their composition, the Fe-Ti oxides are conveniently displayed on a  $\text{TiO}_2\text{-FeO-Fe}_2\text{O}_3$  ternary diagrams (Fig. 4.1) (Haggerty, 1976; Tauxe, 2010; Piper, 1987). Fig. 4.1 represents the ternary diagram showing the classification of the magnetic oxides. In the above figure, the position from left to right indicates increasing ratio of Ferric ( $\text{Fe}^{3+}$ ) and Ferrous ( $\text{Fe}^{2+}$ ) iron while position from bottom to top increases the Ti component (Ti:Fe ratio).

According to Grant and West (1965) it was shown that the igneous and the metamorphic rocks are concentrated over the solid solution series of titanomagnetite and titanohaematite only. This probably accounts for the reason behind rigorous studies of the minerals within these two solid solution series and here also the discussion will remain concentrated to these solid solution series only.

**Titanomagnetite:** Titanomagnetites are generally found to occur within the primary minerals of the igneous rocks. Magnetite is found within volcanic igneous rocks because of high temperature oxidation (Butler, 1992). Substitution of  $Ti^{4+}$  within the

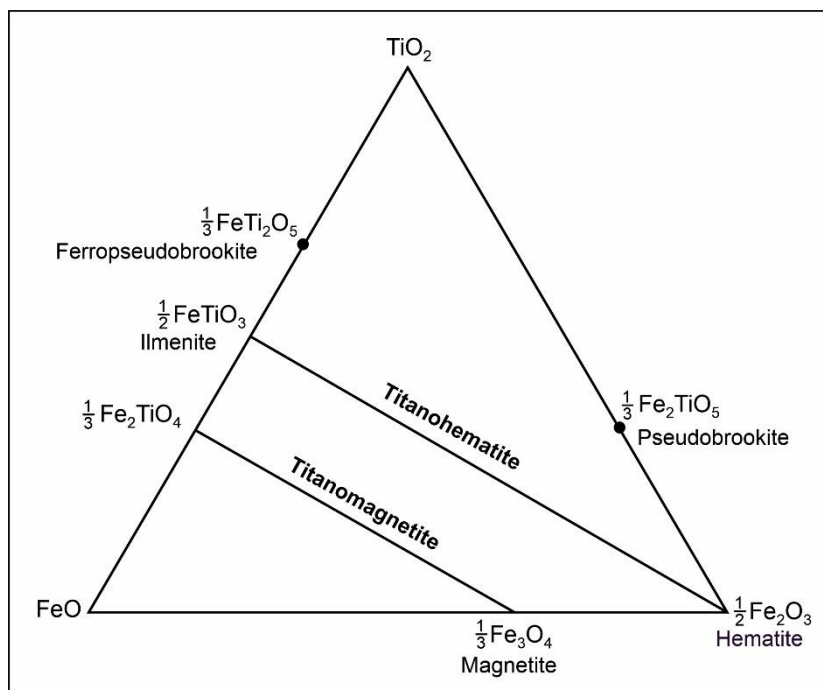


Fig. 4.1: Ternary diagram ( $TiO_2$ - $FeO$ - $Fe_2O_3$ ) showing the classification of the magnetic oxides. Titanomagnetite and titanohaematite solid solution series are indicated (Butler, 1992).

crystal structure of magnetite is a ubiquitous phenomenon and if we consider “x” as the number of titanium cations, replacement by  $Ti^{4+}$  can be represented by the following Fig. 4.2 (Tauxe, 2010).

Considering the palaeomagnetic attributes, the incorporation of titanium within the magnetite has a profound effect (Tauxe, 2010). This is because there is no unpaired electron in  $Ti^{4+}$  and thus the saturated magnetization decreases with the increase in the value of x and further due to increase in the cell dimension, the temperature is decreased (Butler, 1992; Tauxe, 2010).

**Titanohaematites:** Haematite occurs widely in oxidized sediments and dominates the magnetic properties of the red beds. It also occurs as a high temperature phase in certain igneous rocks (Tauxe, 2010; Tarling and Hrouda, 1993). In most igneous rocks, the titanohaematites and their oxidation products constitutes a lesser proportion of ferrimagnetic minerals than do titanomagnetites, but for highly oxidized igneous rocks haematites can be of higher concentration (Butler, 1992). However, haematites and



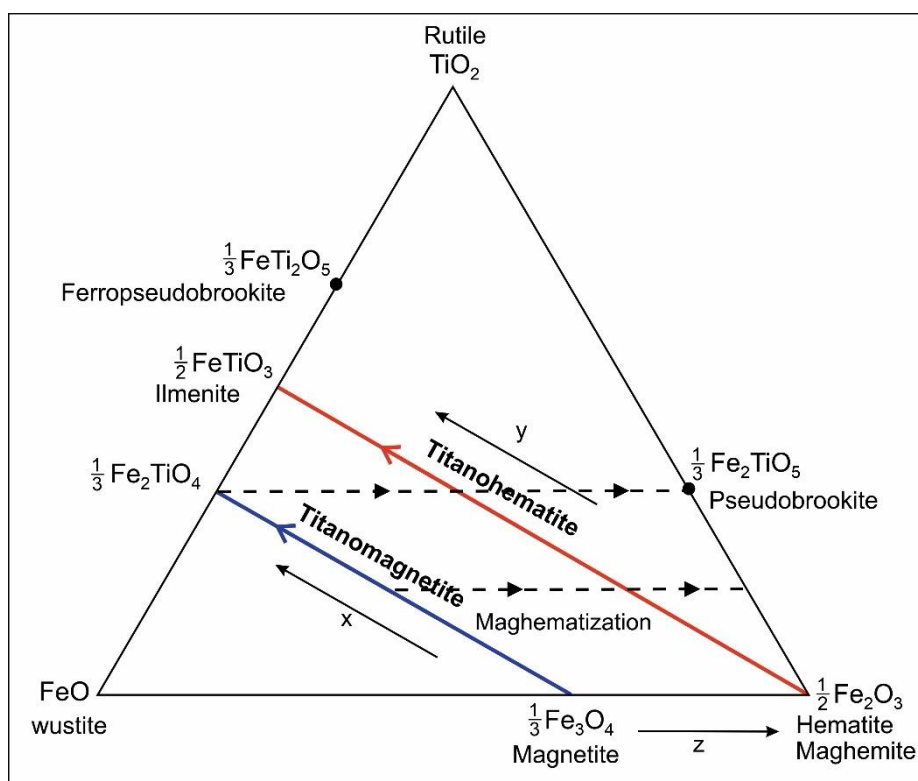


**Fig. 4.2:** Ternary diagram for iron-oxides (modified from O'Reilly, 1984 in Tauxe, 2010). The solid lines are solid solution series with increasing titanium concentration (x and y). The dashed lines with arrows indicate the direction of increasing oxidation (z).

titanohaematites are dominant components of red sediments, which are in turn remarkable sources of palaeomagnetic data (Butler, 1992).

#### 4.1.2. Solid Solution Series of the Fe-Ti Oxides

In palaeomagnetism mainly two solid solution series are important: the ulvospinel-magnetite and ilmeno-haematite series (Fig. 4.3). Both titanomagnetites and titanohaematites crystallizes at  $\sim 1300^\circ\text{C}$  and the solid solution is complete at this temperature. Above about  $600^\circ\text{C}$ , there is complete solid solution between magnetite and ulvospinel and above about  $800^\circ\text{C}$  between ilmenite and haematite (Fig. 4.3). As the temperature goes down, compositional gaps develop below the curves shown in Fig. 4.3. Below these curves, intermediate compositions unmix or exsolve into Ti-rich regions and Ti-poor regions by solid state diffusion of Fe and Ti-cations.

The solid-solution exsolution of the Ti-magnetite series has very close association with the magnetization history. Exsolution of titanomagnetites and titanohaematites is important because unmixing of intermediate-composition grains into composite grains

The solid-solution exsolution of the Ti-magnetite series has very close association with the magnetization history. Exsolution of titanomagnetites and titanohaematites and titanohematites and titanohematites

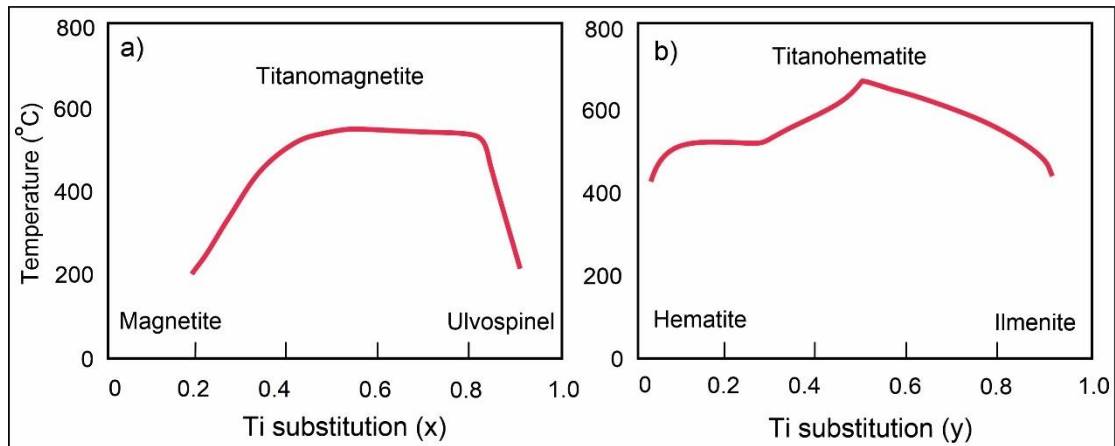


**Fig. 4.3: Phase diagrams (Compositional gaps) for titanohaematite and titanomagnetite. The composition is indicated by x or y. There is complete solid solution above the solid lines. Exsolution begins as the temperature cools below the solid curves. (a) Titanomagnetite series and (b) Ti-haematite series (Redrawn from Dunlop and Ozdemir, 1997 in Tauxe, 2010).**

with Ti-rich (Fe poor) and Ti-poor (Fe rich) regions alters magnetic properties such as  $j_s$  and  $T_C$  that depend on composition and exsolution dramatically decreases effective grain size (Butler, 1992). The Ti-rich (Fe poor) bands have higher magnetization yet lower Curie temperature than the Ti-poor (Fe rich) bands. So, the Ti-poor bands will get magnetized first. After that the Ti-rich bands will become magnetized when the curie temperature of the Ti rich bands riched in the presence of the demagnetizing field of the Ti-poor bands and hence they will acquire a remanence that is antiparallel to the applied field. This causes the NRM to remain antiparallel to the applied field and the rocks thus gets self-reversed (Tauxe, 2010).

## 4.2. Oxidation of Fe-Ti Oxides

Many minerals crystallize under one set of equilibrium conditions and are later subjected to a different set of condition depending on the evolutionary history of the rocks. They will tend to alter in order to come into equilibrium with the new set of conditions. Sometimes the new conditions are more oxidizing than the original condition. In case of Fe-Ti oxide the composition then tends to move along the dashed lines in Fig. 4.2 Showing increasing degree of oxidation (Tauxe, 2010).

High grade rocks are store house of magnetic minerals occurring in different modes. Based on the grain size opaque oxides are mainly bimodal. The coarser variety is primary and the secondary one has thread like appearance. The original phases that originally crystallize from igneous melts are referred to as primary Fe-Ti oxide. During a prolonged period of metamorphism, the magnetic minerals which crystallize initially in igneous rocks have a general tendency for oxidation to make stable phases of all Fe-Ti oxide minerals of metamorphic rock.

Based on the degree of oxidation (which is a function of temperature and corresponding pressure and  $fO_2$ ) the magnetic minerals of primary Fe-Ti oxides are classified as follows.

- (i) High temperature oxidation that occurs above 600° C.
- (ii) Low temperature oxidation that occurs about 350° C or below that temperature.

**(i) High temperature oxidation of Fe-Ti oxides:**

Both titanomagnetite and magnetite crystallize at ~ 1300° C and are early in the crystallization sequence of the igneous rocks. High-grade metamorphic rocks, which consists of the present study, consists of both titanomagnetite and titanohaematite as the primary Fe-Ti oxides. Cooling rate of these rocks have a major effect on the grain size of the titanomagnetite and titanohaematite. High temperature oxidation of the primary Fe-Ti oxides (titanomagnetite and titanohaematite) have two different textural assemblage developed from the oxidation.

**Exsolution:** Exsolution or “oxidation-exsolution” (Buddington and Lindsley, 1964) is the development of ilmenite lamellae along (111) parting planes in titanomagnetite, which is called treills ilmenite (Buddington and Lindsley, 1964). Both titanomagnetite and titanohaematite shows complete solid solution at their crystallization temperature which is above 1300° C. An intermediate composition exsolve into Ti-rich (Fe-poor) and Ti-poor (Fe-rich) regions by solid state diffusion of Fe and Ti cations below this temperature (Buddington and Lindsley, 1964).

By exsolution, a large homogeneous grain is transferred into much smaller Ti-rich (Fe-poor) and complementary Ti-poor (Fe-rich) regions. In titanomagnetite exsolution gives Ti-poor crystals of cubic habit surrounded by Ti-rich region (Fig. 4.6) and resulting composite grain have ferromagnetic fine grain crystals. In case of titanohaematite exsolution occurs along (0001) planes (Butler, 1992) give a tiger-striped composite grain (Fig. 4.13, Fig. 4.14). Exsolution in Titanomagnetite is slow process and generally observed only in slowly cooled plutonic rock because titanomagnetite unmix at fairly low temperature ( $\sim 600^{\circ}\text{C}$ ). In titanohaematite exsolution is more rapid because titanohaematite unmix fairly at higher temperature than titanohaematite. Exsolution of intermediate composition of titanomagnetite and titanohaematite are important because (a) Saturation magnetization and curie temperature depend on composition (b) Decreased effective grain size has a major effect on magnetic properties.

**Duteric oxidation:** Duteric oxidation mainly occurs during the original cooling of an igneous rock. The typical condition of duteric oxidation involve temperature of  $750^{\circ}\text{C}$  and  $f\text{O}_2$  of  $10^{-5}$ -  $10^{-6}$  atmospheres (Butler, 1992) and occurs in the solid state but generally above curie temperature. Both primary titanomagnetite and primary titanohaematite are affected by duteric oxidation. In case of titanomagnetite, resulting grains are not usually homogeneous, commonly they are composite grains with ilmenite lathes along (111) plane of the host titanomagnetite (Fig. 4.5, Fig. 4.6). The composition of host titanomagnetite become enriched in Fe and approaches pure magnetite (Butler, 1992). The change in composition of the titanomagnetite due to duteric oxidation changes the magnetic properties. Primary titanomagnetite of intermediate composition replaced by Fe-rich titanomagnetite and grain size decreased drastically. Primary grains are subdivided into many smaller grains separated by paramagnetic ilmenite. Fe-rich titanomagnetite have high curie temperature and higher saturation magnetization and decreased grain size has a major effect on magnetic properties. Primary Ti-rich titanohaematite also undergoes duteric oxidation, extreme cases give composite grains of rutile ( $\text{TiO}_2$ ), haematite ( $\alpha\text{Fe}_2\text{O}_3$ ) and sometimes pseudobrookite ( $\text{Fe}_2\text{TiO}_5$ ). Similarly, extreme duteric oxidation of primary titanomagnetite can give rutile and haematite. There are stages of duteric oxidation depending on the cooling rate and  $f\text{O}_2$ .

Intensity and stability of palaeomagnetism are commonly maximized where duferite oxidation proceeded to advanced stage ((Butler, 1992).

Haggerty (1976) classified the stages of high temperature oxidation. The letter “C” prefixes each stage of oxidation resulting from Cubic phase:

- C1-Stage:** Optically homogeneous titanomagnetite solid solutions enriched with Ulvospinel.
- C2-Stage:** Titanomagnetite having the small number of “exsolved” ilmenite lamellae along (111) crystallographic plane.
- C3-Stage:** Titanomagnetite with densely crowded “exsolved” ilmenite lamellae along (111) crystallographic plane.
- C4-Stage:** Mottling of lamellar ilmenite – intralamellar titanomagnetite inter-growth and development of ferri-rutile in metailmenite lamellae.
- C5-Stage:** Rutile and titanohaematite extensively develop within the metailmenite lamellae and rutile-titanohaematite assemblages develop incipiently within the titanomagnetite.
- C6-Stage:** Incipient pseudobrookite forms during this stage and three phase assemblages, rutile, pseudobrookite and exsolved spinel develop with or without unoxidized titanomagnetite.
- C7-Stage:** Pseudobrookite (ss) and haematite (ss) coexist with this stage of oxidation.

The progressive stages of high temperature oxidation of rhombohedral phase i.e., discrete ilmenite have been classified and are denoted by prefix with the letter “R”:

- R1-Stage:** Homogeneous ilmenite.
- R2-Stage:** Ferrian ilmenite + ferrian rutile.
- R3-Stage:** Ferrian rutile + (ferrian ilmenite).

**R4-Stage:** Rutile + titanohaematite + ferrian rutile + ferrian ilmenite.

**R5-Stage:** Rutile + titanohaematite.

**R6-Stage:** Rutile + titanohaematite.

**R7-Stage:** Pseudobrookite + (rutile + titanohaematite).

High temperature oxidation of primary titanomagnetite and titanohaematite is observed in the samples taken from granulites, anorthosite and enderbite of KPLC (KP-4, KP-5, KP-7, KP-10, KP-12, KP-14, KP-15, KP-19, KP-21, KP-36, KP-38, KP-39, KP-42). Mainly phenocrysts of primary titanomagnetite and titanohaematite within the studied rocks show characteristic high temperature oxidation features. The titanomagnetite phenocrysts of the studied samples are subhedral in nature and experienced C1, C2, C3, and C4-Stages of high temperature oxidation.

In general, titanomagnetites are light grey in colour with moderate to low reflectivity. In oxidized titanomagnetite titanium diffuses from the host mineral, which results significant changes in colour and reflectivity. The mineral become whiter with an increase in reflectivity. High-grade metamorphic rocks from area under study are characterized by the appearance of (111) fabric developed by trellis ilmenite along (111) parting planes in host titanomagnetite (KP-04, KP-07, KP-10, KP-21, KP-42). Primary titanomagnetites show the degree of high temperature oxidation ranging between C1 to C4-Stage. Discrete primary ilmenites are also present.

In C1-Stage, optically homogeneous titanomagnetites are found as first generation of primary Fe-Ti oxide (Fig. 4.4). In C2-Stage of high temperature oxidation, at least one set of fine hair like 'exsolved' ilmenite lamellae is found in host titanomagnetite along the (111) crystallographic plane (Fig. 4.5). There is a sharp difference in colour between the ulvospinel-poor area with ilmenite lamellae and ulvospinel rich part of the host titanomagnetite. At places two dominant sets of ilmenite lamellae developed along (111) plane. In C3-Stage, with increasing degree of oxidation thin ilmenite lamellas are merged to form relatively thick crowded 'exsolved' lamellae of ilmenite along (111) plane within host titanomagnetite (Fig. 4.6). Ilmenite lamellas parallel to the (111) planes show same degree of anisotropy and pleochroism. Exsolved

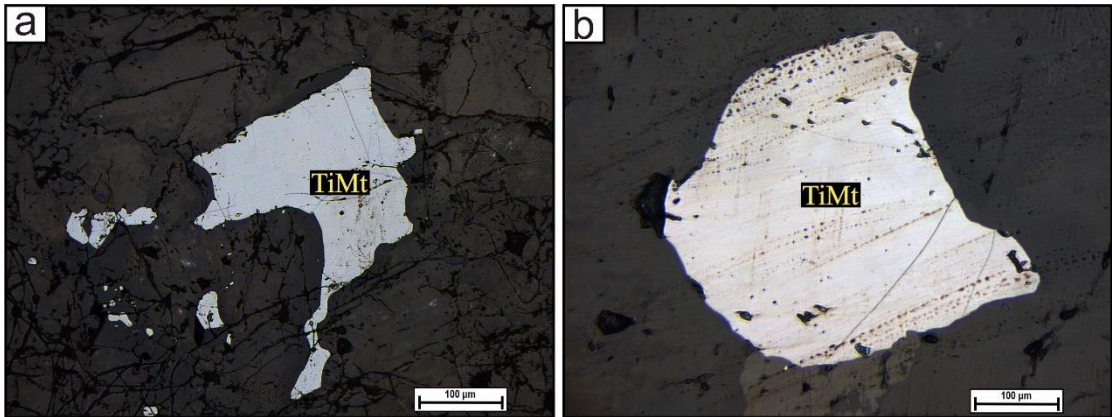


Fig. 4.4: (a) and (b) Primary homogeneous titanomagnetite showing C1 stage of high temperature oxidation (PPL).

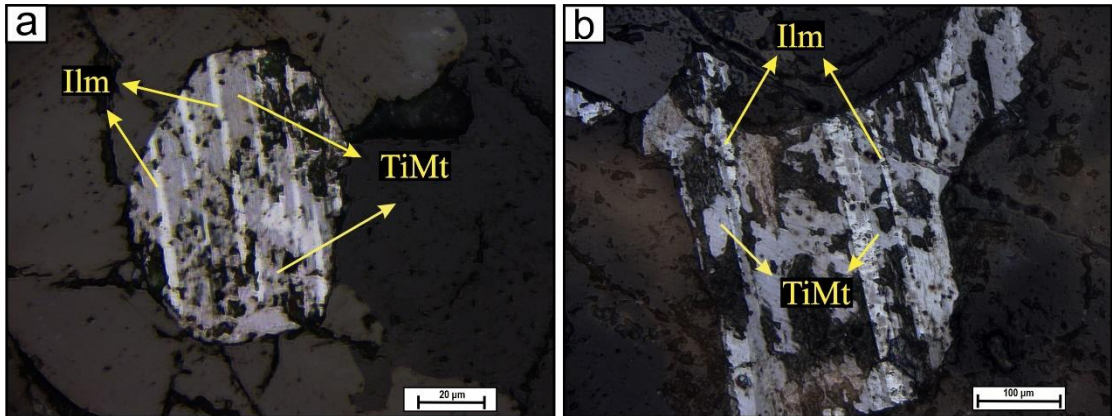


Fig. 4.5: (a) and (b) C2-Stage of high temperature oxidation of titanomagnetite shows one set of thin ilmenite lamellae (PPL).

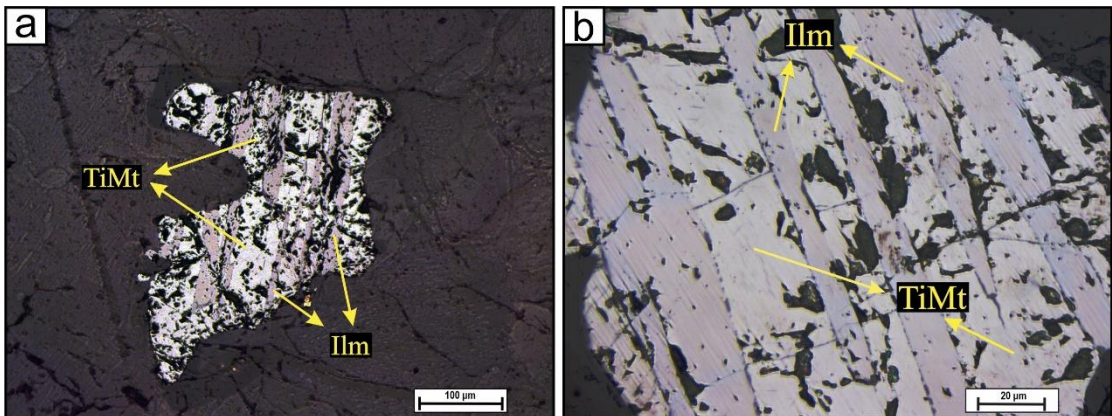


Fig. 4.6: (a) and (b) C3-Stage of high temperature oxidation of titanomagnetite shows crowded thick exsolved lamellae of ilmenite (PPL).

lamellas show sharp and well-defined contacts with the host titanomagnetites and are distinguished by their smooth and parallel outline. Thick sandwich lath (Fig. 4.7) of ilmenite along one set of the octahedral plane are commonly observed. These thick laths

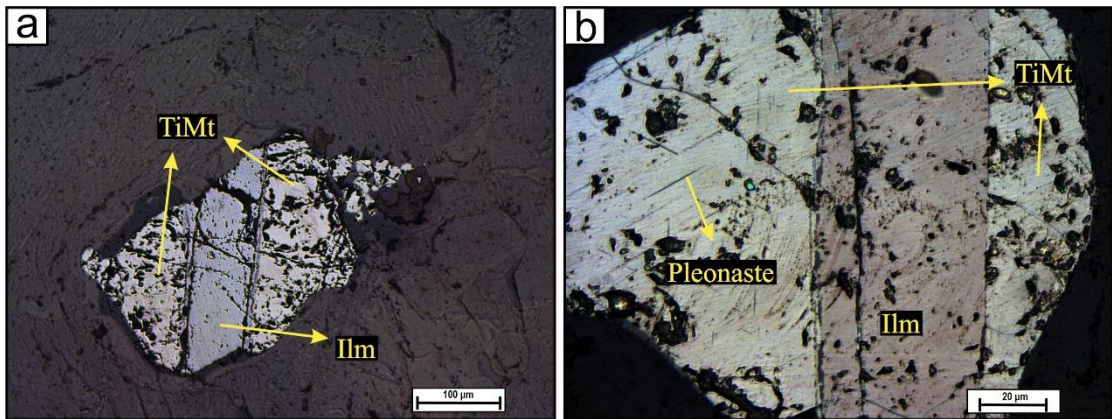


Fig. 4.7: (a) and (b) Thick laths of ilmenite lamellae sandwiched between host titanomagnetite (PPL).

generally, occur in small numbers and a single lath is the most common form in granulitic rocks. Ilmenite lamellae are often concentrated along the cracks of titanomagnetite host (Fig. 4.8). These textural association strongly support the evidence of oxidation which is responsible for the formation of ilmenite lamellae from primary

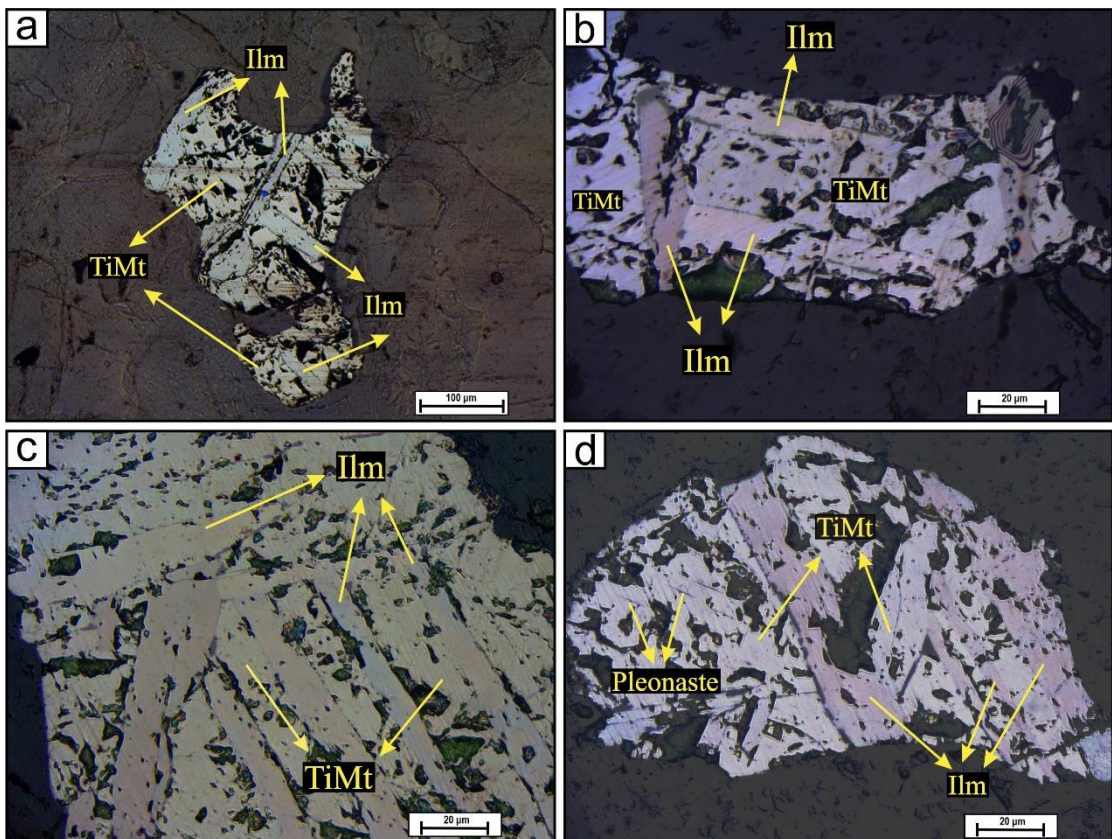
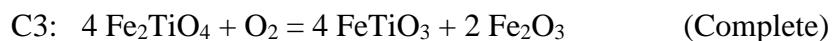


Fig. 4.8: (a), (b), (c) and (d) Secondary ilmenite occurs along the cracks of titanomagnetites. Note that the cracks filled by ilmenite occurs at right angle to exsolved lamellae of previous generation (PPL).



ulvospinel-magnetite solid solution. The typical reaction leading to C1 and C3-Stage of high temperature oxidation are given below (Haggerty, 1976).



In C4-Stage, with increasing oxidation the ‘exsolved’ metailmenite becomes lighter in colour (haematite solid solution) and the titanomagnetite changes from tan to dark brown (magnetite solid solution) (Fig. 4.9). Lenses of ferrian rutile are oriented parallel to the length of meta-ilmenite lamellae (0001) and also present at an angle to

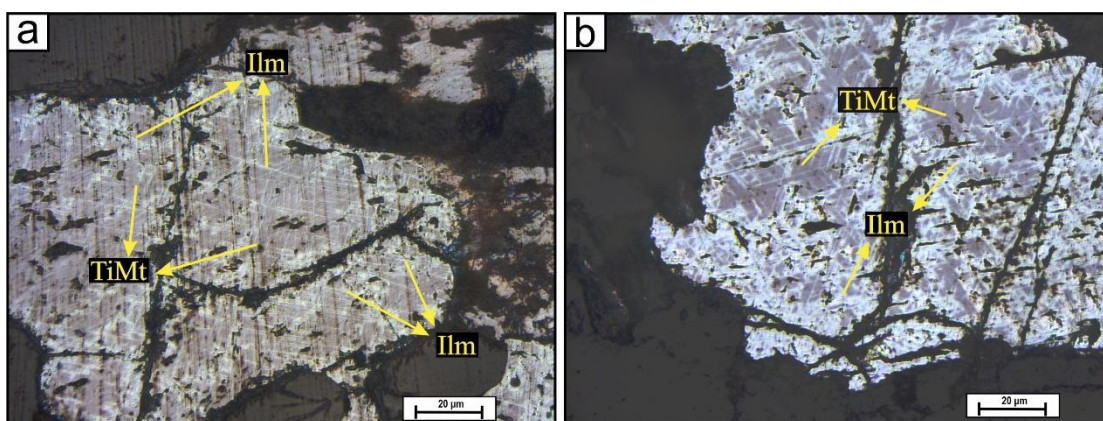


Fig. 4.9: (a) and (b) C4-Stage of high temperature oxidation of titanomagnetite shows mottled appearance of the metailmenite lamellae (PPL).

the lamellae (Haggerty, 1976). The lamellae towards the edges of the titanomagnetite grains are more intensely oxidized than those towards the center (Fig. 4.10). ‘Exsolved’ black rods of spinel (pleonaste) in the titanomagnetite host oriented along (100) plane

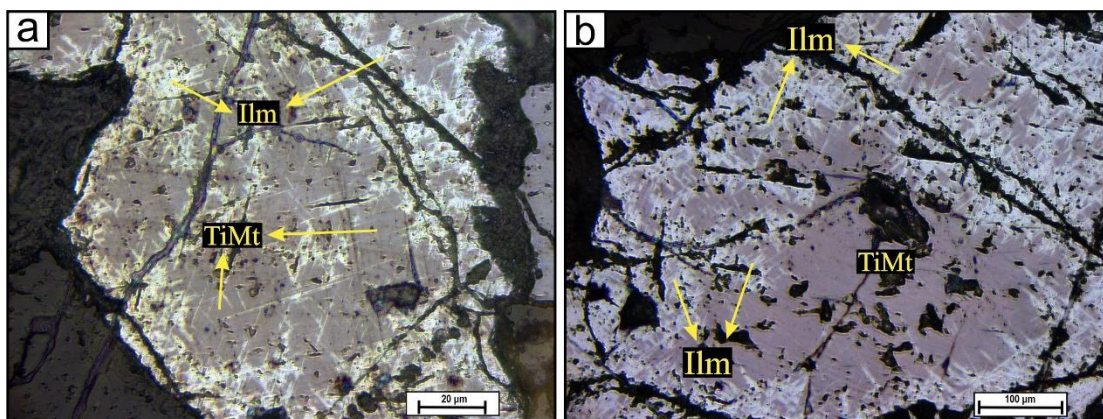


Fig. 4.10: (a) and (b) C4-Stage of high temperature oxidation of titanomagnetite. Oxidation is more intense at the grain boundary (PPL).

(Fig. 4.11). This oxidation stage is characterized by spinel rods, internal reflections and the mottled appearance of the meta-ilmenite lamellae.

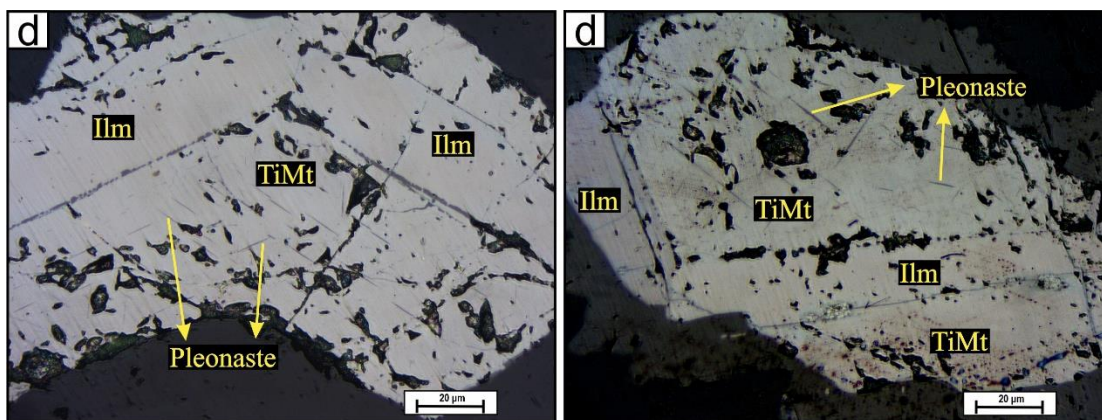


Fig. 4.11: (a) and (b) Suture like spinel rods within the titanomagnetite grains (PPL).

In the present study, it is evident that the ilmenite lamellae are oriented along (111) crystallographic plane and at the same time the clusters of minutes pleonaste lamellae also occur within the host titanomagnetite grains (Fig. 4.12). Pleonastes are the intermediate members of the Spinel-Hercynite solid solution series and oriented

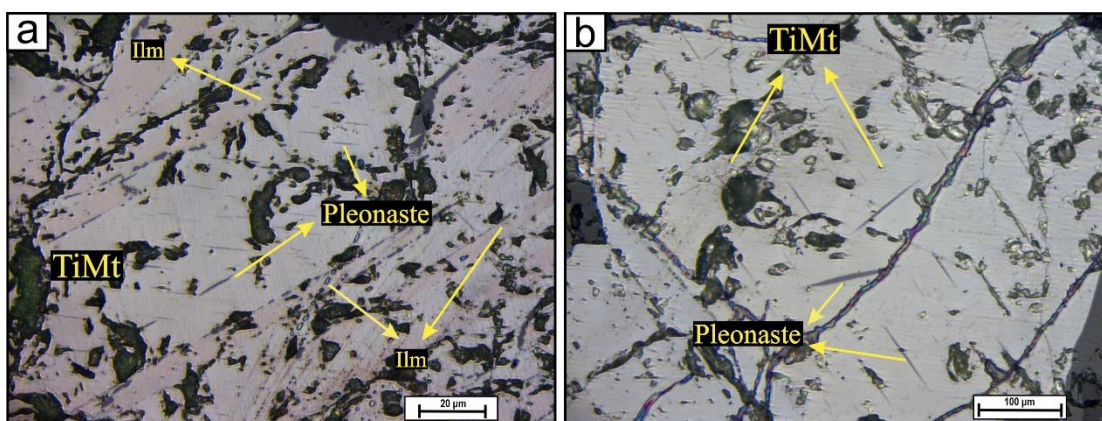
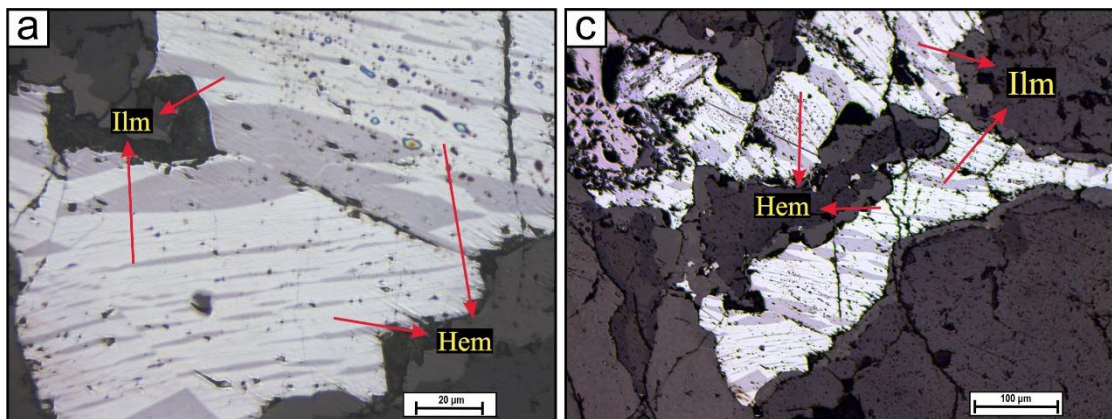


Fig. 4.12: (a) and (b) First generation of pleonaste lamellae showing suture like pattern within the inhomogeneous titanomagnetite (PPL).

along (100) plane within titanomagnetite. These are the common features in titanomagnetites and these pleonaste lamellae often seem to originate from titanomagnetite (Haggerty, 1976a). These tiny droplets of pleonaste or pleonaste lamellae are much higher in Fe than titanomagnetite (Speczik et al., 1988). 'Exsolution' of pleonaste from titanomagnetite happened above the magnetite-ulvospinel solvas and depends on bulk composition (Haggerty, 1976b, Price 1981). Smaller lamellae of pleonaste appeared successively with increasing retrogression. The degree of

fractionation of minor elements between co-existing phases tends to increase with decrease in temperature.

Exsolution of ilmenite from haematite and haematite from ilmenite are restricted to deep-seated intrusions and are particularly characteristic of anorthositic association and other basic suits (Haggerty, 1976). The plane of exsolution is parallel to the (0001) rhombohedral direction and exsolution take place in accord with decomposition as a consequence of slow cooling and solvi-intersection. The growth and distribution of large and finer lamellae results in a syneusis texture i.e., with finer lenses of the solute (exsolving phase) distributed between thicker lenses in the solvent (host dissolving medium, Fig. 4.13). Under condition of prolonged cooling atoll textures formed due to diffusion of the solute migrates towards the crystal boundaries. Commonly, secondary and in some cases tertiary exsolution bodies within the primary



**Fig. 4.13: (a) and (b) Ilmenite lenses occur within the host titanohaematite. Individual grains show sharp termination (PPL).**

lamellae also present (Fig. 4.14). Kretchsmar and McNutt (1971) suggests that exsolution of composition with  $>Ilm_{85}$  is continuous, whereas with initial haematite enriched solid solution, exsolution proceeds discontinuously. This interpretation reflects in the textures illustrated in Fig. 4.15 and Fig. 4.16. There is a greater number of discontinuous or second-generation lenses of exsolved ilmenite solid solution in host grains of haematite solid solution members (Fig. 4.16). For the reverse relationship, the single generation constituents of exsolved haematite solid solution are relatively evenly distributed within hosts ilmenite solid solution (Fig. 4.15).

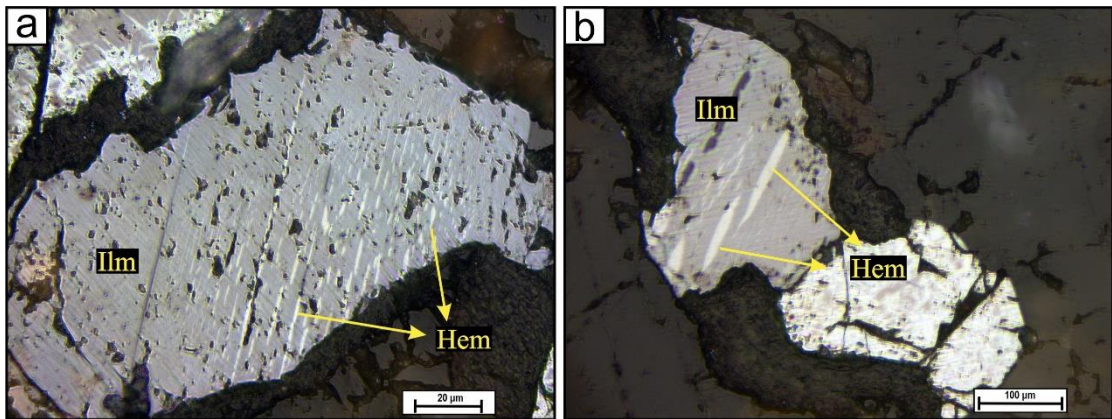


Fig. 4.14: (a) and (b) 2<sup>nd</sup> generation of exsolution lamellae within the primary exsolution lamellae within haematite ilmenite solid solution (PPL).

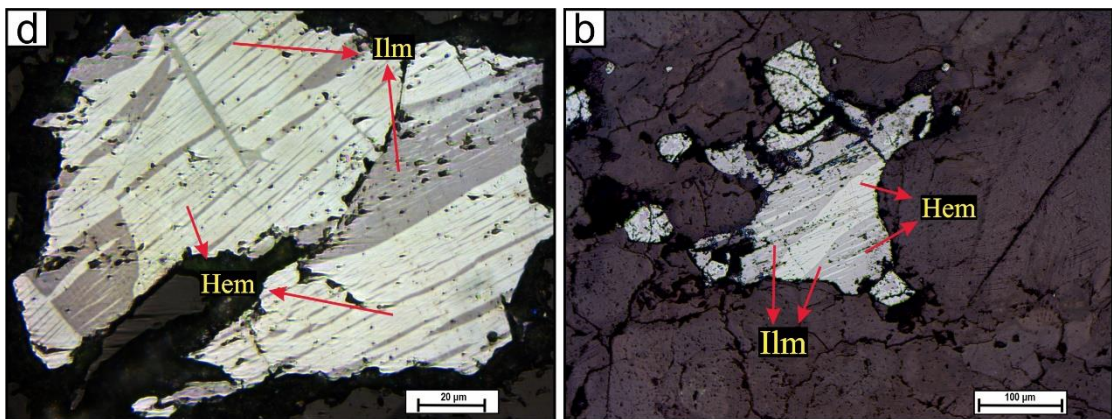


Fig. 4.15: (a) and (b) Reverse relationship is illustrated here for ilmenite hosts and haematite solid solution. The lenses are fine grained and zones of non-exsolution are concentrated along the grain boundary (PPL).

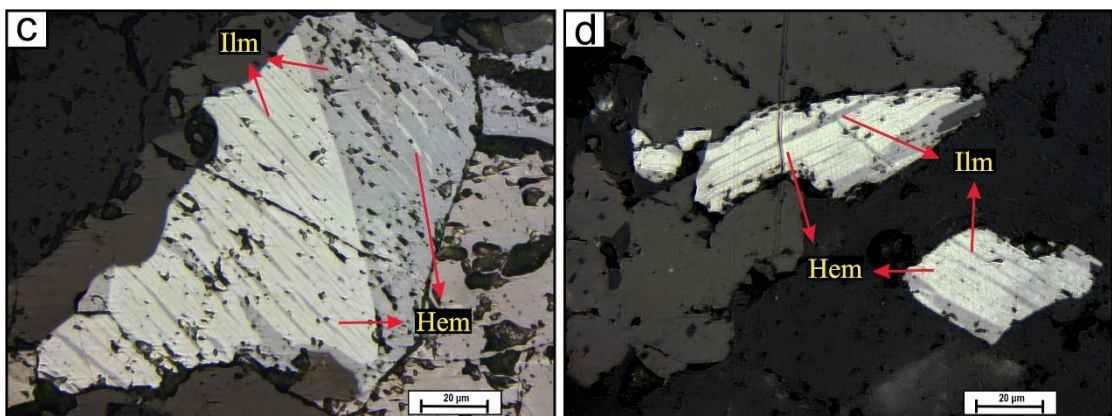


Fig. 4.16: (a) and (b) Both ilmenite and haematite exsolution within the haematite-ilmenite solid solution (PPL).

**(ii) Low temperature oxidation of Fe-Ti oxides:**

The effect of low temperature oxidation of Fe-Ti oxide entirely different from the high temperature oxidation of Fe-Ti oxide. At the time of low temperature (ambient surface temperature) oxidation, weathering of titanomagnetite or some hydrothermal alteration at  $T < 200^{\circ} \text{C}$  leads to the production of cation deficient spinel. This cation deficiency ultimately results in the formation of monophasic non-stoichiometric cation deficient spinel from magnetite, called maghemite ( $\gamma\text{-Fe}_2\text{O}_3$ ) which is chemically equivalent to haematite ( $\alpha\text{-Fe}_2\text{O}_3$ ) but retain the spinel crystal structure. This process of oxidation known as “Maghematization” (Fig. 4.2). The degree of oxidation increases with the increase of cation deficiency in the titanomagnetite-spinel lattice. During “Maghematization” migration of  $\text{Fe}^{2+}$  ions out of the titanomagnetite-spinel lattice occurs by diffusion producing vacancies (Prevot et al., 1968; Johnson and Melson, 1978; Johnson and Hall, 1978; Akimoto et al., 1984, Butler, 1992). Migration also includes some  $\text{Mg}^{2+}$  and  $\text{Mn}^{2+}$  and those migrations occurs due to high mobility of the cations (Akimoto et al., 1984).

The formation of irregular and curvilinear cracks in the titanomagnetite grains are remarkable morphological changes during progressive low temperature oxidation. These cracks were interpreted as the result of change (decrease) in volume due to creation of vacant spaces and these are termed as “shrinkage cracks” (Larson and Strangway, 1969; Johnson and Hall, 1978; Akimoto et al., 1984) within which silicate materials occurs through the cracks. The  $\text{Si}^{4+}$  content within the titanomagnetite is very low and are mainly carried from the surrounding silicate minerals, hydro-circulation being the most probable carrying mechanism of these, which further maintains the chemical potential gradient between the lattice and the environment (Akimoto et al., 1984). The hydro-circulation causes to develop a weak line where the internal stress concentrates and with the release of such internal stress, physical cracks occur (Akimoto et al., 1984).

Johnson and Hall (1978) classified five different stages on the basis of microscopic features associated with the progressive low temperature oxidation of Fe-Ti oxide. The five stages of low temperature oxidation of titanomagnetite are as follows.

- Stage-1:** Unoxidized titanomagnetite: Homogeneous titanomagnetite rich in high titanium, free of cracks (unoxidized).
- Stage-2:** Partial oxidation: The growth of very fine to submicroscopic cracks along the grain boundaries of titanomagnetite is indicated by the change into bright colour.
- Stage-3:** Formation of cracks: Cracks are curvilinear and prominent with the presence of some non-opaque minerals replacing original titanomagnetite towards their grain margins.
- Stage-4:** Formation of veins: Early formed cracks were filled with silicates and numerous new cracks developed from the earlier cracks as branches. Red pigmentary strain appears growing surrounding the silicates.
- Stage-5:** Relic grains: Isolated, bright, greyish white relic grains are left after almost complete replacement of titanomagnetite by non-opaque silicate minerals.

Different types of textural features of low temperature oxidation of titanomagnetite have been observed within the samples collected from the KPLC (KP-04, KP-07, KP-10, KP-15, KP-17, KP-19, KP-36). Titanomagnetite present within these studied samples have numerous visible microcracks shows grayish brown colour. Discrete ilmenites are also present but in very insignificant amount.

Under the reflected light microscopic studies of primary titanomagnetites in the rocks of KPLC revealed that they are oxidized to different stages of low temperature oxidation. The pattern and nature of formation of the cracks shows different textural features experienced by progressive low temperature oxidation. In Stage-1, homogeneous titanomagnetites are free of cracks with corrugated boundary (Fig. 4.17). Minor fine cracks are generated in homogeneous titanomagnetite from its grain boundary to its inner part in Stage-2 (Fig. 4.18). In case of Stage-3 these curvilinear cracks become wider due to further development of newly formed secondary cracks (Fig. 4.19a). In later stages of Stage-3, a third generation of linear cracks developed from secondary cracks. These are very short, fine and makes right angles with early formed cracks. All the cracks become interconnected with each other. So, the

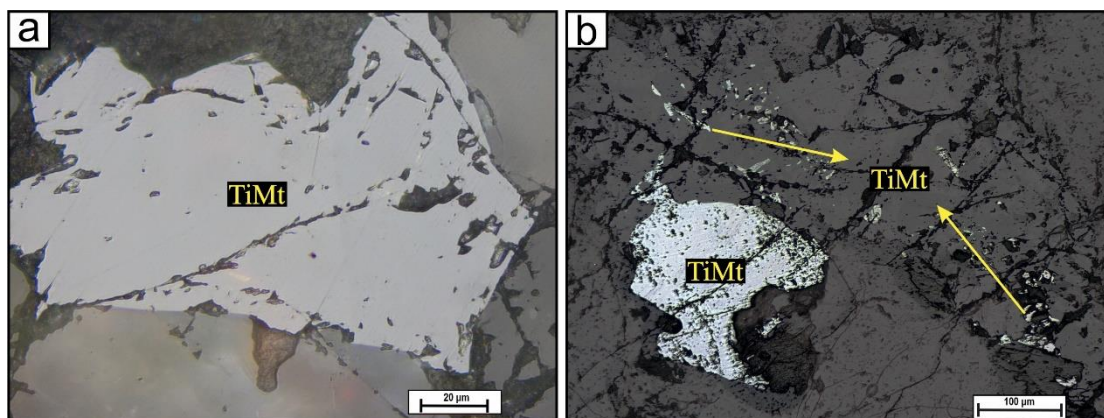


Fig. 4.17: (a) Stage-1 of Low temperature oxidation of titanomagnetite (PPL). (b) Two different generations of Fe-Ti oxide. Coarser one is primary titanomagnetite shows stage-1 of low temperature oxidation and finer one is secondary ferrimagnetic minerals (PPL).

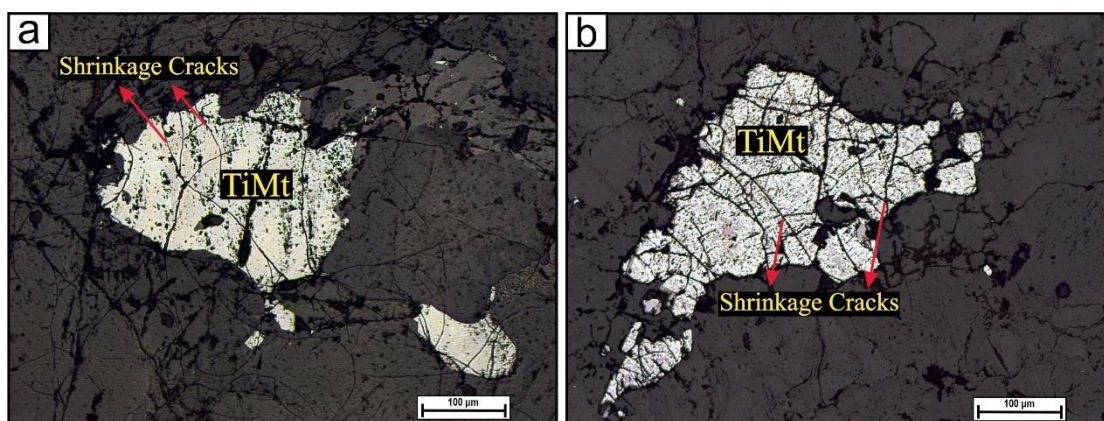
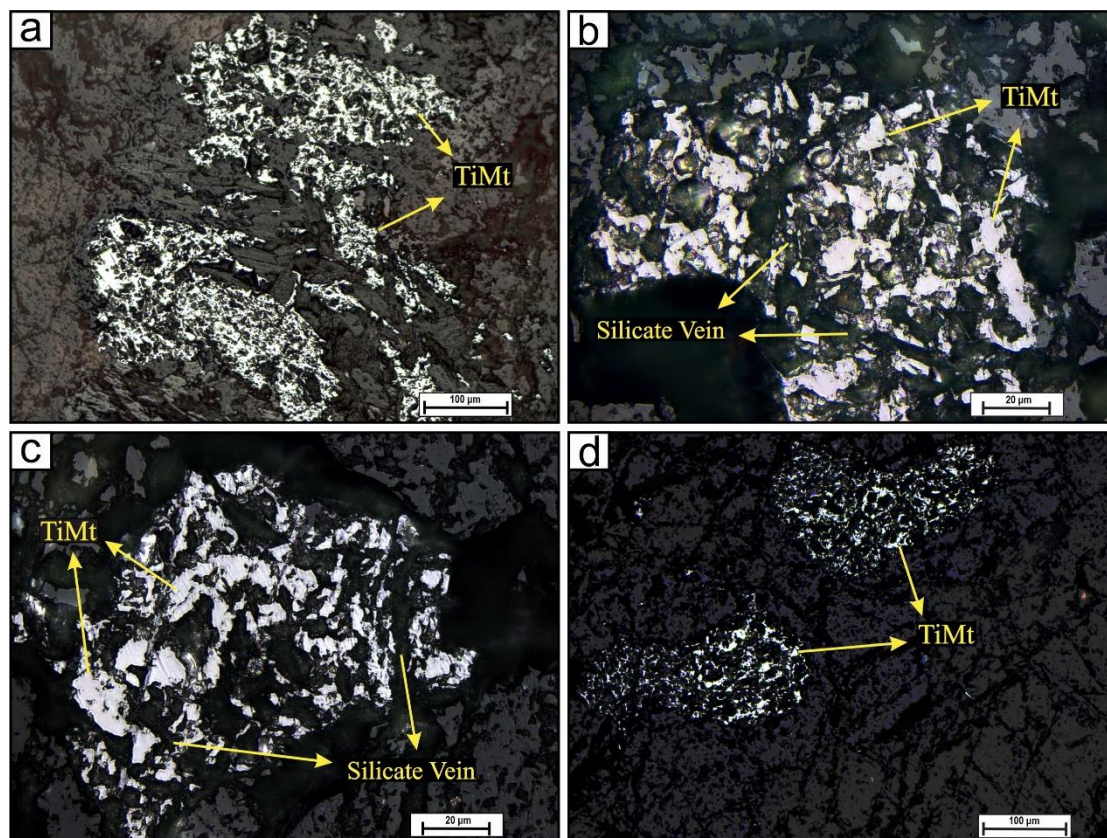


Fig. 4.18: (a) Stage-2 of Low temperature oxidation of titanomagnetite (PPL). (b) Porphyroblast of primary titanomagnetite shows Stage-3 of low temperature oxidation (PPL).

titanomagnetite grain appears as a fragmented grain, which is characteristic features of Stage-4 (Fig. 4.19b and Fig. 4.19c). Further with increasing degree of oxidation the cracks have expanded to a great extent so that an oxidized grain of titanomagnetite is found left with relicts of titanomagnetite in the Stage-5 of low temperature oxidation (Fig. 4.19d). Fine droplet like remains of titanomagnetites are present within the replaced silicate.

Titanomagnetites occurring in granulites and anorthosite of KPLC generally found to be oxidized to mainly Stage-2 (Fig. 4.18) and Stage-3 (Fig. 4.19a). At places low temperature oxidation goes up to Stage-5 (Fig. 4.19d). Most of the titanomagnetite grains show fine cracks and hence, appear to be feebly oxidized to Stage-2 and Stage-3 of low temperature oxidation. Stage-4 and Stage-5 of low temperature oxidation features are evident in few titanomagnetite grains within some sites (KP- 10, KP- 15,

KP- 19). They are found to be completely oxidized and replaced by silicate minerals leaving behind relicts of original titanomagnetite grains as island of microcrystalline titanomagnetite (Fig. 4.19d). In general, the titanomagnetite of the studied rocks shows large number of cracks indicating Stage-3 and Stage-4 of low temperature oxidation. So, “Maghematization” of titanomagnetite is intensely observed.



**Fig. 4.19:** (a) Stage-3 of Low temperature oxidation of titanomagnetite (PPL). (b) and (c) Transition between Stage-4 and Stage-5 (PPL). (d) Low temperature oxidation of primary titanomagnetite shows Stage-5 of low temperature oxidation (PPL).

It is evident from the reflected light studies that both high temperature and low temperature oxidation features of primary Fe-Ti oxide are present within high-grade metamorphic rocks of KPLC. It is also evident that the degree of oxidation not only varies among sites but also within a single site and sometimes within a single section of a particular rock. The granulite samples of the KPLC are dominated by both high temperature oxidation as well as low temperature oxidation while anorthosite and enderbite show mainly low temperature oxidation of Fe-Ti oxide. Beside Primary Fe-Ti oxide ultra-fine grains of secondary Fe-Ti oxides are also present within the studied rocks. Secondary Fe-Ti oxides are associated with other silicate minerals. There are



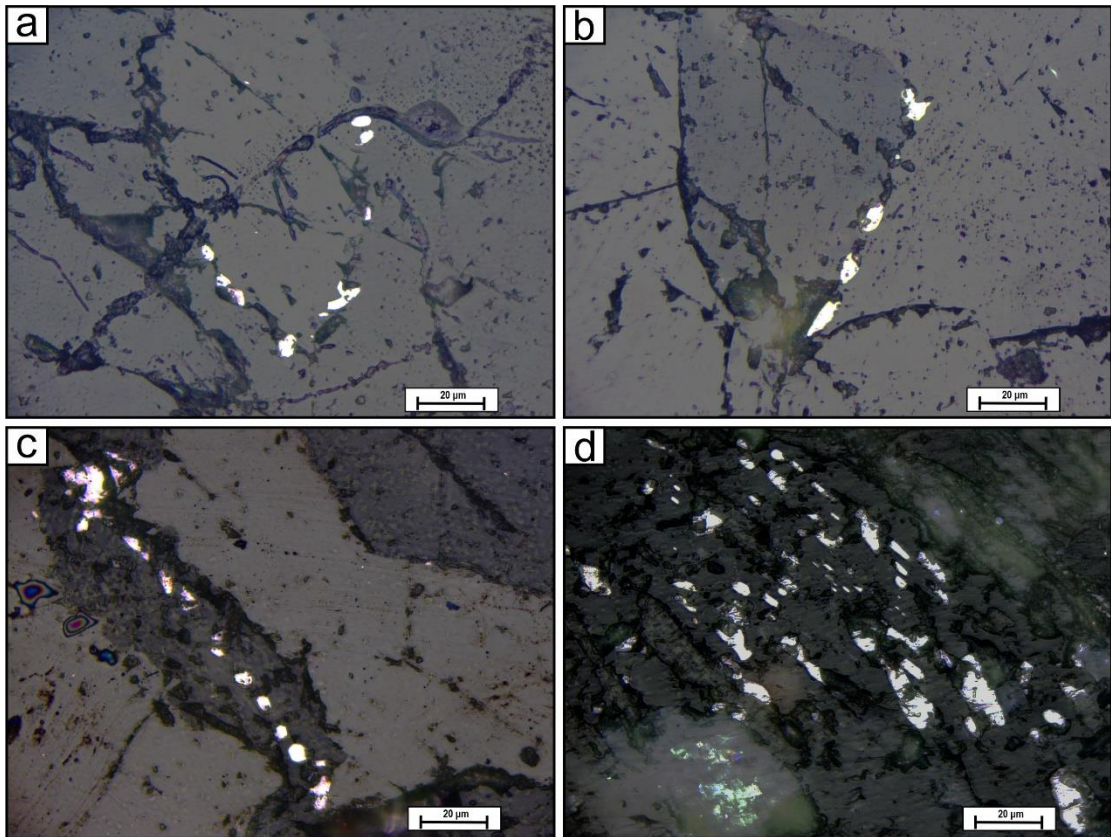


**Fig. 4.20:** (a) and (b) Ultra-fine grain of secondary magnetite along the grain boundary of coarse silicate minerals (PPL). (c) Ultra-fine grain of secondary magnetite along the late generation cracks of silicate minerals (PPL). (d) Ultra-fine grain of secondary magnetite along the cleavage plane of biotite (PPL).

three types of occurrences of secondary Fe-Ti oxide observed within the studied samples. One as very fine emulsion drops along grain boundaries of orthopyroxene and garnet (Fig. 4.20a, Fig. 4.20b). The others occur as microcrystalline / ultrafine grains of secondary magnetite occur along the fractures of orthopyroxene and garnet and along the cleavage planes of biotite (Fig. 4.20c, Fig. 4.20d).

### **4.3. Generations of Fe-Ti oxide and its tectonic implications**

The occurrence and abundance of Fe-Ti oxide minerals in high-grade metamorphic rocks of KPLC of EGB depends on (a) Lithology, (b) metastable phases of mineral assemblage present within the rocks, and (c) pressure and temperature of metamorphism, because the rock-forming minerals will react each other during metamorphism. The compositions of oxides, silicates, and sulfides are interrelated and

are controlled by oxygen fugacity as well as sulfur fugacity of fluid (Nesbitt, 1986a, b; Frost, 1988).

The major minerals as identified from the observations of thin sections under transmitted light microscope are plagioclase, K-feldspar, orthopyroxene, clinopyroxene and quartz with or without minor occurrences of garnet, amphibole and biotite. Grain

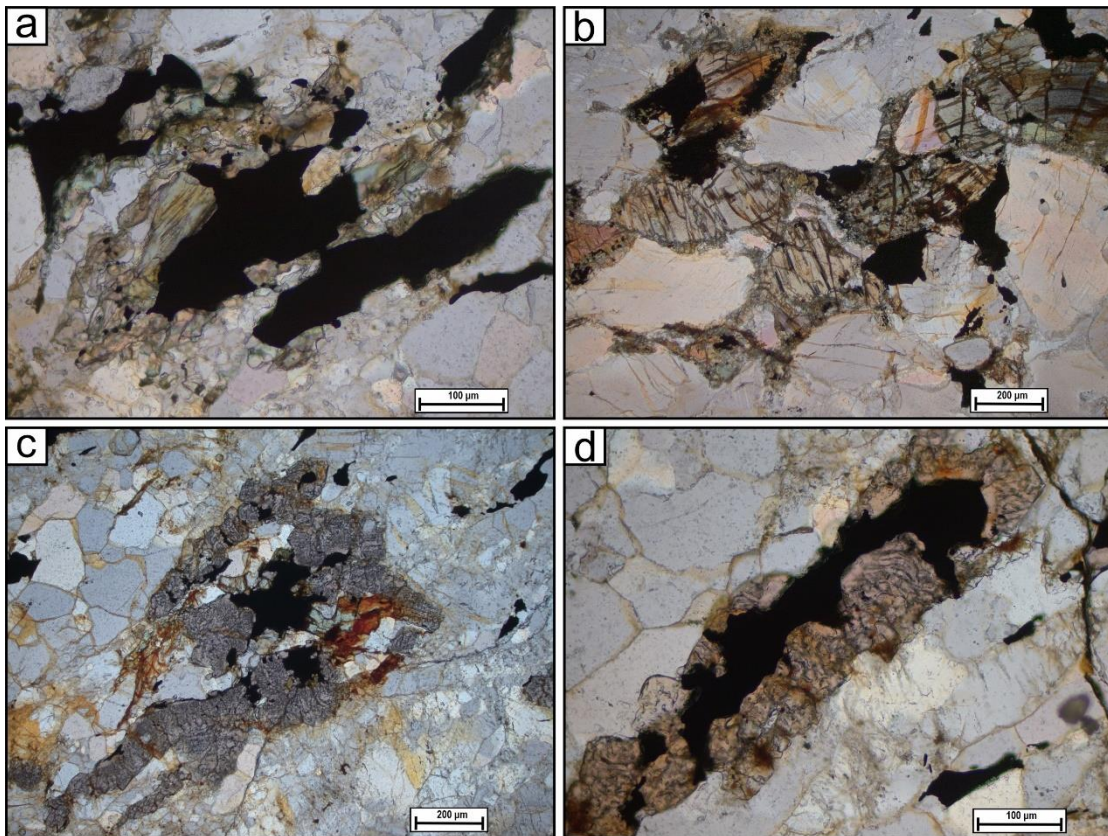


**Fig. 4.21:** (a) and (b) Opaque oxides associated with pyroxene (PPL). (b) and (c) Garnet rims around the opaque oxide (PPL).

sizes of opaque oxides are occurred within a large range from porphyroblast to ultra-fine grains. Opaque oxides are medium to coarse grained and associated with the pyroxenes and in the matrix (Fig. 4.21a, Fig. 4.21b). At places, secondary garnet rimming around the coarse grained primary titanomagnetite (Fig. 4.21c, Fig. 4.21d). Droplets of ultra-fine grained opaque minerals are observed along the fracture / cleavage planes of biotite and along the diffused pyroxene grain boundaries respectively (Fig. 4.22, Fig. 4.23).

The rocks from study area were metamorphosed under extreme pressure - temperature condition (above 8 Kb and  $\geq 1100$  °C) with an anticlockwise P-T trajectory

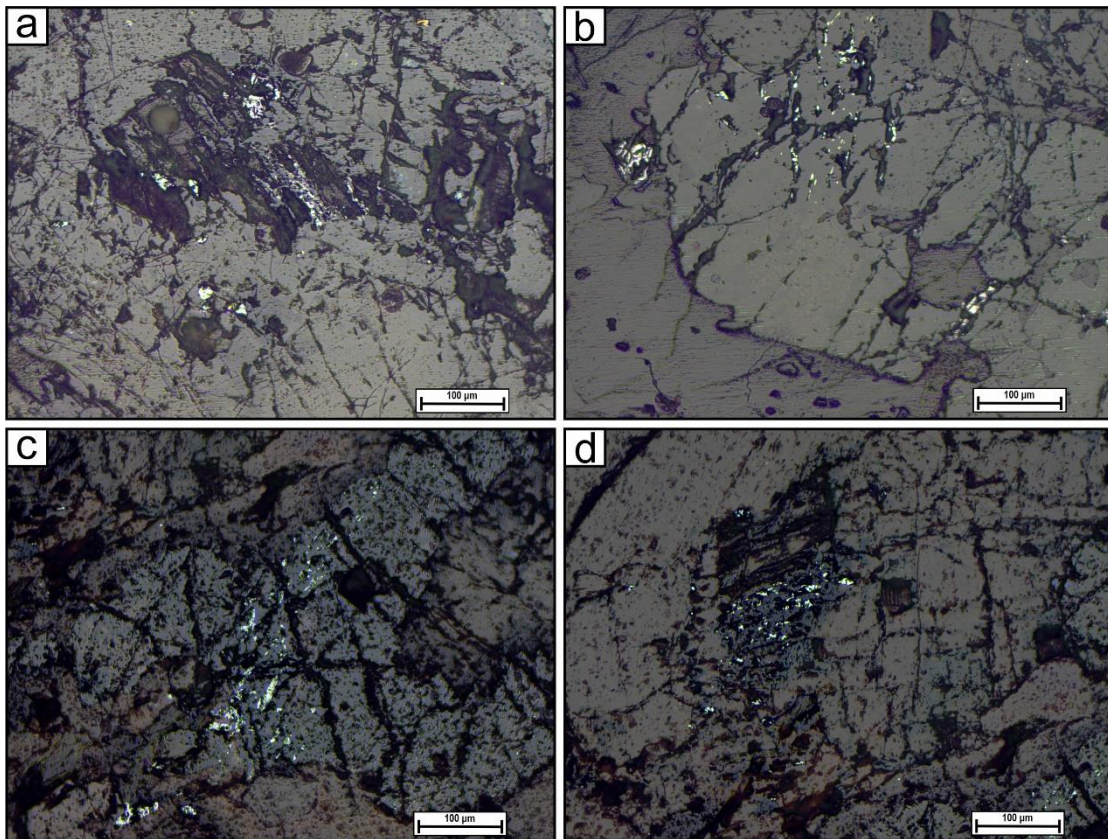


**Fig. 4.22:** (a), (b) and (c) Ultra-fine grain of secondary magnetite along the late generation cracks of silicate minerals (PPL). (d) Ultra-fine grain of secondary magnetite along the cleavage plane of silicate minerals (PPL).

comprising a prograde path and subsequent near-isobaric cooling (Sengupta et al. 1999). Study under the reflected light microscope shows that the dominant Fe-Ti oxides residing in the rocks from KPLC are titanomagnetite and ilmenite with minor amount of haematite, rutile and pleonastes. Both homogeneous and inhomogeneous oxide phases of the titanomagnetites occur within the studied samples, while ilmenite forms as exsolved lamellae within the inhomogeneous titanomagnetite. ‘Exsolution’ of ilmenite in titanomagnetite are restricted in few grains. Most of the titanomagnetite grains shows effect of low temperature oxidation. High-temperature and low-temperature oxidation enhances the possibility of recording stable magnetic remanences in the titanomagnetite grains because these oxidations reduce the effective grain size of the primary titanomagnetites.

From the textural relationship of Fe-Ti oxides in the studied rocks, three generations of Fe-Ti oxide are distinguished. (a) The first generation is primary homogeneous titanomagnetite, which are coarse to medium grained subhedral to

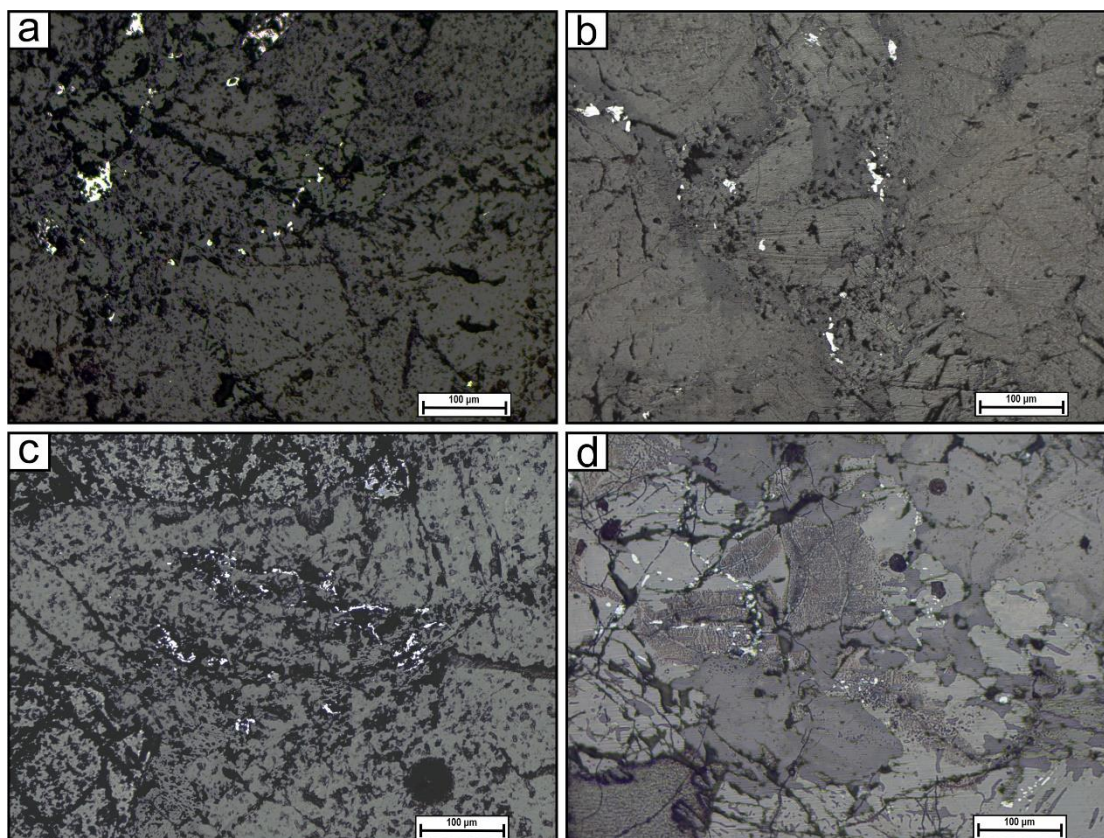


**Fig. 4.23: (a), (b), (c) and (d) Ultra-fine grain of secondary magnetite along the diffused grain boundary of coarse silicate minerals (PPL).**

anhedral occurring individually or associated with pyroxene (Fig. 4.4, Fig. 4.17). The complete solid solution of magnetite-ulvospinel take place only above  $\sim 600^{\circ}\text{C}$ . So, the homogeneous titanomagnetite crystallize at the peak P-T condition of granulite facies metamorphism (Zhang and Piper 1994). (b) The second generation is primary inhomogeneous titanomagnetite described by exsolved ilmenite lamellae within the host titanomagnetite grains (Fig. 4.5, Fig. 4.6) indicating a later thermo-tectonic event. This textural variation indicates that, this ferrimagnetic variety formed during cooling from peak metamorphic condition. (c) The third generation is secondary ultra-fine grained ferrimagnetic variety occurs along the diffused silicate grain boundaries (Fig. 4.20a, Fig. 4.23), along the fracture planes of silicate minerals (Fig. 4.20c, Fig. 4.23a and Fig. 4.23b) and along the cleavage planes of silicates (Fig. 4.20d, Fig. 22c and Fig. 22d). During later stage tectonic upliftment and cooling of high-grade metamorphic terrane, the release of pressure produces solution cracks along the silicate grain and secondary ferrimagnetic variety developed (Hay et al., 1988; Bay et al., 2011).

The primary homogeneous titanomagnetite of KPLC are medium to coarse-grained indicating a slow cooling during prolonged period of metamorphism. The inhomogeneous primary titanomagnetite with the signature of early stages of high temperature oxidation indicate that, these rocks suffered a prolonged period of high temperature metamorphism and followed by upliftment with slow cooling. The presence of exsolution of pleonaste within titanomagnetites indicate that, the studied rocks attained the peak-metamorphic condition, then retrograded to relatively lower grade.

All the features described above suggest that, the rocks from KPLC, which have been studied with the aim of providing some magnetic signatures, are useful for the rock magnetic and palaeomagnetic study leading to identification of pole positions and apparent polar wandering path (APWP) construction for the Indian subcontinent during the Paleoproterozoic-Mesoproterozoic period.

**Chapter 5**  
**Anisotropy of Magnetic**  
**Susceptibility Study**

# ANISOTROPY OF MAGNETIC SUSCEPTIBILITY STUDY

## 5.1. Introduction

Anisotropy of Magnetic Susceptibility (AMS) is a non-destructive technique which represent preferred orientation of magnetic minerals within a rock. The magnetic susceptibility in a natural rock is not always uniform in all directions, it varies in all directions. The variation of magnetic susceptibility with direction is called the Anisotropy of Magnetic Susceptibility (Hrouda, 1982; Tarling and Hrouda, 1993). Maximum susceptibility axis ( $K_1$ ), intermediate susceptibility axis ( $K_2$ ) and minimum susceptibility axis ( $K_3$ ) are the three principal directions along which the numeric values of magnetic susceptibility is maximum, intermediate and minimum respectively where  $K_1 \geq K_2 \geq K_3$ . The fabric developed within a rock defined by these three lineation axes is termed as magnetic fabric. Voight and Kinoshita (1907) considered this AMS technique for fabric studies and later used as a petro-fabric indicator (Ising, 1942; Graham, 1954; Graham, 1966). AMS is a second rank tensor and geometrically represented by a triaxial ellipsoid called susceptibility ellipsoid. The axes of the susceptibility ellipsoid are the three principal susceptibility axes  $K_1$ ,  $K_2$  and  $K_3$  (Tarling and Hrouda, 1993).

The AMS of rocks serves information about the susceptibility and orientation of the grains as it controlled by preferred orientation of magnetic mineral grains. The minerals within a rock and their AMS characteristics, helps to determine the spatial distribution of the grains and the geological processes involved such as water flow in sediments, magma flow in igneous rock, ductile deformation in metamorphic rocks.

To represent the AMS data to determine the petro-fabric of the rocks under study, the values of magnetic foliation (F), magnetic lineation (L), corrected degree of anisotropy ( $P_j$ ), shape parameter (T) and mean susceptibility ( $K_m$ ) were calculated based on the following equations (summarised by Tarling and Hrouda, 1993):

$$\text{Mean Susceptibility } (K_m) = (K_1 + K_2 + K_3) / 3 \quad (\text{Nagata, 1961})$$

$$\text{Magnetic Lineation } (L) = K_1 / K_2 \quad (\text{Balsley and Buddington, 1960})$$

Magnetic Foliation (F) =  $K_2/K_3$  (Stacey et al., 1960)

Corrected degree of anisotropy,

$P_j = \exp \{2[(n_1-n_m)^2 + (n_2-n_m)^2 + (n_3-n_m)^2]\}^{1/2}$ ; where  $n_i = \log K_i$  (Jelinek, 1981)

Shape parameter  $T_j = (2n_2-n_1-n_3) / (n_1-n_3)$ ; where  $n_i = \log K_i$  (Hrouda, 1982)

The parameter  $P_j$  is considered more intrinsic because, it depends on both  $K_1$ ,  $K_2$ ,  $K_3$  and  $K_m$ . The value of the shape parameter (T) lies within -1 and +1, i.e.,  $-1 < T < +1$ .

It is evident that, these parameters are functions of  $K_1$ ,  $K_2$ ,  $K_3$ , which are the magnitude of the principal susceptibility axes and are represented as the axes of an imaginary ellipsoid called susceptibility ellipsoid. Based on these parameters, the shape and magnitude of the magnetic fabrics are classified: disc shaped or oblate ellipsoid ( $K_1 = K_2 > K_3$ ), cigar shaped or prolate ellipsoid ( $K_1 > K_2 = K_3$ ) and triaxial ( $K_1 > K_2 > K_3$ ). Jelinek Plot (after Jelinek, 1981; Hrouda, 1982) of  $P_j$  versus T helps to determine the shape of the magnetic susceptibility ellipsoid.  $K_m$  versus  $P_j$  plot helps to determine the control of the maximum susceptibilities on the degree of anisotropy. To represent the direction of the magnetic susceptibility, the direction of the principle magnetic susceptibility axes are plotted on a lower hemisphere equal area diagram. The  $K_1$ ,  $K_2$  and  $K_3$  are plotted as solid squares, triangles and circles respectively. The plane passing through  $K_1$  axes and  $K_2$  axes is the trace of magnetic foliation and  $K_1$  represents the magnetic lineation.  $K_3$  also represent the pole to the magnetic foliation.

## 5.2. AMS and magnetic fabrics in Rocks of KPLC

### 5.2.1. Introduction

Magnetic fabrics of the high-grade metamorphic rocks are important as it is often related to the metamorphic and tectonic events experienced by a particular geological terrain (Tarling and Hrouda, 1993). AMS analysis is excellent tools for studying deformation and tectonics related fabric development, especially in metamorphic rocks (Hrouda and Janak, 1976; Pares and van der Pluijm, 2002; Ferre et al., 2004). Also, in metamorphic terrains, the AMS ellipsoids are useful indicators of the geometry of the magnetic fabric elements (Borradaile, 1991; Borradaile and Alford,



1987; Till et al., 2010; Ferre et al., 2014; Pares and van der Pluijm, 2002). The geometry of the magnetic fabrics along with the structural data can resolve complex tectonic problems with high precision (Pomella et al., 2011; Georgiev et al., 2014). Large scale deformations can also be traced from AMS signatures (Cifelli et al., 2004, 2009; Borradaile and Jackson, 2004; Agarwal et al., 2021). The high-grade metamorphic rocks form the bulk of the continental crust and are exposed in several geological terrains, but are the least studied in terms of magnetic properties in the Indian context (Raposo and Egydio-Silva, 2001; Viegas et al., 2013). Thus, these terrains are ideal for studying rock magnetic properties and magnetic fabrics in relation to tectonics. The EGB is remarkable among them. AMS has been used in understanding deformation and fabric patterns in high-grade metamorphic rocks (Fodor et al., 2020; Viegas et al., 2013; Ferre et al., 2014; Ferre et al., 2004). Magnetic fabric studies and their tectonic implications are reported in some other metamorphic terrains like the Chhotanagpur Granite Gneissic Complex (Chatterjee et al., 2018b) and Southern Granulite Terrain (Mondal et al., 2009). In this chapter, detailed study of AMS has been done to derive the magnetic fabrics and relate them to the mesoscopic fabrics and tectonics of the KPLC.

The major structural elements that are reported in the KPLC from the present study are represented in lower hemisphere equal area diagrams in (Fig. 5.1) and described earlier. As described earlier, among the 26 block samples, 8 were mafic granulite, 7 were opx-granulite, 3 samples each from anorthosite, leptynite, and enderbite, and 2 from khondalite. From the blocks, a total of 161 cores (height 2.2 cm and diameter 2.54 cm) were drilled out for AMS analysis (6–8 cores per block). Besides, a sufficient amount of mesoscopic structural data was collected for the different structural elements encountered in the field.

The low field AMS analysis was carried out at 0.46 kHz using an MS-2 Susceptibility Meter (Bartington, UK), housed in the Geophysical Laboratory, Department of Geological Sciences, Jadavpur University, Kolkata 700032, India. The Bartington MS-2 Susceptibility Meter works in synchronous operation with the AMS-Bar software which measures the susceptibility of the samples in 18 different orientations. Based on the measurements in these 18 orientations, the directions of the principal susceptibility axes along with the corresponding susceptibility values and

different parameters are provided as output.

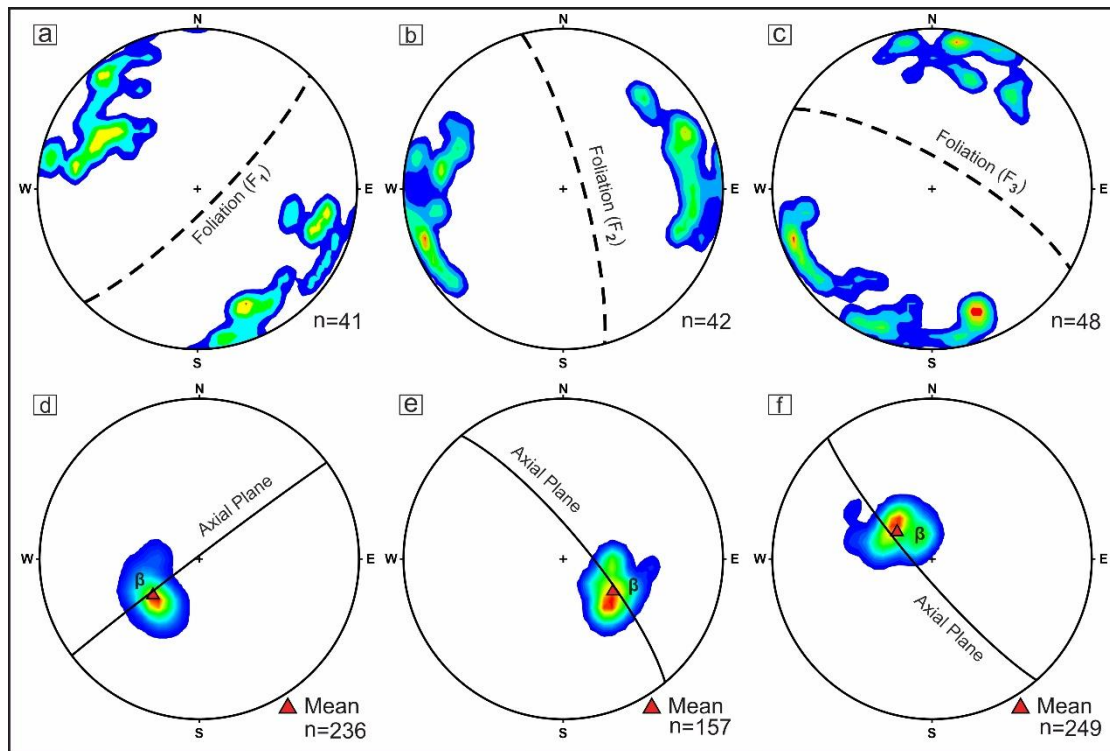


**Fig. 5.1: Mesoscopic fabrics (field data) in the KPLC. Fold axes and corresponding axial planes are averaged using the  $\beta$  pole.**

### 5.2.2. Low field magnetic susceptibility and anisotropy

As the parameters related to AMS are dependent on the rock types, the sample-wise variation of AMS parameters in the KPLC is provided in Table 5.1. The average distribution of the AMS parameters based on the rock types is provided in Table 5.2. The mean magnetic susceptibility ( $K_m$ ) varies from  $0.24 \times 10^{-4}$  SI to  $9.52 \times 10^{-4}$  SI with a standard deviation of  $6.14 \times 10^{-4}$  SI. The highest magnetic susceptibilities are observed in the opx-granulite and khondalite whereas the lowest values are observed in the enderbite. The corrected degree of anisotropy ( $P_j$ ) has a nearly uniform value throughout the study area (Table 5.1) with an average of 1.39. The standard deviation for the same is also 0.08 which is much lower corroborating the contention. The values of  $P_j$  in the rocks range from 1.4 to 1.5 except in those of the mafic granulite where it is 1.10. Thus, although the values range within certain limits, they have values  $>1.05$  which is the threshold value for a magnetic fabric to be tectonically controlled (Mondal et al., 2022; Chatterjee et al., 2018a; Tarling and Hrouda, 1993; Dvorak and Hrouda,

**Table 5.1: The AMS data from representative samples of different rock types in the KPLC.**

Site No.	Rock type	No. of cores	$K_1 (D^\circ/I^\circ)$	$\alpha_{95}$ for $K_1$	$K_3(D^\circ/I^\circ)$	$\alpha_{95}$ for $K_3$	F	L	$P_j$	T	$K_m (\times 10^{-4} S I)$
KP-2	Opx-Granulite	8	162.3 / 5.7	12.9	340.8 / 85.2	6.9	1.18	1.02	1.80	0.62	1.66
KP-3	Opx-Granulite	6	240.6 / 3.4	26.4	47.1 / 78	10.4	1.23	1.01	1.43	0.72	0.26
KP-4	Anorthosite	6	306.6 / 9.8	6.5	53.7 / 73	3.9	1.44	1.08	1.27	-0.10	2.87
KP-5	Anorthosite	8	128.9 / 5.4	10.7	22.9 / 73.5	9.3	1.25	1.13	1.39	0.85	8.60
KP-7	Opx-Granulite	6	323.8 / 14	11.2	82.1 / 62.3	5.5	1.30	1.12	1.60	0.65	22.12
KP-10	Leptynite	6	212.9 / 2.1	24.6	326.7 / 85.4	2.9	1.33	1.04	1.37	0.67	18.03
KP-12	Opx-Granulite	6	125.5 / 16.6	52.2	356.1 / 76	10.8	1.23	1.04	1.44	0.36	0.49
KP-14	Mafic Granulite	6	243.2 / 13.8	13.8	50.5 / 80.1	7.8	1.18	1.06	1.32	-0.41	0.35
KP-15	Mafic Granulite	6	212.3 / 16.8	10.1	103.1 / 56	27.8	1.16	1.19	1.39	-0.53	2.00
KP-16	Opx-Granulite	7	163.3 / 1.2	6.9	68.6 / 85.7	1.7	1.52	1.04	1.46	0.40	16.77
KP-17	Anorthosite	6	213.4 / 26.8	10.2	33.9 / 65.4	23.4	1.08	1.25	1.65	-0.49	5.68
KP-19	Mafic Granulite	6	139.6 / 6.2	14.8	227.4 / 85.1	5	1.40	1.07	1.48	0.10	3.69
KP-21	Mafic Granulite	6	254.1 / 4.2	11.2	16.5 / 80.8	4.1	1.19	1.06	1.55	0.04	0.67
KP-22	Mafic Granulite	6	16.9 / 6.5	7.2	89.5 / 82.8	16.7	1.21	1.08	1.27	0.27	0.75
KP-25	Khondalite	6	32.08 / 5.3	4.5	183.8 / 20.8	16.7	1.10	1.25	1.61	0.34	6.51
KP-26	Khondalite	6	34.4/44.2	7.6	158.8 / 25.2	21.7	1.09	1.33	1.45	0.43	11.04
KP-27	Mafic Granulite	6	345.8 / 10.5	9	247.9 / 32.5	18.6	1.10	1.07	1.27	0.39	5.42
KP-28	Mafic Granulite	6	122.6 / 17.8	11.4	273.4 / 68.7	5.4	1.26	1.22	1.94	-0.47	9.33
KP-31	Leptynite	6	328.6 / 34.0	19.1	129.8 / 55.8	12.1	1.16	1.09	1.55	0.52	3.24
KP-33	Enderbite	6	226.5 / 21.1	42.9	39.5 / 79.5	17.2	1.58	1.19	1.37	0.46	0.07
KP-35	Mafic Granulite	6	22.9 / 12.9	9.2	121.3 / 45.3	21	1.10	1.29	1.44	0.10	12.18
KP-36	Leptnite	6	134.1 / 2.6	5.1	221.9 / 65.1	4.8	1.29	1.23	1.27	0.41	7.28
KP-38	Enderbite	6	223.8 / 10	23.8	81.3 / 76.6	23.7	1.27	1.13	1.47	0.46	0.24
KP-39	Enderbite	6	189.1 / 7.7	14.1	17.6 / 83.4	7.2	1.24	1.09	1.37	1.17	0.42
KP-42	Opx-Granulite	6	170.1 / 3.61	5	274.6 / 75.8	2.4	1.31	1.10	1.43	0.78	3.75
KP-43	Opx-Granulite	6	142.1 / 7.3	50.5	259.3 / 79.8	6.3	1.22	1.04	1.30	0.73	0.45

**Table 5.2: Mean values of AMS parameters for the different rock types in the KPLC.**

Rock type	Mean Susceptibility ( $K_m$ )	Foliation (F)	Lineation (L)	Degree of Anisotropy ( $P_j$ )	Shape Parameter (T)
Opx-granulite	$6.50 \times 10^{-4} SI$	1.28	1.05	1.49	0.66
Mafic Granulite	$4.3 \times 10^{-4} SI$	1.13	1.2	1.10	0.21
Anorthosite	$5.72 \times 10^{-4} SI$	1.26	1.15	1.44	0.19
Leptynite	$9.52 \times 10^{-4} SI$	1.26	1.12	1.40	0.38
Enderbite	$0.24 \times 10^{-4} SI$	1.14	1.14	1.40	0.38
Khondalite	$8.76 \times 10^{-4} SI$	1.1	1.29	1.53	0.46

1975). Thus, the magnetic fabrics are controlled tectonically. Also, the  $K_m$  and  $P_j$  do not show a positive correlation in the plot (Fig. 5.2). The magnetic foliation (F) averages at 1.19 and that of magnetic lineation (L) is 1.16 and they are near-constant throughout

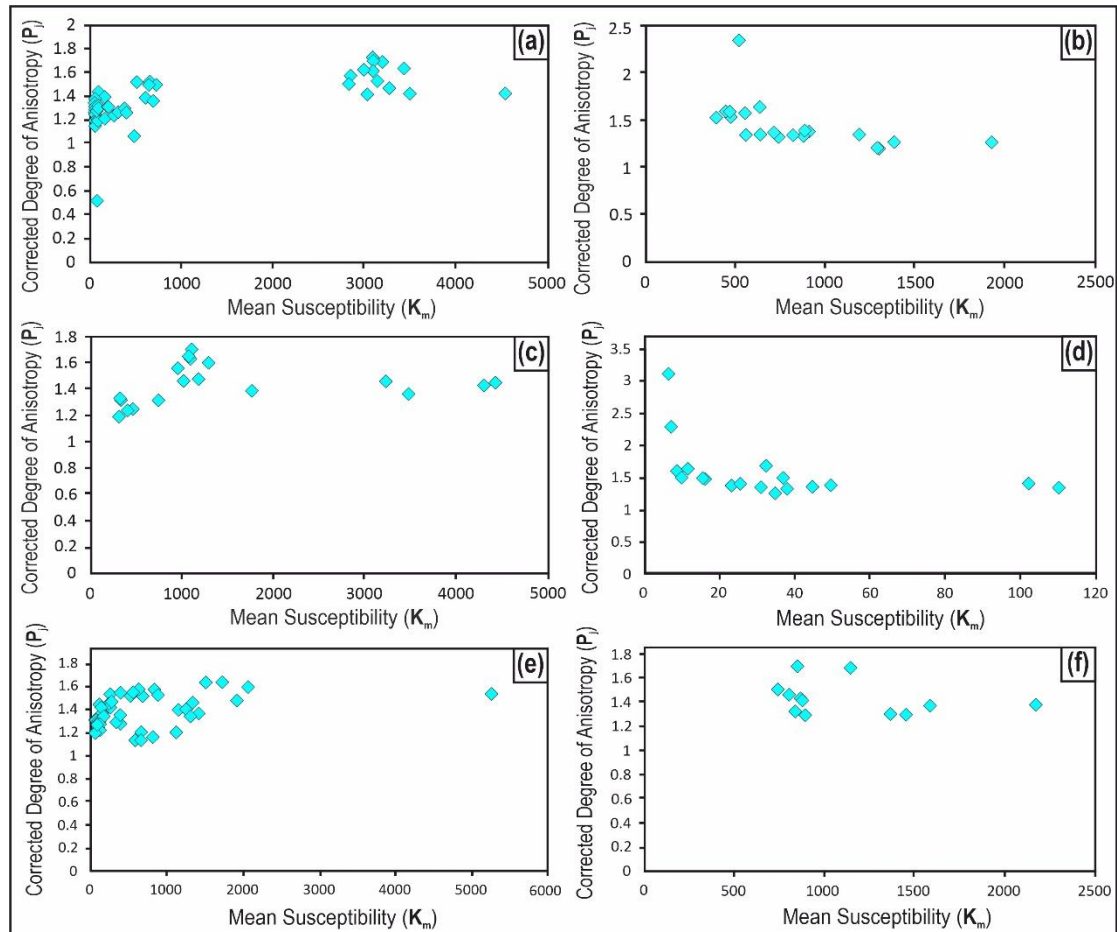


**Fig. 5.2:**  $K_m$  versus  $P_j$  plots for the (a) Opx-granulite, (b) Anorthosite, (c) Leptynite, (d) Enderbite, (e) Mafic Granulite, (f) Khondalite.

the studied area. The shape parameter (T) varies from - 0.46 (for khondalite) to 0.66 (for the opx-granulite). However, khondalite is the only exception with  $T < 0$ . Evidently in the  $P_j$  versus T plots, the Khondalite display prolate ellipsoids, whereas, in the other rocks, the shape of the susceptibility ellipsoids varies within a range from oblate to prolate (Fig. 5.3).

### 5.2.3. Magnetic Fabrics

The distribution of the maximum, ( $K_1$ ), intermediate ( $K_2$ ), and minimum ( $K_3$ ) susceptibility axes is shown in Fig. 5.4. The  $K_1$  (magnetic lineation) and the  $K_2$  are distributed throughout the periphery, and  $K_3$  (poles to magnetic foliation) clusters at

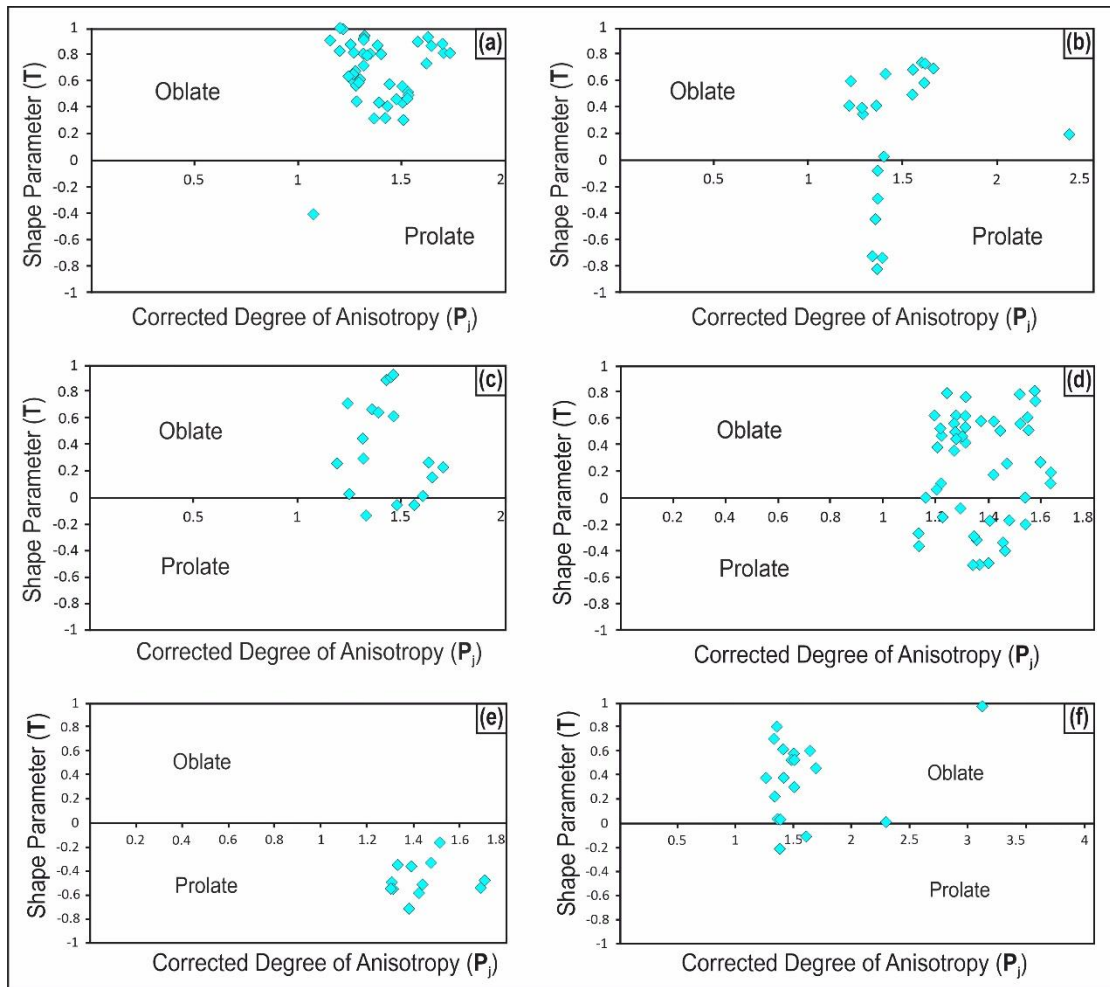


**Fig. 5.3:**  $P_j$  versus  $T$  plots for the (a) Opx-granulite, (b) Anorthosite, (c) Leptynite, (d) Enderbite, (e) Mafic Granulite, (f) Khondalite.

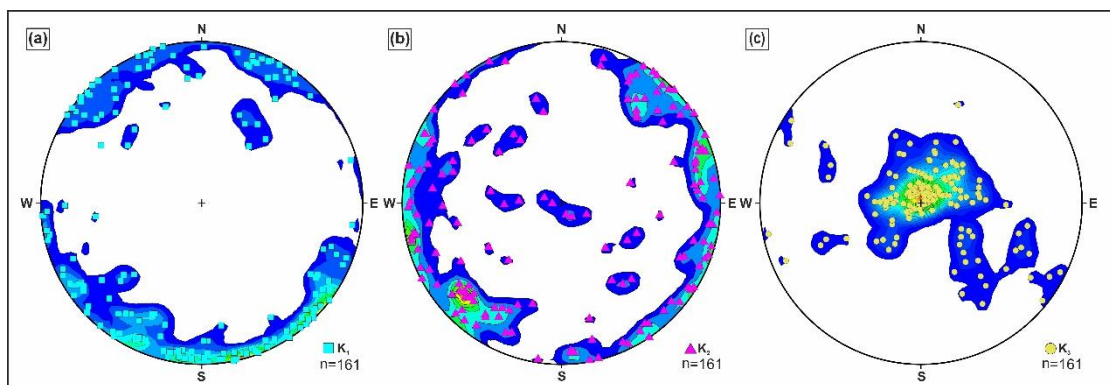


**Fig. 5.4:** Overall distribution of the maximum ( $K_1$ ), intermediate ( $K_2$ ), and minimum ( $K_3$ ) susceptibility axes over the studied area.

the centre, irrespective of the rock types. However, as evident from the  $\alpha_{95}$  values, the clusters are stronger in granulites, leptynite, and anorthosite (average  $\alpha_{95}$  ranging within 6–12) than the khondalite and enderbite (average  $\alpha_{95}$  ranging within 16–19).

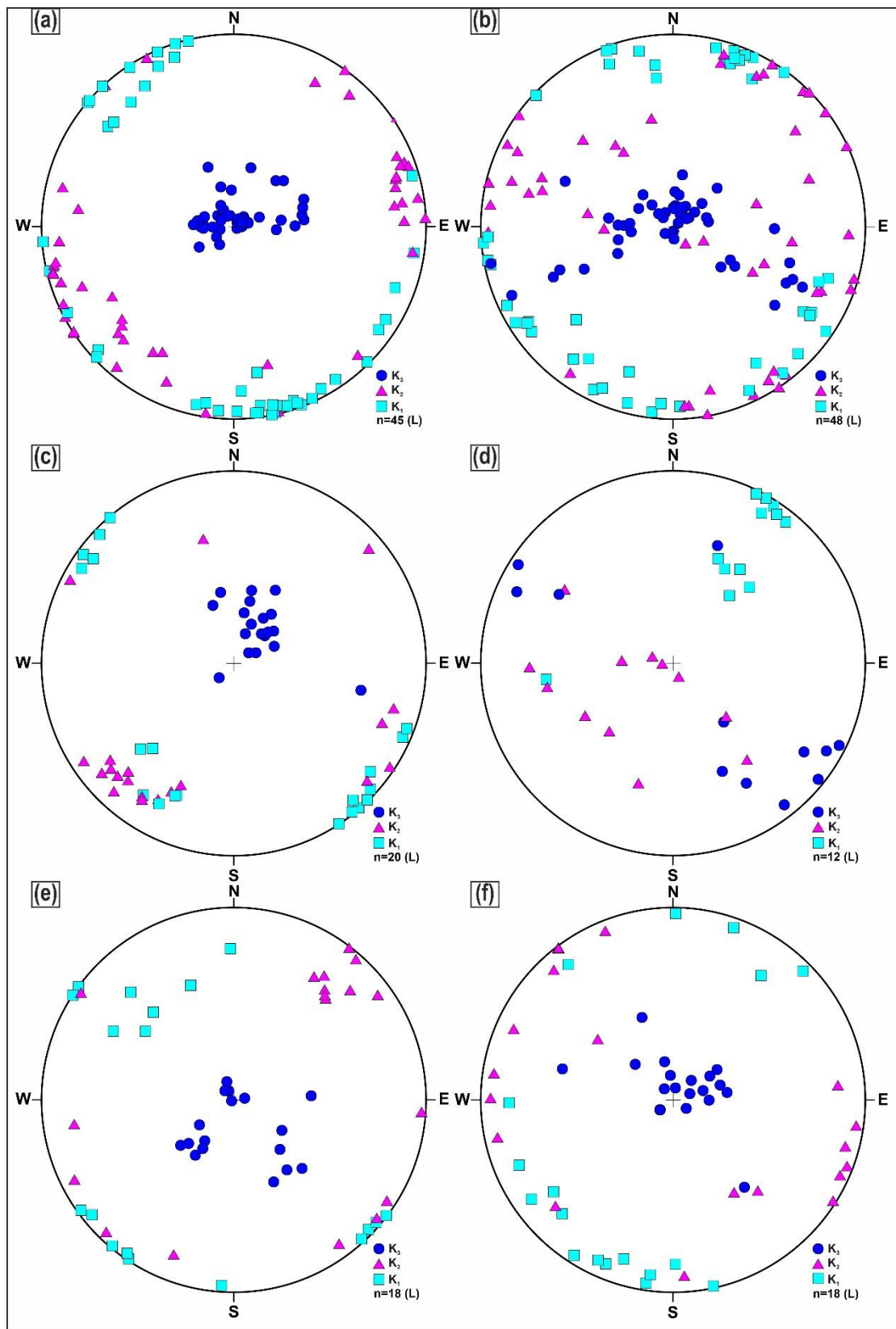


Fig. 5.5: Stereographic projections of the principal susceptibility axes for different rock types in the study area. for the (a) Opx-granulite, (b) Mafic Granulite, (c) Anorthosite, (d) Khondalite. (e) Leptynite, (f) Enderbite.

These show that the magnetic lineation, as well as the foliation, are near horizontal which is common in high-grade rocks (Chatterjee et al., 2018b). The magnetic fabric elements in individual rock types are shown in Fig. 5.5. Although the magnetic lineation is consistently horizontal, their trend varies lithologically. It trends NW-SE in the opx-granulite and anorthosite; NE-SW in the khondalite and enderbite and varies within NW-SE and NE-SW in the mafic granulite and the leptynite. The distribution of the magnetic fabrics in the KPLC is provided by the magnetic foliation map (Fig. 5.6) and lineation map (Fig. 5.7).

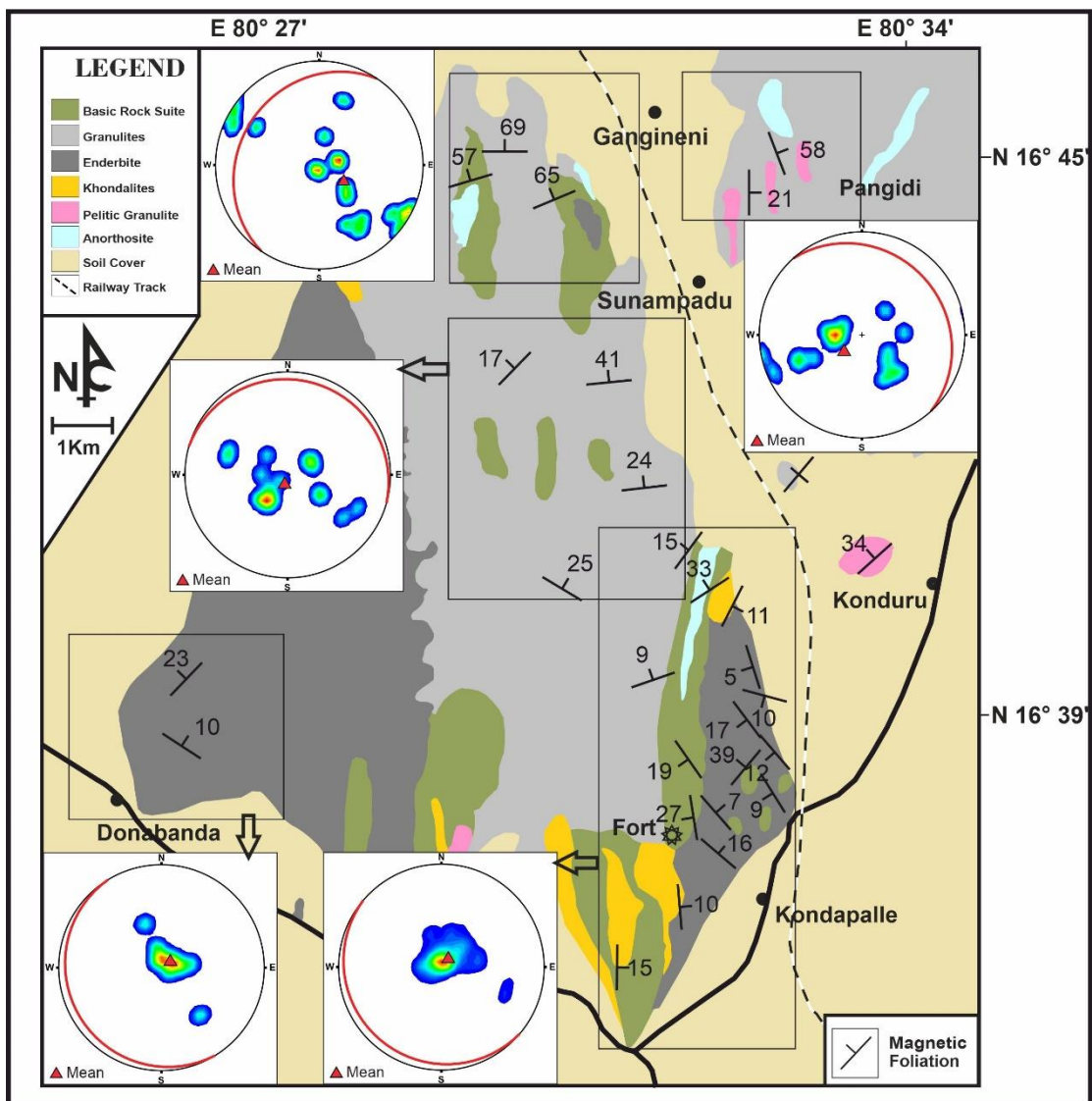


Fig. 5.6: Distribution of the magnetic foliation in the KPLC. The average foliation planes for each sector are represented by the equal-area diagrams.

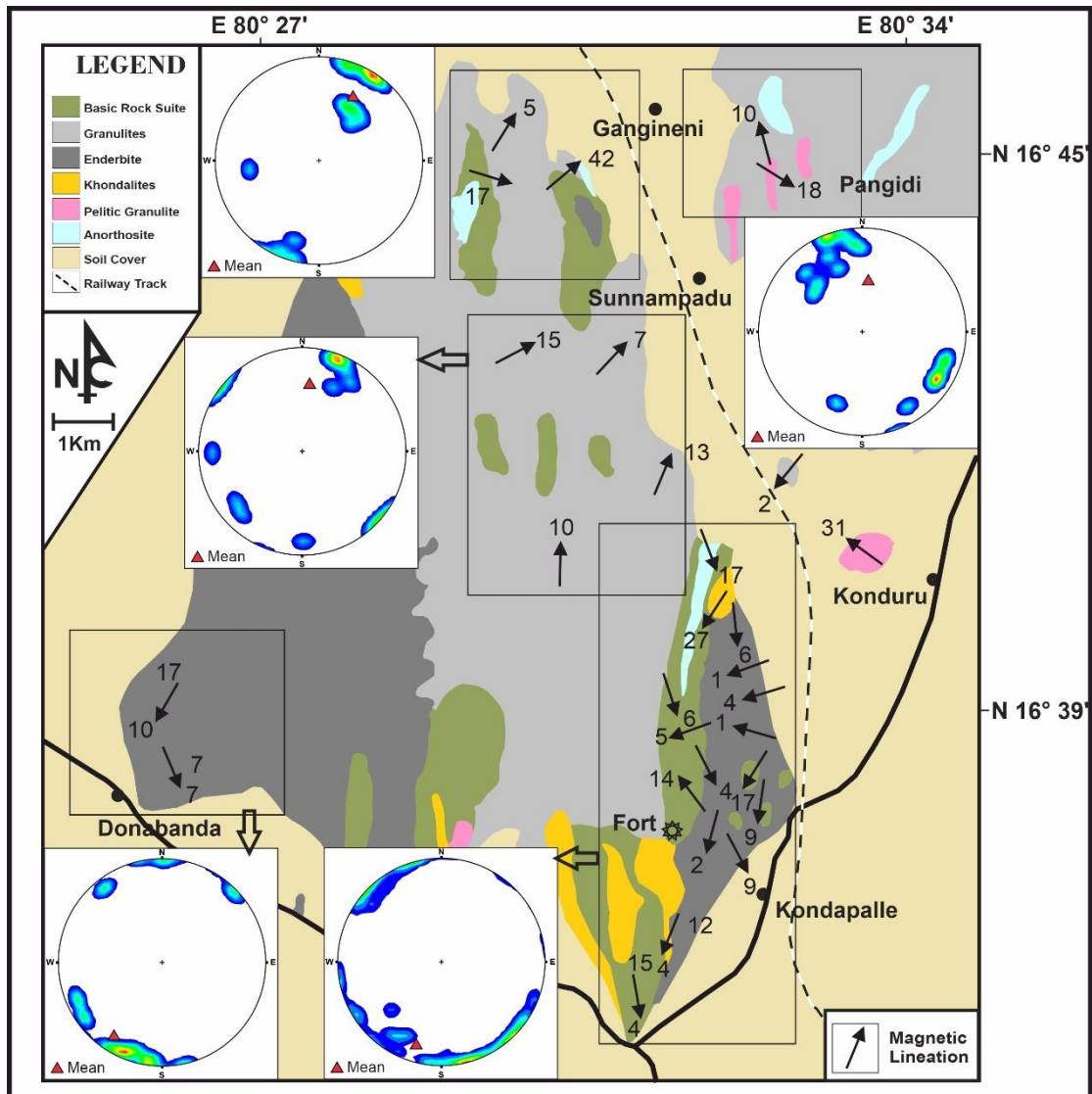


Fig. 5.7: Distribution of the magnetic lineation in the KPLC. The average foliation planes for each sector are represented by the equal-area diagrams.

#### 6.2.4. Magnetic fabric versus mesoscopic fabric

The  $P_j$  values are almost uniform throughout the rock types with an average of 1.45 (Table 5.1). There exists no positive correlation between  $K_m$  and  $P_j$ . It is  $P_j$  that quantifies the extent to which the magnetic fabrics are developed (Tarling and Hrouda, 1993) and  $K_m$  quantifies the amount of ferrimagnetic minerals (Lamali et al., 2013; Basavaiah, 2011; Basavaiah and Khadkikar, 2004; Borradaile et al., 1999). Thus, the negative correlation (or independence) between  $K_m$  and  $P_j$  proves that the magnetic fabrics are controlled by the paramagnetic ones (Fig. 5.2). As the control over the anisotropy is taken by the paramagnetic minerals, the anisotropy will be shape preferred



of the paramagnetic silicates which is in turn related to the mesoscopic fabrics (Tarling and Hrouda, 1993; Borradaile and Jackson, 2004; Mamtani et al., 2013, 2019; Mondal, 2018; Mondal and Mamtani, 2014; Mamtani and Greiling, 2005; Schobel and deWall, 2014).  $K_1$  and  $K_3$  parallel the lineation and pole to foliation respectively. The magnetic fabrics of the rocks are both foliated and lineated as evident from the sub-equal values of the F and L (Table 5.1). Also, the average trends of foliation and lineation have well accordance with those observed mesoscopically (Fig. 5.1, Fig. 5.6 and Fig. 5.7). The magnetic fabrics observed, thus, have a good correlation with the mesoscopic fabrics. The NE-SW trending magnetic lineations are replications of the  $F_1$  folds observed in the Khondalite (Dharma Rao et al., 2012). Also, the NW-SE trend of the magnetic lineations is the outcome of the  $F_2$  deformation event.

Despite the analogy of the magnetic fabrics with the mesoscopic fabrics, there is an interesting deviation of the magnetic fabrics from the mesoscopic ones. Although the magnetic fabrics have trends and dip/plunge directions analogous to different stages of folding in the KPLC, the dip amounts vary. Whereas the axial planar foliations dip at least  $60^\circ$ , the magnetic foliations are near horizontal. The causes for such deviations may be due to superposed deformation chiefly. Unusual variations in trends and dips of the magnetic foliation and mesoscopic foliations ubiquitously result due to superposed folds (Dubey and Cobbold, 1977). This presence of curved fold axes trends corroborates the contention (Fig. 2.3). Moreover, the scattering of  $K_1$  and  $K_2$  along the periphery is due to the occurrence of the  $D_2$  event on an already folded surface (Sen et al., 2012; Tripathi et al., 2019). The Jelinek plots ( $P_j$  versus T) from most of the sites in the KPLC reveal a strong oblate shape of susceptibility ellipsoid (Fig. 5.3). The oblate ellipsoids result from axially symmetric shortening in general strain conditions (Hobbs et al., 1976). The shape of the ellipsoids in most of the rocks of the studied area are chiefly oblate except for those in khondalite. This proves the prevalence of an overall compressive stress regime on a regional scale. However, the interference of ferrimagnetic minerals (titanomagnetite in the present case) may also contribute to such deviations (Borradaile and Jackson, 2004). According to Sengupta et al. (1999) and the present study, the paramagnetic silicate minerals like biotite, sillimanite, etc. parallel to the regional schistosity which are evident from the paramagnetic control over the magnetic fabrics. On the other hand, the titanomagnetite is equant in shape and is randomly distributed as porphyroblast. However, although the Titanomagnetite grains

are equant, they are not magnetically isotropic and thus possess a preferred magnetic fabric that is dissimilar to the ones developed paramagnetically. In such cases, the ferrimagnetic anisotropy tends to distort the penetrative magnetic fabric (Arbaret et al., 2013; Gregoire et al., 1998; Archanjo and Launeau, 1995).

Now, from the above discussion, there emerges a question of the relative strength of the magnetic fabrics and the mesoscopic fabrics. This is, however, debatable because of the following reasons. First, the magnetic fabrics are tectonically controlled as evident from the parallel trends of the mesoscopic and (paramagnetic) magnetic fabrics. This suggests that the tectonic fabrics were stronger to orient the magnetic fabrics in their direction. However, such a situation of parallelism of the magnetic and the mesoscopic fabrics is also possible if the crystallographic preferred anisotropies of the minerals are themselves oriented in the direction of the mesoscopic foliations. But, in the present study, we suggest that the magnetic fabrics are shape preferred firstly because of the higher values of  $P_j$  and an independent relationship between  $K_m$  and  $P_j$  (Chatterjee et al., 2018a). On the other hand, the random equant porphyroblastic titanomagnetite grains interfered in the resultant magnetic fabric by impinging variation in the dip/plunge of the magnetic fabric elements. Nevertheless, no penetrative magnetic fabric was developed due to this. Thus, the mesoscopic fabrics were stronger enough to impinge shape anisotropy in the paramagnetic grains resulting in a magnetic fabric whose trend parallels the mesoscopic fabrics, however, with varying dips. Although, tectonic implications of the magnetic fabrics are not obliterated even if the dip/plunge varies (Chatterjee et al., 2018a; Mamtani et al., 2013; Mamtani and Sengupta, 2010).

### **6.3. Summary: Tectonic implications**

The magnetic fabrics of the high-grade rocks of the KPLC are controlled by the regional mesoscopic fabric broadly defined by the paramagnetic minerals. When the magnetic anisotropy is a function of the paramagnetic minerals, the rocks tend to deform uniformly on a mesoscopic scale (Housen et al., 1995). Hence, the orientation of the magnetic lineation may be directly derived from the orientation of the principal compressive stress ( $\sigma_1$ ), where  $\sigma_1$  is perpendicular to the magnetic lineation (Fig. 5.8). The oldest rocks (the ones which came to existence before the first deformation phase

F<sub>1</sub>) in the succession of the KPLC are the granulite facies rocks followed by the emplacement of the anorthosite and later by the enderbite during F<sub>1</sub> deformation event (Sengupta et al., 1999). The earliest orientation is fossilized in the granulites only. The orientation of the magnetic lineation in the granulites, thus, preserves the signature of the earliest orientation of the  $\sigma_1$  i.e., NW-SE, during F<sub>1</sub>. The F<sub>2</sub> event was coeval with the emplacement of the anorthosite, thus the anorthosite are the best indicators of the second phase deformation. The  $\sigma_1$  was then oriented in a NE-SW trend, as recorded in the anorthosite which have an analogy with the F<sub>2</sub> deformation phase (Dharma Rao et al., 2012). However, there is a hiatus in the magnetic fabric record regarding the F<sub>3</sub> whose signatures are not available in the AMS record which may be due to the lesser intensity to re-orient the magnetic fabrics (Chatterjee et al., 2018a, 2018b).

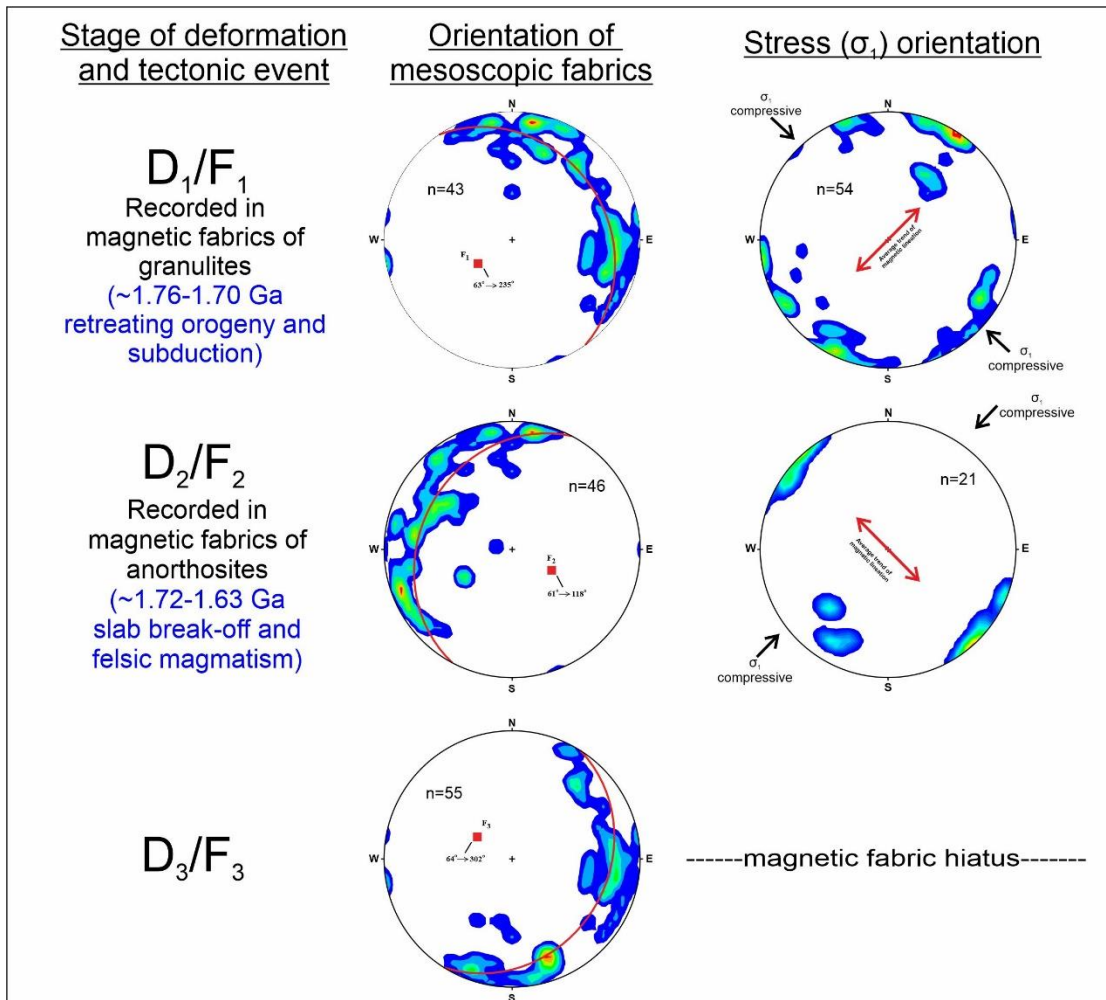


**Fig. 5.8:** Correlation of the magnetic fabric elements with the deformational events and deforming stress acting.

The stress regimes that are defined from the magnetic fabrics, correlate with the tectonic evolution of the Domain 1A of the EGB (Rickers et al., 2001). The Indo-

Antarctic continental blocks started experiencing a post rifting orogenesis phase initiated at ~1.87 Ga due to continued subduction of the riftogenic ocean basin under the Indian continental block (Dasgupta et al., 2013; Vijaya Kumar et al., 2010, 2011). During this period of orogeny (~1.87 - ~1.6 Ga; Dasgupta et al., 2013 and references therein), the paleo-stress field was not constant and that is reflected in the magnetic fabrics of the rocks of the KPLC. The oldest rocks of the KPLC which represent this orogeny are the granulites which recorded the first set of events. These rocks also marked the initiation of the UHT metamorphism during the retreating orogeny phase at ~1.76-1.70 Ga (Dasgupta et al., 2013; Bose et al., 2011; Sengupta et al., 1999). This set of events can thus be correlated with the initial orientation of the  $\sigma_1$  axis. Thus, during the ~1.76 -1.70 Ga accretionary orogeny phase of the Indo-Antarctic blocks, the compressive stress was oriented in an NW-SE direction (as recorded in the granulites). This event was followed by felsic magmatism during the period of ~1.72 to ~1.63 Ga due to the ceasing of the subduction process and slab break-off leading to the emplacement of the anorthosite and enderbite (Dasgupta et al., 2013; Dharma Rao et al., 2012; Kovach et al., 2001). During this period of ceasing of subduction and magmatism, the stress field was reoriented in NE-SW directions (as recorded in the magnetic fabrics of the anorthosite). Thus, the compressive force acting during the accretionary orogeny, related to the formation of the KPLC (and other members of the domain 1A of the EGB) was not unidirectional and marks a change at the boundary between completion of subduction and felsic magmatism.

**Chapter 6**  
**Rock Magnetic Studies**

## ROCK MAGNETIC STUDIES

### 6.1. Introduction

Rock magnetic and mineral magnetic characters of the natural rock samples are used to determine the nature of the carrier of the remanent magnetization including its grain size and composition and characterize the properties of the magnetic minerals residing in it. Rock magnetic properties of the high-grade metamorphic rocks from KPLC of Proterozoic EGB were measured to identify and the nature of the magnetic remanence carrier present within them. The purpose of measuring the rock magnetic parameters include: (a) Identification of the magnetic grain sizes of the different minerals in the rocks, (b) Relate the magnetic properties to petrological observations, (c) Determination of the origin of the remanence carrier, and (d) Short samples that are suitable for palaeomagnetic studies.

Magnetic properties of natural rocks such as magnetic susceptibility and magnetic remanence are highly sensitive to the concentration of the magnetic minerals as well as mineralogy, grain shape and size (e.g., Basavaiah, 2011; Thompson and Oldfield, 1986). The magnetic grain size plays an important role in rock magnetism as it controls the potentiality of a grain to acquire ancient terrestrial magnetic field (Radhakrishnamurty et al., 1978; Basavaiah et al., 2010; Basavaiah, 2011). The magnetic grains are classified into Super paramagnetic (SP), Stable Single Domain (SSD), Pseudo Single Domain (PSD), and Multi domain (MD). SSD grains are more suitable for acquiring ancient terrestrial magnetic field. Rock magnetic studies have revealed the properties of magnetic minerals in terms of concentration, composition and grain size.

In the present study detailed characterization of magnetic mineralogy of rock from KPLC were carried out by measuring a range of rock magnetic and mineral magnetic parameters and calculating the inter-parametric ratios (e.g., Basavaiah et al., 2018; Basavaiah, 2011; Dearing, 1999; Walden et al., 1998; Thompson and Oldfield, 1986) using powdered rock samples. These measurements are rapid, inexpensive, non-destructive and sensitive to even low concentration of magnetic minerals. Rock magnetic parameters includes thermomagnetic curve, Hysteresis curve and Isothermal

Remanent Magnetisation curve. Mineral magnetic parameters include Magnetic Susceptibility ( $\chi$ ), Anhyseretic Remanent Magnetization (ARM), Saturation Isothermal Remanent Magnetization (SIRM) and inter-parametric ratios like  $\chi_{fd}\%$ , SIRM/ $\chi$ , ARM/ $\chi$ , ARM/SIRM, Soft IRM, Hard IRM and S-ratios. These parameters are used to determine magnetic concentration, magnetic grain size and magnetic composition of the studied rocks from KPLC (Table 6.1). The magnetic parameters and the implication from them are listed in the Table 6.2.

The rock magnetic measurements were carried out in the Department of Earth, Ocean, and Ecological Sciences, University of Liverpool, UK and the mineral magnetic measurements were carried out in the Environmental Magnetism Laboratory, Solid Earth Geomagnetism Division, IIG (Navi Mumbai, India).

**Table 6.1: Parameters associated with different types of Magnetic Characterization.**

Characterization	Parameters associated
Magnetic Concentration	$\chi$ , ARM, SIRM
Magnetic grain sizes	$\chi_{fd}\%$ , SIRM/ $\chi$ , ARM/ $\chi$ , ARM/SIRM
Magnetic Composition	Soft IRM, Hard IRM, S-ratio

**Table 6.2: List of all magnetic parameters, their symbols and implications.**

Magnetic parameter	Symbol (Units)	Interpretation
Magnetic Susceptibility	$\chi$ ( $10^{-7} \text{ m}^3 \text{ kg}^{-1}$ )	Indicate the concentration of ferrimagnetic minerals (magnetite, maghemite). It also depends on magnetic particle size and magnetic mineralogy.
Anhyseretic Remanent Magnetization	ARM ( $10^{-5} \text{ Am}^2 \text{ Kg}^{-1}$ )	ARM measures the concentration of ferrimagnetic minerals of fine grained Stable single domain (SSD) magnetic particles ( $0.025 \text{ m} < d < 0.05 \text{ m}$ ). It also sensitive to grain interactions.
Saturation Isothermal Remanent Magnetization	SIRM ( $10^{-5} \text{ Am}^2 \text{ Kg}^{-1}$ )	SIRM depends on concentration and particle size of magnetic minerals. It also relates to magnetic mineral type.
Frequency Dependent Susceptibility	$\chi_{fd}\%$	$\chi_{fd}\%$ indicate the presence of ultra-fine ( $d < 0.025 \text{ m}$ ) superparamagnetic (SP) magnetic particles in the sample.
SIRM/ $\chi$ , ARM/, ARM / SIRM	SIRM/ $\chi$ ( $10^2 \text{ Am}^{-1}$ ), ARM/ $\chi$ ( $10^2 \text{ Am}^{-1}$ )	SIRM/ $\chi$ , ARM/ and ARM / SIRM are grain size indicator and used for magnetic granulometry. They indicate the presence of SSD to PSD magnetic minerals.
Soft IRM and Hard IRM	( $10^{-5} \text{ Am}^2 \text{ Kg}^{-1}$ )	Indicator of magnetic composition. Sensitive to the magnetically soft and hard minerals.
S-ratio	S	Depends on mineralogy. Indicate ferrimagnetic to antiferromagnetic ratio.

## 6.2. Rock Magnetic Measurements

### 6.2.1. Thermo-magnetic Study

Strong field thermo-magnetic curves were generated by heating the chip sample to 700° C in a saturating magnetic field and then cooling it to 100° C. The decreasing saturation remanence (heating curve) was monitored by a horizontal Curie Balance as the temperature increased, until it reached Curie Temperature ( $T_c$ ).  $T_c$  was noted from the point where the magnetization becomes zero which depends on the carrier mineral of magnetization. Similarly, the acquisition of secondary magnetization due to cooling below  $T_c$  was also recorded generating a cooling curve. The thermomagnetic heating and cooling were carried out in an air environment.

The magnetic minerals, in the following rocks such as opx-granulites, mafic granulites, anorthosites and leptynites have  $T_c$  at ~580° C (Fig. 6.1). Also, the heating

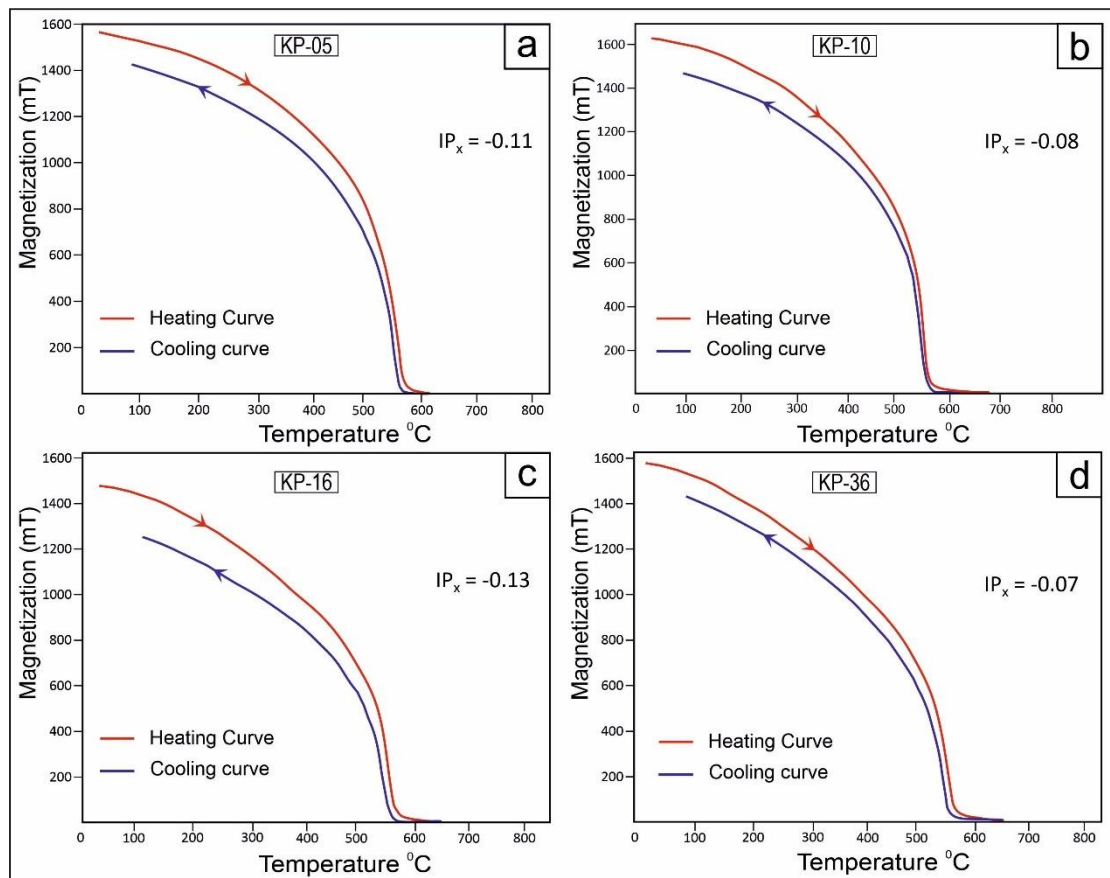


**Fig. 6.1:** Thermo-magnetic (saturation magnetization,  $M_s$ , vs. temperature) for the (a) Anorthosite, (b) Leptynite, (c) Granulite, (d) Leptynite in the high-grade rocks of KPLC. The corresponding values of the Irreversibility Parameter (IP) are provided along with the curves.



and cooling curves are reversible and do not crossover at any point. All these features depict the presence of titanomagnetite as the chief magnetic mineral (Bohnel et al., 2002). In contrast, the curves obtained from khondalite and enderbite (Fig. 6.2) show higher  $T_c$  with the irreversible nature of the heating and the cooling curves. Each of the

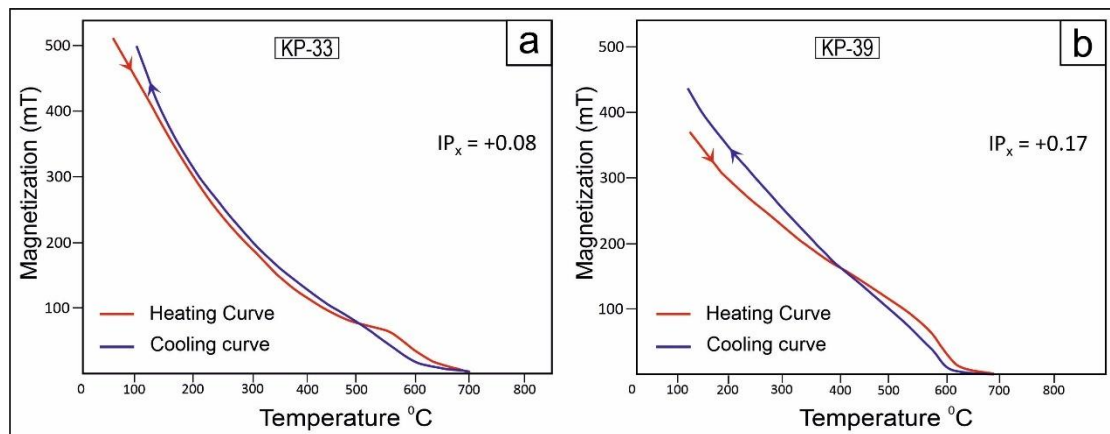


**Fig. 6.2:** Thermo-magnetic (saturation magnetization,  $M_s$ , vs. temperature) for the (a) Khondalite and (b) Enderbite in the high-grade rocks of KPLC. The corresponding values of the Irreversibility Parameter (IP) are provided along with the curves.

curves also have cross-overs at 450°C–500°C. These features observed in the value  $T_c$  and the nature of the heating and cooling curves can be attributed to the exsolution of a Ti-rich lamella (ilmenite as evident from the petrographic studies) which results in the host getting enriched in Fe. Thus, there is an increase in the  $T_c$  and the curves are irreversible (Lattard et al., 2006). The reversibility of the curves and the alteration due to heating are studied based on the “New Irreversibility Parameter (IP<sub>x</sub>)” given by Bohnel et al., 2002. None of the curves in the present study are completely reversible with zero IP<sub>x</sub> value. The IP<sub>x</sub> for the granulites, anorthosites, and leptynites range from - 0.07 to - 0.13. This shows that the samples are oxidized to a certain degree during heating. However, as the IP<sub>x</sub> for these rocks has lesser negative values, it can be assured that there has occurred no formation of haematite due to extreme degrees of oxidation during heating. The khondalites and the enderbites, in contrast, have positive IP<sub>x</sub> of +0.08 and +0.17.

### 6.2.2. Magnetic Hysteresis Study

Hysteresis studies were carried out by subjecting the samples to a cyclic magnetic field from 0 to 800 mT.

The anorthosite and granulites (viz. KP-17, KP-07) have moderate coercivities with relatively high values of saturation remanence (Fig. 6.3a and Fig. 6.3b). The

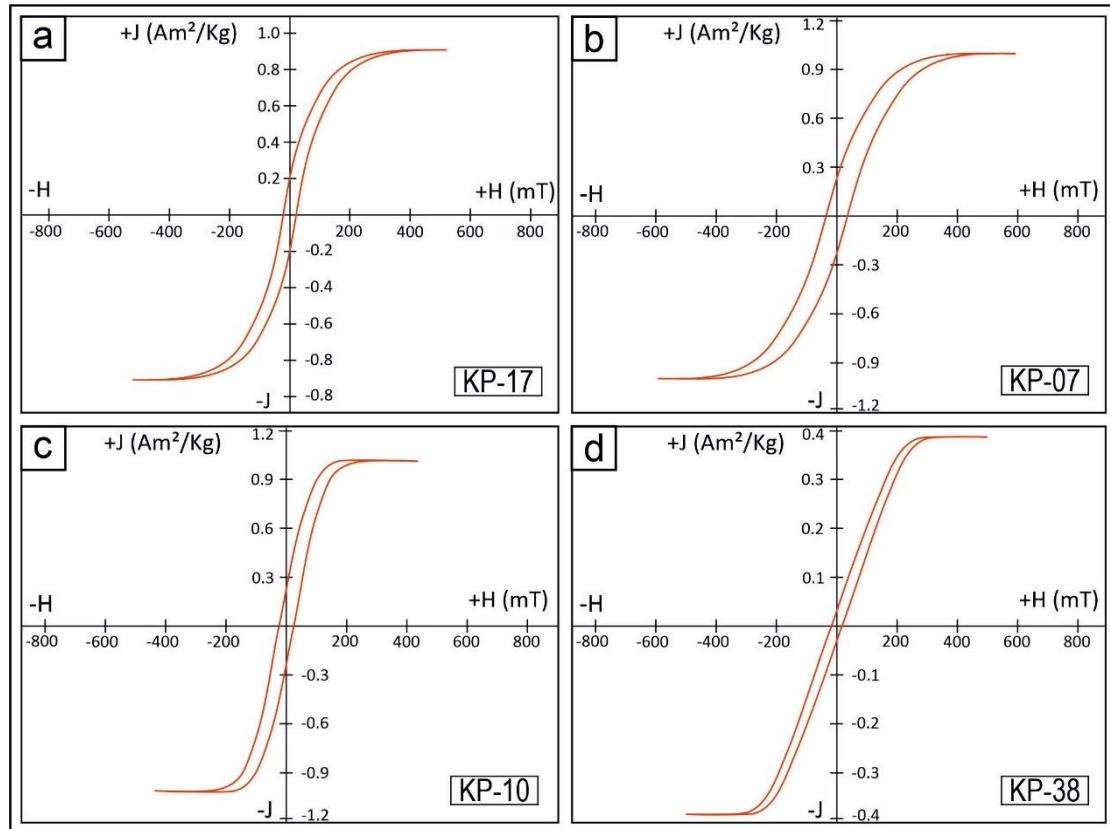


**Fig. 6.3:** Strong field Hysteresis loops for the (a) Anorthosite, (b) Granulites, (c) Leptynite, and (d) Enderbite of the KPLC. The hysteresis loops are corrected to paramagnetic contribution.

leptynite display characteristic ferrimagnetic curves with low coercivity (viz. KP-10, Fig. 6.3c). The enderbites exhibit elongated hysteresis loops with a typical wasp-waisted shape (viz. KP-38, Fig. 6.3d).  $M_{rs}/M_s$  values are calculated which lie between 0.11 (minimum, for the enderbites) and 0.25 (highest, for the granulites and anorthosites) with an average of 0.18. The ratio of remanent coercivity and coercivity of remanence ( $H_{cr}/H_c$ ) lies within 1.24 (in the granulites) to 1.36 (in the leptynite and enderbite) with an average of 1.3. The magnetic hysteresis parameters are represented in a modified Day diagram with theoretical mixing curves (Dunlop, 2002) and the variations in magnetic domain states are shown in Fig. 6.4 (Dunlop, 2002; Tauxe et al., 2002).

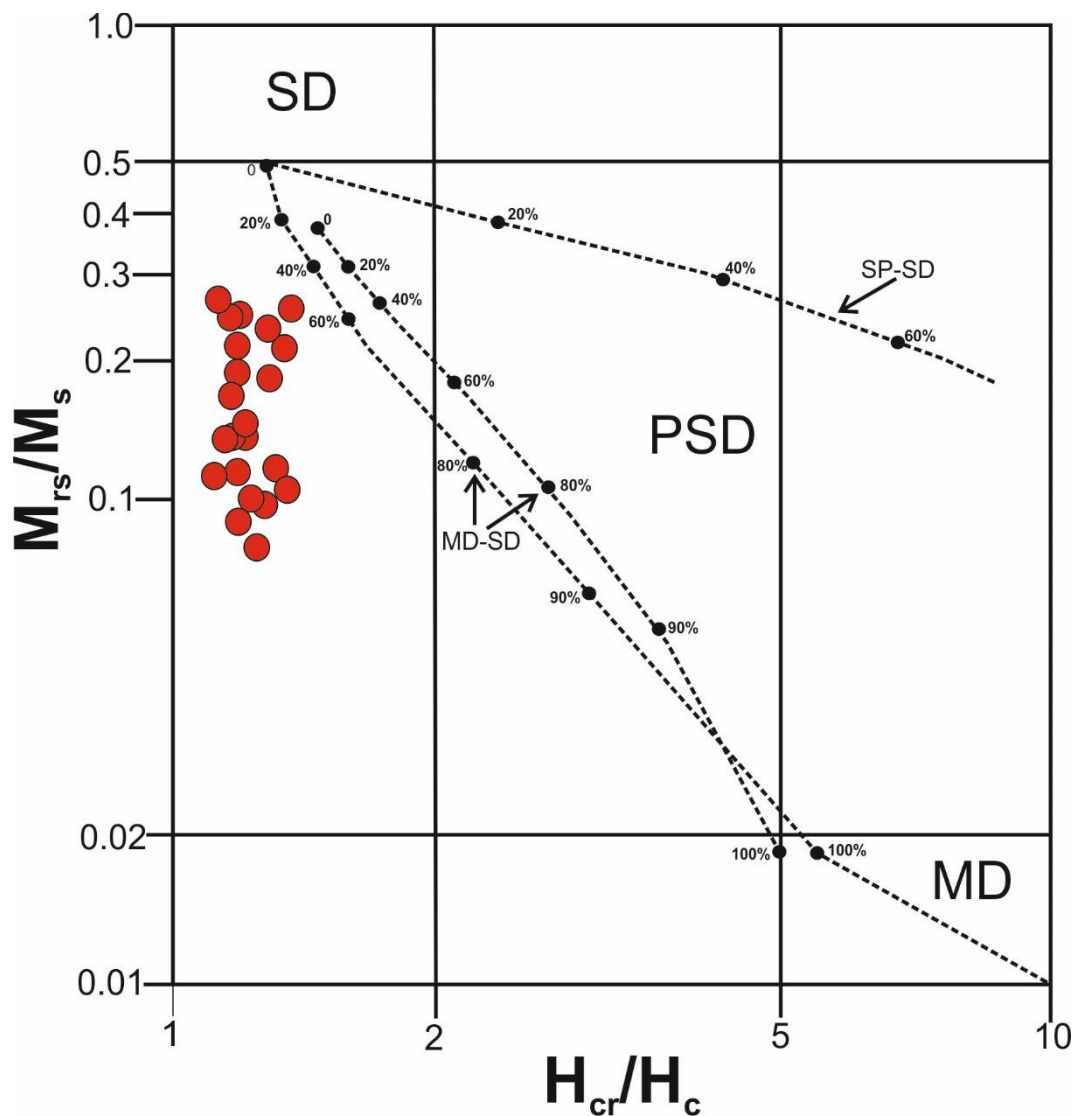
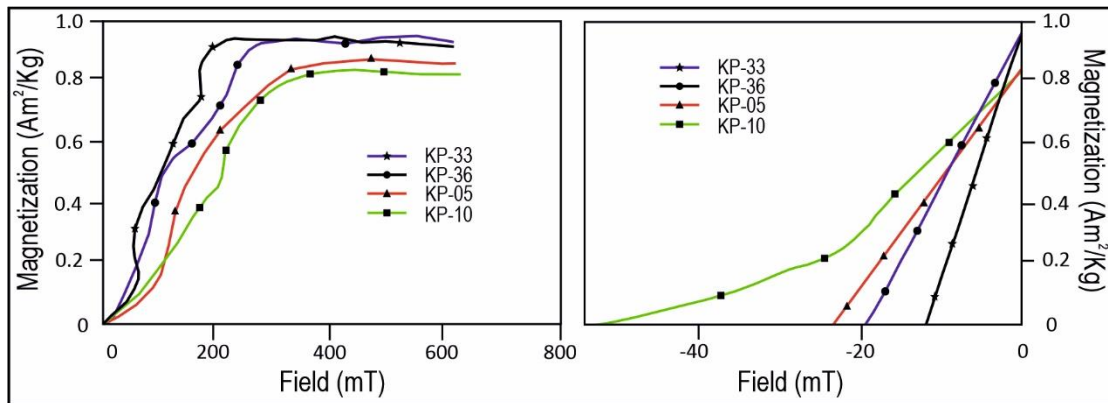


Fig. 6.4: Distribution of the domain states of titanomagnetite in different rocks of the KPLC (Day et al., 1977; Dunlop, 2002).

### 6.2.3. Isothermal Remanent Magnetization (IRM) Study

The Isothermal Remanent Magnetization (IRM) acquisition curves were obtained by subjecting the samples to an applied field at a constant temperature (room temperature) up to 2500 mT using a Pulse Magnetizer.

From the IRM acquisition curves and the corresponding coercivity spectra, it is evident that the samples attained saturation at applied fields below 400 mT (Fig. 6.5). A group of samples (viz. KP-33, KP-36) saturates at around 150 to 200 mT and have coercivities <30 mT. In contrast, others (viz. KP-05, KP-10) saturate at fields of 250–300 mT. The samples have coercivities ranging from <20 mT (for samples with



**Fig. 6.5: Isothermal Remanent Magnetization (IRM) acquisition curves and corresponding coercivity spectra (backfield IRM demagnetization) for the different rocks of the KPLC.**

lower saturating fields) to >40 mT (for samples with higher saturating fields). Although the saturating fields and the coercivities have two ranges, the general signal from the IRM and coercivity spectra is towards a soft magnetic mineral as the chief carrier. The fields of IRM saturation and the corresponding coercivities suggest that the magnetic minerals belong to titanomagnetite solid solution series.

### 6.3. Mineral Magnetic Studies

#### 6.3.1. Magnetic Susceptibility Measurement

Magnetic susceptibility ( $\kappa$ ) is a measure of the ability of a material to acquire magnetization. Magnetic susceptibility ( $\kappa$ ) indicates the degree of magnetization of magnetic material when gets magnetised by externally applied magnetic field. Mathematically,  $\chi$  can be represented as the ratio of bulk magnetization (M) within the material and the applied magnetic field (H);

$$\text{i.e. } \kappa = M/H.$$

Both M and H are measured in A/m in SI units, so  $\kappa$  is dimensionless. The  $\kappa$  is here is mainly volume susceptibility. To obtain mass specific susceptibility we use the following equation:

$$\chi = \kappa/\rho$$

Where,  $\rho$  is the density of the material and  $\chi$  has a unit same as density,  $\text{m}^3/\text{Kg}$ .

A positive  $\chi$  value indicate magnetization acquired by the materials is parallel to the direction of the applied magnetic field and negative  $\chi$  value implies that the acquired magnetic field is antiparallel to the applied magnetic field. In case of the natural rock samples, the applied magnetic field is the geomagnetic field prevailing during the magnetization of the rock. It should be noted that a rock body may not get magnetised during its formation, but that point when its temperature is below its Curie temperature of magnetic minerals present rocks. So, it is precise to deal with the magnetic field during the magnetization of that rock rather the same during its formation.

Variation in  $\chi$  value reflects gross changes in relative concentration of magnetic minerals (Verosub and Roberts, 1995). The  $\chi$  value of the natural rock samples depends on the amount of ferrimagnetic minerals present within the rocks or more accurately the amount of magnetite and Titanomagnetite. This parameter is mainly related to the concentration of ferrimagnetic minerals in a sample, but is also influenced by diamagnetic and paramagnetic materials (Lepland and Stevens, 1996).

Table 6.3 represents the variation of magnetic susceptibility ( $\chi$ ) values in different rock types of the study area. The distribution of the  $\chi$  values in the studied area is represented in Fig. 6.6. From the analysis of data in the studied area it is observed that it ranges from  $178.49 \times 10^{-7} \text{ m}^3 \text{ kg}^{-1}$  to  $2.88 \times 10^{-7} \text{ m}^3 \text{ kg}^{-1}$ . The highest  $\chi$  value is

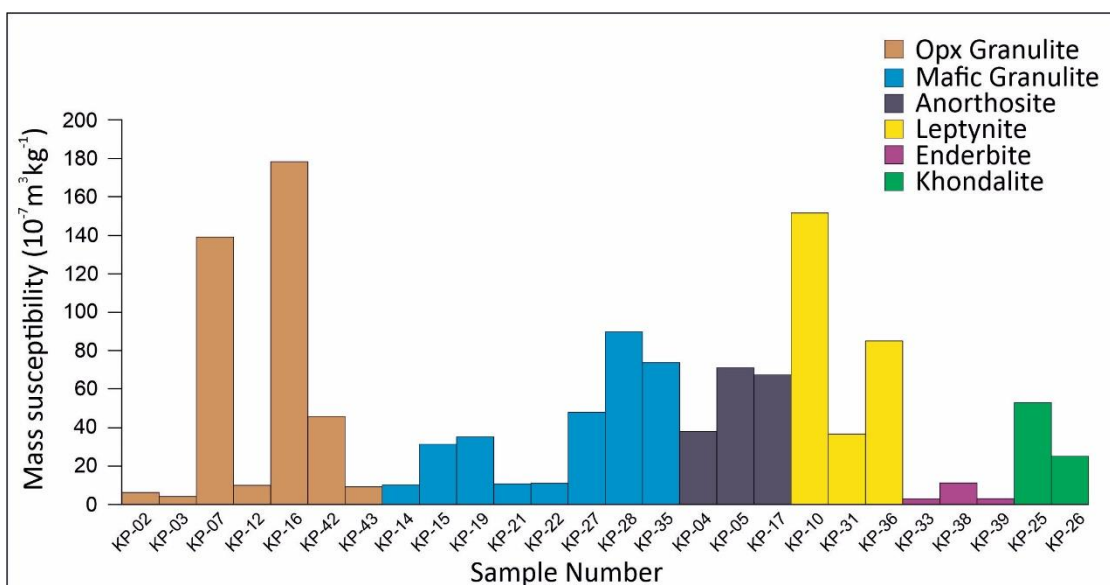


Fig. 6.6: Distribution of Magnetic Susceptibility in different rock types of KPLC.

**Table 6.3: Distribution of magnetic susceptibility, ARM and SIRM in KPLC rocks.**

Sample	Mass (gm)	$\kappa$ , $10^{-5}$	$\chi$ ( $10^{-7} \text{ m}^3 \text{ kg}^{-1}$ )	ARM ( $10^{-5} \text{ Am}^2 \text{ Kg}^{-1}$ )	SIRM ( $10^{-5} \text{ Am}^2 \text{ Kg}^{-1}$ )
KP- 02	9.672	60.375	6.24	1.317	230.21
KP- 03	10.358	44.417	4.28	1.0081	187.05
KP- 07	9.531	1326.8	139.28	22.2709	5090.92
KP- 12	10.068	101.48	10.07	4.8758	566.32
KP- 16	9.846	17.57.5	178.49	25.9748	5328.16
KP- 42	9.114	418.22	45.88	15.9115	1395.68
KP- 43	9.912	91.761	9.25	3.9945	334.90
KP- 14	8.168	83.595	10.23	5.2205	165.19
KP- 15	9.146	287.28	31.41	6.1412	1042.44
KP- 19	9.139	322.78	35.31	11.7654	1454.60
KP- 21	10.358	111.56	10.74	14.2635	2749.92
KP- 22	9.255	101.83	11.00	11.0358	719.12
KP- 27	9.243	445.41	48.18	13.9207	6746.82
KP- 28	8.987	809.13	90.03	12.0119	3349.10
KP- 35	8.317	615.27	73.97	11.4347	1990.58
KP- 04	8.594	326.54	37.99	5.2380	1080.12
KP- 05	8.828	627.92	71.12	11.7115	2676.68
KP- 17	8.721	589.72	67.62	8.7092	1615.97
KP- 10	9.481	1437.6	151.62	32.7176	5428.00
KP- 31	9.506	349.55	36.77	7.3831	1085.52
KP- 36	7.595	645.28	84.96	9.0371	1872.14
KP- 33	8.288	23.872	2.88	0.7569	172.38
KP- 38	9.868	110.82	11.23	5.1715	997.29
KP- 39	9.112	27.002	2.96	0.5903	86.79
KP- 25	9.688	514.75	53.13	13.6508	3918.31
KP- 26	8.46	212.02	25.06	5.7349	1830.89

observed within orthopyroxene granulite and the lowest  $\chi$  value within enderbite with an average  $\chi$  value of  $48.06 \times 2.88 \times 10^{-7} \text{ m}^3 \text{ kg}^{-1}$ . Comparing these with standard values, it suggests that the magnetic minerals residing in the studied rocks are mainly magnetite/titanomagnetite. It is observed from the petrographic studies that the ferrimagnetic titanomagnetites are mainly primary. Thus, the higher observed  $\chi$  values (average  $48.06 \times 10^{-7} \text{ m}^3 \text{ kg}^{-1}$ ) are due to primary occurrences. Notably enderbite have relatively low  $\chi$  values compared to the other rock types. So,  $\chi$  is weakened by the presence of ilmeno-haematite. The  $\chi$  values also point towards the presence of ilmeno-haematite which is also evident from the petrographic study.

### 6.3.2. Anhyseretic Remanent Magnetization (ARM) Measurement

Anhyseretic remanent magnetization (ARM) is a laboratory remanence acquired by a sample during treatment in a decaying, alternating magnetic field (peak field about 100 mT) with a superimposed steady field (usually 50-100  $\mu$ T) at room temperature (Hunt et al., 1995a). This imparts a magnetization in a known direction.

ARM can be highly sensitive to the presence of Stable single domain (SSD) (Hunt et al., 1995a; Dunlop and Ozdemir, 1997). Higher ARM depicts presence of higher concentration of SSD magnetic minerals in the samples. ARM can also be influenced (decrease with increasing concentration) by magnetic interactions among the magnetic particles (Sugiura, 1979; Yamazaki and Ioka, 1997). ARM was measured by imparting a DC bias field of 0.05mT superimposed on a peak AF of 100 mT with ASC's D-Tech Alternating Field (AF) demagnetizer.

The distribution of the ARM values in the studied area are shown in the bar diagram (Fig. 6.7) and listed in the Table 6.3 The average ARM value of the studied area is  $10.07 \times 10^{-5} \text{ m}^3 \text{ kg}^{-1}$  with the highest value of  $32.7 \times 10^{-5} \text{ m}^3 \text{ kg}^{-1}$  in leptynite and the lowest value of  $0.59 \times 10^{-5} \text{ m}^3 \text{ kg}^{-1}$  in enderbite.

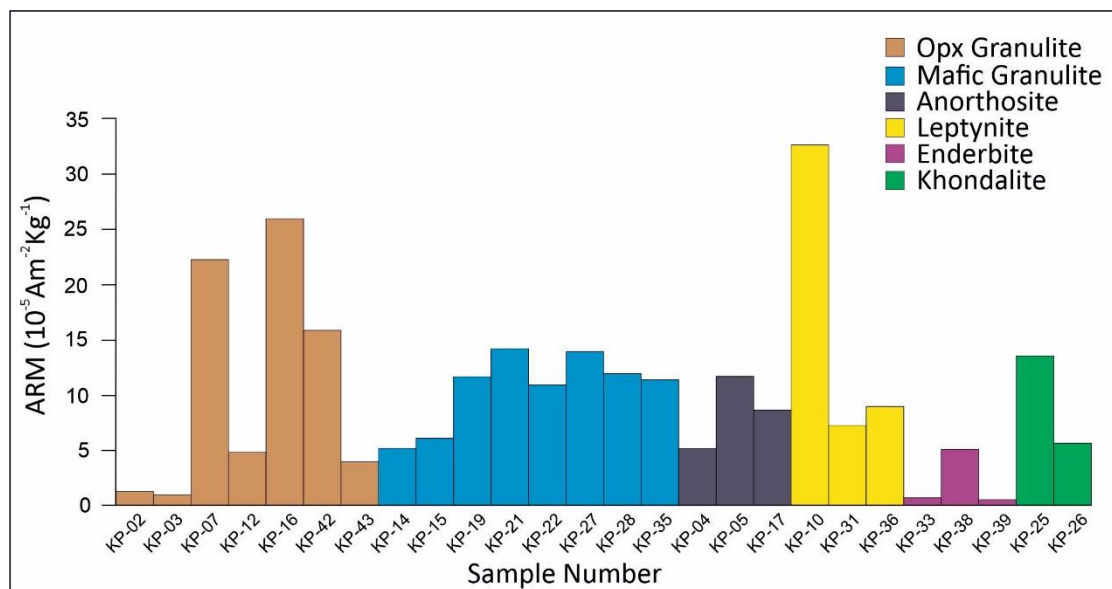


**Fig. 6.7: Distribution of ARM in different rock types of KPLC.**

From the studies of the generation of the Fe-Ti oxide in the studied samples, it is evident that the studied samples contain both primary granoblastic (coarser/finer) titanomagnetite grains and ultra-fine grains of secondary magnetite grains present along

the grain boundary, cleavage plane of the silicate minerals. In many cases titanomagnetites are oxidised with high temperature oxidation (C1-Stage to C4-Stage) and low temperature oxidation (Stage-1 to Stage-5) evident from the petrographic studies. Due to oxidation the effective grain size of the titanomagnetite is reduced. Thus, it is evident from the ARM studies that the primary and secondary titanomagnetite and magnetite observed in the studied samples, belong to the SSD nature, which are capable of recording remanences.

All the rock types except enderbite shows high ARM values (except KP-02, KP-03). The average values of ARM in different rock types as follows: Orthopyroxene granulite-  $10.76 \times 10^{-5} \text{ m}^3 \text{ kg}^{-1}$ , mafic granulite-  $10.72 \times 10^{-5} \text{ m}^3 \text{ kg}^{-1}$ , anorthosite-  $8.55 \times 10^{-5} \text{ m}^3 \text{ kg}^{-1}$ , leptynite-  $16.37 \times 10^{-5} \text{ m}^3 \text{ kg}^{-1}$ , khondalite-  $9.69 \times 10^{-5} \text{ m}^3 \text{ kg}^{-1}$ . These high values indicate that, they contain SSD titanomagnetite and are mainly magnetically soft. The samples having relatively low ARM values are mainly contain Pseudo Single Domain (PSD) grains to MD grains. So, the concentration of phenocrysts of titanomagnetite grains (Stage-1 and C1-Stage) is high within these samples along with the secondary ultra-fine grains of secondary magnetite, which is also evident from the petrographic studies. Enderbite shows average low values of ARM ( $2.17 \times 10^{-5} \text{ m}^3 \text{ kg}^{-1}$ ), which indicate the magnetic minerals residing in the samples shows PSD to MD behaviour.

So, overall high values of ARM signify, that the magnetic minerals (here titanomagnetite and magnetite) residing within the studied samples are SSD to PSD in nature and capable of recording magnetic remanence.

### **6.3.3. Saturation Isothermal Remanent Magnetization (SIRM) Measurement**

Saturation Isothermal Remanent Magnetization (SIRM) is the maximum Isothermal Remanent Magnetization (IRM) that a sample can obtain and is determined by recording IRM in progressively higher magnetic field over a short period of time at constant temperature. After reaching saturation, IRM does not increase further with higher applied magnetic field. Stepwise acquisition of IRM in a forward field up to 1T followed by stepwise demagnetization in backfield up to 300mT was carried out using Pulse magnetizer and a Molspin/JR-6A spinner magnetometer.



The distribution (based on rock types) and the graphical representation of the SIRM values for the KPLC rocks are provided in Table 6.3 and Fig. 6.8 respectively. The ferrimagnetic minerals (e.g., magnetite, titanomagnetite) have the property of getting saturated with magnetization after the applied field is increased to a certain value (here it is 1T). However, the paramagnetic and diamagnetic minerals are not associated with saturation of magnetization and thus the values of SIRM are proportional to the amount of ferrimagnetic minerals and thus can directly define the

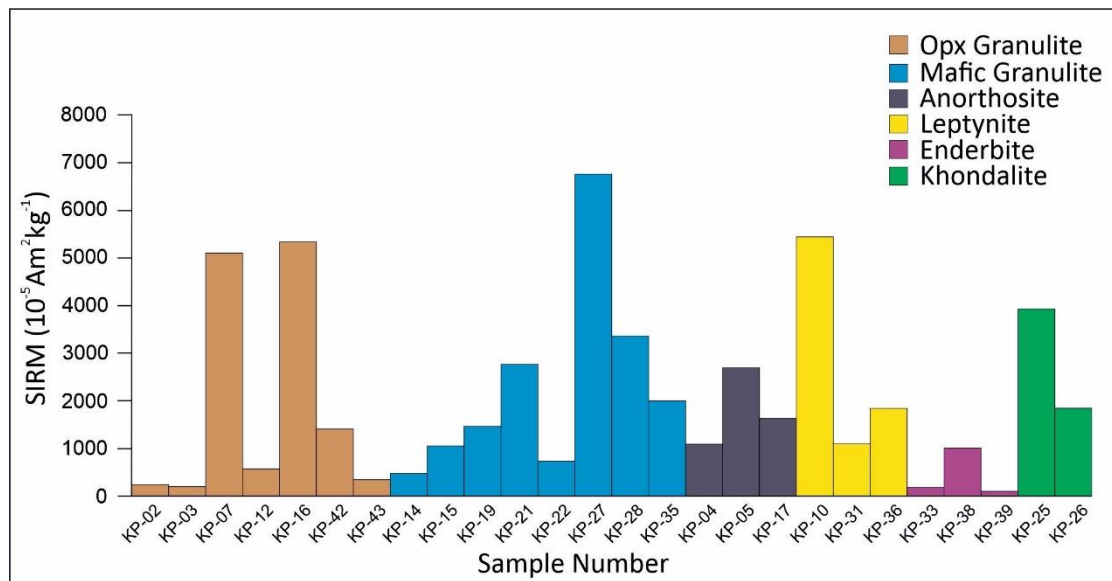


**Fig. 6.8: Distribution of SIRM in different rock types of KPLC.**

potentiality of a sample in recording ancient magnetic field. From the values of SIRM in the studied area, it is revealed that the orthopyroxene granulite (average  $\sim 1876.2 \times 10^{-5} \text{Am}^2 \text{kg}^{-1}$ ), mafic granulite (average  $\sim 2314.7 \times 10^{-5} \text{Am}^2 \text{kg}^{-1}$ ), anorthosite (average  $\sim 1790.9 \times 10^{-5} \text{Am}^2 \text{kg}^{-1}$ ), leptynite (average  $\sim 1876.2 \times 10^{-5} \text{Am}^2 \text{kg}^{-1}$ ) and khondalite (average  $\sim 1876.2 \times 10^{-5} \text{Am}^2 \text{kg}^{-1}$ ) have high saturating remanences and these rocks are suitable for recording magnetic remanences. The samples which have higher values of SIRM, also have higher values of  $\chi$  and ARM. Again, the high values of  $\chi$  are higher where the magnetic grains are present as primary in nature. Thus, combination of the results assures that the dominant ferrimagnetic components which can record ancient magnetic field are mainly primary magnetite/titanomagnetites in the studied area. The lower trends of SIRM in enderbite (average  $\sim 418.8 \times 10^{-5} \text{Am}^2 \text{kg}^{-1}$ ) reveal that the concentration of magnetic minerals is much lower in them. This may be due to the interferences of the high concentration of paramagnetic minerals like the silicates.

### 6.3.4. Frequency-dependent Susceptibility ( $\chi_{fd}$ %) Measurement

Frequency-dependent Susceptibility ( $\chi_{fd}$  %) is used to detect the presence of very fine super paramagnetic (SP) grains (0.02  $\mu\text{m}$ ) within the sample (Zhou et al., 1990; Worm, 1998; Liu et al., 2005a). In presence of SP grains, the samples exhibit frequency dependence in initial  $\chi$  value (Thompson and Oldfield 1986). Susceptibility measured at higher frequencies is always equal or lower than that measured at lower frequencies (Basavaiah, 2011). The  $\chi_{fd}$  express the difference between  $\chi$  measured at low frequency (often 470 Hz) and  $\chi$  measured at high frequency (often 4.7 kHz):

$$\chi_{fd} = \chi_{lf} - \chi_{hf}$$

And the percentage frequency dependence factor ( $\chi_{fd}\%$ ) expressed as:

$$\chi_{fd} \% = (\chi_{lf} - \chi_{hf} / \chi_{lf}) \times 100 \% (\chi_{fd} \%)$$

High values of  $\chi_{fd}$  % indicate the presence of very fine-grained metastable magnetic grains ranging between the SP and SSD boundary (Eyre, 1997; Worm, 1998). Generally, a parallel increase of  $\chi$  and  $\chi_{fd}$  % point towards secondary origin whereas the variation of  $\chi$  not associated with corresponding variation of  $\chi_{fd}$  % indicates contribution of ferrimagnetic mineral of primary origin (Basavaiah, 2011). Interpretations from  $\chi_{fd}$  % values derived from samples shown in the Table 6.4.

**Table 6.4: Interpretation of the value  $\chi_{fd}$  % (Fajri et al., 2019).**

Value of $\chi_{fd}$ (%)	Information
< 2.0%	None or contains less than 10% superparamagnetic grain.
2.0 - 10.0%	A coarser mixture of superparamagnetic and non-superparamagnetic grains, or superparamagnetic grain measuring <0.005 $\mu\text{m}$ .
10.0 - 14.0%	Overall or consists of more than 75% superparamagnetic grain.

In the present study, the value of  $\chi_{fd}$  % ranges from 0.89% to 4.44% with an average value of 2.07%. The distribution of the value of  $\chi_{fd}$  % is listed in Table 6.5 and sample wise variation of  $\chi_{fd}$  % in the studied samples are represented in Fig. 6.9. In case of orthopyroxene granulite, mafic granulite and khondalite, the average value of  $\chi_{fd}$  % is > 2%. Which indicate superparamagnetic behaviour; the rocks contain a mixture of

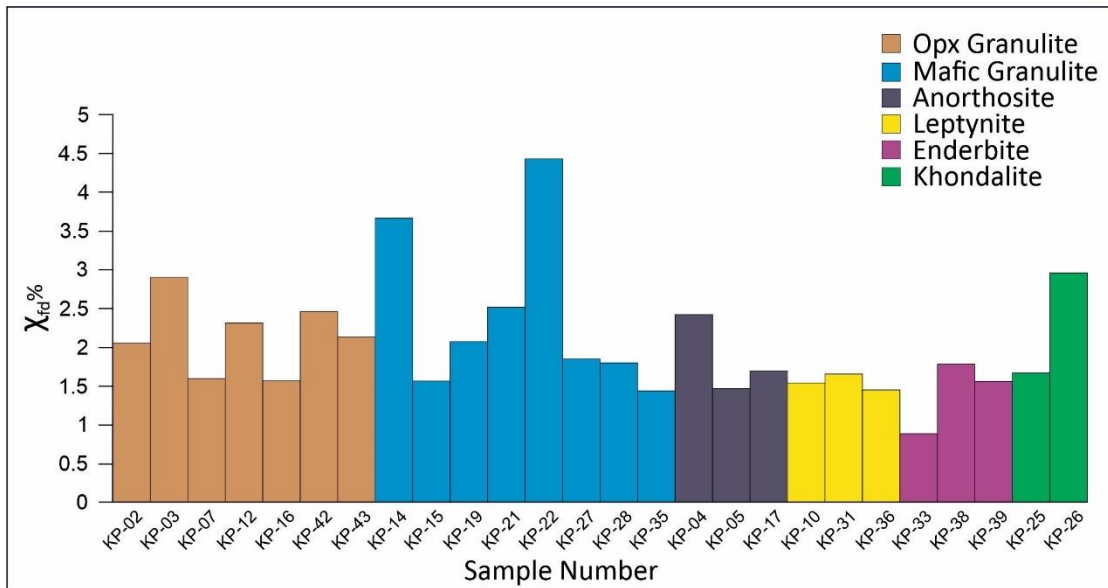


Fig. 6.9: Distribution of  $\chi_{fd}$  % in different rock types of KPLC.

SP grains and coarser magnetic grains. However, most of the samples (e.g., KP-7, KP-16, KP-15, KP-27, KP-28, KP-35, KP-25) have  $\chi_{fd}$  % values < 2%, which suggests non-superparamagnetic behaviour, i.e., they contain less than 10% of superparamagnetic grains. Also, the other rock types also show low average  $\chi_{fd}$  % value, which is < 2%, which indicates non-superparamagnetic behaviour. Based on the  $\chi$  vs  $\chi_{fd}$  % diagram (Fig. 6.10), it is evident that there is no positive correlation between  $\chi$  and  $\chi_{fd}$  %. So, it can say that the titanomagnetite grains within the studied samples are

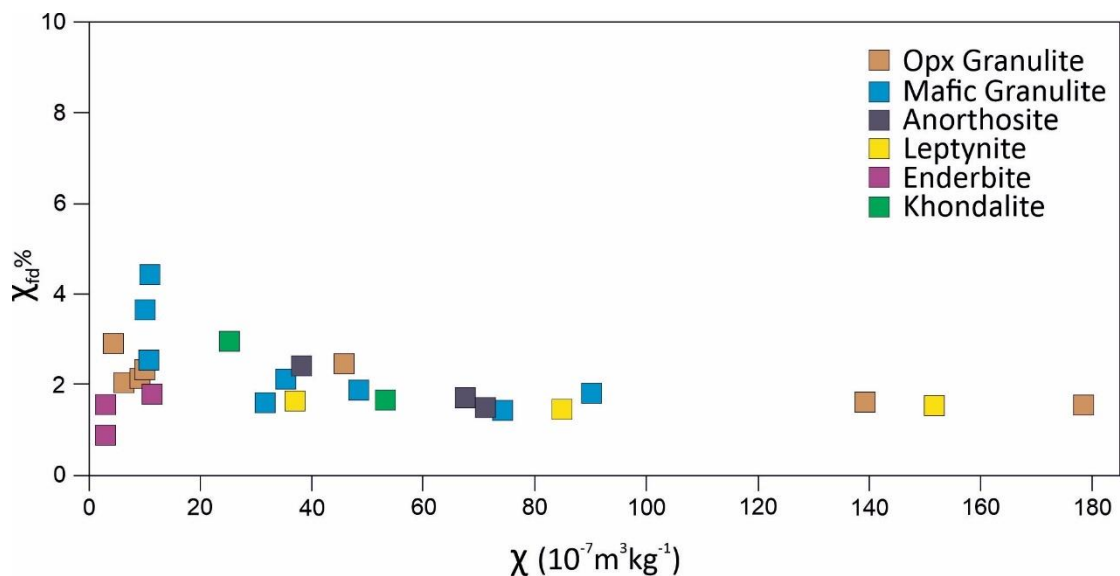


Fig. 6.10. Relationship between  $\chi$  and  $\chi_{fd}$  % in different rock types of KPLC.

Table 6.5: Distribution of  $\chi_{fd}$  %, ARM/SIRM, SIRM/ $\chi$ , ARM/ $\chi$  in KPLC rocks.

Sample	Mass (gm)	$\chi_{lf}$ ( $10^{-5}$ )	$\chi_{hf}$ ( $10^{-5}$ )	$\chi_{fd}$ %	ARM / SIRM	SIRM/ $\chi$ ( $10^2 \text{ Am}^{-1}$ )	ARM/ $\chi$ ( $10^2 \text{ Am}^{-1}$ )
KP- 02	9.672	60.375	59.113	2.06	0.0057	36.88	0.211412
KP- 03	10.358	44.417	43.12	2.92	0.0054	43.62	0.23509
KP- 07	9.531	1326.8	1305.4	1.61	0.0044	36.57	0.159982
KP- 12	10.068	101.48	99.048	2.33	0.0086	56.22	0.484075
KP- 16	9.846	17.57.5	1729.7	1.58	0.0049	29.84	0.145518
KP- 42	9.114	418.22	407.84	2.48	0.0114	30.41	0.346748
KP- 43	9.912	91.761	89.801	2.14	0.0119	36.17	0.43148
KP- 14	8.168	83.595	80.526	3.67	0.0112	45.43	0.509839
KP- 15	9.146	287.28	282.74	1.58	0.0059	33.18	0.195513
KP- 19	9.139	322.78	316.02	2.09	0.0081	41.18	0.333119
KP- 21	10.358	111.56	108.74	2.53	0.0052	255.98	1.32777
KP- 22	9.255	101.83	97.311	4.44	0.0153	65.35	1.003005
KP- 27	9.243	445.41	437.19	1.85	0.0021	140.00	0.288878
KP- 28	8.987	809.13	794.48	1.81	0.0036	37.19	0.133416
KP- 35	8.317	615.27	606.35	1.45	0.0057	26.90	0.15457
KP- 04	8.594	326.54	318.6	2.43	0.0048	28.42	0.137854
KP- 05	8.828	627.92	618.61	1.48	0.0044	37.63	0.164653
KP- 17	8.721	589.72	579.62	1.71	0.0054	23.89	0.128795
KP- 10	9.481	1437.6	1415.3	1.55	0.0060	35.79	0.215774
KP- 31	9.506	349.55	343.73	1.66	0.0068	29.52	0.200784
KP- 36	7.595	645.28	635.87	1.46	0.0049	21.50	0.106368
KP- 33	8.288	23.872	23.659	0.89	0.0044	59.84	0.262776
KP- 38	9.868	110.82	108.84	1.79	0.0052	88.80	0.460494
KP- 39	9.112	27.002	29.577	1.57	0.0068	29.28	0.199207
KP- 25	9.688	514.75	506.11	1.68	0.0035	73.75	0.256919
KP- 26	8.46	212.02	205.74	2.96	0.0031	73.75	0.228832

mainly primary in origin. Such implication also supported by the petrographic observation. Some samples show little higher values are may be due to presence of ultra-fine grained secondary magnetite grains along the grain boundary, cleavage planes and fracture planes of the silicate minerals, also evident in the petrographic observation.

Thus, from the  $\chi_{fd}$ % results, it can be said that, the studied samples bear primary and secondary magnetic grains varies from SSD to SP range. There is no such positive correlation between the variation of  $\chi$  and the corresponding  $\chi_{fd}$ %, thus the dominance of primary magnetic grains is reflected. From the petrographic studies, it is evident that the primary titanomagnetite undergone high temperature oxidation (C1-Stage to C4-

Stage) and low temperature oxidation (Stage-1- Stage-5) resulting the reduction of effective grain size, which is also evident from the ARM results.

### 6.3.5. SIRM/ $\chi$ , ARM/ $\chi$ and ARM/SIRM

The ratios between SIRM and  $\chi$ , ARM and  $\chi$  and ARM/SIRM are widely used as grain size indicators of magnetic minerals. Small particles yield higher values because they are highly efficient for acquiring remanence, particularly ARM (Maher, 1988; Dunlop and Xu, 1993; Dunlop, 1995).

In case of SIRM/  $\chi$ , size dependent SIRM coupled with the size independent  $\chi$  (Heider et al., 1996), which leads to higher values, where smaller particles are more abundant. SIRM/ $\chi$  is useful in terms of differentiating between different types of magnetic behaviours. For instance, if both SIRM and  $\chi$  are low and the ratio is high that indicates a large amount of haematite. Again, if  $\chi$  is positive with low remanence the magnetic minerals are mostly paramagnetic (Basavaiah, 2011; Basavaiah and Khadkikar, 2004). Thus, a comparative analysis of the values of SIRM,  $\chi$  and SIRM/  $\chi$  helps to identify the magnetic behaviour of the samples as well as the minerals contributing towards such behaviour. The distribution of SIRM/ $\chi$  is listed in Table 6.5 and the variation is also represented in Fig. 6.11. The highest SIRM/ $\chi$  value of  $\sim 255.98 \times 10^2 \text{ Am}^{-1}$  with an average  $\sim 80.65 \times 10^2 \text{ Am}^{-1}$  are observed in mafic granulite and

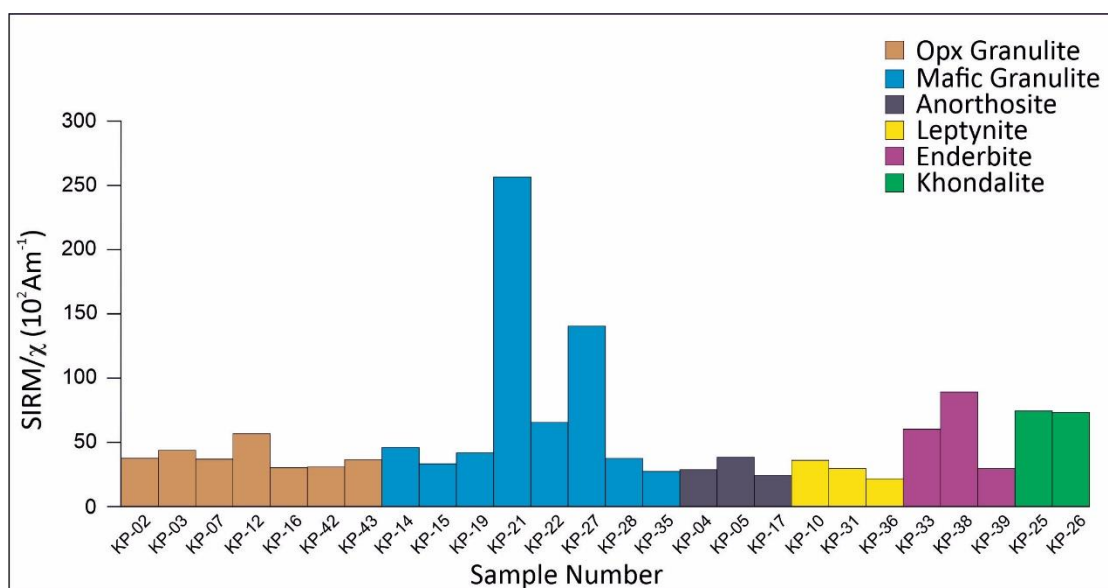
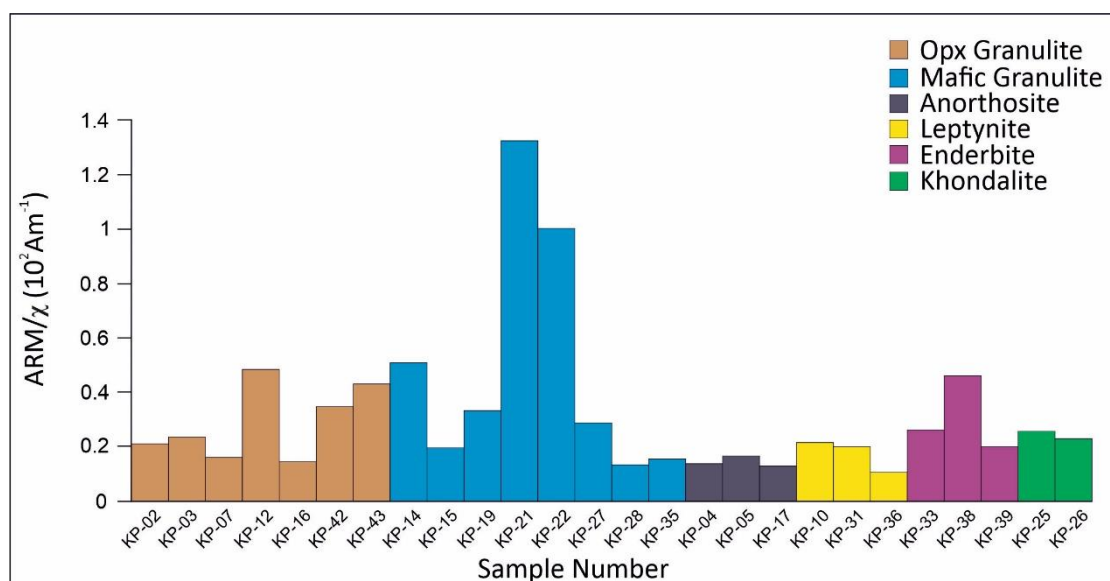


Fig. 6.11: Distribution of SIRM/ $\chi$  in different rock types of KPLC.

the lowest SIRM/ $\chi$  value of  $\sim 21.50 \times 10^2 \text{ Am}^{-1}$  in leptynite with an average  $\sim 28.94 \times 10^2 \text{ Am}^{-1}$ . In case of orthopyroxene granulite, mafic granulite and anorthosite both the SIRM and  $\chi$  are high (Table 6.3) resulting in high values of the ratio. Thus, the SIRM/ $\chi$  ratio is implicative towards the presence of high susceptibility and high remanence bearing minerals like magnetite and Titanomagnetite. In case of the anorthosite, both the SIRM and  $\chi$  are high resulting in low values of the ratio which also indicate the presence of high susceptibility and high remanence bearing minerals like magnetite or Titanomagnetite. Values of  $\chi$  are relatively low in enderbite and khondalite which is causing a rise in the SIRM/ $\chi$  which indicate coarser grain size of the magnetic minerals. The low values for clearly indicate lower concentration of magnetite but the high SIRM indicates the presence of some minerals which have high capability of recording remanences which further indicates the presence of iron sulphides like pyrrhotite or greigite (Roberts et al., 1996).

ARM/ $\chi$  also indicate the grain size dependence. Higher ARM/ $\chi$  value signifies abundance of small SSD to PSD grains of magnetic minerals. Decreasing value of ARM/ $\chi$  indicate the increasing concentration of larger grains. The values of ARM/ $\chi$  are represented in the Fig. 6.12 and listed in the Table 6.5. The values range from  $0.11 \times 10^2 \text{ Am}^{-1}$  in leptynite to  $1.33 \times 10^2 \text{ Am}^{-1}$  in mafic granulite with an average value of  $0.32 \times 10^2 \text{ Am}^{-1}$ . Both average ARM and  $\chi$  value of the studied samples are high, so the ratio of ARM and  $\chi$  also high within the studied samples which indicate the magnetic



**Fig. 6.12: Distribution of ARM/ $\chi$  in different rock types of KPLC.**

minerals residing in the studied samples are mainly SSD in nature. Relatively lower values indicate the presence of PSD to MD grains.

The ratio of ARM and SIRM serves as a measure of the strength of grain interaction. The samples containing a higher fraction of SD-PSD particles will give higher ARM/SIRM ratios and MD grains will yield lower ARM/SIRM ratios (Basavaiah and

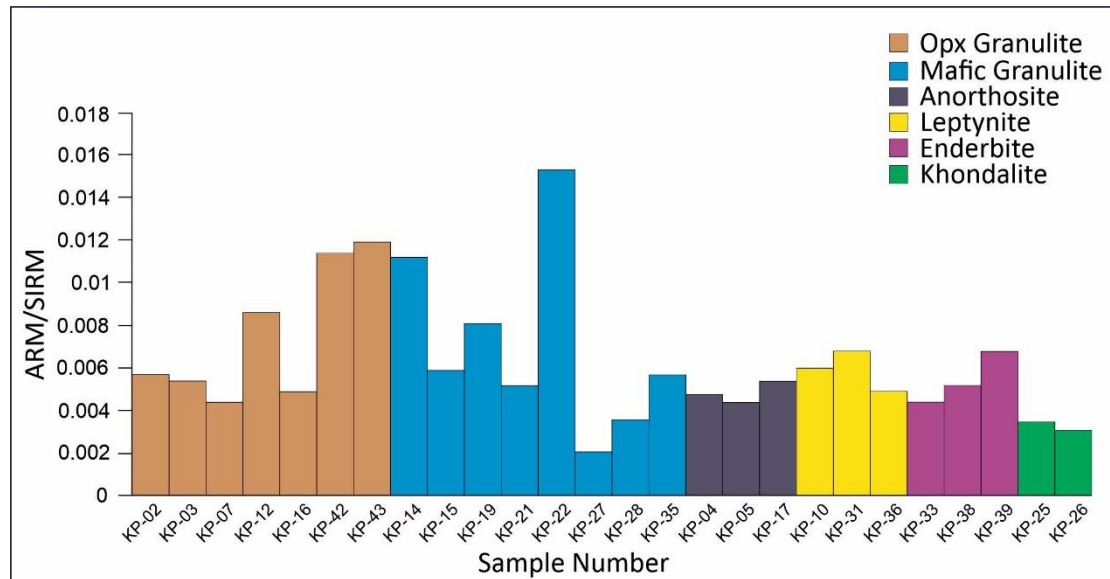


**Fig. 6.13: Distribution of ARM/ $\chi$  in different rock types of KPLC.**

Khadkikar, 2004). The values of ARM/SIRM of the studied samples are represented in the Fig. 6.13 and listed in the Table 6.5. The values range from 0.0021 in mafic granulite to 0.0153 in mafic granulite with an average value of 0.0063. The overall values of ARM/SIRM indicate that the studied samples contain mainly SSD to PSD grains of magnetic minerals. Some samples show lower ARM/SIRM value indicating presence of large MD grains which is also evident from petrographic studies (porphyroblasts of C1-Stage and Stage-1 of primary titanomagnetite).

### 6.3.6. Partial IRMs: Hard IRM, Soft IRM and S-ratio

Partial IRMs includes Hard IRM (HIRM), Soft IRM and S-ratio. HIRM is absolutely concentration dependent parameter and used as a measure of the mass concentration of high coercivity antiferromagnetic minerals (e.g., haematite and goethite) to the saturation remanence (Basavaiah, 2011, Liu et al., 2012). HIRM refers to the hard fraction of the magnetic component, which is determined by the formula:  $HIRM = (SIRM + IRM_{-0.3T})/2$ , where  $IRM_{-0.3T}$  is IRM remaining after exposed to a

**Table 6.6: Distribution of Soft IRM, Hard IRM and S-ratio in KPLC rocks.**

Sample	Mass (gm)	Soft IRM ( $10^{-5} \text{ Am}^2 \text{ Kg}^{-1}$ )	Hard IRM ( $10^{-5} \text{ Am}^2 \text{ Kg}^{-1}$ )	Sratio-300mT	S-ratio-100mT
KP- 02	9.672	178.6884	14.8728	1.0646	0.931938706
KP- 03	10.358	158.4789	8.4335	1.0451	0.855070616
KP- 07	9.531	3698.4577	339.7104	1.0667	0.943679882
KP- 12	10.068	439.0817	3.3306	1.0059	0.834722777
KP- 16	9.846	3954.9868	350.3768	1.0658	0.953581433
KP- 42	9.114	1046.8192	572.4128	1.4101	1.186594603
KP- 43	9.912	320.9115	20.1064	0.9400	0.677018968
KP- 14	8.168	316.9105	10.2510	1.0220	0.865991974
KP- 15	9.146	746.6219	5.8441	0.9944	0.7879996933
KP- 19	9.139	1154.0239	32.4762	1.0223	0.86100003
KP- 21	10.358	1711.4174	107.5156	1.0391	0.920958612
KP- 22	9.255	675.0972	37.1277	0.9484	0.671827511
KP- 27	9.243	5759.8431	871.0776	0.8709	0.469119111
KP- 28	8.987	2713.3231	54.6990	0.9837	0.855611214
KP- 35	8.317	1543.7399	13.4916	0.9932	0.8690752224
KP- 04	8.594	764.9673	62.7729	1.0581	0.905405592
KP- 05	8.828	2093.6184	150.2821	1.0561	0.937668511
KP- 17	8.721	1098.0690	91.6053	1.0567	0.942096416
KP- 10	9.481	4683.0166	196.9972	1.0363	0.864451983
KP- 31	9.506	861.4798	28.0665	0.971	0.776649333
KP- 36	7.595	1466.7966	4.0579	0.9978	0.86591781
KP- 33	8.288	170.3314	2.8257	0.9836	0.723311568
KP- 38	9.868	750.1792	10.0719	0.9899	0.806461165
KP- 39	9.112	66.6758	4.7896	1.0552	0.880893975
KP- 25	9.688	3914.6928	21.1447	0.9946	0.967692572
KP- 26	8.46	1755.3960	72.4846	0.9604	0.632951093

reversed field of 0.3T after SIRM acquisition in the opposite direction (Liu et al., 2012). The soft fraction of magnetic component is quantified through the relative term S-ratio, calculated from measurements of SIRM and of the IRM subsequently acquired in back fields of 100 mT (IRM<sub>-100</sub>) or 300 mT (IRM<sub>-300</sub>). The S-ratio is defined as,  $S_{-100} = (-\text{IRM}_{-100}/\text{SIRM})$  or  $S_{-300} = (-\text{IRM}_{-300}/\text{SIRM})$  (King and Channell, 1991). S-ratio can be used to identify magnetic mineralogy (Bloemendal et al., 1992). S-ratio close to +1.0 are indicative of soft ferrimagnetic minerals (e.g., magnetite and titanomagnetite), while low S-ratios ( $< 0.6$  or even  $< 0$ ) are caused by the presence of antiferromagnetic minerals (Mooney et al., 2002). This basically normalizes the data to express the overall concentration of the ferrimagnetic minerals as indicated by SIRM.



The values of HIRM in the studied samples ranges from  $2.8 \times 10^{-5} \text{Am}^2 \text{kg}^{-1}$  in enderbite to  $87 \times 10^{-5} \text{Am}^2 \text{kg}^{-1}$  in mafic granulite with an average value of  $118.72 \times 10^{-5} \text{Am}^2 \text{kg}^{-1}$ . The distribution of HIRM is shown in the bar diagram (Fig. 14) and listed in the Table 6.6. From the values of Hard IRM in the studied samples, it is seen that the

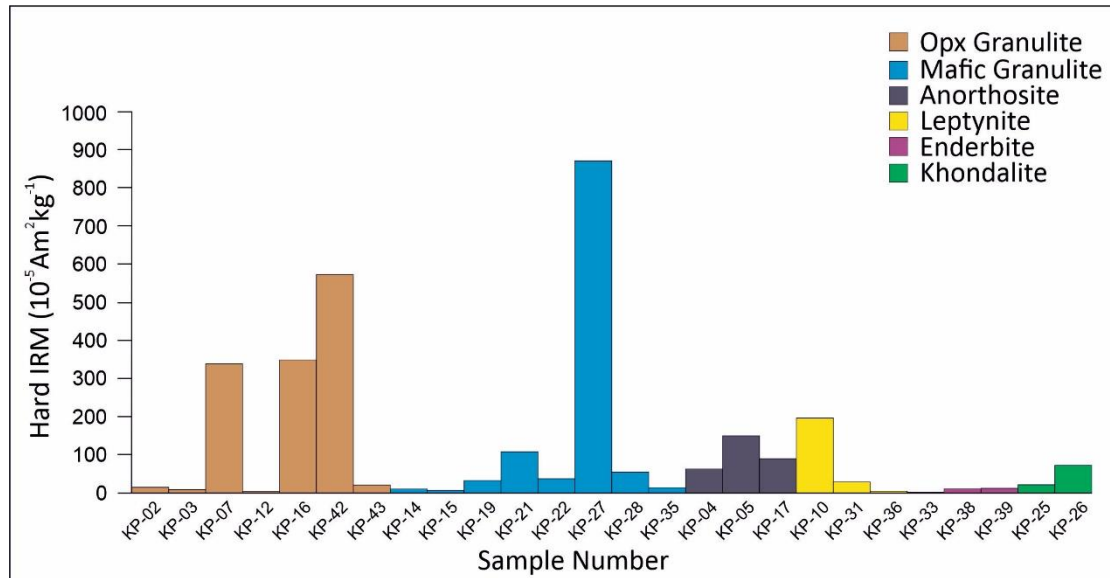


**Fig. 6.14: Distribution of HIRM in different rock types of KPLC.**

overall components of the magnetically hard minerals are low. Some samples show relatively high HIRM values (KP- 07, KP- 16, KP- 27, KP- 42). This is due to the presence of ilmeno-haematite within these samples which is also evident from the petrographic studies. Comparing the values of HIRM and Soft IRM (Table 6.6 and Fig. 14 and Fig. 15), it is noted that, the Soft IRM dominates over the HIRM in all the samples, indicating that the chief remanence carriers are soft titanomagnetite and magnetite with minor concentration of haematite (Basavaiah et al., 2018).

The values of S-ratio can be calculated corresponding to all backfield IRM acquisitions during measurements. Here S-ratio corresponds to 100 mT ( $S_{100}$ ). The values of S-ratio are represented in the Fig. 6.16 and listed in the Table 6.6. The values of S-ratio ranges 0.67 in mafic granulite to 1.18 in orthopyroxene granulite with an average value of 0.84. The values of S-ratio of most of the samples irrespective of rock types are close to 1, which signifies titanomagnetite and magnetite are the chief remanence carrier within the studied rocks. Apparently lower values suggest the presence of ilmeno-haematite within the studied samples as evident from the

petrographic studies. Also, the higher HIRM values corroborates that contention (Basavaiah and khadkikar, 2004).

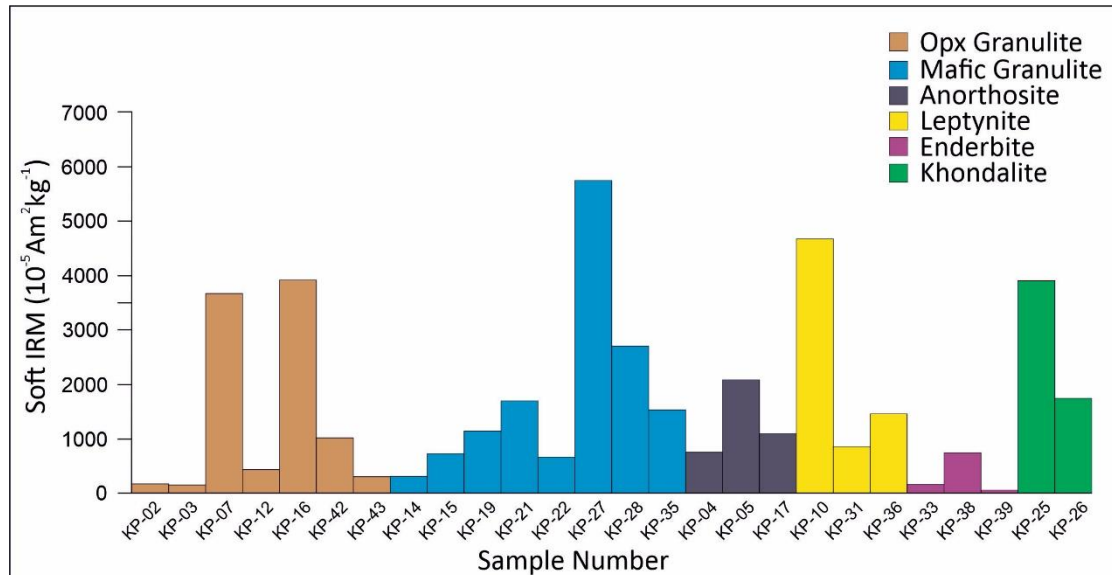


Fig. 6.15: Distribution of Soft IRM in different rock types of KPLC.

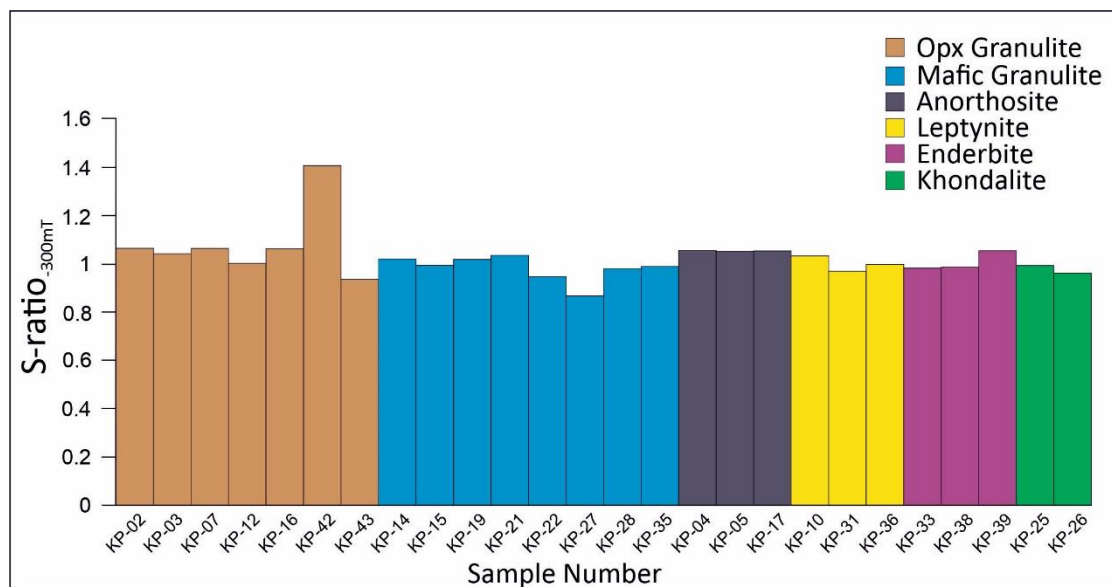


Fig. 6.16: Distribution of S-ratio in different rock types of KPLC.

### 6.3.7. SIRM versus Magnetic Susceptibility ( $\chi$ ) Plot

In the bi-logarithmic Plot of saturation remanence (SIRM) versus magnetic susceptibility ( $\chi$ ), the distribution of high  $\chi$  and high SIRM is defined by the presence of large amount of Stable Single Domain (SSD) magnetite and titanomagnetite and both low  $\chi$  and low SIRM characterised by high haematite to magnetite ratio. It is used to

characterize the maximum possible ranges of magnetic minerals within the rocks. Also, SIRM versus  $\chi$  can unravel the controlling factors (ferrimagnetic or paramagnetic minerals) of AMS and magnetic fabrics.

In bi-logarithmic Plot of SIRM versus  $\chi$  of the rocks from KPLC is represented in Fig. 17. It shows positive correlation irrespective of rock types i.e., samples have high  $\chi$ , also have high SIRM (Fig. 6.6 and Fig. 6.8). Hence it is evident that the mineral contributing towards high susceptibility also contributing towards high saturating remanence. Such a relation can only be obtained by the presence

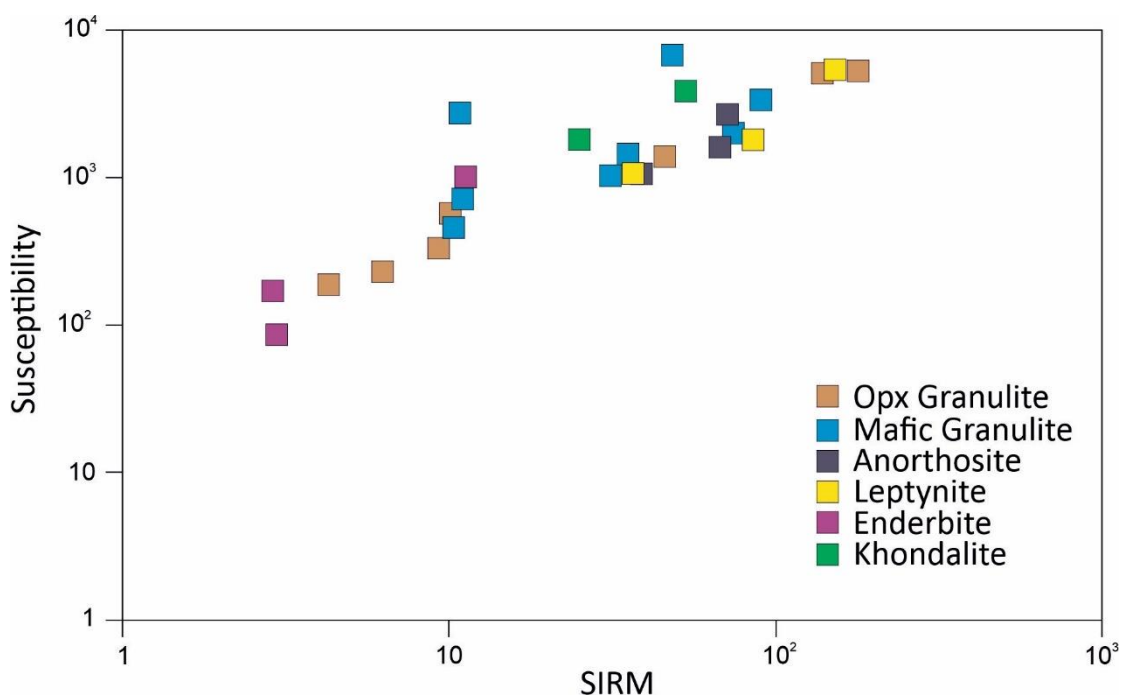


**Fig. 6.17: SIRM versus Magnetic Susceptibility ( $\chi$ ) Plot of different rock types of KPLC.**

of titanomagnetite or magnetite. Their high  $\chi$  and SIRM values are due to the presence of large amounts of SSD titanomagnetite and magnetite. Thus, it is evident that the titanomagnetite and magnetite are the chief remanence carrier in the studied rocks. This scenario thus explained is also evident from the near constant values of SIRM/  $\chi$ .

#### 6.4. Summary of Rock Magnetic Studies

The main objective of this chapter is to characterize the magnetic properties of the rocks from KPLC, in terms of rock magnetic and mineral magnetic measurements. Petrographic study under reflected light microscope revealed that, the rocks under study

contain chiefly ferrimagnetic minerals (magnetite and titanomagnetite) along with some ilmeno-haematite with a broad range of grain size distribution indicating multiple origins of these Fe-Ti oxide minerals. Evidently, the generations of Fe-Ti oxides and their textural relationship with the silicates are different in all rock types. Also, the Fe-Ti oxide grain sizes are bimodal.

The magnetic hysteresis studies and day plot (Fig. 6.3 and Fig. 6.4) shows that the chief remanence carriers belong to fine-grained SD to PSD titanomagnetite. Several factors can contribute to the observed magnetic domain states (Roberts et al., 2018). The most important factor is the degree of low temperature and high temperature oxidation. With increasing degrees of low temperature oxidation, the effective grain sizes shift from the MD-PSD boundary towards the PSD field. High degrees of low temperature and high temperature oxidations are observed in the present study (up to Stage-4, according to Johnson and Hall, 1978 and up to C4-Stage, according to Haggerty, 1976). Thus, despite the presence of petrographically coarser grains, no plots fall in the MD field. Secondly, if the magnetic grains with random orientation, have tendencies to decrease the  $M_{rs}/M_s$  values and the net grain size comes to PSD. From the petrographic studies, it is evident that the magnetic grains display no preferred orientations and thus may have effectively contributed to the PSD affinity. Thirdly and finally, the titanomagnetite grains are near equant and are rarely elongated in any preferred orientation, thereby increasing tendencies to come under PSD (Roberts et al., 2018). The results from the IRM studies and the coercivity spectra (Fig. 6.5) also denote that the chief magnetic mineral is titanomagnetite depicted by the lower fields of saturation (150 to 200 mT) and lower values of coercivity. However, the fields at which the IRM saturates and the corresponding coercivity spectra can be subdivided into two groups. One belongs to a magnetically very soft group, mainly titanomagnetite. The other samples which have relatively higher saturation fields (250–300 mT) and coercivities are indicative of evidence of maghemitization (Thompson and Oldfield, 1986). Maghemitization is associated with low-temperature oxidation (Basavaiah, 2011), which is abundant in these samples. The presence of titanomagnetite is also confirmed by the thermo-magnetic curves and the corresponding  $IP_x$  values (Fig. 6.1). Thus, based on the magnetic mineralogy and magnetic grain sizes in the rocks under study it can be stated that the rocks are ferrimagnetic and they have considerably high remanence recording potentials. Certain deviations from ferrimagnetism are evident

due to oxidations, however, that does not by any means nullify the remanence recording potentials (Basavaiah, 2011; Basavaiah and Khadkikar, 2004; Chatterjee et al., 2021).

Mineral magnetic measurements of  $\chi$ , ARM, SIRM and the inter-parametric ratios allowed quantifying magnetic minerals and their properties as parameters related to them. Magnetic susceptibility ( $\chi$ ), SIRM and ARM are concentration indicator. They determine the concentration of remanence carriers i.e., ferrimagnetic minerals within the samples. Here, in the studied samples of KPLC, the overall values of these parameters are high which indicate the rocks from the studied area have high concentration of magnetic minerals (magnetite and titanomagnetite) which is also evident from the petrographic study. The average  $\chi$  values of the different rock types (ranges  $39.1 \times 10^{-7} \text{ m}^3 \text{ kg}^{-1}$  to  $91.1 \times 10^{-7} \text{ m}^3 \text{ kg}^{-1}$ ) are high except enderbite ( $5.69 \times 10^{-7} \text{ m}^3 \text{ kg}^{-1}$ ). This is due to presence of weak ferrimagnetic ilmeno-haematite which is also evident from the petrographic studies. Also, higher ARM values (ranges  $8.55 \times 10^{-5} \text{ Am}^2 \text{ kg}^{-1}$  to  $16.37 \times 10^{-5} \text{ Am}^2 \text{ kg}^{-1}$ ) also indicate the presence of Stable Single Domain (SSD) magnetic minerals as it is very sensitive to the small sized particles except emderbite. In enderbite the average value of ARM is  $2.17 \times 10^{-5} \text{ Am}^2 \text{ kg}^{-1}$  indicate presence of coarse MD grains which corresponds to the coarse porphyroblasts of fresh titanomagnetite grains. Grain size indicator parameter frequency dependence susceptibility ( $\chi_{fd} \%$ ), determine the amount of magnetic grain of superparamagnetic (SP) range present within the studied samples. Values of  $\chi_{fd} \%$  of studied samples have two groups, one is  $< 2\%$  and another one is  $> 2\%$  but far less than  $10\%$  indicating studied samples contain either no SP grains or a mixture of coarse magnetic grains and SP grains. Inter-parametric ratios,  $\text{ARM}/\chi$ ,  $\text{SIRM}/\chi$ ,  $\text{ARM}/\text{SIRM}$  determine the grain size of the magnetic minerals. Overall values of the  $\text{ARM}/\chi$  (ranges  $0.14 \times 10^2 \text{ Am}^{-1}$  in anorthosite to  $0.49 \times 10^2 \text{ Am}^{-1}$  in mafic granulite) and  $\text{SIRM}/\chi$  (ranges  $28.94 \times 10^2 \text{ Am}^{-1}$  in leptynite to  $80.65 \times 10^2 \text{ Am}^{-1}$  in mafic granulite) in the studied samples are moderate to higher, indicating the grains of magnetic mineral within the samples are SSD to PSD in nature. Presence of oxidised (oxidised up to C4-Stage of high temperature oxidation according to Haggerty, 1976 and up to Stage-5 of low temperature oxidation according to Johnson and Hall, 1978) primary titanomagnetite and ultra-fine grains of secondary magnetite are responsible for SSD to PSD range.  $\text{ARM}/\text{SIRM}$  values (ranges 0.0033 to 0.0075) determined the presence of both SSD

and PSD-MD grains of magnetic minerals. The unoxidized fresh porphyroblasts of titanomagnetite (Stage-1 of low temperature oxidation according to Johnson and Hall, 1978 and C1-Stage of high temperature oxidation according to Haggerty, 1976) are responsible for these PSD-MD range values. Composition indicator Soft IRM, Hard IRM and S-ratio Determined the type of the magnetic minerals. Overall, the values of Soft IRM (average value ranges  $329.06 \times 10^{-5} \text{Am}^2 \text{kg}^{-1}$  in enderbite to  $2835.04 \times 10^{-5} \text{Am}^2 \text{kg}^{-1}$  in khondalite) are higher which is dominant over Hard IRM (average value ranges  $5.89 \times 10^{-5} \text{Am}^2 \text{kg}^{-1}$  in enderbite to  $187.03 \times 10^{-5} \text{Am}^2 \text{kg}^{-1}$  in opx-granulite) indicating the predominant remanence carrier is soft titanomagnetite and magnetite. Also, the narrow range of high S-ratio (close to 1) values of the studied samples indicate the predominant remanence carrier is soft titanomagnetite and magnetite. SIRM vs Susceptibility graph indicates the high magnetite to haematite ratio within the studied sample.

The magneto mineralogical characteristics of studied rocks based on the mineral magnetic properties are summarised in Table 6.7. The estimation of the composition, concentration and grain size is mainly based on the analysis of primary rock magnetic and mineral magnetic parameters such as  $\chi$ , ARM and SIRM; and inter-parametric ratios like ARM/ $\chi$ , SIRM/ $\chi$ , ARM/SIRM, Soft IRM, HIRM and S-ratio and may also have important palaeomagnetic implications.

**Table 6.7: Summary of magneto mineralogical characteristics of KPLC rocks based on the mineral magnetic parameters.**

Rock type	Magnetic Signature	Magnetic Nature and Mineralogy	Petrological Signature	Potential of recording remanence
Opx-Granulite	High $\chi$ ( $56.2 \times 10^{-7} \text{m}^3 \text{kg}^{-1}$ ), High SIRM ( $1876.18 \times 10^{-5} \text{Am}^2 \text{kg}^{-1}$ ), High ARM ( $10.76 \times 10^{-5} \text{Am}^2 \text{kg}^{-1}$ ), Moderate $\chi_{\text{rd}}$ % (2.16), High ARM/SIRM,	Ferrimagnetic. Magnetite and titanomagnetite of SSD to PSD nature. Small amount of SP grains.	Low (Stage-2- Stage-5) and High (C2- Stage to C4- Stage) temperature oxidation of primary titanomagnetite and ultra-fine grains of secondary magnetite.	High

	High ARM/ $\chi$ , High SIRM/ $\chi$ (38.53), $S_{-100}=0.91$ , Low HIRM, Soft IRM $\gg$ HIRM.			
Mafic Granulite	High $\chi$ ( $38.9 \times 10^{-7} \text{ m}^3 \text{ kg}^{-1}$ ), High SIRM ( $2314.72 \times 10^{-5} \text{ Am}^2 \text{ kg}^{-1}$ ), High ARM ( $10.72 \times 10^{-5} \text{ Am}^2 \text{ kg}^{-1}$ ), Moderate $\chi_{fd}$ % (2.43), High ARM/SIRM, High ARM/ $\chi$ , High SIRM/ $\chi$ (80.65), $S_{-100}=0.78$ , Low HIRM, Soft IRM $\gg$ HIRM.	Ferrimagnetic. Magnetite and titanomagnetite of SSD to PSD nature. Small amount of SP grains.	Low (Stage-2 to Stage-5) and High (C2- Stage to C4- Stage) temperature oxidation of primary titanomagnetite and ultra-fine grains of secondary magnetite.	High
Anorthosite	High $\chi$ ( $58.9 \times 10^{-7} \text{ m}^3 \text{ kg}^{-1}$ ), High SIRM ( $1790.92 \times 10^{-5} \text{ Am}^2 \text{ kg}^{-1}$ ), High ARM ( $8.55 \times 10^{-5} \text{ Am}^2 \text{ kg}^{-1}$ ), Low $\chi_{fd}$ % (1.88), High ARM/SIRM, Moderate ARM/ $\chi$ , Moderate SIRM/ $\chi$ (29.98), $S_{-100}=0.92$ , Low HIRM, Soft IRM $\gg$ HIRM.	Ferrimagnetic. Magnetite and titanomagnetite of SSD to PSD nature. Small MD grains. No or <10% SP grains.	Low (Stage-2 to Stage-5) and High (C2- Stage to C4- Stage) temperature oxidation of primary titanomagnetite and ultra-fine grains of secondary magnetite. Coarse primary titanomagnetite (C1-Stage and Stage-1)	High
Leptynite	High $\chi$ ( $91.1 \times 10^{-7} \text{ m}^3 \text{ kg}^{-1}$ ), High SIRM ( $2780.22 \times 10^{-5} \text{ Am}^2 \text{ kg}^{-1}$ ),	Ferrimagnetic. Magnetite and titanomagnetite of SSD to PSD	Low (Stage-2 to Stage-5) and High (C2- Stage to C4- Stage) temperature oxidation of primary titanomagnetite	High

	High ARM ( $16.37 \times 10^{-5} \text{ Am}^2 \text{ kg}^{-1}$ ), Low $\chi_{fd}$ % (1.56), High ARM/SIRM, Moderate ARM/ $\chi$ , Moderate SIRM/ $\chi$ (28.94), $S_{100}=0.83$ , Low HIRM, Soft IRM $\gg$ HIRM.	nature. Small MD grains. No or <10% SP grains.	and ultra-fine grains of secondary magnetite. Coarse primary titanomagnetite (C1-Stage and Stage-1)	
Enderbite	Low $\chi$ ( $5.69 \times 10^{-7} \text{ m}^3 \text{ kg}^{-1}$ ), Moderate SIRM ( $1876.18 \times 10^{-5} \text{ Am}^2 \text{ kg}^{-1}$ ), Low ARM ( $2.17 \times 10^{-5} \text{ Am}^2 \text{ kg}^{-1}$ ), Low $\chi_{fd}$ % (1.42), High ARM/SIRM, High ARM/ $\chi$ , High SIRM/ $\chi$ (59.31), $S_{100}=0.80$ , Low HIRM, Soft IRM $\gg$ HIRM.	Ferrimagnetic and antiferromagnetic. Magnetite and titanomagnetite of SSD to PSD nature. Ilmeno-haematite. No or <10% SP grains.	Low Stage-2- Stage-5) and High (C2- Stage to C4-Stage) temperature oxidation of primary titanomagnetite and ultra-fine grains of magnetite. Ilmeno- haematite also present.	Moderate to High
Khondalite	High $\chi$ ( $39.1 \times 10^{-7} \text{ m}^3 \text{ kg}^{-1}$ ), High SIRM ( $2874.18 \times 10^{-5} \text{ Am}^2 \text{ kg}^{-1}$ ), High ARM ( $9.69 \times 10^{-5} \text{ Am}^2 \text{ kg}^{-1}$ ), Moderate $\chi_{fd}$ % (2.32), Moderate ARM/SIRM, High ARM/ $\chi$ , High SIRM/ $\chi$ (73.40), $S_{100}=0.80$ , Low HIRM, Soft IRM $\gg$ HIRM.	Ferrimagnetic. Magnetite and titanomagnetite of SSD to PSD nature. No or <10% SP grains.	Low (Stage-2 to Stage-5) and High (C2- Stage to C4-Stage) temperature oxidation of primary titanomagnetite and ultra-fine grains of secondary magnetite	High



It is evident from the rock magnetic and mineral magnetic studies that the ferrimagnetic properties and remanence recording potential of rocks from the KPLC are chiefly due to the presence of titanomagnetite and magnetite. It may be noticed that the magnetic susceptibility is much higher in the granulite facies metamorphic rocks than in the magmatic suite (Table 6.3). This has occurred due to the enhancement of titanomagnetite in the rocks due to a prolonged period of metamorphism to granulite facies (Frost and Shive, 1986; Shive and Fountain, 1988; Shive et al., 1992; Liu et al., 2013). The correlation between the rock magnetic properties of deep crustal rocks and metamorphic grades is dubious to date (Wang et al., 2015), however, from the present study it is quite evident that the ferrimagnetism increases with increasing grades of metamorphism. The same is reported in the Chilka lake domain of the EGB (Chatterjee et al., 2016). According to Wang et al. (2015), prograde metamorphism to granulite facies enhances the rocks in Fe-Ti oxides like ferrimagnetic magnetite and titanomagnetite but retrograde metamorphism of the granulites impinges para-magnetism. The same is the case for the KPLC where the para-magnetism is strengthened during the retrograde P-T-t path of metamorphism (Sengupta et al., 1999) whereby uplift-related oxidation processes come to play.

**Chapter 7**  
**Palaeomagnetic Studies**

## PALAEOMAGNETIC STUDIES

### 7.1. Introduction

The main aim of the palaeomagnetic study is the recognition and separation of NRM components acquired by the rocks at different time of their geological history. Usually most of the high-grade metamorphic rocks acquire more than one component of magnetization. The primary magnetization component acquired at the time of formation of the rocks and the secondary one acquired later subsequent to their formation. Sometimes, a soft viscous remanence magnetization (VRM) is acquired in the present EMF. To isolate the ChRM, selective removal of secondary NRM is needed. Demagnetization technique can be used to separate out various magnetization components (primary and secondary) comprises the total NRM in the high-grade metamorphic rocks. Demagnetization technique is also known as “cleaning” of remanent magnetization. The different magnetization components usually have different coercivity spectra and blocking temperature. Depending upon this, there are two different demagnetization techniques, which have been largely used. First one is Alternating Field (AF) demagnetization, where a rock specimen is exposed to a decaying alternating magnetic field in the absence of external direct magnetic fields. And second one is Thermal demagnetization, which involves heating a specimen to an elevated temperature below the Curie temperature of the constituent ferrimagnetic minerals and then cooling to room temperature in a zero magnetic field.

In case of AF demagnetization processes a decaying alternating magnetic field is applied to a sample in the absence of any external direct magnetic field. Any remanent magnetization of coercivity less than the peak intensity of applied AF then ‘cleaned’ from the sample. Thus, AF demagnetization is used to remove secondary NRM carried by the low coercivity grains and leave the ChRM unaffected.

### 7.2. Natural Remanent Magnetization (NRM)

The NRM is the permanent magnetism of rock and preserve a record of the EMF through geologic time since its formation. The bulk remanent magnetization presents in the rock before any demagnetization treatment, described as NRM (J) and defined

by the vector sum of multiple remanent components. The NRM possess direction (Declinations and Inclinations) and magnitude (Intensity of magnetization) and have been determined in the laboratory. The NRM is expressed as:

$$J = J_i + J_r \quad (\text{Butler, 1992})$$

where  $J_i$  is induced magnetizations (acquired parallel to the direction of EMF) and  $J_r$  is remanent magnetizations. However, acquisition of induced magnetization is a reversible process without effect of the past magnetic fields. So, for palaeomagnetism, the remanent magnetization acquired by the rock at the time of its formation is important (Butler, 1992; Tarling, 2007).

NRM consists of both primary and secondary NRMs. Primary NRM acquired during the formation of the rocks is parallel to the ambient Earth's magnetic field, whereas secondary NRM is acquired during the subsequent geological processes suffered by the rocks (Butler, 1992). The directions of NRM from demagnetization of samples from KPLC therefore represent the direction of ChRM.

The frequency distribution of NRM intensity of the samples collected shown in the Fig. 7.1. It shows that the majority of the samples possess high NRM intensity. The range for majority of the samples varies from 10 mA/m to 1349 mA/m. It is observed that the sites showing high concentration of ferrimagnetic minerals (or high SIRM) show high NRM intensities. Based on the distribution of the NRM intensities, the rock types showing high NRM intensity from intensities are examined for palaeomagnetic study.

The distribution of NRM directions of samples from the area under study are plotted mostly along the NE and NW direction with positive inclination (Fig. 7.2). The present Earth's magnetic field directions are Declination (D)/Inclination (I) =  $0^\circ/23^\circ$  or the equivalent reversed direction  $D/I = 180^\circ/-23^\circ$ . The NRM direction of the samples from KPLC do not possess any significant record of the present EMF.

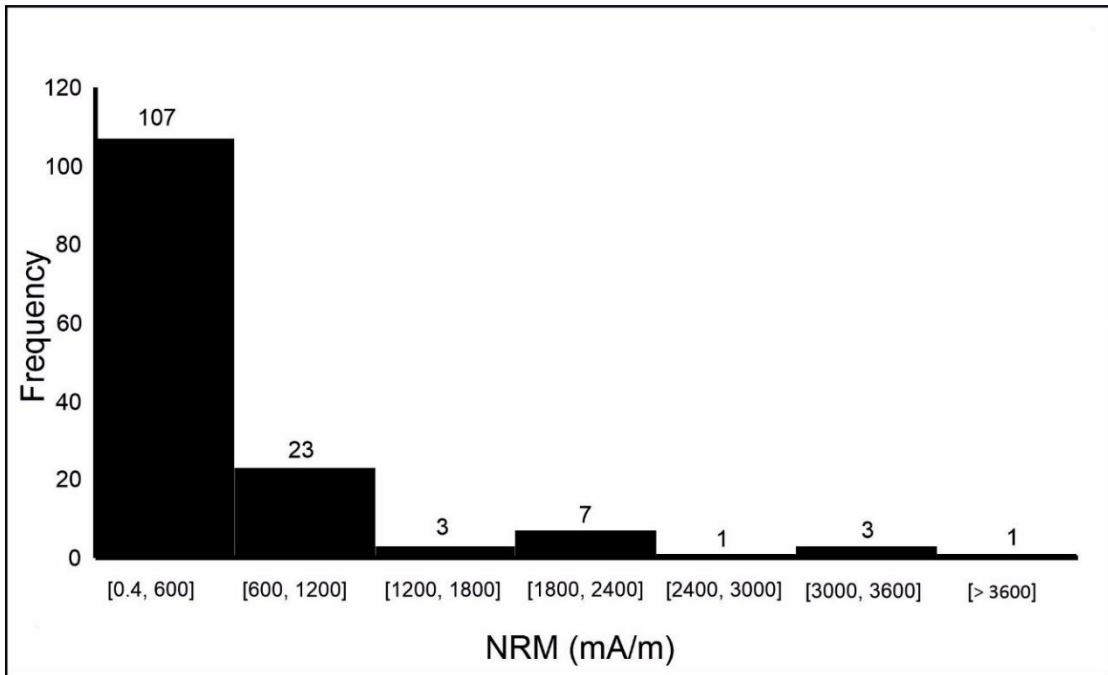


Fig. 7.1: Frequency distribution of NRM in KPLC.

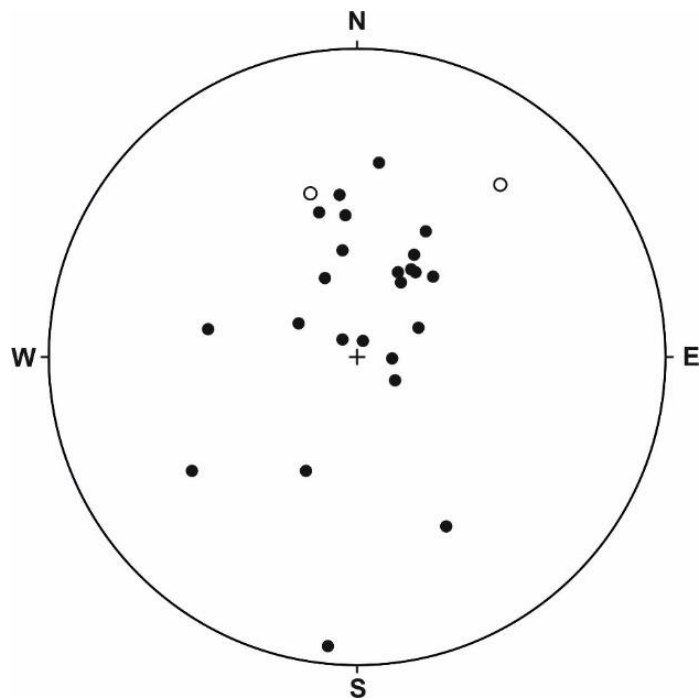


Fig. 7.2: Equal area diagram showing distributions of NRM directions of studied samples. Hollow circles denotes negative inclination.

### 7.3. Koenigsberger (Q) Ratio

The relative proportion of the remanent magnetization and the induced magnetization in natural rocks is known as the Koenigsberger ratio. It is also denoted as the Q ratio. The Q ratio physically signifies the ratio between NRM and  $\chi$  within a rock. i.e.,

$$Q = \text{NRM}/\chi$$

Q ratio is used as a measure of stability to indicate a rock's capability of maintaining stable remanence. Thus, Q ratio greater than 1 indicates that the remanence properties contribute the majority of the total magnetization of the rocks.

In the present study, the Q-ratio of different samples is calculated by dividing the NRM by the low frequency susceptibility ( $\chi$ ). The frequency distribution of the Q-ratio is represented in Fig. 7.3. The Q ratio of the studied samples ranges 0.2 to 4.7. The majority of the samples have Q-ratio ranges between 0.1 to 1.137. The NRM and susceptibility of the studied rocks are high, which results in low Q ratio. Low Q ratio

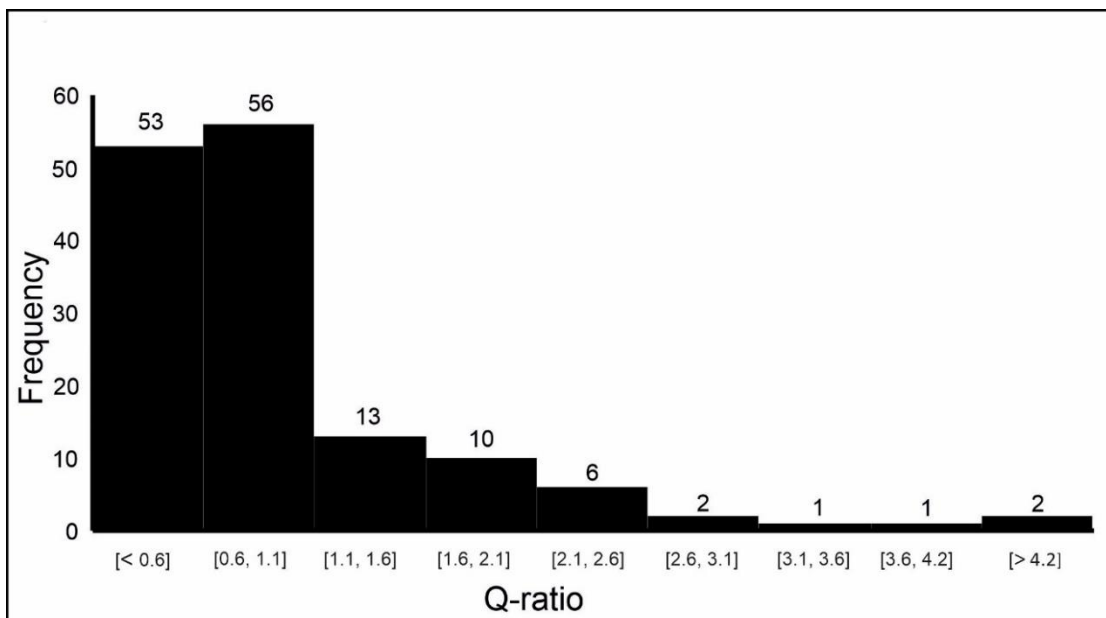


Fig. 7.3: Frequency distribution of Q-ratio in KPLC.

indicate that, in situ magnetization of those rocks is larger than their induced magnetization. Thus, the in-situ magnetization is dominated by remanent magnetization

than an instantaneous magnetization induced by Earth's magnetic field. The samples which have high NRM and high Q-ratio ( $>1$ ) were selected for palaeomagnetic studies and subjected to the AF demagnetization.

#### 7.4. AF Demagnetization

Step wise AF demagnetization was carried out with the high-grade metamorphic rocks from the studied area by applying fields varying from 2.5 mT to 100 mT. The field was applied initially with lower field difference (2.5 mT-5 mT) and larger differences (10 mT-20 mT) after. Each step of the demagnetization process magnetic declination, inclination and intensity of magnetization (Appendix I) were measured using Molspin Spinner Magnetometer.

To determine the stable magnetic vectors from the results of AF demagnetization of high-grade rocks, three types of diagrams were used i.e., orthogonal plot, intensity plot and stereo plot. In orthogonal plot (Zijderveld, 1967), projection of magnitude and direction (declination and inclination) plotted on a horizontal and vertical plane. This diagrams also known as Zijderveld diagram. In case of intensity plot, intensity of magnetization of each step was plotted with respect to the applied magnetic field. Intensity plot shows the behaviours of magnetization vectors giving coercivity spectrum. The magnetization directions of each step of demagnetization were plotted on a lower hemisphere equal stereo net in stereo plot. Stereo plot exhibits the movement of vectors.

The samples of high-grade metamorphic rocks from KPLC possess multi-component magnetization vector. The relative contributions of them are different in different samples. Sample KP-10.01 shows a movement of magnetic vector from  $D/I = 20.9^\circ/54.5^\circ$  to  $14.1^\circ/36.5^\circ$  (Appendix I, Fig. 7.4c), which indicates that the presence of multi-component magnetization vector within the sample. The orthogonal plot of sample KP-10.01 shows two more or less straight segments (Fig. 7.4a), indicating multi-component vectors of magnetization. These segments correspond to AF ranges 0 mT to 15 mT and 20 mT to 100 mT. The former one is low coercivity range and the later one is high coercivity range. This is also evident from the Intensity plot of the sample KP-10.01 (Fig. 7.4b). The samples KP-2.01, KP-7.01, KP-36.01, KP-25.01

show the similar AF demagnetization behaviour (Fig. 7.5, Fig. 7.6, Fig. 7.7 and Fig. 7.8). The magnetization component in these samples is highly stable with a little and relatively weak but stable component. The stereo plots exhibit that, the magnetic vectors lie in north easterly direction with moderate inclination (KP-10.01, Fig. 7.5c) and north westerly direction with moderate inclination (KP-36.01, Fig. 7.7c).

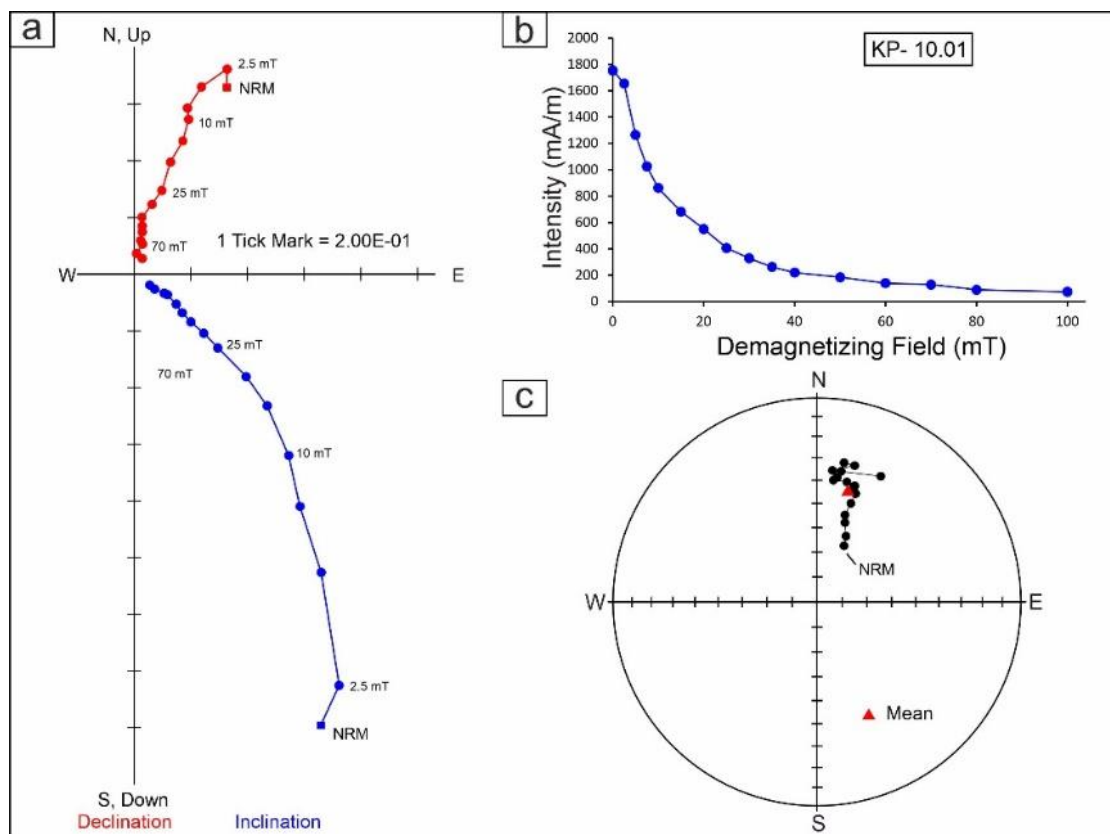


Fig. 7.4: (a) Orthogonal plot, (b) Intensity plot and (c) Stereo plot of demagnetization data of sample KP-10.01.



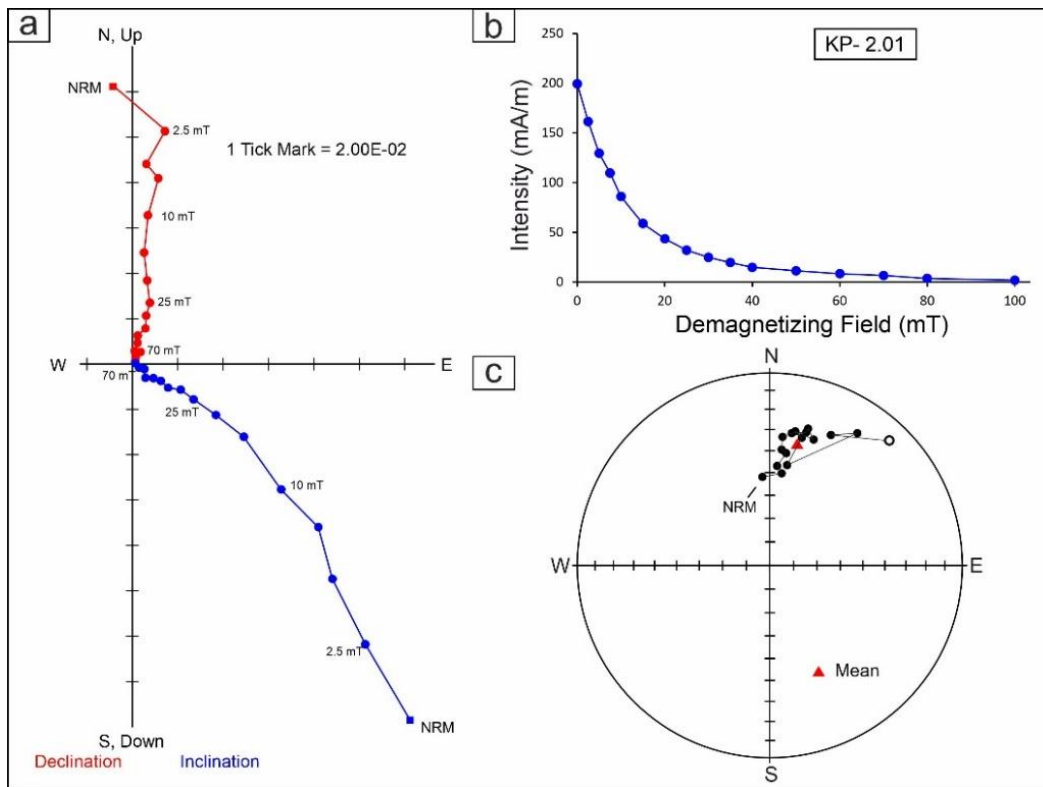


Fig. 7.5: (a) Orthogonal plot, (b) Intensity plot and (c) Stereo plot of demagnetization data of sample KP-2.01.

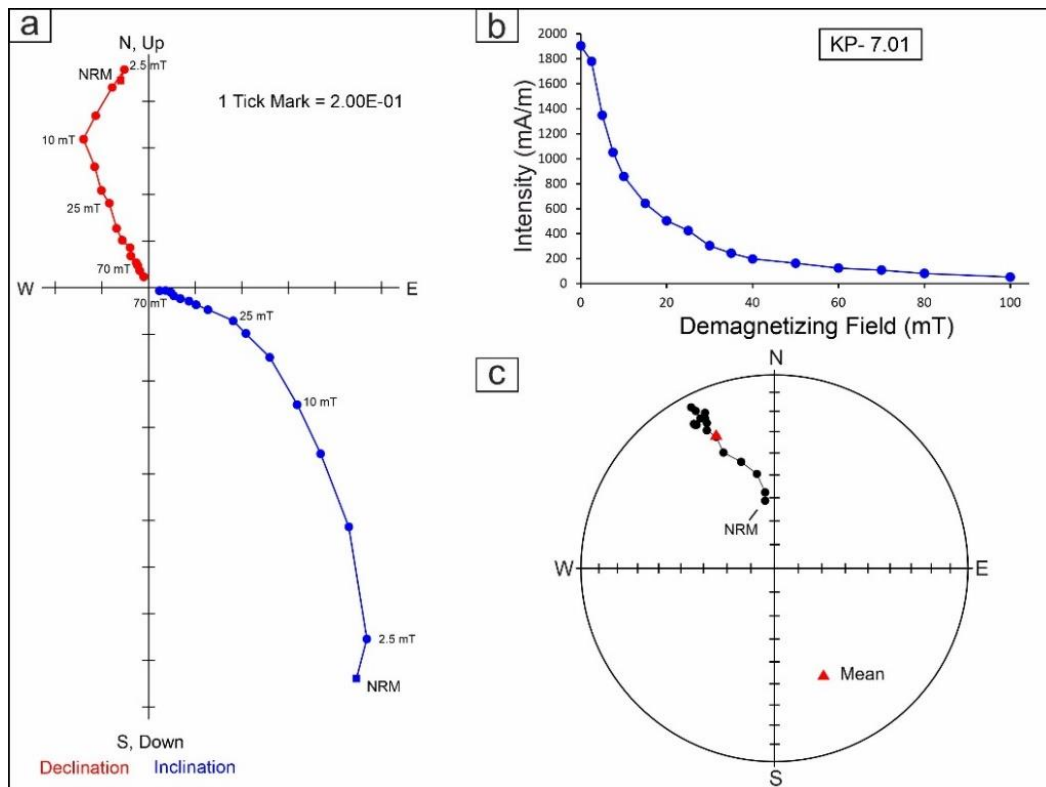


Fig. 7.6: (a) Orthogonal plot, (b) Intensity plot and (c) Stereo plot of demagnetization data of sample KP-7.01.

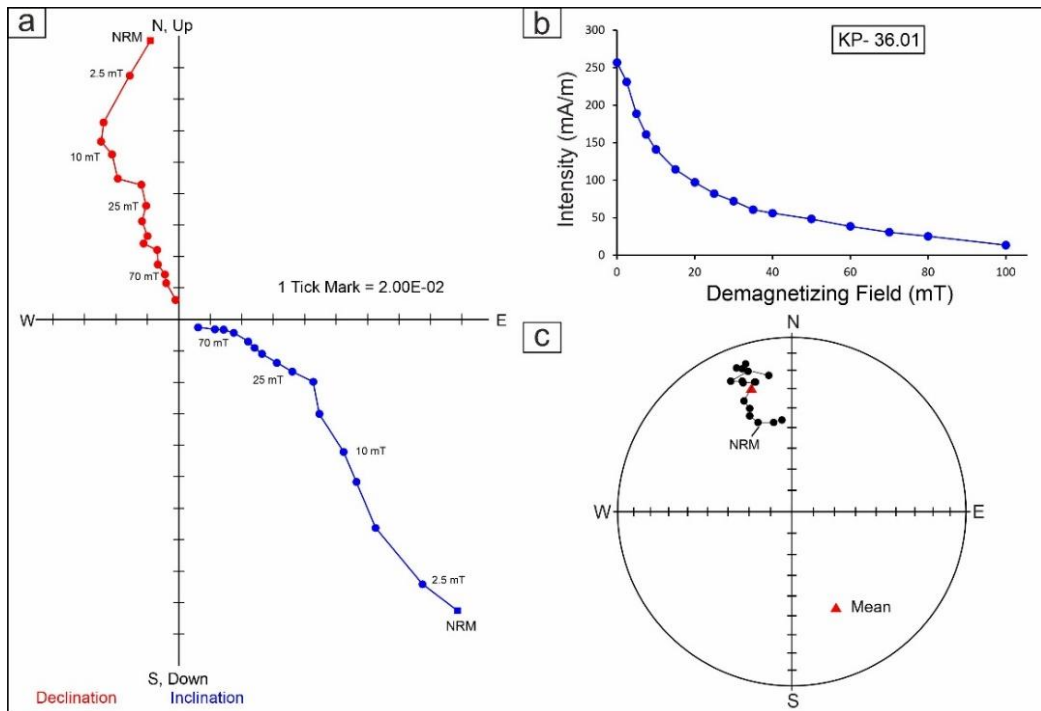


Fig. 7.7: (a) Orthogonal plot, (b) Intensity plot and (c) Stereo plot of demagnetization data of sample KP-36.01.

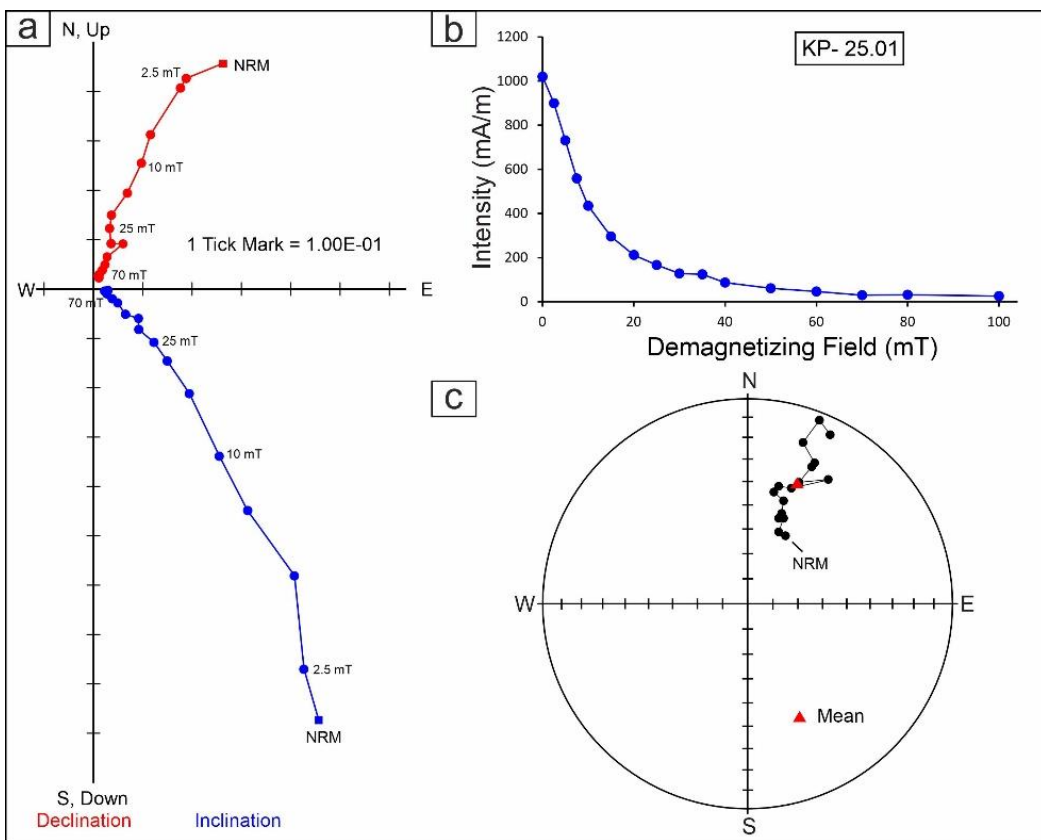
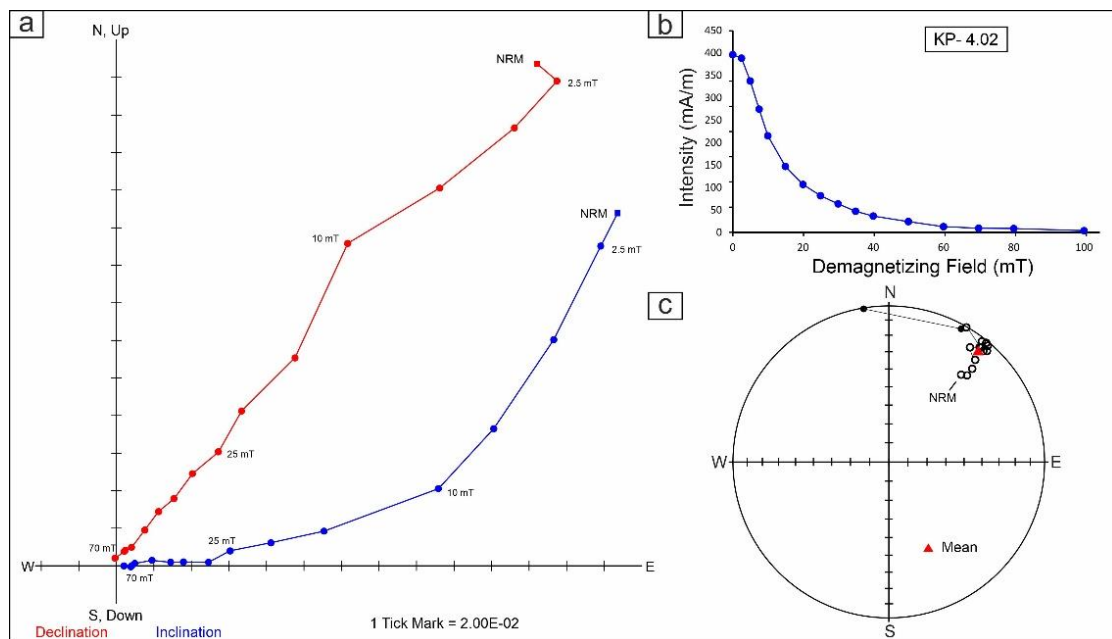


Fig. 7.8: (a) Orthogonal plot, (b) Intensity plot and (c) Stereo plot of demagnetization data of sample KP-25.01.

The AF demagnetization curve of KP-4.02 (Fig. 7.9) shows that initial rapid decrease in magnetization up to 20 mT, after that, it decreases slowly up to 100 mT. The steady and gentle segment of demagnetization curve between applied field 25 mT and 100 mT, indicate a stable magnetic component. In stereo plots, the change in magnetization direction is not visible, because of superimposition of magnetic vectors, which is observed in the orthogonal plot.



**Fig. 7.9: (a) Orthogonal plot, (b) Intensity plot and (c) Stereo plot of demagnetization data of sample KP-4.02.**

In samples KP- 12.02, KP-16.01, KP-19.01 (Fig. 7.7), it is evident that a steep fall of magnetization intensity between 0 mT and 5 mT, suggest removal of secondary VRM component. From 10 mT to 80 mT the intensity of magnetization then become steady indicating stable magnetic vector. Which is also observed from the orthogonal and Stereo plot (Fig. 7.10, Fig 7.11, and Fig. 7.12).

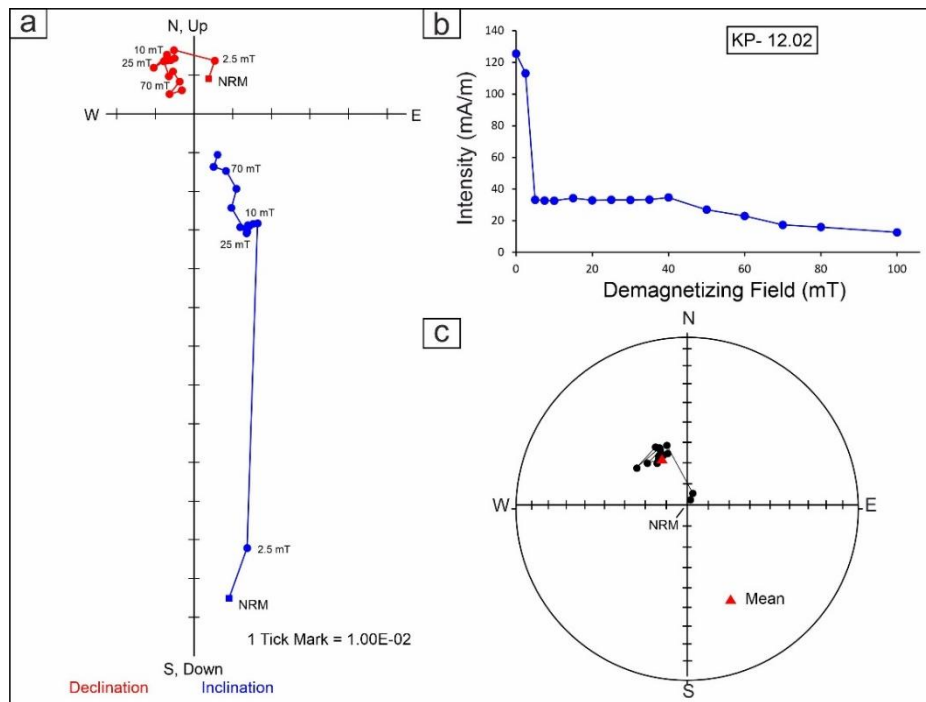


Fig. 7.10: (a) Orthogonal plot, (b) Intensity plot and (c) Stereo plot of demagnetization data of sample KP-12.02.

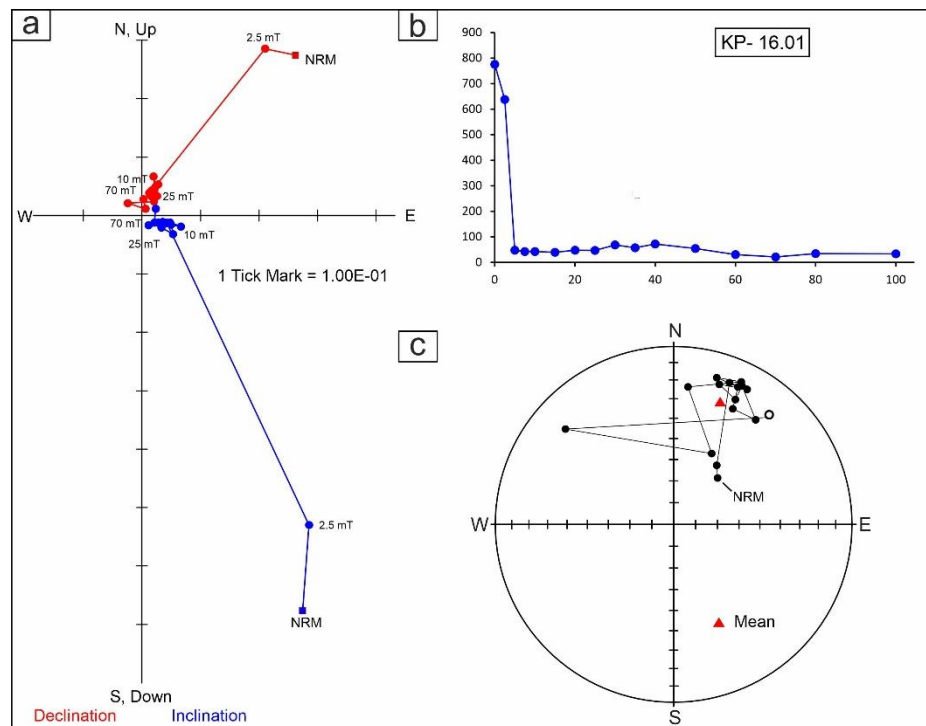


Fig. 7.11: (a) Orthogonal plot, (b) Intensity plot and (c) Stereo plot of demagnetization data of sample KP-16.01.

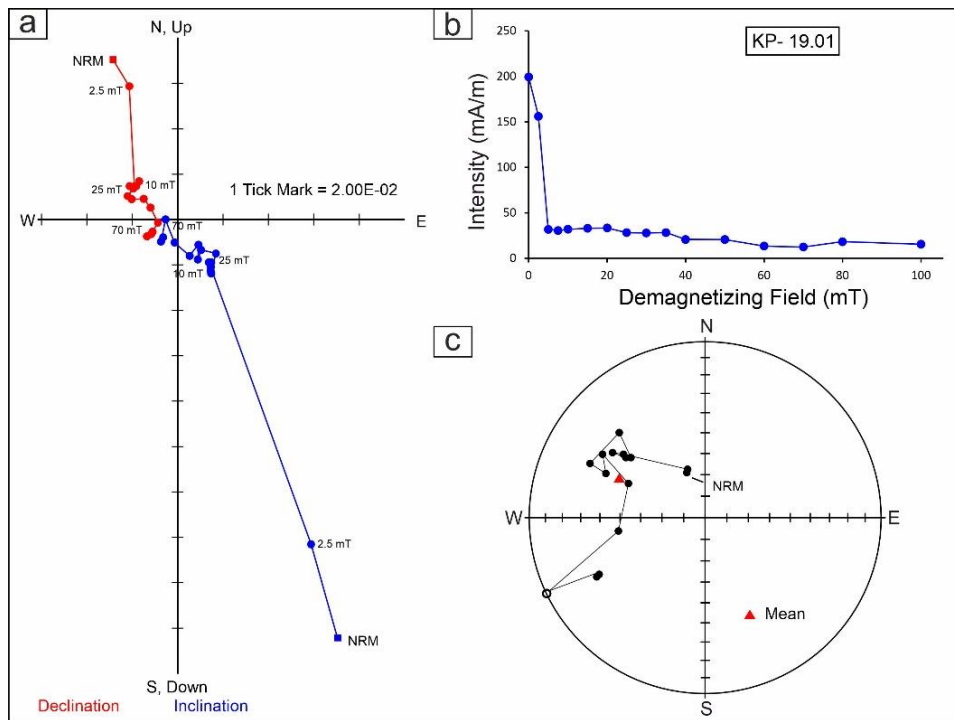


Fig. 7.12: (a) Orthogonal plot, (b) Intensity plot and (c) Stereo plot of demagnetization data of sample KP-19.01.

## 7.5. ChRM and Pole Positions

The metamorphic rocks from study area record a wide range of magnetization directions. From the total stereo plots for all components three groups of directions are visible. These are moderately dipping north easterly ( $D_1$ ), moderately dipping north westerly ( $D_2$ ) and shallow dipping north easterly ( $D_3$ ) clusters. The mean directions of these three groups, yield three components of magnetization (Table 7.1 and Fig. 7.13). From these three mean directions, three Palaeomagnetic pole positions (pole latitude  $\lambda_p$  and pole longitude  $\phi_p$ ) were calculated by the following equations (Butler, 1992):

$$\lambda_p = \sin^{-1}(\sin \lambda_s \cdot \cos p + \cos \lambda_s \cdot \sin p \cdot \cos D_m)$$

Where,  $\lambda_s$  and  $\phi_s$  are the present latitude and longitude of the site,  $D_m$  is the mean declination of the site NRM and  $p$  is the colatitude of the site. Colatitude of the site is given by:

$$p = \tan^{-1}(2/\tan I_m).$$

where,  $I_m$  is the mean inclination of the site NRM.

There are two possibilities for pole longitude  $\varphi_s$ ,

$$\text{if } \cos p \geq (\sin \lambda_s \cdot \sin \lambda_p), \text{ then } \varphi_p = (\varphi_s + \beta),$$

$$\text{or } \cos p < (\sin \lambda_s \cdot \sin \lambda_p), \text{ then } \varphi_p = \varphi_s + (180^\circ - \beta),$$

where,  $\beta = \sin^{-1}(\sin p \cdot \sin D_m / \cos \lambda_p)$ . Here,  $\beta$  denote the longitudinal difference between pole and site. The polar error, given by  $dp$  and  $dm$  is termed the oval of ninety-five percent confidence about the pole position. The  $dp$  and  $dm$  are given by:

$$dp = \frac{1}{2} \alpha_{95} (1 + 3 \cos^2 p),$$

$$dm = \alpha_{95} (\sin p / \cos I_m).$$

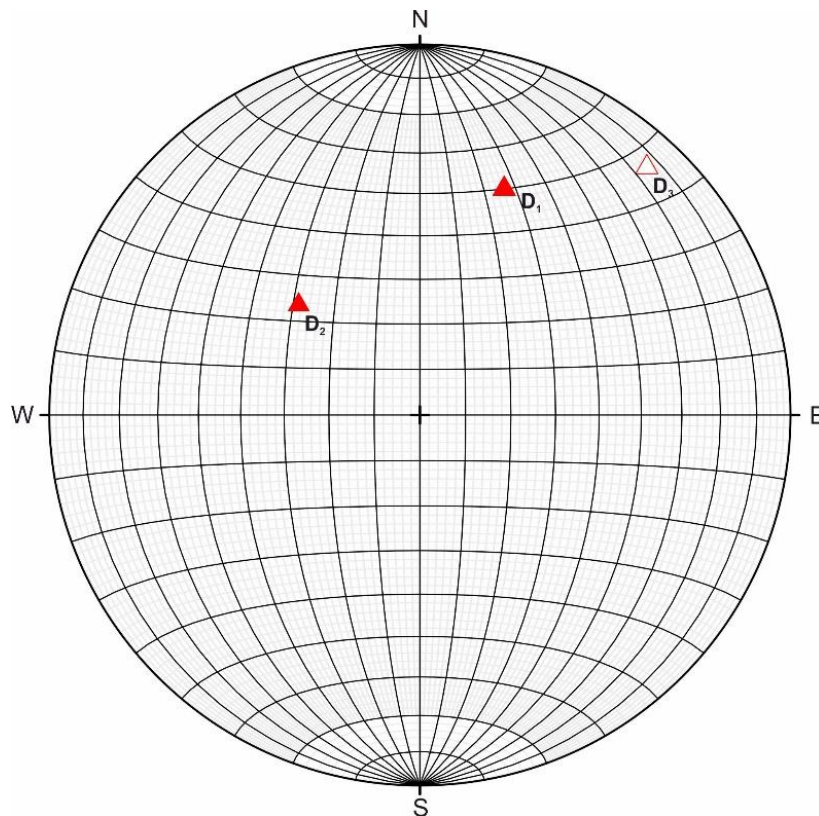


**Fig.7.13: Equal area projections of the mean ChRM vectors obtained from AF demagnetization. Hollow triangle denotes negative inclination.**

**Table 7.1: Mean ChRM vectors recorded in the studied samples.**

Mean Vectors	Mean Declination (in degrees)	Mean Inclination (in degrees)	$\alpha_{95}$	k
D <sub>1</sub>	20.8	35.1	2.7	34.6
D <sub>2</sub>	312.5	53.7	3.9	31.6
D <sub>3</sub>	42.6	-10.3	6.1	30.1

## 7.6. Pole Positions and its Geological Implications

Pole positions and palaeo-latitudes are obtained from the mean ChRM vectors obtained from AF demagnetization are listed in Table 7.2. The pole positions are plotted on an equal area projection (Fig. 7.14) to correlate with the existing determined and dated pole positions and estimate the age of the poles calculated from the present study.

The three poles K<sub>1</sub>, K<sub>2</sub>, and K<sub>3</sub> have decreasing geological ages following the generalized APWP of Indian Subcontinent. Pole K<sub>1</sub> has the maximum age (~ 1900 Ma), K<sub>2</sub> has the intermediate and K<sub>3</sub> has the minimum age (~ 1100 Ma). Each of these poles have correspondence with the different tectonic events in the history of the Indian Subcontinent.

The pole K<sub>1</sub> which has an average age of ~ 1900-1700 Ma (Mohanty et al., 2006; Chalapathi Rao et al., 1999; Bhimasankaram, 1964). During this time period the Indian Subcontinent witnessed a range of collisional tectonics and magmatism. The AMS studies (see Gain et al., 2022) revealed that this period was marked by retreating orogeny and subduction bringing the Indo-Antarctic continental block together. Evidently this subduction and orogeny created a high temperature regime which led to the rocks to undergo UHT metamorphism (Dasgupta et al., 2013; Vijaya Kumar, 2010). Thus, during this peak stage of metamorphism the high temperature phases of titanomagnetite is formed and the magnetic vector of this pole (K<sub>1</sub>) is recorded by the titanomagnetite formed during peak metamorphism.

Table 7.2: Pole positions and palaeolatitudes obtained from the studied samples.

Pole	Pole position ( $\lambda_p/\phi_p$ )	Palaeolatitude	$d_p/d_m$
K <sub>1</sub>	70.04°N/159.61°E	19.36 °N	1.8/3.1
K <sub>2</sub>	44.12°N/22.43°E	34.24 °N	3.8/5.4
K <sub>3</sub>	42.56°S/14.28°E	5.2 °S	3.1/6.2

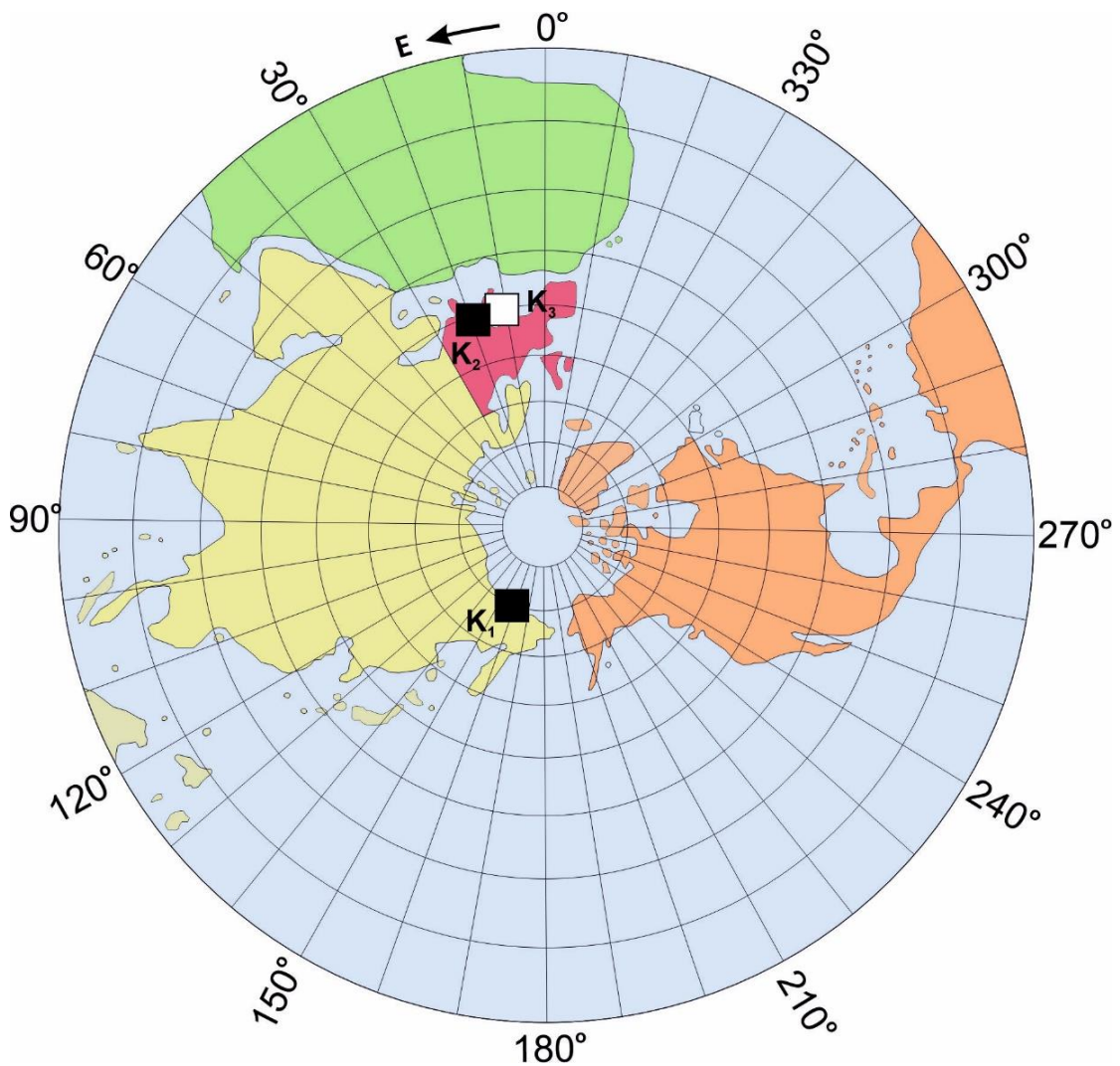


Fig.7.14: Pole positions obtained from the studied samples. Hollow square represents pole position on southern hemisphere.



The second pole  $K_2$  is analogous to an age of ~1500-1700 Ma (Paul, 2006; Biswal et al., 2003; Verma et al., 1977). This pole ( $K_2$ ) marks the most important tectonic event in the evolution of the Eastern Ghats Belts i.e., the Eastern Ghats Orogeny, during which the major folding event and magmatism occurred. Thus, this age of the pole may also be correlated with the origin of the anorthosite and other suite of igneous rocks in the area. The remanence carrier for these rocks are also high temperature phases of titanomagnetite.

The pole  $K_3$  is the youngest in the area and only reverse pole present in the studied rocks. This pole has an age of ~1000-1200 Ma (Mohanty, 2006 and reference therein). During this time the post peak metamorphic upliftment and exhumation processes occurred in the EGB. During this upliftment, the titanomagnetite remanence carriers changed to low temperature phases due to uplift related oxidation processes. that's also evident in the textural characters of Fe-Ti oxides present in the studied samples.

Thus, the pole positions obtained can be summarized as follows:

<b>Pole</b>	<b>Age</b>	<b>Vector Carriers</b>	<b>Event</b>
$K_1$	~1700-1900 Ma (Mohanty et al., 2006; Chalapathi Rao et al., 1999; Bhimasankaram, 1964)	High temperature primary phases	Collision and UHT metamorphism
$K_2$	~1500-1700 Ma (Paul, 2006; Biswal et al., 2003; Verma et al., 1977)	High temperature primary phases	Eastern Ghats Orogeny
$K_3$	~1100-1200 Ma (Mohanty, 2006 and reference therein)	Low temperature phases	Upliftment of deep crustal rocks

**Chapter 8**  
**Conclusions**

## CONCLUSIONS

The present study is the first attempt to determine the rock magnetic, anisotropy of magnetic susceptibility (AMS) and palaeomagnetic characteristics of the rocks from Kondapalle Pangidi Layered complex, Eastern Ghats Belt, India in relation with petrological and tectonic evolution. On the basis of field and experimental observations, following major conclusions can be drawn:

1. The identification of rock types in terms of petrological and mineralogical characteristics are important for interpreting the magnetic properties. The petrological studies revealed that the major rock types are orthopyroxene granulite, mafic granulite, leptynite, khondalite, enderbite and anorthosite.
2. Three generations of Fe-Ti Oxides are observed under reflected light microscopic study and their textural relationship suggests that, the rocks suffer a prolonged period of metamorphism. Also, the textural features of secondary Fe-Ti oxides indicate the evidence of uplift related oxidations, that suggest metamorphism is followed by uplift related slow cooling. Exsolution of pleonaste within host titanomagnetite indicates the rocks retrograded to relatively lower grade after attaining the peak-metamorphic condition.
3. The rock magnetic studies suggest that the ferrimagnetic properties and remanence recording potential of rocks are chiefly due to the presence of titanomagnetite. Ferrimagnetism increases with increasing grades of metamorphism. The grain size of the chief remanence carrier ranges from SSD to PSD range. Mineral magnetic parameters also corroborate all the above contention. Both the rock magnetic and mineral magnetic properties suggest that the rock from KPLC are suitable for recording magnetic remanence.
4. The magnetic fabrics of the high-grade rocks of the KPLC are controlled by the regional mesoscopic fabric broadly defined by the paramagnetic minerals. The AMS studies in the KPLC revealed that the stress directions/patterns during the different stages of evolutions of the KPLC. It is evident, that the principal

compressional stress orientation was not uniform during the tectonic events and changed throughout the geological history of the KPLC.

5. The palaeomagnetic studies revealed three well defined mean ChRM components  $D_1$ ,  $D_2$  and  $D_3$  were recorded in the rocks acquired at different geologic times:

$D_1$ :  $D / I = 20.8^\circ / 35.1^\circ$ ,  $k = 34.6$  and  $\alpha_{95} = 2.7^\circ$ ;

$D_2$ :  $D / I = 312.5^\circ / 53.7^\circ$ ,  $k = 31.6$  and  $\alpha_{95} = 3.9^\circ$ ; and

$D_3$ :  $D / I = 42.6^\circ / -10.3^\circ$ ,  $k = 41.8$  and  $\alpha_{95} = 19.3^\circ$ .

6. The following palaeomagnetic pole positions derived from each component are:

$K_1$  from  $D_1$  at  $\lambda_P = 70.04^\circ$  N;  $\varphi_P = 159.61^\circ$  E and  $dp / dm = 1.8/3.1$ ;

$K_2$  from  $D_2$  at  $\lambda_P = 44.12^\circ$  N;  $\varphi_P = 22.43^\circ$  E and  $dp / dm = 11.9/12.4$ ; and

$K_3$  from  $D_3$  at  $\lambda_P = 42.56^\circ$  S;  $\varphi_P = 14.28^\circ$  E and  $dp / dm = 33.0/35.7$ .

The position of the poles changed during the tectonic evolution of the KPLC signifying the blocking and unblocking of remanence carriers (titanomagnetite) occurred due to varying temperature regimes of evolution of KPLC.

## **Appendix**

**APPENDIX**  
**AF DEMAGNETIZATION DATA**

<b>Sample no.</b>	<b>Demagnetizing Field (mT)</b>	<b>Declination (Deg.)</b>	<b>Inclination (Deg.)</b>	<b>Intensity (mA/m)</b>
<b>KP2.01</b>	<b>NRM (0)</b>	355.5	52.1	199.4
	2.5	7.9	50.1	161.4
	5	4.4	47.3	129.6
	7.5	8.1	41	109.7
	10	6.3	39.7	86.1
	15	6	33.3	58.9
	20	9.7	31.3	43.6
	25	15.5	29.3	32.1
	30	16	27.1	24.9
	35	19.5	31.7	19.7
	40	10.8	29.8	14.8
	50	14.3	32.5	11.4
	60	10.3	46	8.4
	70	33.8	18.8	6.7
	80	25.4	26.1	3.7
100	43.8	-11	1.9	
<b>KP3.02</b>	<b>NRM (0)</b>	344.3	-44.4	147
	2.5	2	-46.7	142.5
	5	352	-39.1	103.9
	7.5	357.6	-31.6	69.6
	10	10.9	-25.7	47.5
	15	9.3	-19.8	22.1
	20	26.9	-30.6	12.3
	25	7.7	-45.3	8.1
	30	11.1	-20	4
	35	325.4	-66.9	3.2
	40	0.6	0.7	4.2
	50	31.9	12.6	3.9
	60	315.7	22.5	8.4
	70	7.1	-27.6	3.6
	80	317.6	23.2	5.3
100	262.3	34.5	6.2	
<b>KP4.02</b>	<b>NRM (0)</b>	40	-28.3	396.2
	2.5	42.3	-26	388.3
	5	42.3	-20.9	337.4
	7.5	40.6	-15.4	274.7
	10	35.7	-11	215.3
	15	40.7	-7.2	147.2
	20	39	-6.6	106.8

25		41.9	-5.6	81.9
30		39.6	-1.7	63.7
35		40.7	-2.5	47.2
40		37.9	-3	36.7
50		38.6	-6.9	24.4
60		39.3	-5.8	12.8
70		30.1	-0.4	9.5
80		28.7	3.3	8.8
100		350.9	1.2	4.1
<b>KP5.01</b>	<b>NRM (0)</b>	235.2	35.4	494
	2.5	231.5	20.9	493.7
	5	234.5	18.6	416.8
	7.5	232.8	16.4	350.6
	10	229.7	12.7	302.7
	15	242	11	205.4
	20	242.5	6.7	163.8
	25	246.3	3.7	137.3
	30	246.3	-0.4	120.9
	35	244.8	-2.5	99.4
	40	246.7	-8.7	87.5
	50	246.1	-8.5	71.1
	60	243.9	-15.2	53.9
	70	247	-18.3	43.8
	80	246.5	-22	37.2
	100	242.2	-25.8	26.1
<b>KP7.01</b>	<b>NRM (0)</b>	352.3	61.8	1904.6
	2.5	353.7	58	1778.5
	5	349.7	49.6	1348.7
	7.5	342.9	42.7	1051.3
	10	336.3	35.8	858.7
	15	336	27.7	642.9
	20	334.1	22.9	503.8
	25	335.1	19.5	424.9
	30	331.7	18.1	304.3
	35	331	17.5	244.5
	40	335.3	16.8	198.4
	50	331	16.6	163
	60	333.6	15.9	124.9
	70	333.5	11.1	108.6
	80	332.8	8.4	82.3
	100	336.1	14.3	53.6
<b>KP10.01</b>	<b>NRM (0)</b>	26.4	65.2	1753.8
	2.5	24.4	61.3	1654.5
	5	19.8	56.3	1265.2
	7.5	17.9	53.1	1025.4
	10	19.4	47.9	862.7
	15	20.1	42.9	682.8

20		18	41	551.2
25		18.4	39.9	406.4
30		14.3	39.4	329
35		8	39.8	263.4
40		9.5	38.4	219.9
50		10.8	35.2	184.8
60		11.3	31.2	140.1
70		15.8	31.6	128.9
80		7	35.6	89.7
100		27.4	31.7	73.7
<b>KP12.02</b>	<b>NRM (0)</b>	22.7	85.5	125.5
	2.5	21.4	82.5	113.1
	5	342.6	58.6	33.1
	7.5	340.6	62.3	32.7
	10	336.6	62.3	32.6
	15	333	63.1	34.2
	20	332.6	61.4	32.8
	25	331.5	61.6	33.1
	30	335.4	59.4	33
	35	318.8	61.6	33.3
	40	330.1	63.1	34.6
	50	326.2	64.3	26.9
	60	333.7	57.7	22.9
	70	335.7	58.3	17.3
	80	308.7	59.3	15.9
	100	332.8	57.1	12.6
<b>KP14.03</b>	<b>NRM (0)</b>	29	51.9	24
	2.5	52.1	81.1	25.6
	5	20.2	29.5	13.3
	7.5	16.9	27.1	13.1
	10	11.7	25	14
	15	18.5	42.9	12.4
	20	8.6	43.1	10.2
	25	15.1	50.4	10.7
	30	14	42.5	9.3
	35	13.3	17	6.3
	40	21.8	54.4	8.7
	50	326.2	50.2	11.5
	60	214.6	-18.5	5.3
	70	219.5	47.1	6.7
	80	326.2	40.7	4
	100	271.3	-10.1	3.1
<b>KP15.02</b>	<b>NRM (0)</b>	65.6	72.1	63.8
	2.5	65.3	74.3	51
	5	327.4	59	5.6
	7.5	308	48.1	4.6
	10	330.4	56.3	4.3



15		327.4	50.9	4.9
20		357.1	57.6	5.2
25		270.7	52.8	3.1
30		318.6	54.4	5.1
35		318.2	42.1	4.8
40		322.5	73.5	5.2
50		303.4	49.2	4.4
60		321.9	39.8	4
70		325.9	67.2	2.9
80		300.3	66.7	1.9
100		355.8	45.8	2.5
<b>KP16.01</b>	<b>NRM (0)</b>	43.7	60.7	775.6
	2.5	36.4	56.2	637.6
	5	21.7	15.8	47.9
	7.5	28.7	15.1	42.4
	10	18.3	18.6	42.7
	15	26.5	22.8	39.8
	20	26.6	14.5	47.8
	25	38.2	26.2	47.1
	30	27.4	27.8	68
	35	25.2	16.1	57.5
	40	16.4	15.2	72.2
	50	25.4	12.6	54.4
	60	6.1	23.7	30.4
	70	28.6	52.7	21.3
	80	311.3	20.6	34.4
	100	41.2	-19.6	33.4
<b>KP17.01</b>	<b>NRM (0)</b>	35.1	62.8	261.3
	2.5	32.8	57.4	193
	5	25.2	26.4	12.9
	7.5	24.8	25.4	12
	10	23.1	27.6	11.6
	15	24.4	30.1	13.9
	20	18.9	37.5	10.9
	25	25.5	14.1	12.2
	30	18.6	35.7	11.7
	35	45.7	36.1	9.9
	40	26.9	44.2	11.5
	50	33	42.2	9.4
	60	40.9	23.9	8.5
	70	23.8	50.4	5.6
	80	134.6	49.1	2.7
	100	17.1	-3.9	4
<b>KP19.01</b>	<b>NRM (0)</b>	338	67.6	199.4
	2.5	340.1	66.4	156.1
	5	307.5	41.1	31.8
	7.5	305.1	38.2	30.4

10		305	36.2	31.9
15		307.1	43	32.9
20		309	45.3	33.3
25		314.9	32.1	28.2
30		295.2	28.8	27.8
35		293.8	38.4	28.3
40		301.5	32.4	20.7
50		293.8	50.8	20.6
60		261.1	48.9	13.4
70		244.3	-0.2	12.3
80		241.5	32.4	18.2
100		241.1	30.4	15.4
<b>KP21.01</b>	<b>NRM (0)</b>	31.7	62.7	237.6
	2.5	21.2	53.4	116.3
	5	20.7	44.2	89.3
	7.5	25.1	49.3	75.4
	10	41.8	22.5	47.2
	15	52.9	44	44.9
	20	74	-1.7	24.6
	25	120.9	7.2	14.9
	30	101.2	30.5	38.4
	35	37	19.2	32.6
	40	71.2	-7.6	30.6
	50	76.7	36.9	27.6
	60	64.3	20.2	28.4
	70	33.5	9.4	18.5
	80	85.9	-41.5	17.5
	100	58.9	59	12.5
<b>KP22.01</b>	<b>NRM (0)</b>	121.6	78.2	169.3
	2.5	127.1	76.6	162
	5	125.1	76.3	159.3
	7.5	153.9	76.4	152.1
	10	142.4	75.1	145.2
	15	137.2	75.1	130.3
	20	152.7	72.9	114.6
	25	159.8	71.8	100.5
	30	155.7	69.3	83.5
	35	143.9	71.8	70.6
	40	159.3	68.6	57.9
	50	153.5	66.4	39
	60	157.8	62.9	27.7
	70	144.5	54.7	20
	80	146.9	56	14.1
	100	129.6	42	7.6
<b>KP25.01</b>	<b>NRM (0)</b>	29.9	58.9	1020.2
	2.5	23.8	58.8	900.4
	5	23.4	52.6	731.2

7.5		20.3	53.4	558.8
10		20.9	51.1	435.2
15		19.5	45.8	295.6
20		13.7	43.4	212.3
25		14.9	40.4	166.9
30		21.2	39.8	128
35		33.2	28.5	124.5
40		23.1	36	87.2
50		25.4	27.1	61.1
60		25.8	25	46.4
70		19.3	18.2	30
80		21.7	4.4	32.1
100		26.2	9.4	25.9
<b>KP26.01</b>	<b>NRM (0)</b>	321.2	84.1	677.1
	2.5	348.6	82.2	523.8
	5	346.3	76.2	349.6
	7.5	335.1	70.7	234.4
	10	339.6	65.4	169.8
	15	346.7	53.2	108.2
	20	344.4	41.3	78
	25	347.5	33.8	60.1
	30	351	28.5	49.8
	35	352.4	20.5	45
	40	353.7	20.4	36.8
	50	350.9	19.4	30.4
	60	349	9.8	24.4
	70	355.4	16.8	21.5
	80	348.9	13.4	17.7
	100	1.6	9.8	12.8
<b>KP27.01</b>	<b>NRM (0)</b>	185.6	6.3	717.8
	2.5	184.7	5.8	701.7
	5	182.5	8.8	652.1
	7.5	183.4	11.1	574.7
	10	179	13	501
	15	188.2	18.8	368.6
	20	189.2	21.6	276.2
	25	181.9	23.4	214.7
	30	179.3	26.6	168.5
	35	186	31.9	130.1
	40	191.2	34.2	112.5
	50	200.8	44.5	85.6
	60	209.1	50.5	64.7
	70	221.8	60.5	54
	80	246.9	62.2	48.3
	100	268.6	65.2	44
<b>KP28.01</b>	<b>NRM (0)</b>	280.6	49.6	404
	2.5	281.5	48.3	352

5		281.6	38.4	278.8
7.5		281.6	31.6	221.4
10		281.4	23	192.4
15		283.3	15.1	149.3
20		285.1	7.8	139.5
25		289.7	2.3	134.3
30		288	0.4	124.9
35		287.4	-1.2	119.8
40		289.6	-1.6	114.2
50		288.6	-1.7	96.2
60		289.9	-0.1	89.9
70		288	-3.9	82.8
80		289.2	-3	76.9
100		290.7	1.4	66.5
<b>KP31.01</b>	<b>NRM (0)</b>	92.6	80.4	141.1
	2.5	68.5	81.7	118.9
	5	48.3	79.1	87
	7.5	39.2	78.8	64.1
	10	30.3	78.8	49.3
	15	32.1	65.1	32.7
	20	6.1	74	24.6
	25	16.9	62.5	21.4
	30	26.6	60.5	16.2
	35	26.1	60.7	14.8
	40	180	62	9.6
	50	324	68.4	4.6
	60	327	39	5.6
	70	351.6	29.4	7.4
	80	336.7	1.8	1.4
	100	6.7	28.7	5.8
<b>KP33.02</b>	<b>NRM (0)</b>	6.5	36.7	10.7
	2.5	7.6	34.9	9.6
	5	357.6	37.6	7.6
	7.5	342.2	42.9	5.4
	10	353.1	39.3	4.1
	15	291.4	68.5	3.7
	20	343.3	48.9	2.8
	25	31.8	65.6	1.9
	30	112.6	69.2	1.8
	35	333.9	41.2	1.1
	40	206.8	-20.8	1.1
	50	114.9	-18.3	2.7
	60	170.3	42.3	1.3
	70	128.2	-53.1	2.6
	80	327.2	7.2	0.7
	100	217	-15.4	2.9
<b>KP35.01</b>	<b>NRM (0)</b>	31.6	67.2	702

2.5		31.9	65.8	556.6
5		25.1	63.8	395.3
7.5		25.6	62.3	279.2
10		26.9	52.4	222.9
15		25.8	48.3	153.4
20		23.1	43.8	103.8
25		21.8	45.4	78.7
30		25.5	36.8	62.8
35		29.4	31.2	50.7
40		16.7	31.2	40.4
50		26.8	31.8	27.9
60		17.5	20.8	25.7
70		14.2	17.3	15.8
80		359.8	11.6	14.1
100		22.6	30.6	7.4
<b>KP36.01</b>	<b>NRM (0)</b>	354.2	46.1	256.9
	2.5	348.6	46.8	230.9
	5	339.1	44.7	188.5
	7.5	336.4	40	160.9
	10	338	36.7	141.1
	15	336.5	31.7	114.5
	20	344.5	24.1	97.2
	25	344	23.9	82.2
	30	339.5	22.5	72.1
	35	339.4	21.2	60.7
	40	335.1	18.9	56.1
	50	342.8	17	48.3
	60	339.1	12.9	38.4
	70	342.8	12.5	30.6
	80	340.9	14.7	25.2
	100	350.5	22.1	13.5
<b>KP38.01</b>	<b>NRM (0)</b>	203.6	56.7	56.8
	2.5	201.7	28.9	43.2
	5	197.7	27.3	31.1
	7.5	187.2	12.3	29.9
	10	199.1	-2.3	22
	15	186.1	-15.8	23.7
	20	190.2	5.3	27.5
	25	123.2	-33.1	19.8
	30	118.4	9.2	20.1
	35	109.3	-43.9	22.2
	40	71.5	42.1	10.5
	50	354.3	-78.2	22.6
	60	81.7	68	36.6
	70	145.1	-1.5	25.9
	80	114	47	20.2
	100	67.8	43.4	16.6

<b>KP39.03</b>	<b>NRM (0)</b>	151.9	37.7	314.4
	2.5	166.2	10.1	192.8
	5	162.7	10	110
	7.5	160.4	28.6	92.2
	10	122.4	26.6	32.7
	15	331.3	2.9	14.1
	20	57.1	-16	10.7
	25	141.7	-71.4	14
	30	12.3	19.9	50.4
	35	354.2	71	48.7
	40	5	-17.7	54.5
	50	359.3	39.9	31.4
	60	350	12.2	67
	70	0.8	7.5	52.3
	80	8.5	17.1	24.6
100	204	-35.2	61.6	
<b>KP42.01</b>	<b>NRM (0)</b>	345.5	50.1	263.2
	2.5	340.3	52.4	205
	5	342.3	48.8	168.8
	7.5	344.5	45.3	141.6
	10	339.3	43.4	110.8
	15	338.3	42.1	76.7
	20	329.7	43.9	65.1
	25	325.6	36.8	50
	30	321.5	50.2	42.3
	35	301.3	47.2	41.7
	40	306.2	38.4	34.2
	50	273.3	43.6	28.6
	60	279.2	44.6	32.1
	70	290	44.8	22.7
	80	256	28.2	20.7
100	271.4	12.2	15.9	
<b>KP43.03</b>	<b>NRM (0)</b>	298.9	72.4	29.4
	2.5	288.7	69.6	28.8
	5	293.7	69.1	27.4
	7.5	289.7	67.4	26.7
	10	285.8	65.4	25.8
	15	304.3	66	24
	20	284.8	62.1	22.4
	25	286.5	59.7	20.7
	30	282.1	57.5	19.1
	35	285.4	56	17.7
	40	281	52.1	15.8
	50	283.2	49.5	15
	60	271.5	45.4	12.8
	70	273.1	46.7	11.8
	80	276.5	46.8	10.9

100

276.6

39.9

8.9

---

## **References**



## REFERENCES

- Aftalion, M., Bowes, D.R., Dash, B. and Dempster, T.J., 1988. Late Proterozoic charnockites in Orissa, India: U-Pb and Rb-Sr isotopic study. *J. Geol.*, vol. 96, pp. 663–676.
- Agarwal, A., Srivastava, D.C., Shah, J., Mamtani, M.A., 2021. Magnetic fabrics in an apparently undeformed granite body near Main Boundary Thrust (MBT), Kumaun Lesser Himalaya, India. *Tectonophysics* 815. <https://doi.org/10.1016/j.tecto.2021.228996>, 228996.
- Akimoto, T., Kinoshita, H., Furuta, T., 1984. Electron probe microanalysis study on process of low temperature oxidation of titanomagnetite. *Earth Planet. Sci. Lett.* 71, 263–278.
- Arbaret, L., Launeau, P., Diot, H., Sizaret, S., 2013. Magnetic and shape fabrics of magnetite in simple shear flows. *J. Volcanol. Geotherm. Res.* 249, 25–38.
- Archanjo, C.J., Launeau, P., Bouchez, J.L., 1995. Magnetic fabric vs. magnetite and biotite shape fabrics of the magnetite-bearing granite pluton of Gameleiras (Northeast Brazil). *Phys. Earth Planet. Inter.* 89 (1–2), 63–75.
- Aswathanaryan, U., 1964. Isotopic ages from the Eastern Ghats and Cuddapahs of India. *J. Geophys. Res.*, vol. 69, pp. 3479–3486.
- Balsley, J.R. and Buddington, A.F., 1960. Magnetic susceptibility anisotropy and fabric of some Adirondack granites and orthogenesis. *Am. J. Sci.*, V. 258A, pp. 6–20.
- Basavaiah, N., 2011. *Geomagnetism: Solid Earth and Upper Atmosphere Perspective*. Springer, Netherlands, pp. 291–386.
- Basavaiah, N., Appel, E., Lakshmi, B.V., Deenadayalan, K., Satyanarayana, K.V.V., Misra, S., Juyal, N., Malik, M.A., 2010. Revised magnetostratigraphy and characteristics of the fluviolacustrine sedimentation of the Kashmir basin, India, during Pliocene-Pleistocene. *J. Geophys. Res.*, V.115, pp. B08-105.
- Basavaiah, N., Khadkikar, A.S., 2004. Environmental magnetism and its application towards paleo monsoon reconstruction. *J. Indian Geophys. Union* 8 (1), 1–14.
- Basavaiah, N., Satyanarayana, K.V.V., Deenadayalan, K., Prasad, J.N., 2018. Does Deccan Volcanic Sequence contain more reversals than the three-Chron N-R-N flow magnetostratigraphy? – a palaeomagnetic evidence from the dyke swarm near Mumbai. *Geophys. J. Int.*, V.213, pp. 1503-1523.

- Bay, R.E., Appel, E., Paudel, L., Neumann, U., Setzer, F., 2011. Palaeomagnetic remanences in high-grade metamorphic rocks of the Everest region: indication for Late Miocene crustal doming. *Geophys. J. Int.* 186 (2), 551–566. <https://doi.org/10.1111/j.1365-246X.2011.05078.x>.
- Bhattacharya, S. and Kar, R., 2002. High temperature dehydration melting and decompressive P-T path in a granulite complex from the Eastern Ghats, India. *Contrib Mineral Petrol*, vol. 143, pp. 175–191.
- Bhattacharya, S., 1996. Eastern Ghats granulite terrain of India: an overview. *J. Southeast Asian Earth Sci.*, vol. 14, pp. 165–174.
- Bhattacharya, S., Sen, S.K. and Acharyya, A., 1994. Structural setting of the Chilka Lake granulite-migmatite-anorthosite suite with emphasis on the time relation of charnockites. *Precambrian Res.*, vol. 66, pp. 393–409.
- Bhimasankaram, V. L. S. 1964. A preliminary investigation of the palaeomagnetic direction of the charnockite of Andhra Pradesh. *Current Science* 33, 465–465.
- Bhowmik, S.K., 1997. Multiple episodes of tectonothermal processes in the Eastern Ghats granulite belt. *Proceedings of the Indian Academy of Science* 106, 131 – 146.
- Bhui, U.K., Sengupta, P., Sengupta, P., 2007. Phase relations in mafic dykes and their host rocks from Kondapalle, Andhra Pradesh, India: implications for the time-depth trajectory of the Palaeoproterozoic (late Archaean?) granulites from southern Eastern Ghats Belt. *Precambrian Res.* 156, 153–174.
- Biswal T. K., Sinha S., Mandal A., Ahuja H. and Das M. K. 2003. Deformation pattern of Bastar craton adjoining Eastern Ghats Mobile Belt, NW Orissa. *Gondwana Geological Society Special Publication* 7, 101-108.
- Bloemendal, J., King, J. W., Hall, F. R. and Doh, S. J., 1992 Rock magnetism of late Neogene and Pleistocene deep-sea sediments: Relationship to sediment source, diagenetic processes, and sediment lithology, *J. Geophys. Res.*, 97, 4361–4375, doi:10.1029/91JB03068.
- Bohnel, G., McIntosh, G., Sherwood, G., 2002. A parameter characterising the irreversibility of thermomagnetic curves. *Phys. Chem. Earth Parts A/B/C* 27, 1305–1309.
- Borradaile, G.J., 1991. Correlation of strain with anisotropy of magnetic susceptibility (AMS). *Pure Appl. Geophys.* 135, 15–29.

- Borradaile, G.J., Alford, C., 1987. Relationship between magnetic susceptibility and strain in laboratory and experiments. *Tectonophysics* 133, 121–135.
- Borradaile, G.J., Jackson, M., 2004. Anisotropy of magnetic susceptibility (AMS): Magnetic petrofabrics of deformed rocks. In: Martín Hernández, F., Lüneburg, C.M., Aubourg, C., Jackson, M. (Eds.), *Magnetic Fabric: Methods and Applications*, Geological Society, London, Special Publication, vol. 238, pp. 299–360.
- Borradaile, J.G., Werner, T., Lacroix, F., 1999. Magnetic fabrics and anisotropy controlled thrusting in the Kapuskasing Structural Zone, Canada. *Tectonophysics* 302, 241–256.
- Bose, S., Dunkley, D.J., Dasgupta, S., Das, K., Arima, M., 2011. India–Antarctica–Australia–Laurentia connection in the Paleoproterozoic–Mesoproterozoic revisited: evidence from new zircon U–Pb and monazite chemical age data from the Eastern Ghats Belt, India. *Bull. Geol. Soc. Am.* 123, 2031–2049.
- Bowen, N.L., and Tuttle, O.F., 1950. The system NaAl- Si<sub>3</sub>O<sub>8</sub>-KAlSi<sub>3</sub>O<sub>8</sub>-H<sub>2</sub>O. *The Journal of Geology*, v. 58, p. 489–51. <https://doi.org/10.1086/625758>.
- Buddington, A. F. and Lindsley, D. H., 1964. Iron- titanium oxide minerals and synthetic equivalents. *Jour. Petrol.*, V. 5, pp. 310-357.
- Butler, R. F., 1992. *Palaeomagnetism: Magnetic Domains to Geologic Terranes*, Blackwell Scientific Publications.
- Chalapathi Rao N. V., Miller J. A., Gibson S. A., Pyle D. M. and Madhavan V. 1999. Precise 40Ar/39Ar age determinations of the Kotakonda kimberlite and Chelima lamproite, India: Implication to the timing of mafic dyke swarm emplacement in the Eastern Dharwar craton. *Journal of the Geological Society of India* 53, 425-432.
- Chatterjee, S., Basavaiah, N., Mondal, S., Gain, D., 2021. Rock magnetic signatures of the Dalma Formation in the Singhbhum Mobile Belt, Eastern India. *J. Geol. Soc. India* 97 (6), 635–642.
- Chatterjee, S., Gain, D., Mondal, S., 2016. Magneto-mineralogy characterization and analysis of magnetic fabrics of the high-grade rocks from Chilka Lake Area, Eastern Ghats Belt, India. *Earth Sci. India* 9 (1), 29–47.
- Chatterjee, S., Mondal, S., Gain, D., Baidya, T.K., Mazumdar, D., 2018a. Interpretation of magnetic fabrics in the Dalma volcanic rocks and associated metasediments of the Singhbhum mobile belt. *J. Earth Syst. Sci.* 127 (11), 89.

- Chatterjee, S., Mondal, S., Roy, P., Gain, D., Bhattacharya, A., 2018b. Magnetomineralogical characterization and manifestations of magnetic fabrics from the gneissic rocks and associated intrusive bodies in and around Bankura and Purulia districts, West Bengal, India. *Curr. Sci.* 114 (9), 1894–1902.
- Chetty, T.R.K., Murthy, D.S.N. (1994) Collision tectonics in the late Precambrian Eastern Ghats Mobile Belt: mesoscopic to satellite-scale structural observations. *Terra Nova*, 6 (1). 72-81 doi:10.1111/j.13653121.1994.tb00635.x
- Cifelli, F., Mattei, M., Chadima, M., Lenser, S., Hirt, A.M., 2009. The magnetic fabric in “undeformed clays”: AMS and neutron texture analyses from the Rif Chain (Morocco). *Tectonophysics* 466, 79–88. <https://doi.org/10.1016/j.tecto.2008.08.008>.
- Cifelli, F., Mattei, M., Hirt, A.M., Günther, A., 2004. The origin of tectonic fabrics in “undeformed” clays: the early stages of deformation in extensional sedimentary basins. *Geophys. Res. Lett.* <https://doi.org/10.1029/2004GL019609>.
- Clark, G. S., and Subbarao, K. V., 1971. Rb-Sr isotopic ages of the Kunavaram series—a group of alkaline rocks from India: *Can. Jour. Earth Sci.*, v. 8, p. 1597-1602.
- Coney, P. J., Jones, D. L. & Monger, J. W. H., 1980. Cordilleran suspect terranes. *Nature* 288, 329–333.
- Dasgupta, S. and Sengupta, P., 2003. Indo-Antarctic Correlation: A Perspective from the Eastern Ghats Granulite Belt, India. In: Yoshida, M., Windley, B.F. and Dasgupta, S., Eds., *Proterozoic East Gondwana: Supercontinent Assembly and Breakup*, Geological Society, London, Special Publications 206, 131-143. <http://dx.doi.org/10.1144/gsl.sp.2003.206.01.08>
- Dasgupta, S., 1995. Pressure-temperature evolutionary history of the Eastern Ghats granulite province: Recent advances and some thoughts. *Mem. Geol. Soc. Ind.*, V. 34, pp. 101-110.
- Dasgupta, S., Bose, S., Das, K., 2013. Tectonic evolution of the eastern Ghats Belt, India. *Precambrian Res.* 227, 247–258.
- Dasgupta, S., Sengupta, P., 1995. Ultrametamorphism in Precambrian granulite terrains—evidence from Mg-Al granulites and calc-granulites of the Eastern Ghats, India. *Geol J* 30:307–318.
- Dasgupta, S., Sengupta, P., 1998. Re-working of an isobarically cooler deep continental crust: evidence of decompressive P-T trajectory from the Eastern Ghats Belt, India. *Ind. J. Geol.*, v. 70, No. 1& 2, pp. 133-144.

- Day, R., Fuller, M.D., Schmidt, V.A., 1977. Hysteresis properties of titanomagnetites: grain size and composition dependence. *Phys. Earth Planet. Inter.* 13, 260–266.
- Dearing, J.A., 1999. *Environmental Magnetic Susceptibility: Using the Bartington MS2 System*. Chi Publishing, Kenilworth.
- Dharma Rao, C.V. & Santosh, M., 2011. Continental arc magmatism in a Mesoproterozoic convergent margin: petrological and geochemical constraints from the magmatic suite of Kondapalle along the eastern margin of the Indian plate. *Tectonophysics*, 510, 151–171.
- Dharma Rao, C.V., 1998. Petrological evolution of Pangidi granulites, Eastern Ghats, India: evidence for decompressive and cooling retrograde trajectories. *Neues Jahrbuch für Mineralogie: Abhandlungen Abh 173*, 305–326.
- Dharma Rao, C.V., Kumar, Satish, K. M. 2001. Petrological and stable isotope evidence for late-stage fluid infiltration and micro-vein formation in high-grade calcsilicate rocks from Pangidi complex, Eastern Ghats, India. *Gondwana Res.* 4, 605.
- Dharma Rao, C.V., Santosh, M., Dong, Y., 2012. U–Pb zircon chronology of the Pangidi–Kondapalle layered intrusion, Eastern Ghats belt, India: constraints on Mesoproterozoic arc magmatism in a convergent margin setting. *J. Asian Earth Sci.*, 362–375.
- Dharma Rao, C.V., Vijay Kumar, T., Bhaskar Rao, Y.J., 2004. The Pangidi anorthosite complex, Eastern Ghats Granulite belt, India: mesoproterozoic Sm–Nd isochron age and evidence for significant crustal contamination. *Curr. Sci.* 89, 1614–1618.
- Dobmeier, C.J., Raith, M.M., 2003. Crustal architecture evolution of the Eastern Ghats Belt and adjacent regions of India. In: Yoshida, M., Windley, B.F., Dasgupta, S. (Eds.), *Proterozoic East Gondwana: Supercontinent Assembly and Breakup*, vol. 206. Geological Society of London Special Publication, pp. 145–168.
- Dubey, A.K., Cobbold, P.R., 1977. Noncylindrical flexural slip folds in nature and experiment. *Tectonophysics* 38, 223–239.
- Dunlop, D.J., 1995. Magnetism in rocks. *J. Geophys. Res.* 100 (B2), 2161–2174.
- Dunlop, D.J., 2002. Theory and application of the day plot (Mrs/Ms versus Hcr/Hc) 1. Theoretical curves and tests using titanomagnetite data. *J. Geophys. Res. Solid Earth* 107 (Issue B3) p. EPM 4-1-EPM 4-22.

- Dunlop, D.J., and Xu, S., 1994. Theory of partial thermoremanent magnetization in multidomain grains. 1. Repeated identical barriers to wall motion single microcoercivity. *Journal of Geophysical Research*, 99: 9005–9023.
- Dunlop, D.J., Ozdemir, O., 1997. *Rock magnetism. Fundamentals and Frontiers*. Cambridge University Press, 573 pp.
- Dvorak, J., Hrouda, F., 1975. The reflection of the deeper structure of the artmanvosoblaha block (Nizky Jesenik Mountains, Czechoslovakia) in the magnetic anisotropy and deformation history of overlying palaeozoic sediments. *Vest. Ustred. Ust. Geol.* 50, 285–296.
- Eyre, J. K., 1997. Frequency dependence of magnetic susceptibility for populations of single-domain grains, *Geophys. J. Int.*, 129, 209–211, doi:10.1111/j.1365-246X.1997.tb00951.x.
- Fajri, R. N., Putra, R., Maisonneuve, C. B. de., Fauzi1, A., Yohandri. and Rifai, H., 2019. Analysis of magnetic properties rocks and soils around the Danau Diatas, West Sumatra. *IOP Conf. Series: Journal of Physics: Conf. Series* 1185 (2019) 012024 doi:10.1088/1742-6596/1185/1/012024.
- Ferre, E.C., Gebelin, A., Till, J.L., Sassier, C., Burmeister, C.K., 2014. Deformation and magnetic fabrics in ductile shear zones: a review. *Tectonophysics* 629, 179–188.
- Ferre, E.C., Martin-Hernandez, F., Teyssier, C., Jackson, M., 2004. Paramagnetic and ferrimagnetic anisotropy of magnetic susceptibility in migmatites: measurements in high and low fields and kinematic implications. *Geophys. J. Int.* 157, 1119–1129.
- Fodor, L.I., Marton, E., Vrabec, M., et al., 2020. Relationship between magnetic fabrics and deformation of the Miocene Pohorje intrusions and surrounding sediments (Eastern Alps). *Int. J. Earth Sci. (Geol. Rundsch.)* 109, 1377–1401. <https://doi.org/10.1007/s00531-020-01846-4>.
- Frost, B. R., 1988. A review of graphite- sulfide- oxide- silicate equilibria in metamorphic rocks. *Rendiconti Societa Italiana Mineral. Petrol.*, V. 43, pp. 25-40.
- Frost, B.R., Shive, P.N., 1986. Magnetic mineralogy of the lower continental crust. *J. Geophys. Res.* 91, 6513–6521.
- Gain, D., Chatterjee, S., Mondal, S., 2022. Rock magnetism and AMS studies in Kondapalle-Pangidi layered complex, Eastern Ghats Belt, India: Remanence carriers and tectonic implications.

- Georgiev, N., Henry, B., Jordanova, N., Jordanova, D., Naydenov, K., 2014. Emplacement and fabric-forming conditions of plutons from structural and magnetic fabric analysis: a case study of the Plana pluton (Central Bulgaria). *Tectonophysics* 629, 138–154.
- Graham, J. W., 1966. “Significance of magnetic Anisotropy in Appalachian Sedimentary rocks,” in *The Earth Beneath the Continents*. Geophysical Monograph Series 10, eds S. Steinhart and T. J. Smith (Washington, DC: American Geophysical Union), 627–648.
- Graham, J.W., 1954. Magnetic susceptibility anisotropy, an unexploited Petro-fabric element. *Bull. Geol. Soc. Am.*, V.65, pp. 1257.
- Grant, F.S. and West, G.F., 1965. *Interpretation Theory in Applied Geophysics*. McGraw-Hill Book Co., New York, 583 pp.
- Gregoire, V., Darrozes, J., Gaillot, P., N´ed´elec, A., Launeau, P., 1998. Magnetite grain shape fabric and distribution anisotropy vs rock magnetic fabric: a three-dimensional case study. *J. Struct. Geol.* 20 (7), 937–944.
- Grew, E.S. and Manton, W.I., 1986. A new correlation of sapphirine granulites in the Indo-Antarctic metamorphic terrain: Late Proterozoic dates from the Eastern Ghats Province of India. *Precambrian Res.*, vol. 33, pp. 123–137.
- Gupta, S., Dobe, R., Sawant D. A., Mishra, S and Mohanty K.W., 2020. Northern Margin of the Eastern Ghats Mobile Belt: Evidence for Strike-Slip Tectonics Along a Craton-Mobile Belt Boundary. *Structural Geometry of Mobile Belts of the Indian Subcontinent*, Springer. DOI: [https://doi.org/10.1007/978-3-030-40593-9\\_7](https://doi.org/10.1007/978-3-030-40593-9_7).
- Haggerty, S. E., 1976a. Oxidation of opaque mineral oxides in basalts. In: D. Rumble (Editor), *Oxide Minerals*. Mineral. Soc. Am., Short Course Notes, No. 3, Hg1 – Hg100.
- Haggerty, S.E., 1976b. Opaque mineral oxides in terrestrial igneous rocks. In: Rumble, D. (Ed.), *Oxide minerals*. Mineral. Soc. Am., Short Course Notes 3, Hg101–Hg300.
- Harley, S. L., 1989. The origins of granulites: a metamorphic perspective. *Geological Magazine*, 126 (3). 215-247 doi:10.1017/s0016756800022330.
- Hay, S. J., Hall, J., Simmons, G. and Russel, M. J., 1988. Sealed microcracks in the Lewisian of NW Scotland: a record of 2 billion years of fluid migration. *Jour. Geol. Soc. London*, V. 145, pp. 819-830.

- Heider, F., A. Zitzelsberger, and K. Fabian (1996), Magnetic susceptibility and remanent coercive force in grown magnetite crystals from 0.1  $\mu\text{m}$  to 6 mm, *Phys. Earth Planet. Inter.*, 93, 239–256, doi:10.1016/0031-9201(95)03071-9.
- Hobbs, B.E., Means, W.D., Williams, P.F., 1976. *An Outline of Structural Geology*. John Wiley & Sons.
- Hopgood, A. M., 1968. The structural geology and tectonic history of Precambrian rocks exposed in the Kinarsani River, eastern Andhra Pradesh. *J INDIAN GEOSCI ASSOC* 8, 13–34.
- Housen, B.A., van der Pluijm, B.A., Essense, E.J., 1995. Plastic behaviour of magnetite and high strains obtained from magnetic fabrics in the Parry Sound shear zone, Ontario Grenville Province. *J. Struct. Geol.* 17, 25–278.
- Hrouda, F., 1982. Magnetic anisotropy of rocks and its application in geology and geophysics. *Geophys. Surv.*, V.5, pp. 37-82.
- Hrouda, F., Janak, F., 1976. The changes in shape of the magnetic susceptibility ellipsoid during progressive metamorphism and deformation. *Tectonophysics* 34, 135–148.
- Hunt, C. P., B. M. Moskowitz, and S. K. Banerjee., 1995a. Magnetic properties of rocks and minerals, in *Rock Physics and Phase Relations: A Handbook of Physical Constants*, edited by T. J. Ahrens, pp. 189–204, AGU, Washington, D. C., doi:10.1029/RF003p0189.
- Ising, G., 1942. On the magnetic properties of varved clay. *Ark. Mat. Astron. Fys.*, V. 29, pp. 1–37.
- Jelinek, V., 1981. Characterisation of the magnetic fabrics of rocks. *Tectonophysics*, V.79, pp. 63-67.
- Johnson, H.P., Hall, J.M., 1978. A detailed rock magnetic and opaque mineralogy study of the basalts from Nazca Plate. *Geophys. J. R. Astr. Soc.* 52, 45–64.
- Johnson, H.P., Melson, W.G., 1978. Electron microprobe analyses of some titanomagnetite grains from Hole 395A. *Initial Reports of the Deep-Sea Drilling Project* 45, 575–579.
- Kaila, K. L. and Bhatia, S. C., 1981. Gravity study along Kavali-Udipi deep seismic sounding profile in the Indian peninsular shield- Some inferences about origin of anorthosites and eastern Ghats orogeny. *Tectonophys.* V. 79, pp. 129-143.



- Katz, M. B., 1978. Tectonic evolution of the Archaean granulite facies belt of Sri Lanka-South India. *Jour. Geol. Soc. Ind.* V. 19, pp. 185-205.
- Keary, P., Klepeis, K.A. and Vine, F.J., 2009. *Global Tectonics*, Willey-Blackwell, pp. 54-68.
- King, J., and Channell, J. E. T., 1991. Sedimentary magnetism, environmental magnetism, and magnetostratigraphy, in U.S. National Report to the International Union of Geodesy and Geophysics, vol. 29, pp. 358–370, AGU, Washington, D. C.
- Kovach, V.P., Simmat, R., Rickers, K., Berezhnaya, N.G., Salnikova, E.B., Dobmeier, C., Raith, M.M., Yakovleva, S.Z., Kotov, A.B., 2001. The Western Charnockite Zone of the Eastern Ghats Belt, India – an independent crustal province of late Archean (2.8 Ga) and Paleoproterozoic (1.7–1.6 Ga) terrains. *Gondwana Res.* 4, 666–667.
- Kretchsmar, U. H. and R. H. McNutt, 1971. A study of the Fe-Ti oxides in the Whitestone anorthosite, Dunchruch, Ontario. *Can. J. Earth Sci.* 8, 947.
- Lal, R. K., Ackermant, D. and Upadhyay, H., 1987. P-T-X relationships deduced from corona textures in sapphirine-spinel-quartz assemblages from Paderu, South India. *Jour. Petrol.*, V. 28, pp. 1139-1168.
- Lamali, A., Merabet, N., Henry, B., Maouche, S., Graine-Tazerout, K., Mekkaoui, A., Ayache, M., 2013. Polyphased geodynamical evolution of the Ougarta (Algeria) magmatic complexes evidenced by paleomagnetic and AMS studies. *Tectonophys.* 588, 82–99.
- Larson, E. E. and Strangway, D. W., 1969. Magnetization of the Spanish peak dyke swarm, Colorado and Shipwrick Dyke, New Mexico. *Jour. Geophys. Res.*, V. 74, pp. 1505-1514.
- Lattard, D., Engelmann, R., Kontny, A., Sauerzapf, U., 2006. Curie temperatures of synthetic titanomagnetites in the Fe-Ti-O system: effects of composition, crystal chemistry, and thermomagnetic methods. V. 111, B12S28. <https://doi.org/10.1029/2006JB004591>.
- Leelanandam, C. 1967. Occurrence of anorthosites from the\ chamockitic area of Kondapalli, Andhra Pradesh. *Bull. Geol. Soc. India*, v.4, pp.5-7.
- Leelanandam, C., 1990. The anorthosite complexes and Proterozoic mobile belt of Peninsular India. In: S.M.Naqvi (Ed.) *Precambrian Continental Crust and Its Economic Resources (Developments in Precambrian Geology, v.8)*, Elsevier, Amsterdam, pp.409-435.

- Leelanandam, C., 1997. The Kondapalle Layered Complex, Andhra Pradesh, India: a synoptic overview. *Gondwana Res.* I (1), 95–114.
- Leelanandam, C., 1998. Alkaline magmatism in the Eastern Ghats Belt—a critique. *Geol. Surv. India Spl. Publ.*, vol. 44, pp. 170–179.
- Lepland, A. and Stevens, R.L., 1996. Mineral magnetic and textural interpretations of sedimentation in the Skagerrak, Eastern North Sea. *Mar. Geol.*, 135, 51–64.
- Liu, Q. S., Torrent, J., Maher, B. A., Yu, Y. J., Deng, C. L., Zhu, R. X., and Zhao, X. X., 2005a. Quantifying grain size distribution of pedogenic magnetic particles in Chinese loess and its significance for pedogenesis, *J. Geophys. Res.*, 110, B11102, doi:10.1029/2005JB003726.
- Liu, Q., Roberts, A. P., Larrasoña, J. C., Banerjee, S. K., Guyodo, Y., Tauxe, L. and Oldfield, F., 2012. Environmental magnetism: Principles and applications, *Rev. Geophys.*, 50, RG4002, doi:10.1029/2012RG000393.
- Liu, Q.S., Wang, H.C., Zheng, J.P., Zeng, Q.L., Liu, Q.S., 2013. Petromagnetism properties of granulite-facies rocks from the northern North China craton: implications for magnetic and evolution of the continental lower crust. *J. Earth Sci.* 24, 12–28.
- Mahalik, N. K., 1996. Lithology and tectonothermal history of the Precambrian rocks of Orissa along the Eastern coast of India. *Journal of Asian Earth Sciences*, 14, 209–219.
- Maher, B. A., 1988. Magnetic properties of some synthetic submicron magnetites, *Geophys. J.*, 94, 83–96, doi:10.1111/j.1365-246X.1988.tb03429.x.
- Mamtani, M.A., Bhatt, S., Rana, V., Sen, K., Mondal, T.K., 2019. Application of AMS in understanding regional deformation fabric development and granite emplacement: examples from Indian cratons. *Geol. Soc. Lond. Spl. Publ.*, V. 489 (1). SP489-2019-292.
- Mamtani, M.A., Greiling, R.O., 2005. Granite emplacement and its relation with regional deformation in the Aravalli Mountain belt (India) - inferences from magnetic fabric. *J. Struct. Geol.* 27, 2008–2029.
- Mamtani, M.A., Pal, T., Greiling, R.O., 2013. Kinematic analysis using AMS data from a deformed granitoid. *J. Struct. Geol.* 50, 119–132.
- Mamtani, M.A., Sengupta, P., 2010. Significance of AMS analysis in evaluating superposed folds in quartzites. *Geol. Mag.* 147, 910–918.

- Mathez, E.A., 1989. Interactions involving fluids in the Stillwater and Bushveld complexes: observations from the rocks. In: A.J. Naldrett and J. Whitney (Eds.) Ore Deposition Associated with Magmas. Soc. Economic Geologists Short Course Notes, pp. 167- 179.
- McClelland Brown, E., 1982. Discrimination of TRM and CRM by blocking-temperature spectrum analysis. *Physics of the Earth and Planetary Interiors*, 30: 405–411.
- Mezger, K. and Cosca, M.A., 1999. The thermal history of the Eastern Ghats Belt (India), as revealed by U-Pb and  $^{40}\text{Ar}/^{39}\text{Ar}$  dating of metamorphic and magmatic minerals: implications for the SWEAT correlation. *Precambrian Res.*, vol. 94, pp. 251–271.
- Mezger, K., Cosca, M.A. and Raith, M.M., 1996. Thermal history of the Eastern Ghats Belt (India) deduced from U-Pb and  $^{40}\text{Ar}/^{39}\text{Ar}$  dating of metamorphic minerals. (Abstract) V.M. Goldschmidt Conference, 1, p. 401.
- Mohanty, S., 2006. Apparent Polar wandering path of the Proterozoic system of India: Implication for tectonic evolution of the Indian subcontinent. *Indian Journal of Geology*, V. 78(1-4), pp. 19- 35.
- Mondal, S., Piper, J.D.A., Hunt, L., Bandopadhyay, G., Basu Mallick, S., 2009. Palaeomagnetic and rock magnetic study of charnockites from Tamil Nadu, India and the 'Ur' protocontinent in early Palaeoproterozoic times. *J. Asia Earth Sci.* 34 (493), 506.
- Mondal, T.K., 2018. Evolution of fabric in Chitradurga granite (South India) – a study based on microstructure, anisotropy of magnetic susceptibility (AMS) and vorticity analysis. *Tectonophysics* 723, 149–161.
- Mondal, T.K., Chowdhury, A., Sain, A., Chatterjee, S., 2022. Understanding the maturity of columnar joints and its spatial relationship with eruptive centre: a critical appraisal from the Rajmahal Basalt, India. *Phys. Earth Planet. Inter.* 326, 106867.
- Mondal, T.K., Mamtani, M.A., 2014. Fabric analysis in rocks of the Gadag region (southern India) – implications for time relationship between regional deformation and gold mineralization. *Tectonophysics* 629, 238–249.
- Mooney, D. S., Geiss, C., Smith, A. M., 2002. The Use of Mineral Magnetic Parameters to Characterize Archaeological Ochres. *Journal of Archaeological Science* (2002) 29, 000–000. doi:10.1006/jasc.2002.0856.

- Murthy, M. V. N., Viswanathan, T. V. and Roy Chowdhury, S., 1971. The Eastern Ghats Group. *Rec. Geol. Surv. Ind.*, V. 101, Pt. 2., pp. 15-42.
- Nagata, T., 1961. *Rock Magnetism*, 2nd edition, Maruzen, Tokyo, 350pp.
- Naldrett, A.J., Bruegmann, G.E. and Wilson, A.H. (1990) Models for the concentration of PGE in layered intrusions. *Can. Min.*, v.28, pp.389-408.
- Nanda, J.K., Natarajan, V., 1980. Anorthosites and related rocks of the Kondapalle hills, Andhra Pradesh. *Geol. Surv. India Rec.* 113, 57–67.
- Narayanaswami, S., 1966. Tectonic problems of Precambrian rocks of peninsular India. *Symposium on Tectonics. Indian Geophys. Union spec. Pub.* pp. 77-94.
- Narayanaswami, S., 1975. Proposal for charnockite-khondalite system in the Archean shield of Peninsular India. *Geol. Surv. India, Misc. Publ. No.23, Part-1*, pp.1-16.
- Natarajan, V., Nanda, J. K., 1981. Large Scale Basin and Dome Structures in the High Grade Metamorphics, Near Visakhapatnam, South India. *Geology*.
- Nesbitt, B. E., 1986a. Oxide – sulfide - silicate equilibria associated with metamorphosed ore deposits. Part-I. Theoretical Considerations. *Econ. Geol.*, V. 81, pp. 831-840.
- Nesbitt, B. E., 1986b. Oxide – sulfide - silicate equilibria associated with metamorphosed ore deposits. Part-II. Pelitic and felsic terrains. *Econ. Geol.*, V. 81, pp. 841-856.
- Newton, R. C., 1987. Petrologic aspects of Precambrian granulite facies terrains bearing on their origins. A. Kroner (Ed.), *Proterozoic Lithospheric Evolution. American Geophysical Union, Geodynamic Series, Washington DC, vol. 17 (1987)*, pp. 11-26.
- O'Reilly, W. (1984) *Rock and Mineral Magnetism*. Blackie, New York.
- Pares, J.M., van der Pluijm, B.A., 2002. Evaluating magnetic lineations (AMS) in deformed rocks. *Tectonophysics* 350, 283–298.
- Paul S. 2006. Facies, paleogeography and depositional sequence analyses in parts of Meso- to Neoproterozoic rocks of Chattishgarh Supergroup, India. Unpublished Ph.D. Thesis, Indian School of Mines, Dhanbad, 177 p.
- Paul, D.K., Ray Barman, T., McNaughton, N.J., Fletscher, I.R., Potts, P.J., Ramakrishnan, M. and Augustine, P.F., 1990. *Archaean-Proterozoic evolution*

- of Indian charnockites: isotopic and geochemical evidence from granulites of the Eastern Ghats Belt. *J. Geol.*, vol. 98, pp. 253–263.
- Perraju, P., Kovach, A. and Svingor, E., 1979. Rubidium-strontium ages of some rocks from parts of the Eastern Ghats in Orissa and Andhra Pradesh, India. *J. Geol. Soc. India*, vol. 20, pp. 290–296.
- Piper, J.D.A., 1987. *Palaeomagnetism and the Continental Crust*, First Edition, John Wiley and sons, Halsted Press, Newyork.
- Pomella, H., Klotzli, U., Scholger, R., Stipp, M., Fügenschuh, B., 2011. The Northern Giudicarie and the Meran-Mauls fault (Alps, Northern Italy) in the light of new paleomagnetic and geochronological data from boudinaged Eo-/Oligocene tonalities. *Int. J. Earth Sci.* 100, 1827–1850. <https://doi.org/10.1007/s00531-010-0612-4>.
- Prevot, M., Remond, G., Caye, R., 1968. Etude de la transformation d'une titanomagnetite en titanomaghemite dans une roche volcanique. *Bull. Soc. Fr. Minéral. Cristallogr.* 91, 65.
- Price, G. D., 1981. Subsolidus phase relations in the titanomagnetite solid solution series. *Am. Miner.* V. 66, pp. 751-758.
- Radhakrishnamurty, C., Likhite, S.D., Deutsch, E.R., Murthy, G.S., 1978. Nature of magnetic grains in basalts and implications for palaeomagnetism. *Proc. Indian Acad. Sci. (Earth Planet Sci.)*, V.87A, pp. 235-243.
- Ramakrishnan, M., Nanda, J. K., & Augustine, P. F., 1998. Geological evolution of the Proterozoic Eastern Ghats Mobile Belt. *Geological Survey of India Special Publication*, 44, 1–21.
- Raposo, M.I.B., Egydio-Silva, M., 2001. Magnetic fabric studies of high-grade metamorphic rocks from the Juiz de Fora Complex, Ribeira Belt, Southeastern Brazil. *Int. Geol. Rev.* 43 (5), 441–456.
- Ray, S., Bose, M. K., 1975. *Chayanica Geol.* 11.
- Rickers, K., Mezger, K., Raith, M.M., 2001. Evolution of the continental crust in the Proterozoic Eastern Ghats Belt, and new constraints for Rodinia reconstruction: implications from Sm–Nd, Rb–Sr and Pb–Pb isotopes. *Precambrian Res.* 112, 183–212.
- Roberts, A.P., R.L. Reynolds, K.L. Verosub & D.P. Adam 1996 Environmental magnetic implications of greigite (Fe<sub>3</sub>S<sub>4</sub>) formation in a 3 m.y. lake sediment record from Butte Valley, northern California – *Geophys. Res. Lett.* 23: 2859–2862.

- Roberts, A.P., Tauxe, L., Heslop, D., Zhao, X., Jiang, Z., 2018. A critical appraisal of the “Day” diagram. *J. Geophys. Res. Solid Earth* 123, 2618–2644. <https://doi.org/10.1002/2017JB015247>.
- Roberts, S., Foster, R.P. and Nesbitt, R.M. (1990) Mineralisation associated with early Precambrian basic magmatism. In: R. P. Hall and D. J. Hughes (Eds.) *Early Precambrian Basic Magmatism*, Blackie, Glasgow, pp.157-188.
- Santosh M, Harris NBW, Jackson DH, Matthey DP (1990) Dehydration and incipient charnockite formation: a phase equilibria and fluid inclusion study from South India. *J Geol* 98:915–926.
- Santosh, M., Jackson, D.H., Harris, N.B.W. et al., 1991. Carbonic fluid inclusions in South Indian granulites: evidence for entrapment during charnockite formation. *Contr. Mineral. and Petrol.* 108, 318–330. <https://doi.org/10.1007/BF00285940>.
- Sarkar, A., 1994. Wilson cycle signature in a Precambrian orogen: a case study on the Eastern Ghats belt. *Workshop on Eastern Ghats Mobile Belt, Visakhapatnam*, pp. 76-78 (abs.).
- Sarkar, A., Bhanumathi, L. and Balasubramanyan, M.N., 1981. Petrology, geochemistry, and geochronology of the Chilka Lake igneous complex, Orissa State, India. *Lithos*, vol. 14, pp. 93–111.
- Sarkar, T., Schenk, V., Berndt, J., 2015. Formation and evolution of a Proterozoic magmatic arc: geochemical and geochronological constraints from meta-igneous rocks of the Ongole domain, Eastern Ghats Belt, India. *Contrib Mineral Petrol.*, 169:5, DOI 10.1007/s00410-014-1096-1.
- Schobel, S., deWall, H., 2014. AMS–NRM interferences in the Deccan basalts: toward an improved understanding of magnetic fabrics in flood basalts. *J. Geophys. Res. Solid Earth* 119, 2651–2678.
- Sen, K., Dubey, A.K., Tripathi, K., Pfänder, J.A., 2012. Composite mesoscopic and magnetic fabrics of the Paleo-Proterozoic Wangtu Gneissic Complex, Himachal Himalaya, India: implications for ductile deformation and superposed folding of the Himalayan basement rocks. *J. Geodyn.* 61, 81–93.
- Sen, S.K., Bhattacharya, S. and Acharyya, A., 1995. A multi-stage pressure–temperature record in the Chilka Lake granulites: the epitome of the metamorphic evolution of Eastern Ghats, India? *Journal of Metamorphic Geology*, 14, 287–298.

- Sengupta, P., Sen, J., Dasgupta, Raith, M., Bhui, U.K., Ehl, J., 1999. Ultra-high temperature metamorphism of Metapelitic Granulites from Kondapalle, Eastern Ghats Belt: implications for the Indo-Antarctic Correlation. *J. Petrol.* 40 (7), 1065–1087.
- Shive, P.N., Blakely, R.J., Frost, B.R., Fountain, D.M., 1992. Magnetic properties of the lower continental crust. In: Fountain, D.M., Arculus, R., Kay, R.W. (Eds.), *Continental Lower Crust*. Elsevier, pp. 145–178.
- Shive, P.N., Fountain, D.M., 1988. Magnetic mineralogy in an Archean crustal cross section: implications for crustal magnetization. *J. Geophys. Res.* 93, 12177–12186.
- Sinha, R. C. and Mall, A. P., 1974. The charnockite-bearing ultrabasics of Kondapalli and Gangineni (A.P.) and the petrogenetic relations between associated Charnockite series of rocks. *Proc. Indian Natl. Sci. Acad.*, v. 40 A, pp. 46-56.
- Speczik, S., Wiszniewska, J., Diedel, R., 1988. Minerals, exsolution features and geochemistry of Fe-Ti ores of the Suwalki District (Northeast Poland). *Mineral. Deposita*, V. 23, pp. 200-210.
- Stacey, F.D., Joplin, G., Lindsay, J., 1960. Magnetic anisotropy and fabric of some foliated rocks from S.E. Australia. *Geophysica. Pura Appl.*, V.47, pp. 30-40.
- Subrahmanyam, C., 1978. On the relation of gravity anomalies to geotectonics of the Precambrian terrain of south Indian shield. *Jour. Geol. Soc. Ind.*, V. 19, pp. 251- 261.
- Sugiura, N., 1979. ARM, TRM and magnetic interactions: Concentration dependence, *Earth Planet. Sci. Lett.*, 42, 451–455, doi:10.1016/0012-821X(79)90054-2.
- Tarling, D., Hrouda, F., 1993. *Magnetic Anisotropy of Rocks*. Springer.
- Tarling, D.H., 2007. *Palaeomagnetism: Principles and applications in Geology, Geophysics and Archaeology*. Chapman and Hall, New York and London.
- Tauxe, L., 2010. *Essentials of palaeomagnetism*, University of California Press, Berkley-Los Angeles-London. ISBN: 978-0-520-26031-3.
- Tauxe, L., Bertman, H.N., Sebwrino, C., 2002. Physical interpretation of hysteresis loops: micromagnetic modelling of fine particle magnetite. *Geochem. Geophys. Geosyst.* 3 (10), 1–22.
- Thompson, R., Oldfield, F., 1986. *Environmental Magnetism*. Allen and Unwin, Winchester, MA. <https://doi.org/10.1007/978-94-011-8036-8>.

- Till, J.L., Jackson, M.J., Moskowitz, B.M., 2010. Remanence stability and magnetic fabric development in synthetic shear zones deformed at 500°C. *Geochem. Geophys. Geosyst.* <https://doi.org/10.1029/2010GC003320>.
- Tilley, C. E., 1936. Enderbite, A new member of the charnockite series. *Geol. Mag.*, V. 73, pp. 312-316.
- Tripathi, K., Dubey, A.K., Jayangondaperumal, R., 2019. Mesoscopic, magnetic and petrofabric study of the High Himalayan gneisses and leucogranite along oblique and frontal ramps of the Vaikrita Thrust in Satluj and Bhagirathi valleys: thrust locking and superposed folding. *J. Earth Syst. Sci.* 128, 77. <https://doi.org/10.1007/s12040-019-1094-9>.
- Upadhyay, D., Raith, M.M., Mezger, K., Hammerschmidt, K., 2006a. Mesoproterozoic rift related alkaline magmatism at Elchuru, Prakasam Alkaline Province, SE India. *Lithos* 89, 447–477.
- Verma R. K., Samaddar A. K. and Murti K. S. 1977. Palaeomagnetic study of Gunderdehi Shale of Raipur Group from Chhatisgarh basin in India. *Indian Journal of Earth Science* 4, 183-191.
- Verosub, K.L. & A.P. Roberts 1995 Environmental magnetism: Past, present, and future – *J. Geophys. Res.* 100: 2175–2192.
- Viegas, G.F., Archanjo, C.J., Vauchez, A., 2013. Fabrics of migmatites and the relationships between partial melting and deformation in high-grade transpressional shear zones: the Espinho Branco anatexite (Borborema Province, NE Brazil). *J. Struct. Geol.* 48, 45–56.
- Vielzeuf, D. and Vidal Ph. (Editors), 1990. *Granulites and Crustal Differentiation*. Kluwer, Dordrecht.
- Vijaya Kumar, K., Ernst, W.G., Leelanandam, C., Wooden, J.L., Grove, N.J., 2010. First Paleoproterozoic ophiolite from Gondwana: geochronologic-geochemical documentation of ancient oceanic crust from Kandra, SE India. *Tectonophysics* 487, 22–32.
- Vijaya Kumar, K., Leelanandam, C., Ernst, W.G., 2011. Formation and fragmentation of the Palaeoproterozoic supercontinent Columbia: evidence from the Eastern Ghats Granulite Belt, southeast India. *International Geology Review*, <http://dx.doi.org/10.1080/00206814.2010.527658>.
- Vinogradov, A., Tugarinov, A., Zhykov, C., Stapnikova, N., Bibikova, E. and Korre, K., 1964. Geochronology of the Indian Precambrian. Report 22nd International Geological Congress, Part 10, pp. 553–567.



- Viswanathan, T.V., 1969. The granulitic rocks of the Indian Precambrian shield. *Mem. geol. Sum. India*, 100: 37-66.
- Voight, W., Kinoshita, S., 1907. Bestimmung absoluter Werte von Magnetisierungszahlen, insbesondere für Kristalle. *Annale der Physic*, V.24, pp. 492–514.
- Walden J., Oldfield F. and Smith J., 1999. *Environmental magnetism: a practical guide*. Quaternary Research Association, London.
- Wang, X. Y., Yi, S., Lu, H., Vandenberghe, J., and Han, Z. (2015). Aeolian process and climatic changes in loess records from the northeastern Tibetan Plateau: response to global temperature forcing since 30 ka. *Paleoceanography* 30, 612–620. doi: 10.1002/2014PA002731.
- Windley, B. F., 1973. Crustal development in the Precambrian. *Phil. Trans. Roy. Soc. London.*, V. A-273, pp. 321-341.
- Worm, H. U., 1998. On the superparamagnetic-stable single domain transition for magnetite, and frequency dependence of susceptibility, *Geophys. J. Int.*, 133, 201–206, doi:10.1046/j.1365-246X.1998.1331468.x.
- Yamazaki, T., and Ioka, N., 1997. Cautionary note on magnetic grain-size estimation using the ratio of ARM to magnetic susceptibility, *Geophys. Res. Lett.*, 24, 751–754, doi:10.1029/97GL00602.
- Zhang, J. and Piper, J. D. A., 1994. Magnetic fabric and post-orogenic uplift and cooling magnetisations in a Precambrian granulite terrain: The Datong-Huai'an region of the North China Shield. *Tectonophysics*, V. 234, pp. 227-246.
- Zhou, L. P., Oldfield, F., Wintle, A. G., Robinson, S. G. and Wang, J. T., 1990. Partly pedogenic origin of magnetic variations in Chinese loess, *Nature*, 346, 737–739, doi:10.1038/346737a0.
- Zijderveld, J. D. A., 1967. A. C. demagnetization of rocks: analysis of results, in *Methods in Palaeomagnetism* (eds D. W. Collinson, K. M. Creer and S. K. Runcorn), Elsevier, Amsterdam.